NOTICE

The quality of this microform is heavily dependent upon the quality of the original thesis submitted for microfilming. Every effort has been made to ensure the highest quality of reproduction possible.

If pages are missing, contact the university which granted the degree.

Some pages may have indistinct print especially if the original pages were typed with a poor typewriter ribbon or if the university sent us an inferior photocopy.

Reproduction in full or in part of this microform is governed by the Canadian Copyright Act, R.S.C. 1970, c. C-30, and subsequent amendments.

AVIS

La qualité de cette microforme dépend grandement de la qualité de la thèse soumise au microfilmage. Nous avons tout fait pour assurer une qualité supérieure de reproduction.

S'il manque des pages, veuillez communiquer avec l'université qui a conféré le grade.

La qualité d'impression de certaines pages peut laisser à désirer, surtout si les pages originales ont été dactylographiées à l'aide d'un ruban usé ou si l'université nous a fait parvenir une photocopie de qualité inférieure.

La reproduction, même partielle, de cette microforme est soumise à la Loi canadienne sur le droit d'auteur, SRC 1970, c. C-30, et ses amendements subséquents.

DYNAMIC ANAYLSIS OF A HYDROPNEUMATIC SUSPENSION SYSTEM

Frank R. Joo

A Thesis

in

The Department

of

Mechanical Engineering

Presented in Partial Fulfillment of the Requirements
for the Degree of Master of Engineering at
Concordia University
Montreal, Quebec, Canada

December 1991

ISBN 0-315-73616-X

ABSTRACT

DYNAMIC ANALYSIS OF A HYDROPNEUMATIC SUSPENSION SYSTEM

Frank R. Joo

Variable road surface quality imposes a wide shock and vibration environment on ground vehicles. The requirement to isolate the vehicle chassis, occupants and cargo from potentially harmful shock and vibration exposure, without reducing vehicle handling performance, has created several contradictory design requirements. Alternative suspension designs have thus been investigated to achieve an improved compromise between ride and handling performance criteria. In this thesis, the shock and vibration isolation potentials of hydropneumatic suspension are investigated through systematic modeling and computer simulation.

The shock and vibration isolation potentials of hydropneumatic suspension are investigated through two mathematical models characterizing the dynamic behaviour of the suspension. The mathematical models incorporate nonlinearities due to: polytropic nature of the gas spring; turbulent hydraulic fluid flow; Coulomb damping; compressible hydraulic fluid, and elastic motion limiting bump stops. Shock isolation potential is evaluated for rounded step and rounded pulse displacement excitations. Vibration isolation is investigated for harmonic displacement excitation, employing a direct integration and frequency sweep method. A frequency dependent linearization technique, based on

dissipation/storage of energy, is employed to derive local linear equivalent suspension characteristics; frequency response of the linearized suspension model is investigated to establish validity of the linearization technique. The influence of various suspension characteristics are investigated via parametric sensitivity analyses.

Shock and vibration isolation potentials of hydropneumatic suspension are also investigated via a vehicle application study. A pitch-plane, seven degrees-of-freedom ride dynamic model of a tracked military vehicle is employed for this analysis. Vibration isolation performance is predicted for harmonic displacement excitation, via a direct integration and frequency sweep technique. Shock isolation performance is predicted for the vehicle traversing semi-circular bump obstacles at different approach speeds.

The hydropneumatic suspension is very nonlinear in nature due to the progressively stiffening gas spring characteristic and orifice and Coulomb damping. Shock and vibration isolation response characteristics of the hydropneumatic suspension tend to be superior compared to those of a conventional suspension, particularly under severe excitations. Parametric analyses revealed that the significant design parameters are initial gas pressure and initial gas volume, whereas the significant operating parameters are hydraulic fluid bulk modulus and gas polytropic exponent. Ride analysis of the tracked vehicle revealed that hydropneumatic suspension provides superior vibration isolation characteristics throughout the entire frequency range of interest, and improved shock isolation characteristics when the vehicle is subjected to severe bump excitations.

ACKNOWLEDGEMENTS

The author would like to thank his supervisors Dr. S. Sankar and Dr. S. Rakheja for their continuous support and guidance in the preparation of this thesis.

The author would also like to thank the members of the faculty, staff and students of the CONCAVE (CONcordia Computer Aided Vehicle Engineering) Research Centre, Department of Mechanical Engineering, Concordia University, for their time and assistance during the evolution of this work.

Appreciation and thanks is acknowledged for the support provided by the Fonds FCAR fellowship during the course of this research.

Special thanks is owed to the Product Engineering Department of General Motors of Canada for their continued support, encouragement and patience during the completion of this thesis.

This thesis is dedicated to the author's parents, Ferenc and Rita Joo and to his wife Lauretta Joo for their love, patience and encouragement to achieve excellence; without them this thesis would not have been possible.

TABLE OF CONTENTS

CHAPTER 6

TRACKED VEHICLE RIDE PERFORMANCE ANALYSIS

CHAPTER 7

CONCLUSIONS AND RECOMMENDATIONS FOR FUTURE WORK

LIST OF FIGURES

LIST OF TABLES

NOMENCLATURE

SYMBOL	*DESCRIPTION*
A_e	Effective cross-section area of actuating piston, (m^2)
A_{fp}	Cross-section area of floating piston, (m^2)
A_o	Cross-section area of damper plate orifice, (m^2)
A_p	Cross-section area of main piston, (m^2)
C	Polytropic gas constant, ($P_\phi \cdot V_\phi^\gamma$)
C_c	Viscous damping coefficient of Coulomb damping, (N•s/m)
C_d	Coefficient of drag for turbulent fluid flow through an orifice
C_{eqi}	Equivalent viscous damping coefficient of damper 'i', (N•s/m)
C_o	Viscous damping coefficient of fluid flow through an orifice, (N•s/m)
d_1, d_2	Distance between elastic bump stops and main piston in compression and expansion modes, respectively, for hydropneumatic suspension, (m)
d_i	Distance between hull c.g. and trailing arm pivot 'i', (m)
d_{si}	Distance between hull c.g. and shock absorber pivot 'B_i', (m)
E_c	Energy dissipated in one cycle by Coulomb damping, (J)
E_d	Energy dissipated in one cycle by orifice damping, (J)
E_{gas}	Energy stored in a quarter cycle by gas spring, (J)
F_c	Coulomb friction force acting on main piston, (N)

F_{cf}	Coulomb friction force acting on floating piston, (N)
F_f	Dynamic friction force, (N)
F_{Hi}	Combined spring and damping force generated by hydropneumatic suspension system 'i', (N)
F_s	Force due to elastic bump stops, (N)
g	Acceleration due to gravity, (m/s^2)
J_h	Mass moment of inertia of tracked vehicle about hull center of gravity, ($kg \cdot m^2$)
k_b	Tracked vehicle elastic bump stop stiffness coefficient, (N/m)
K_{eq}	Equivalent linear spring stiffness coefficient, (N/m)
K_{gas}	Static gas spring stiffness coefficient, (N/m)
K_s	Elastic bump stop stiffness coefficient for hydropneumatic suspension system, (N/m)
K_{lin}	Linear spring stiffness coefficient, (N/m)
K_{peff}	Effective stiffness coefficient of road wheel and elastic track pad, (N/m)
K_{ti}	Torsional stiffness coefficient of torsion bar 'i', (N•m/rad)
L_{ID}	Distance between idler gear and hull center of gravity, (m)
L_{sp}	Distance between sprocket and hull center of gravity, (m)
M	Isolator mass, (kg)
M_{fp}	Floating piston mass, (kg)
M_h	Mass of tracked vehicle hull, (kg)
m_{wi}	Mass of road wheel 'i', (kg)

n	Number of orifices in damper plate of hydropneumatic suspension
P_1, P_2	Internal pressures of oil chambers 1 and 2 of hydropneumatic suspension system, (N/m^2)
P_{at}	Atmospheric pressure, (N/m^2)
P_{gas}	Internal pressure of gas chamber in hydropneumatic suspension, (N/m^2)
P_{gi}	Dynamic gas pressure of hydropneumatic suspension, (N/m^2)
$P_{i\phi}$	Initial gas charge pressure of hydropneumatic suspension, (N/m^2)
Q_i	Flow rate into/out of oil chamber 'i', (m^3/s)
R	Trailing arm length, (m)
r_b	Distance between trailing arm pivot and elastic bump stop, (m)
r_B	Radius of bump displacement excitation, (m)
r_s	Distance between trailing arm pivot and shock absorber mount 'A', (m)
t	Time, (s)
V_{Ai}, V_{Bi}	Velocity of shock absorber endpoints 'A' and 'B' along shock absorber axis, (m/s)
V_{gi}	Dynamic gas volume of hydropneumatic suspension, (m^3)
$V_{i\phi}$	Initial gas charge volume of hydropneumatic suspension, (m^3)
V_t	Constant forward speed of tracked vehicle, (m/s)
x_i	Longitudinal displacement of trailing arm pivot 'i', (m)

x_{Ai}	Longitudinal displacement of shock absorber endpoint 'A_i', (m)
x_{Bi}	Longitudinal displacement of shock absorber endpoint 'B_i', (m)
x_o	Initial distance between center of semi-circular bump obstacle and leading contact point of tracked vehicle, (m)
x_{wi}	Longitudinal displacement of road wheel 'i', (m)
y_i	Vertical displacement of trailing arm pivot, 'i', (m)
y_{Ai}	Vertical displacement of shock absorber endpoint 'A_i', (m)
y_{Bi}	Vertical displacement of shock absorber endpoint 'B_i', (m)
y_{wi}	Vertical displacement of road wheel 'i', (m)
y_h	Vertical, (bounce), displacement of tracked vehicle hul' center of gravity, (m)
y_{Ri}	Vertical displacement excitation experienced at road wheel 'i' due to terrain irregularities, (m)
z	Relative displacement between main and floating pistons of hydropneumatic suspension, (m)
z_{fp}	Vertical displacement of floating piston, (m)
z_o	Vertical displacement excitation experienced by hydropneumatic suspension, (m)
z_p	Vertical displacement of main piston, (m)
α	Ratio of main to floating piston cross-section areas of hydropneumatic suspension
α_i	Angle between the horizontal and the line between trailing arm pivot 'i' and hull c.g., (rad)

β	Hydraulic fluid bulk modulus, (N/m^2)
β_i	Angle between the horizontal and the line between shock absorber point 'B_i' and hull c.g., (rad)
β_o	Nominal value of hydraulic fluid bulk modulus, (N/m^2)
ε, ε_d, ε_k	Error parameters
ζ	Angle between trailing arm centerline and a line passing through the trailing arm pivot and shock absorber point 'A', (rad)
γ	Polytropic exponent
θ_i	Swing angle of trailing arm 'i', (rad)
θ_o	Static inclination angle of trailing arms with horizontal, (rad)
λ	Inclination angle of hydraulic shock absorbers, (rad)
μ	Ratio of floating piston mass to isolator mass
μ_{eff}	Effective ratio of floating piston mass to isolator mass
μ_{ID}	Track stiffness coefficient of leading portion of track, (N/m)
μ_{SP}	Track stiffness coefficient of trailing portion of track, (N/m)
μ_w	Track stiffness coefficient of track portions between road wheels, (N/m)
ν	Shock severity parameter
ρ	Hydraulic fluid mass density, (kg/m^3)
ϕ_H	Pitch angle of tracked vehicle hull about hull center of gravity, (rad)
ω	Excitation frequency, (rad/s)

CHAPTER 1
INTRODUCTION AND LITERATURE REVIEW

1.1 INTRODUCTION

The function of a vehicle suspension system is to isolate the vehicle chassis from road or terrain irregularities and to control dynamic forces experienced under various driving maneuvers. The ability to isolate the chassis from road irregularity induced shock and vibrations is a measure of vehicle ride comfort, and the ability to control dynamic forces, experienced during cornering, acceleration and deceleration, is a measure of vehicle handling and control performance. The conflicting requirements imposed by the ride comfort, handling and control performance of a vehicle necessitate a compromise between the characteristics of the spring and hydraulic shock absorber elements selected during the suspension design stage.

Ride comfort requires a soft and lightly damped suspension system to effectively isolate the vehicle chassis from road induced shock and vibrations. Although low natural frequency and soft damping characteristics of a suspension provide good vibration isolation at frequencies well above resonance, they yield poor attenuation and control at resonance. Conversely, a suspension with stiff damping characteristic provides good displacement control at resonance, but exhibits poor shock and vibration isolation.

Conventional suspension systems consist of steel springs and hydraulic shock absorbers. The steel springs, either coil or leaf type, are employed extensively on passenger vehicles and provide approximately linear force deflection characteristics. Compressed air springs, with

nonlinear force deflection characteristic, are employed almost exclusively on heavy vehicles such as buses, dump trucks and tractor trailers. Springs isolate the vehicle chassis from road irregularities by allowing relative motion between the suspension linkages and the chassis, and by temporarily storing the shock and vibration energy emparted by the road irregularities. Dual-tube telescopic hydraulic shock absorbers are typically employed on all forms of ground vehicles. Energy dissipation, or damping, is achieved by forcing hydraulic fluid through restricted passages, valves and orifices, within the shock absorber. The dissipated kinetic energy is converted to heat energy which in turn is dissipated to the surrounding environment.

Owing to the design compromise imposed by ride comfort and handling and control performance, conventional suspension systems have inherent limitations. Steel springs possess a fixed and unadjustable spring rate, and impose a considerable weight penalty on the vehicle. The corresponding increase in the unsprung mass reduces vehicle fuel economy and degrades suspension performance. A significant amount of space is also required to package steel springs, imposing another constraint on the suspension designer. Increased spring size and complexity robs valuable space from other hardware, restricting designer's options.

Efforts to avoid the limitations associated with conventional passive suspension systems have lead designers to investigate alternate suspension designs such as hydropneumatic, semi-active and active suspensions. Hydropneumatic suspension combines a compressed nitrogen gas spring and hydraulic shock absorber into a single suspension unit. The compressed nitrogen gas provides a light weight spring with low static stiffness and nonlinear progressively stiffening spring rate.

Further, the construction of a hydropneumatic suspension aids heat dissipation, reducing the effects of damper heat fade. The single suspension unit design also requires less space to package on the vehicle and reduces the overall unsprung mass of the suspension system due to the light weight of the gas spring.

1.2 REVIEW OF RELEVANT LITERATURE

The performance characteristics of hydraulic shock absorbers in view of ride comfort, handling and control performance of vehicles has been the subject of many investigations. Fukushima, *et al* [1] investigated the ride/handling improvements provided by optimum damping characteristics dependent on piston stroke. The authors experimentally measured suspension vertical reaction force for a vehicle equipped with a coil and strut suspension arrangement. Coil spring and damper forces were quantified as a percentage of the total suspension force, and were measured under various steering maneuvers. Ride comfort was assessed for random terrains and discrete rectangular obstacles. The results revealed that the coil spring provided the majority of the suspension control force under various steering maneuvers, and the shock absorber provided the majority of the suspension control force related to ride comfort and ride harshness. The authors postulated that damping force dependent on piston stroke can provide optimum vehicle ride/handling characteristics.

Anderson and Fan [2] performed an experimental and theoretical analysis of a dual-tube hydraulic shock absorber with rubber bushings fitted at the ends, as shown in Figure 1.1. Dynamic testing of the shock absorber was performed on an electro-hydraulic shaker at various excitation frequencies up to 10 Hz. A five parameter mathematical model

was developed to predict the shock absorber performance. Model assumptions included: linear valve characteristic, negligible fluid leakage, effective compressibility and linear stiffness due to rubber end bushings. Gauss-Newton method was employed to estimate the unknown parameters, such as effective bulk modulus, using the nonlinear time domain analysis. The study provided good correlation with the experimental results, and the authors concluded that the effective compressibility is the primary factor leading to hysteresis and the linear valve assumption provides adequate accuracy although valve leakage does occur.

A dual-tube AC Delco hydraulic shock absorber, shown in Figure 1.2, has been modeled and investigated using the continuous system modeling program (CSMP) [3]. The mathematical model incorporated the effects of valve dynamics, hydraulic fluid compressibility, and entrapped air. Assuming negligible leakage flows, constant reserve chamber pressure, and viscous valve plate damping, the study concluded that an integration time step greater than 10^{-5} seconds resulted in errors which terminated program execution. When compared to previously published experimental results, the proposed shock absorber model displayed good correlation of force-velocity characteristic. Four dual-tube shock absorber models were further considered to study their ride performance potentials: linear approximation; bi-linear approximation; nonlinear approximation, excluding hysteresis, and detailed model as developed by the authors. The two degrees-of-freedom quarter vehicle model, incorporating tire stiffness and unsprung mass, was subjected to a weighted white noise excitation in order to evaluate the ride comfort in relation to ISO-standard 2631 [4]. The study demonstrated that the less detailed

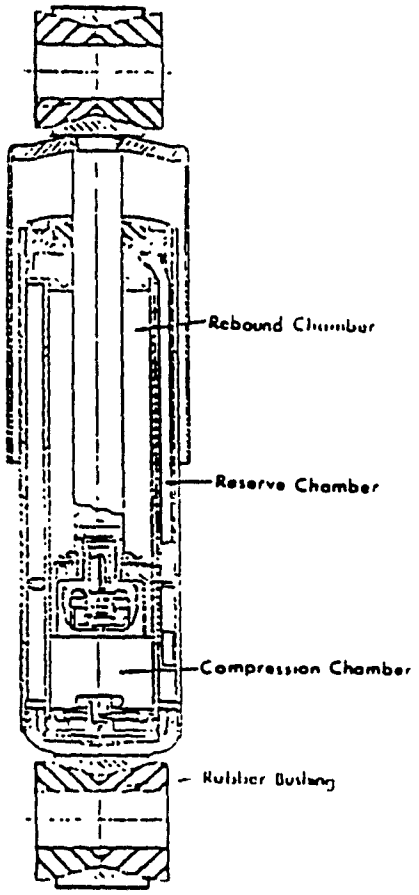

Figure 1.1 Schematic of bus dual-tube shock absorber with rubber end bushings [2].

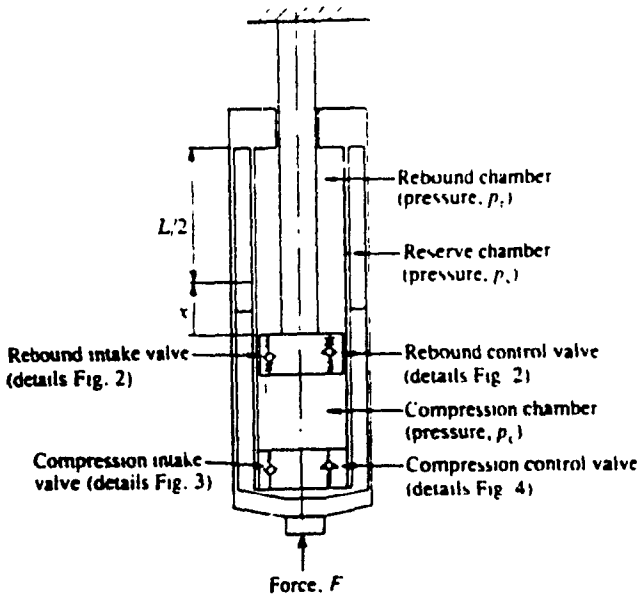

Figure 1.2 Schematic of automotive dual-tube shock absorber [3].

shock absorber models produced significantly more favorable ride predictions than does the detailed model. The authors also concluded that entrained gascs have a detrimental effect on shock absorber performance by increasing the size o' the hysteresis loop.

Several authors have investigated passive hydraulic shock absorbers which incorporate unique pressure control schemes. Su *et al* [5] proposed a tunable passive sequential hydraulic damper, shown in Figure 1.3, employing external pressure control valves which modulate the pressure across the damper piston. A mathematical damper model is developed assuming turbulent orifice flow, high fluid bulk modulus, negligible seal friction and negligible leakage flow. The contribution of the gas column is modeled as a nonlinear restoring force following a polytropic compression/expansion characteristic. An ideal sequential damping scheme is proposed incorporating the dynamics of the external pressure relief valves. For pressure differential below a preset limit, the relief valves remain closed allowing constant orifice damping; the relief valves open providing reduced damping force when the pressure differential exceeds the preset limit. The simulation results indicated that a properly tuned sequential damper can provide considerably improved vibration isolation at frequencies beyond resonance.

The application of compressed air as a spring medium has been treated by several authors. In a study presented by Bank [6], the use of pneumatic springs in heavy vehicle suspensions, including trucks and buses, is discussed. The advantages of pneumatic springs over conventional steel springs include: inherently low static spring rate and low natural frequency; almost constant natural frequency over the load range of the vehicle; potentials for adjustable ride height

allowing full suspension travel regardless of loading condition; improved control of shock forces experienced near the end of suspension compression travel, and reduced vehicle mass. The effects of operating pressure and assembly height on spring performance were investigated, and the force-deflection characteristics of a rolling sleeve-type pneumatic spring, Figure 1.4, were compared to those of a spring with fixed rate, as shown in Figure 1.5. The study also showed that an improved attenuation of shocks can be achieved by increasing operating pressure and decreasing spring diameter. Burkley and Meyers [7] presented equations governing pressure and volume changes in rolling lobe pneumatic springs, and demonstrated the differences in force-deflection characteristics due to adiabatic and isothermal assumptions.

Pneumatic springs and damping mechanisms have also been investigated to achieve isolation from shocks. A shock isolator comprising of a single acting pneumatic spring with fixed and variable volume chambers, separated by an orifice, as shown in Figure 1.6, has been proposed by Hundal [8]. Assuming adiabatic compression process and negligible Coulomb friction, the shock isolator performance was evaluated analytically for a constant velocity pulse of finite duration. The isolator's performance was evaluated for undamped and damped conditions. A self-damped pneumatic shock isolator comprising of a cylinder divided, by a piston, into two equal volume chambers, as shown in Figure 1.7, was further proposed to achieve improved shock isolation [9]. Each chamber was connected to its own surge tank via an orifice passage which provided the damping for the system. The piston was connected to the isolator mass via a ram, and was capable of axial

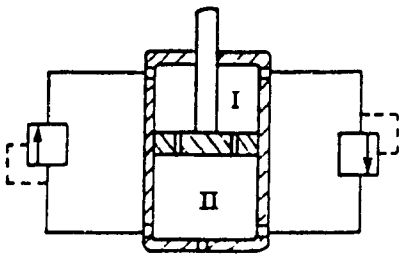

Figure 1.3 Schematic of sequential passive hydraulic damper [5].

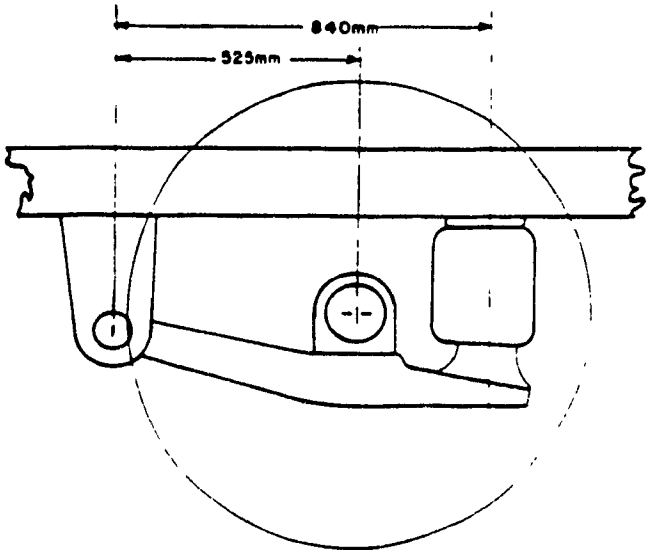

Figure 1.4 Schematic of rolling sleeve-type pneumatic spring [6].

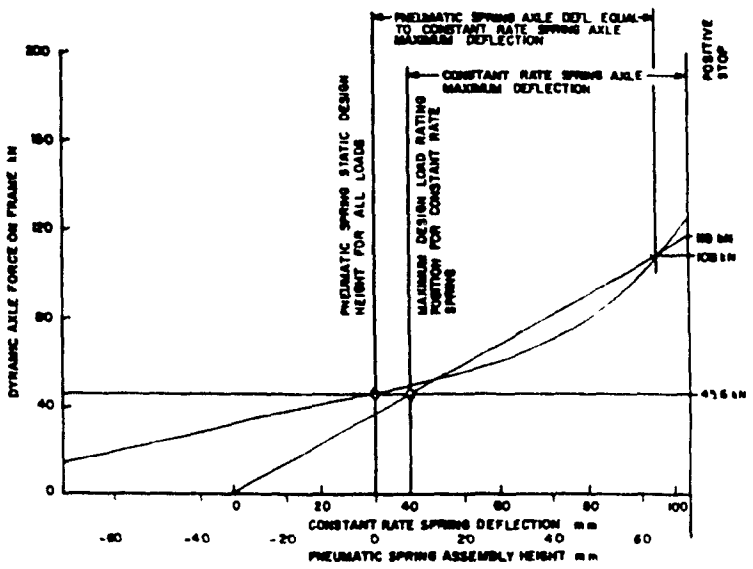

Figure 1.5 Comparison of force-deflection characteristics of linear steel spring and rolling sleeve pneumatic springs for various pneumatic spring assembly heights [6].

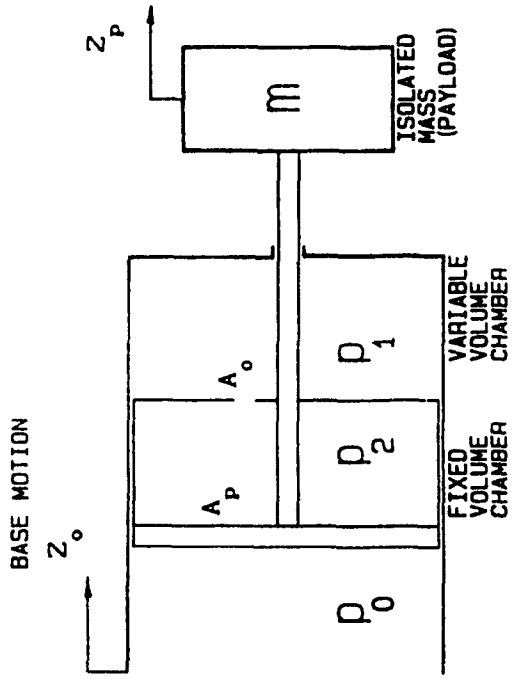

Figure 1.6 Schematic of damped pneumatic isolator [8].

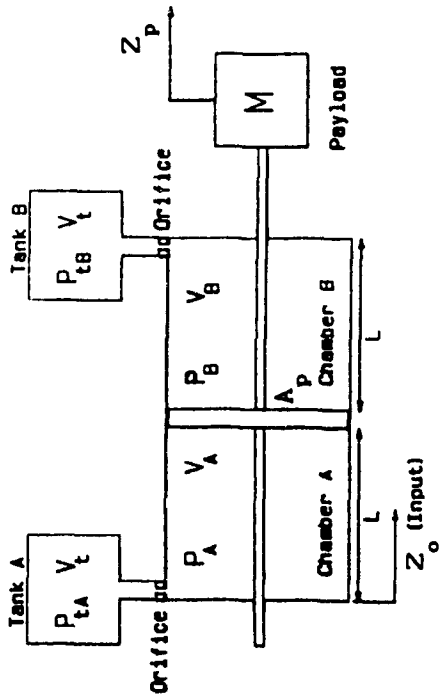

Figure 1.7 Schematic of a symmetrically damped pneumatic isolator [9].

movement within the cylinder. Assuming negligible Coulomb friction, negligible leakage flows and adiabatic process, the shock isolation performance of the isolator model was evaluated for a rectangular acceleration pulse of finite duration.

The investigation of shock absorber performance is not limited to the ground vehicle industry; the aircraft industry has also performed extensive design and analysis of oleopneumatic shock struts employed as aircraft landing gear. These struts are a combination spring/shock absorber employing compressed nitrogen as the spring medium and hydraulic fluid as the damping medium. The hydraulic fluid and the nitrogen gas may be separated by a floating piston or may interface directly depending on the strut design, as shown in Figure 1.8. A mathematical model of the oleopneumatic strut was developed incorporating metering and snubber orifice discharge coefficients as a function of the Reynolds number, orifice shape and orifice orientation, snubber valve hydraulic forces during compression and expansion, and the effects of internal strut Coulomb friction, wing lift, strut inclination angle, wheel spin-up and drag loads [10],[11]. The gas is assumed to follow a polytropic compression/expansion process, and the polytropic exponent is selected as 1.1. Transient response characteristics of the resulting two degrees-of-freedom model of the aircraft and oleopneumatic strut were evaluated on an analog computer for drop test and landing situations. The simulation results revealed good correlation with the experimental results obtained during actual landing and drop tests.

The influence of oil compressibility and gas polytropic exponent on the strut performance was further investigated by Wahl [11]. The study concluded that entrained air has a detrimental effect on strut

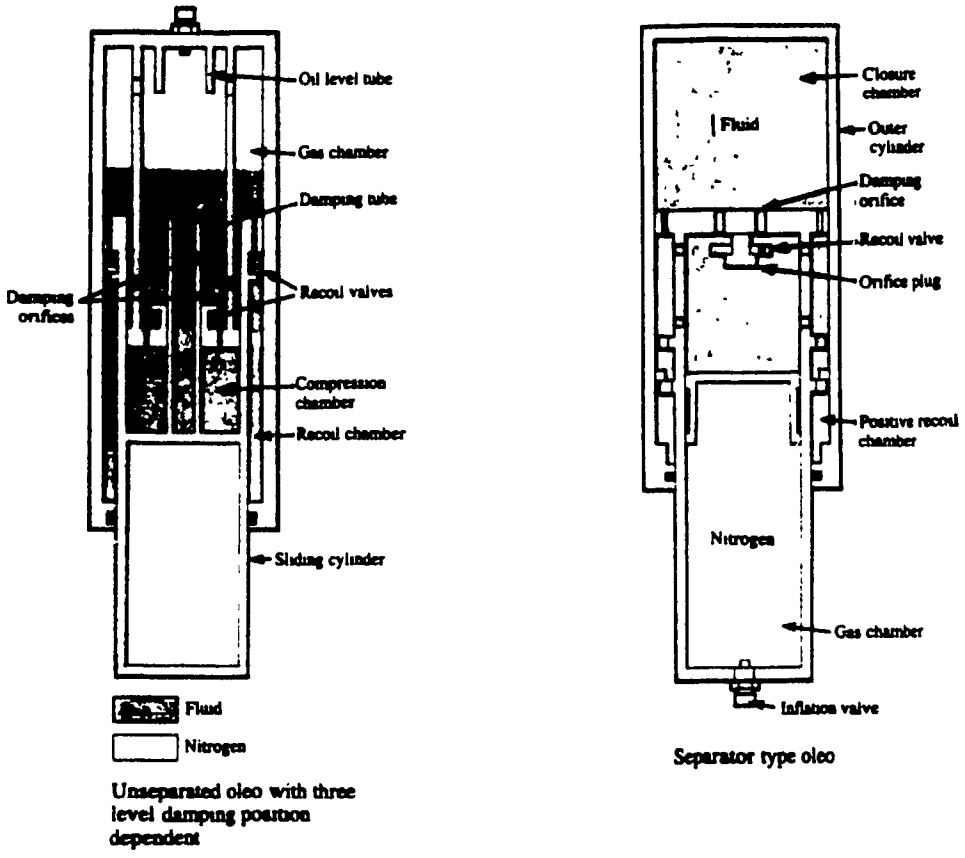

Figure 1.8 Schematic of typical unseparated and separated oleo-pneumatic aircraft struts [21].

load-stroke performance, and the polytropic exponent is indeed not constant during the compression/expansion process.

Hydropneumatic suspension is primarily a form of an oleopneumatic shock strut. Hydropneumatic suspension combines compressed nitrogen gas, as a spring medium, and conventional orifice damping into a single suspension unit. The hydraulic fluid and nitrogen gas are separated by a flexible diaphragm or floating piston. Moulton and Best [12] proposed the design of a hydropneumatic suspension 'Hydragas', shown in Figure 1.9. The history of the suspension development, properties and advantages of Hydragas suspension, and potential ride benefits were discussed. The Hydragas suspension consists of two hermetically sealed spherical containers stacked vertically. The top container is divided into two chambers separated by an elastic diaphragm: the upper chamber is filled with compressed nitrogen gas and the lower chamber is filled with hydraulic fluid. The lower container is also divided into two chambers by a flexible diaphragm. The upper chamber is filled with hydraulic fluid, while the underside of the diaphragm is acted upon by a tapered piston connected to a suspension link. Hydraulic fluid travels between the upper and lower containers through a damper valve with different jounce and rebound flow characteristics. The authors concluded that the advantages of Hydragas suspension include lower natural frequency, lighter suspension weight, stiffening spring characteristic leading to constant natural frequency, and damping properties less affected by changes in operating temperature. A pitch-plane schematic model of a generic automobile equipped with leading arm front link, trailing arm rear link and interconnected front-rear Hydragas suspension has been presented. Based on road measurements, the study presented the

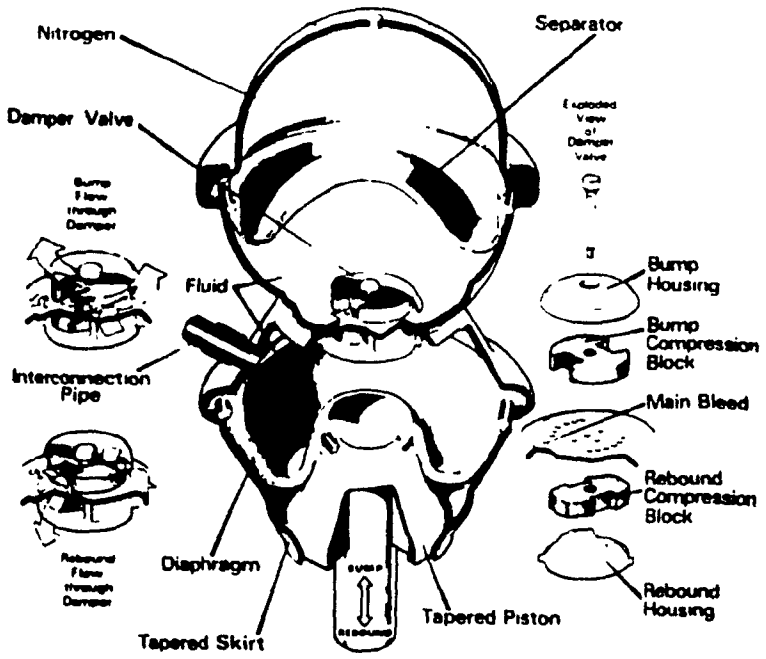

Figure 1.9 Schematic of Hydragas suspension system [12].

ride vibration levels of different vehicles with dissimilar suspension properties. Although the ride vibration characteristics of vehicles such as an Austin Mini equipped with Hydragas suspension were compared to those of a Volkswagen Polo equipped with the conventional suspension, the study failed to demonstrate definitive conclusions.

Several other authors have also investigated the performance potentials of hydropneumatic suspension or derivatives of hydropneumatic suspension. Félez and Vera [13] investigated the response of a heavy crane vehicle equipped with three forms of hydropneumatic suspension: independent cylinder suspension; linked cylinder suspension, and active suspension, as shown in Figure 1.10. Mathematical models developed employing bond graph techniques were simulated to evaluate vehicle response to roll input caused by constant speed turning maneuver, and by a vertical displacement at one side of the vehicle. The simulation results for the vehicle negotiating a curve at constant speed revealed that the chassis vertical displacement response of the independent and linked cylinder suspension configurations were almost identical. The active suspension, however, provided the compensation for the centrifugal forces thereby reducing vehicle roll.

In another study on performance potentials of hydropneumatic suspension, Craighead and Brown [14] investigated the shock and vibration response of two off-road vehicles equipped with conventional and hydropneumatic suspensions. The two vehicles studied were a 25 tonne articulated dump truck, and a 39 tonne Vickers Main Battle Tank with six suspension units per side. The responses characteristics of the dump truck were compared for two suspension configurations: no suspension, except for pneumatic tires, and leading arm front hydropneumatic

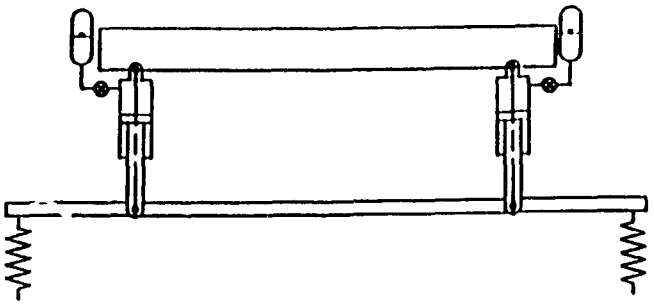

(a) Independent cylinder suspension configuration.

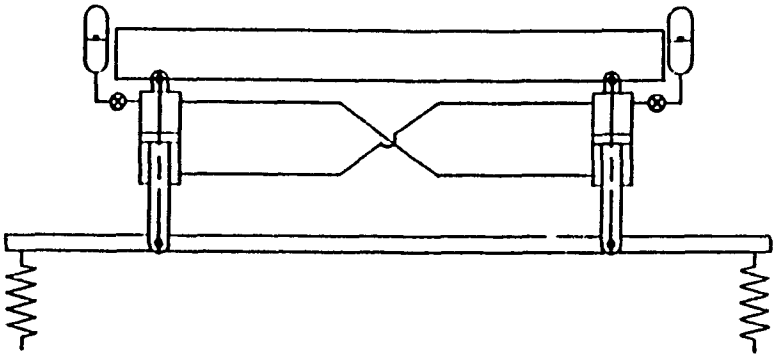

(b) Linked cylinder suspension configuration.

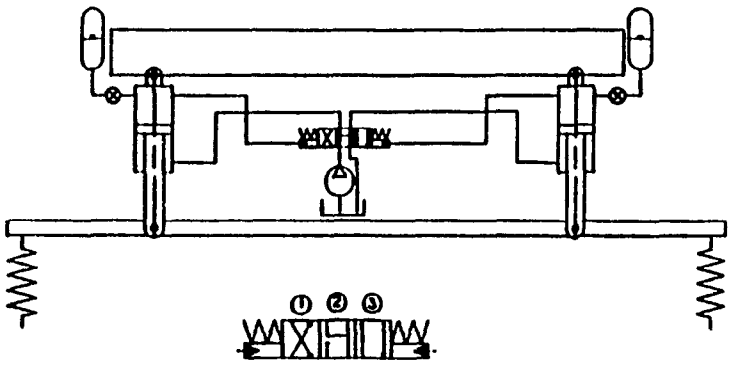

(c) Active suspension configuration.

Figure 1.10 Schematic of three hydropneumatic suspension configurations: (a) Independent cylinder suspension; (b) Linked cylinder suspension, and (c) Active suspension [13].

suspension with rigid rear axle, as shown in Figure 1.11. A six degrees-of-freedom dump truck model was developed assuming adiabatic nature of the nitrogen gas, stiff travel limiting bump stops with linear characteristic, damping forces generated by viscous flow through suspension piping, linear tire characteristic and constant damping characteristics. A simplified eight degrees-of-freedom pitch-plane mathematical model of the battle tank was developed for the conventional torsion bar and hydropneumatic suspension used in the study. Figure 1.12 illustrates the schematic of the hydropneumatic suspension employed in the study. The natural frequencies and damping ratios were computed through eigen value analysis of the linearized homogeneous equations. Continuous Systems Modeling Package (CSMP) was employed, to simulate the transient response characteristics of the vehicles traversing a discrete obstacle at a constant speed. The vibration attenuation performance was evaluated for random terrains at constant speeds. The results indicated that the addition of front suspension to the truck lowers the bounce and pitch mode natural frequencies while increasing the damping factor of these two modes. All other truck modes were not affected by the addition of the front suspension. The addition of hydropneumatic suspension to the tank resulted in a reduction of the hull pitch, roll and heave mode natural frequencies while the damping factors of each mode remain virtually unchanged. The study also concluded that the addition of hydropneumatic suspension to the truck reduced peak acceleration and displacement at the c.g., while the tank experienced reduced acceleration but higher displacement at the hull c.g. Ride response of the truck traversing random terrain showed that the hydropneumatic suspension significantly reduced transmitted vibrations. The ride

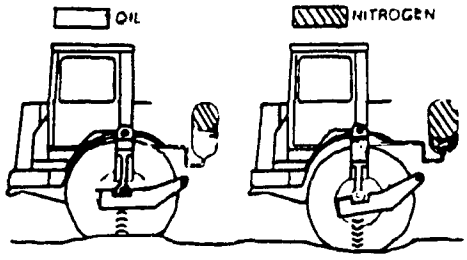

Figure 1.11 Schematic of hydropneumatic truck suspension system [14].

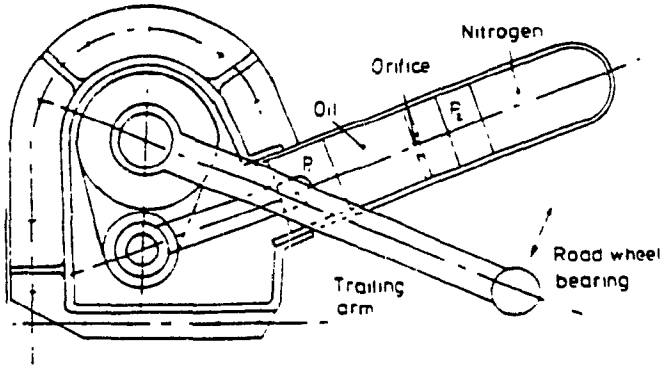

Figure 1.12 Schematic of Vickers battle tank hydropneumatic suspension system [14].

responses of the tank traversing random terrain, however, indicated that the hydropneumatic suspension yields inferior vibration isolation at certain vehicle speeds.

Maclaurin [15] reviewed the configurations and principles of operation of current British tracked military vehicle suspensions. In particular, the shock and vibration isolation performance of a Challenger main battle tank, equipped with hydropneumatic suspension, and the Mechanized Combat Vehicle 80, (MCV-80), equipped with conventional torsion bar suspension were compared. The suspension of the MCV-80 comprises a torsion bar, pivoting on roller bearings, and a rotary vane hydraulic damper. There are six suspension stations per side of the vehicle; torsion bars are at each station, and dampers at stations 1, 2 and 6. The Challenger also has six wheel stations per side, each fitted with a hydropneumatic suspension as shown in Figure 1.13. Vehicle ride performance was evaluated for the following MVEE test courses: sinewave course, 4.5 m, 7.0 m, and 12.0 m wavelengths; ramps, 30%, 40% and 50%, and a random profile course 205 m long of spectral characteristic typical of natural off-road terrains. For the 7.0 m wavelength sinewave course, the Challenger tank, equipped with hydropneumatic suspension, displayed superior isolation performance. When subjected to the 30% ramp, both vehicles displayed similar performance, being able to achieve the same approach speed before reaching the permissible acceleration level at the driver's seat. When subjected to the random course, the Challenger tank displayed inferior isolation performance, attaining higher levels of RMS acceleration through the speed range.

Another military application of hydropneumatic suspension is

discussed in a report by Murphy [16]. The ride vibration and shock isolation characteristics of an M60 battle tank equipped with a combination of hydropneumatic suspension system (HSS) and advanced torsion bar suspension (ATB), referred to as the M60 HSS/ATB hybrid tank, were investigated. The performance characteristics of the M60 HSS/ATB hybrid tank were compared to those of an M60 tank equipped with standard torsion bar suspension (STB) for various test courses. The measured data was analyzed in terms of ride performance, the speed at which a limiting vertical absorbed power is experienced, and ride quality, the vertical absorbed power experienced at a given speed. The study concluded that ride performance of the two vehicles is quite similar; the M60 HSS/ATB hybrid tank, however can negotiate discrete obstacles at faster speeds. The study further concluded that the ride quality of the M60 HSS/ATB hybrid tank was superior to that of the M60 STB tank on some of the random test courses.

Multiple uses and configurations of hydropneumatic suspension have been investigated by various researchers in an attempt to achieve improved shock and vibration isolation performance. Hydropneumatic suspension has been studied for applications such as adaptive, semi-active and fully active suspensions. Karnopp and Margolis [17] discussed the influence of suspension parameters on vibration isolation, and proposed an adaptive suspension scheme to achieve optimal isolation performance. The study was based on simulation of a single degree-of-freedom model of an isolator comprising adiabatic gas spring, viscous damping, negligible friction and a load leveler.

Horton and Crolla [18] presented a theoretical analysis of hydropneumatic semi-active suspension comprising three staged gas

springs and capable of automatic self-leveling, as shown in Figure 1.14. A quarter vehicle model incorporating adiabatic gas spring, viscous damper and linear spring and damping representation of the tire and control pendulum system, was developed. A three dimensional, ten degrees-of-freedom vehicle model was also developed for a small truck with independent front suspension, solid rear axle and three suspension control pendula. Vehicle response was simulated for two terrain excitations: a double ramp 1.0 m long and 0.14 m high traversed by one side of the vehicle only, and digital representation of a 100 m length of the National Institute of Agricultural Engineering, (N.I.A.E.), test track representing a typical farm road. Simulation results were obtained for vehicles equipped with passive, semi-active and no suspension. The results revealed that for the application of a static load, the semi-active suspension is superior due to its self-leveling properties. However, when subjected to discrete ramp displacement excitations and when traversing the N.I.A.E. test course, the vehicles equipped with passive and semi-active suspension experienced almost identical responses for both laden and unladen conditions. The shock and vibration isolation potentials of farm tractors, equipped with the proposed semi-active suspension, have been investigated through analytical and experimental means [19]. Comparison of analytical and experimental results revealed that simulation predicts poorer ride performance than that obtained experimentally for the vehicle traversing the triangular bumps. Vertical RMS acceleration response was measured at the driver's seat of four vehicles, (a 4 wheel drive tractor with unequal sized wheels, a 2 wheel drive tractor with sprung front axle wheels, a utility vehicle with axle suspension, and the farm tractor with semi-active

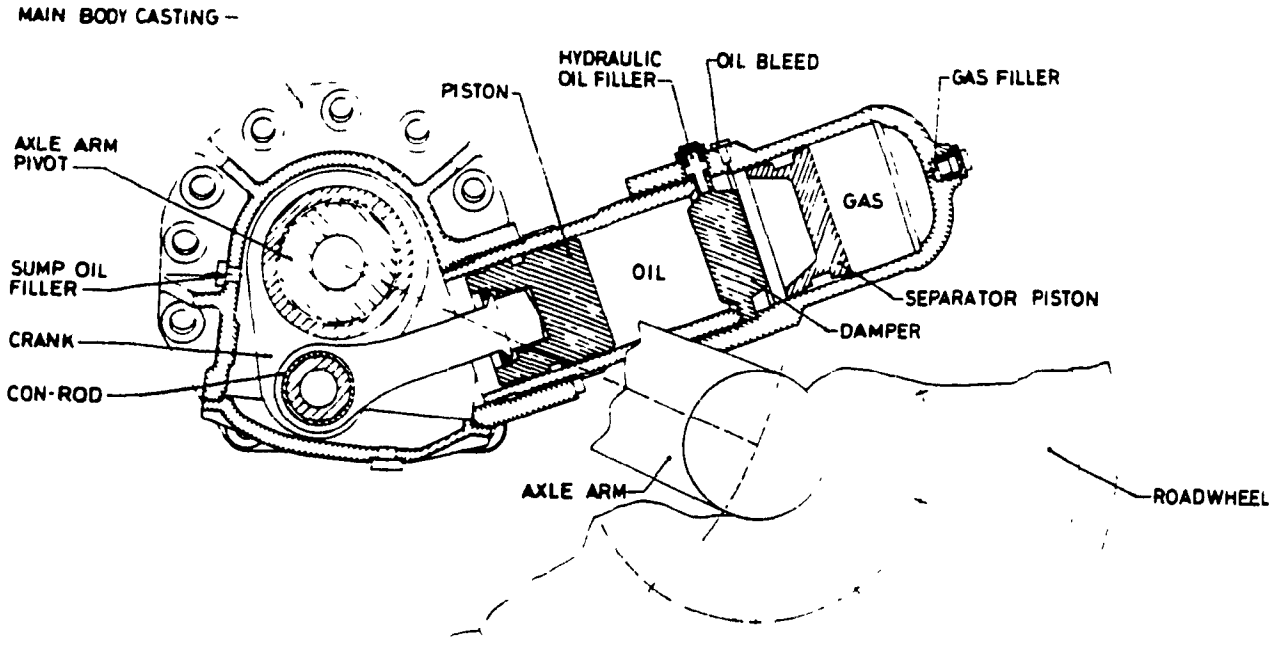

Figure 1.13 Schematic of Challenger battle tank hydropneumatic suspension system [15].

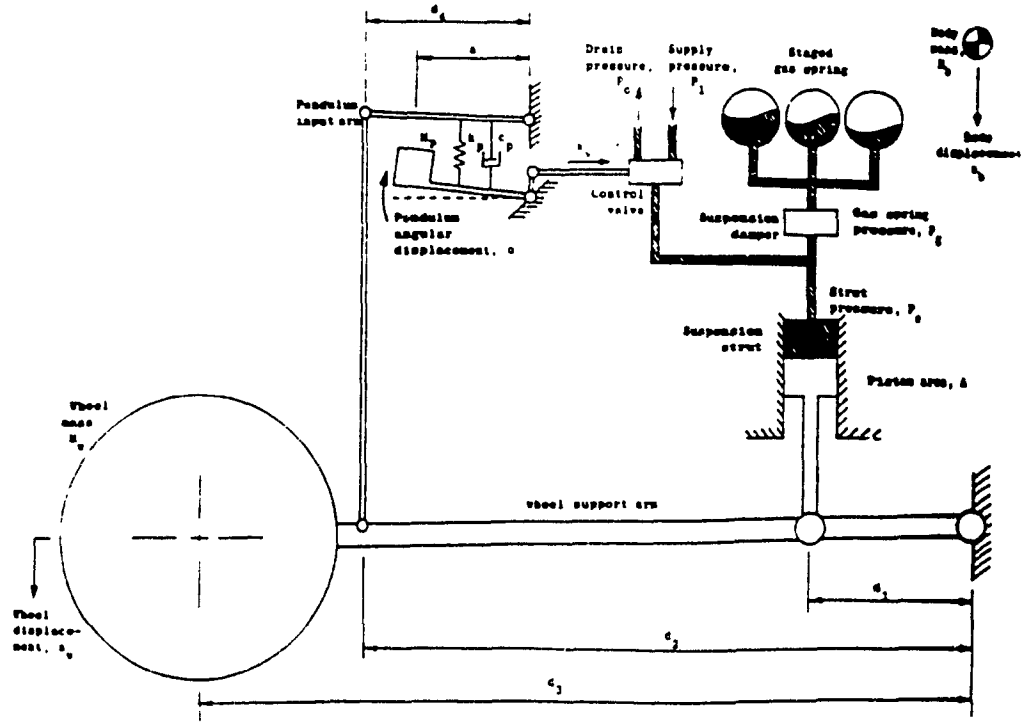

Figure 1.14 Schematic of proposed off-road semi-active hydropneumatic suspension system [18].

suspension), traversing the N.I.A.E. test courses. Comparison of experimental results revealed that the vibration isolation of the test vehicle with semi-active suspension is superior to the isolation experienced by the two tractors, but inferior to that of the utility vehicle.

The unique nature of hydropneumatic suspension has also been extended for use in sports vehicles. Dominy and Bulman [20] proposed a semi-active suspension for use on a Formula One Grand Prix Racing car, as shown in Figure 1.15. The suspension performance was analyzed by considering a quarter vehicle model influenced by chassis and road inputs. The analysis, incorporating the spring mass interactions, control valve dynamics, control flows, negligible tire compliance, adiabatic gas spring, negligible Coulomb friction, and turbulent hydraulic flows, was carried out for a gradually increasing load due to aerodynamic downforce and bump excitation. The study revealed that adequate selection of suspension parameters can significantly reduce chassis movement.

1.3 SCOPE OF THE PRESENT RESEARCH WORK

The primary objectives of this thesis research are to evaluate the ride performance potentials of passive hydropneumatic suspension via computer simulation. The specific objectives of the thesis research are as follows:

1) To develop a comprehensive mathematical model of a passive, nonlinear hydropneumatic suspension system, including effects of polytropic gas compression, orifice flows, Coulomb friction, and hydraulic fluid compressibility.

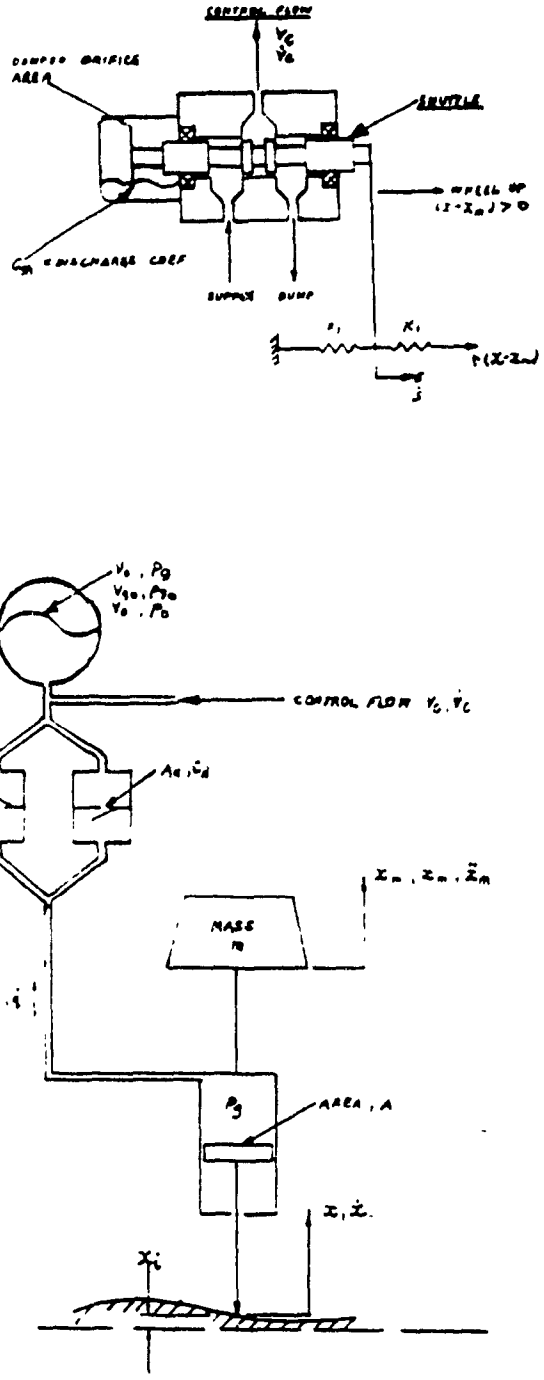

Figure 1.15 Schematic of proposed Formula One hydropneumatic active suspension system [20].

2) To predict the shock and vibration isolation of the hydropneumatic suspension subject to shock and harmonic displacement excitations.

3) To perform a parametric sensitivity analysis to identify significant design and operating suspension parameters, and illustrate the effects of fluid compressibility on suspension performance.

4) To develop a ride-dynamic model of a multiple road wheels tracked vehicle incorporating kinematics and dynamics of the linkage suspension.

5) Investigate the relative ride performance potentials of hydropneumatic suspension systems, employed in tracked vehicles, for excitations arising from discrete obstacles and harmonic displacements.

In Chapter 2, the design details and potential benefits of various passive hydropneumatic suspension systems are discussed. Two nonlinear mathematical models of the hydropneumatic suspension are developed: one assuming hydraulic fluid to be incompressible, and the other considering hydraulic fluid compressibility. The analytical models incorporating nonlinearities due to seal friction, dynamics of the floating piston, orifice flows and bump stops are derived and discussed.

In Chapter 3, analytical techniques and deterministic excitations used for evaluating shock and vibration isolation performance are presented. The nonlinear hydropneumatic suspension model is linearized using a local linearization technique based on balancing the dissipated/stored energy. The nonlinear forces due to gas spring, orifice damping and Coulomb friction are expressed by an array of local

equivalent constants as a function of excitation and response characteristics. The effectiveness of the linearization technique is demonstrated by comparing the response characteristics of the linearized suspension model to those of the nonlinear model.

In Chapter 4, a multi-wheeled tracked vehicle is presented for a vehicle application study. The tracked vehicle is modeled yielding a pitch-plane, seven degrees-of-freedom mathematical model. Modeling assumptions and highlights are also discussed.

In Chapter 5, the shock and vibration isolation performance of the hydropneumatic suspension is evaluated via computer simulation. The response of the linearized hydropneumatic suspension is compared to the nonlinear hydropneumatic model to evaluate accuracy of the linear modeling technique. A parametric sensitivity analysis is performed to identify significant design and operating suspension parameters. The results of the parametric study are discussed to highlight the influence of various design and operating parameters on the suspension performance.

In Chapter 6, the ride performance potentials of hydropneumatic suspension are evaluated for the tracked vehicle subjected to excitations arising from discrete obstacles and harmonic displacement. Relative performance benefits of hydropneumatic suspension are demonstrated by comparing the sprung mass displacement and acceleration response characteristics to those of the tracked vehicle with conventional torsion bar suspension. The conclusions drawn from the study and recommendations for future work are presented in Chapter 7.

CHAPTER 2

ANALYTICAL MODELING OF A HYDROPNEUMATIC VEHICLE SUSPENSION

2.1 GENERAL

The desired functions of a suspension system are to provide support and guidance to the vehicle, and to isolate the vehicle chassis, passengers and cargo from shocks and vibrations induced by roadway irregularities. Adequate suspension designs can provide improved ride quality and handling performance of the vehicle, and reduce the risks of vehicle component/cargo damage. Vehicle ride vibrations are of whole body nature and are predominant around low frequencies (1 - 8 Hz) [30]. Prolonged exposure to such vibrations causes driver fatigue and loss of driving proficiency [4]. Effective vibration isolation via vehicle suspension can thus improve vehicle ride quality and driver safety by reducing the magnitude of transmitted vibration. Furthermore, effective isolation from sudden shocks can reduce the risk of driver injury, loss of vehicle control, and the magnitude of cargo/component damage.

Handling and control characteristics of vehicles are also dependent upon vehicle suspension designs. Ride comfort, handling and control performance, however, impose conflicting design requirements on the vehicle suspension system. Lightly damped and soft suspension systems yield improved vibration isolation, and thus improved ride quality, at the expense of poor handling and control performance of the vehicle. A lightly damped and soft suspension further yields excessive chassis/suspension deflections, considerable variations in the ride height between laden and unladen conditions, and low effective roll

stiffness. Conversely, suspension systems with stiff springs are more desirable to achieve improved roll stability, handling and control performance of the vehicle. Consequently, suspension designs necessitate a compromise between ride quality, roll stability, and handling and control performance characteristics of the vehicle.

Hydropneumatic suspension systems offer considerable performance potentials in view of ride height control, ride quality, and vehicle handling and control. Variations in ride height due to sprung weight, under laden and unladen conditions, can be conveniently compensated via a simple control system. Since the restoring force is generated by compressed gas, addition of a control valve and a gas reservoir can provide the desired ride height control. The gas spring of a hydropneumatic suspension provides low spring rate, and thus low natural frequency, under static conditions. Low frequency terrain induced vibrations and shocks can thus be effectively isolated to yield improved ride quality. The ride quality can be further improved via the addition of variable damping that may be realized by introducing blow-off valves within the damper plate assembly.

The nonlinear progressively stiffening spring characteristic of the gas spring offers considerable advantages in controlling relative deflection of the sprung mass with respect to the unsprung mass. Vehicle handling and control performance are also improved due to the progressively hardening gas spring characteristic. As the relative suspension travel increases, the restoring force increases sharply. During an abrupt steering maneuver, a sufficiently large restoring force generated with small suspension travel, limits the vehicle roll and pitch.

In this chapter, construction and principles of operation of various commercially developed hydropneumatic suspension systems are briefly described, and their performance benefits and limitations are discussed. An analytical model of a hydropneumatic suspension system is derived in a systematic manner in order to investigate its shock and vibration isolation potentials.

2.2 HYDROPNEUMATIC SUSPENSION

A number of hydropneumatic suspension systems have been developed for road as well as off-road vehicle applications [12, 14, 22, 23]. Although these suspension systems exhibit several design variations, their operation is primarily an identical principle. A hydropneumatic suspension consists of an energy storage element (spring), and an energy dissipating element (damper), contained in a single unit, as illustrated in Figure 2.1. The suspension system contains both hydraulic fluid and compressed gas, usually nitrogen, separated by either a floating piston or a flexible diaphragm. The suspension forces are generated by fluid pressure acting on the main piston. Damping forces are generated by the flow of hydraulic fluid through constrictions provided by either a damper plate or a valve housing, while the restoring forces are generated by the compression/extension of the gas charge.

A hydropneumatic suspension may be used as an alternative suspension system for a wide range of vehicles. It is particularly well suited for heavy load carrying vehicles due to its ability to generate high spring forces while providing a low static natural frequency. In view of its potentials to provide ride height control, hydropneumatic suspension can be effectively employed in freight vehicles which

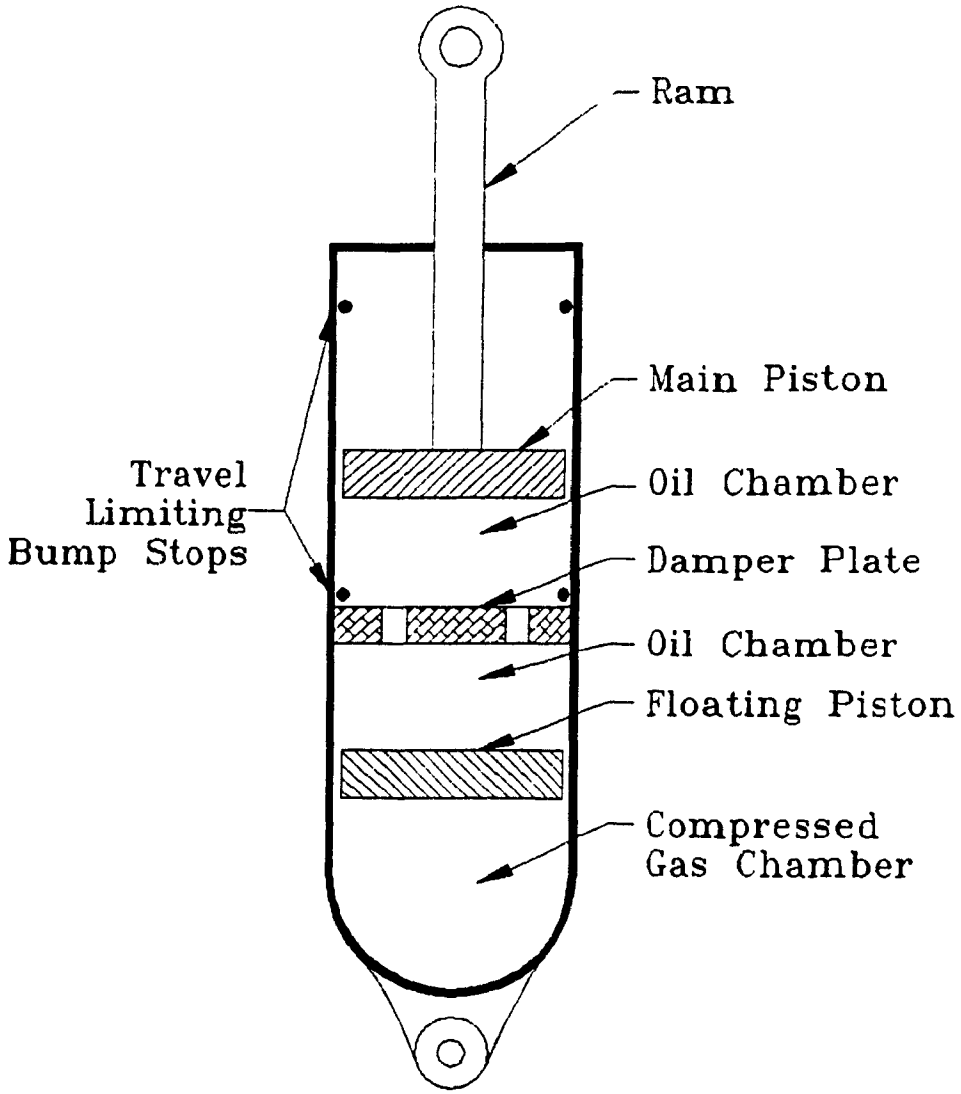

Figure 2.1 Schematic of typical hydropneumatic suspension system.

experience considerable variations in sprung weight during laden and unladen conditions. Conventional primary suspensions, in general, employ stiff spring characteristics to compensate for the large variations in sprung weight. Such a design philosophy provides adequate handling and control, and good ride quality when laden. However, the shock and vibration isolation performance deteriorates considerably when the vehicle is in the unladen condition. Hydropneumatic suspension is also well suited for passenger cars and other light weight vehicles due to its compact and light weight design The compressed gas spring generates significant restoring forces at a fraction of the weight of a conventional spring.

Figure 2.2 illustrates the "Hydragas" suspension design, developed by Moulton and Best [12]. The suspension system consists of two hermetically sealed spherical chambers in a vertical arrangement. A rubber separator (diaphragm), divides the upper chamber into two sections. The upper section is charged with compressed nitrogen, while the lower section contains hydraulic fluid. The lower spherical chamber is filled only with hydraulic fluid that acts upon a tapered piston. The lower chamber is sealed against this piston by means of a rolling diaphragm. A damper assembly, with bump and rebound valves, is mounted between the two chambers, as shown in Figure 2.2. The "Hydragas" suspension system was designed for passenger cars, and offers the possibility of coupled front-rear suspension by means of interconnecting hydraulic lines. Moulton and Best conducted experimental studies and concluded that this suspension design provides superior ride quality and improved handling, while maintaining a low natural frequency and reduced unsprung weight.

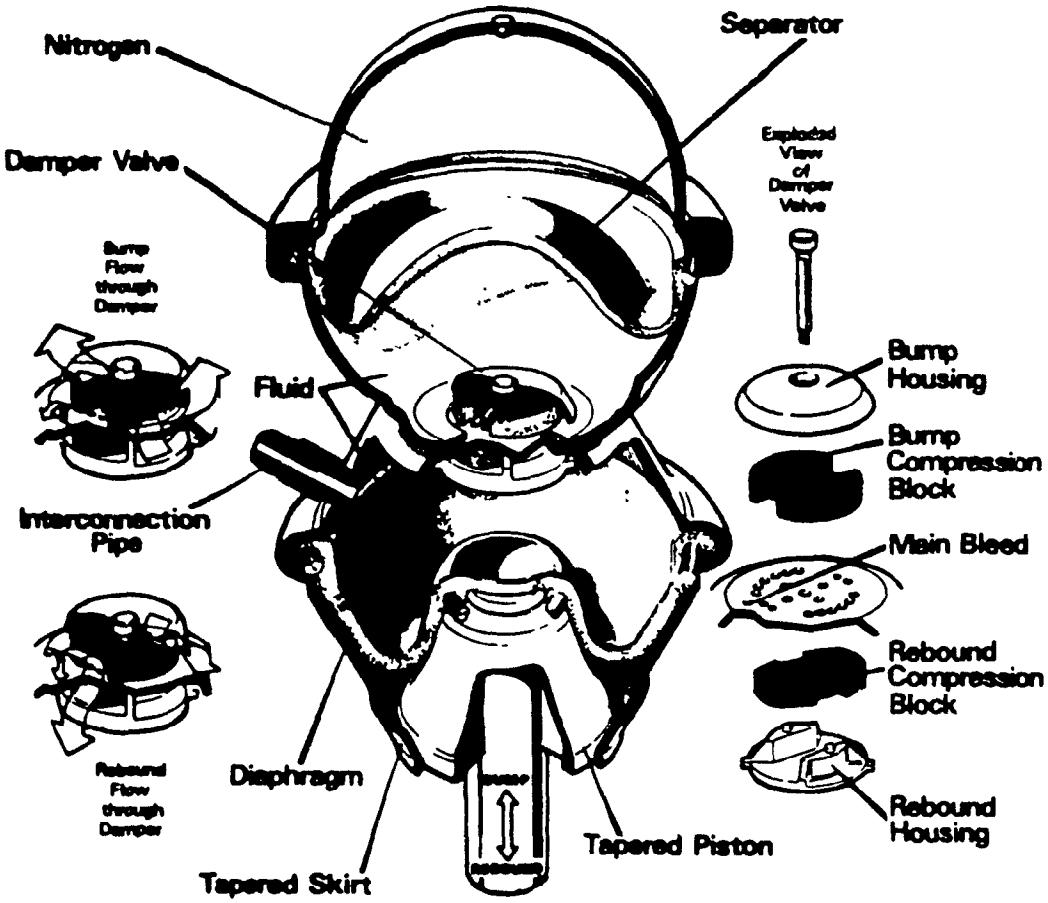

Figure 2.2 Schematic of 'Hydragas' suspension system[12].

Figure 2.3 illustrates the schematic of a hydropneumatic suspension system, developed by Dunlop Industries [22], for tracked military vehicles. The suspension system comprises a cylinder, as an integral part of a main housing, which is bolted to the hull of the vehicle. The cylinder is divided into two chambers: one containing hydraulic fluid and the other containing compressed nitrogen gas. The two fluid mediums are separated by means of a 'floating' piston. The main piston acts directly on the hydraulic fluid and is connected to the suspension trailing arm via crank and connecting rod links. Damping is achieved by forcing hydraulic fluid through a damper assembly which is located within the hydraulic chamber. Extremely secure seals are used to prevent leakage past both the main and floating pistons, since any loss of hydraulic fluid or nitrogen gas would degrade suspension performance.

Figure 2.4 shows a schematic of a hydropneumatic suspension system developed by Teledyne Continental Motors [23]. This suspension system consists of two cylinders; an actuator, and an accumulator. The cylinders are located within the road arm in a parallel arrangement. A damping manifold is used to port the hydraulic fluid from one chamber to the other, and a floating piston separates the hydraulic fluid from the nitrogen gas. The main piston, connected to the mounting plate via crank and connecting rod links, acts directly on the hydraulic fluid. The pistons are installed with high precision seals to prevent leakage and formation of an oil/gas mixture. The entire suspension system is contained within the trailing arm assembly which is bolted directly to the hull of the vehicle.

The hydropneumatic suspension system offers many advantages and limitations when compared to a conventional suspension. The light weight

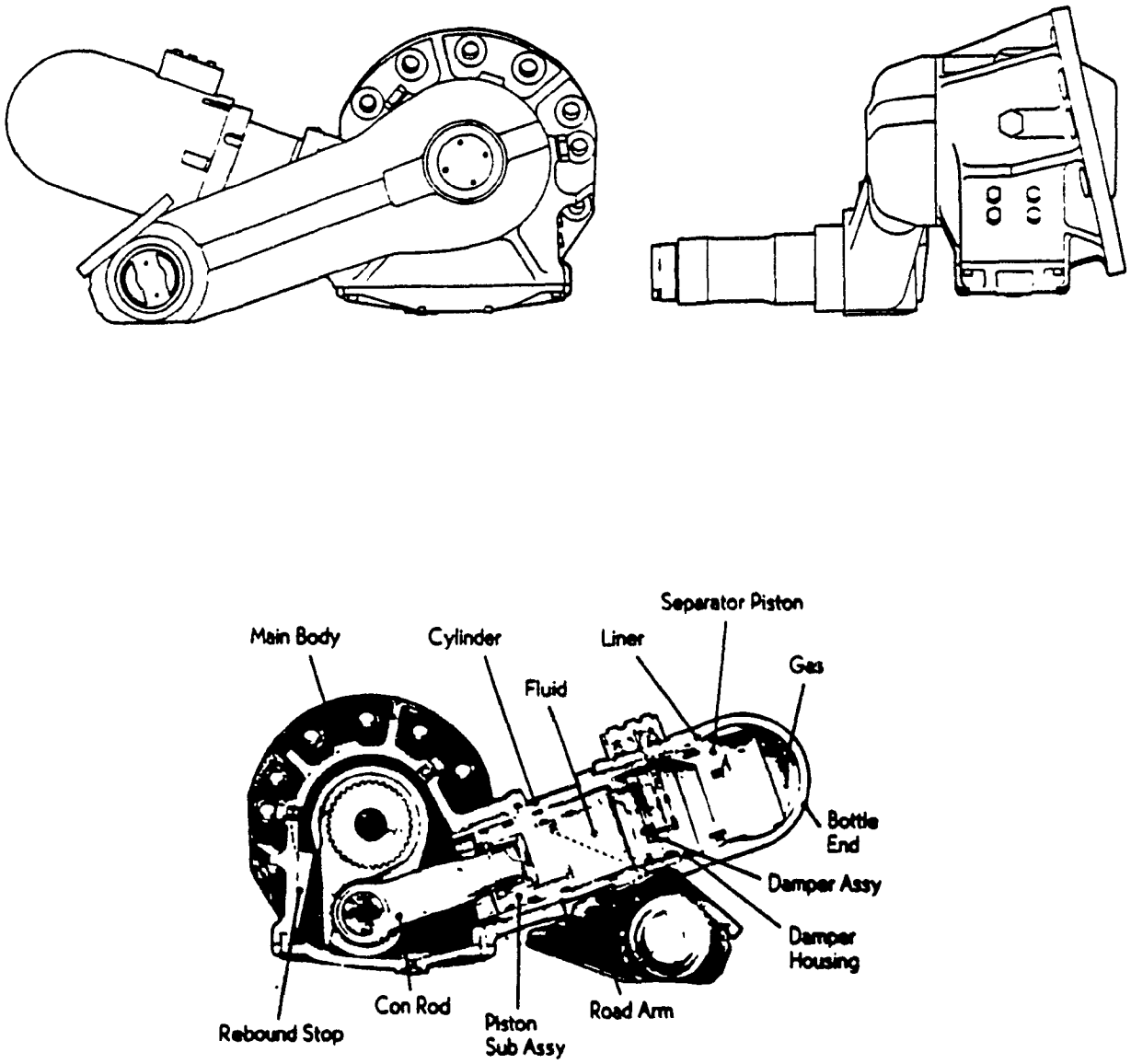

Figure 2.3 Schematic of Dunlop Industries hydropneumatic suspension system [22].

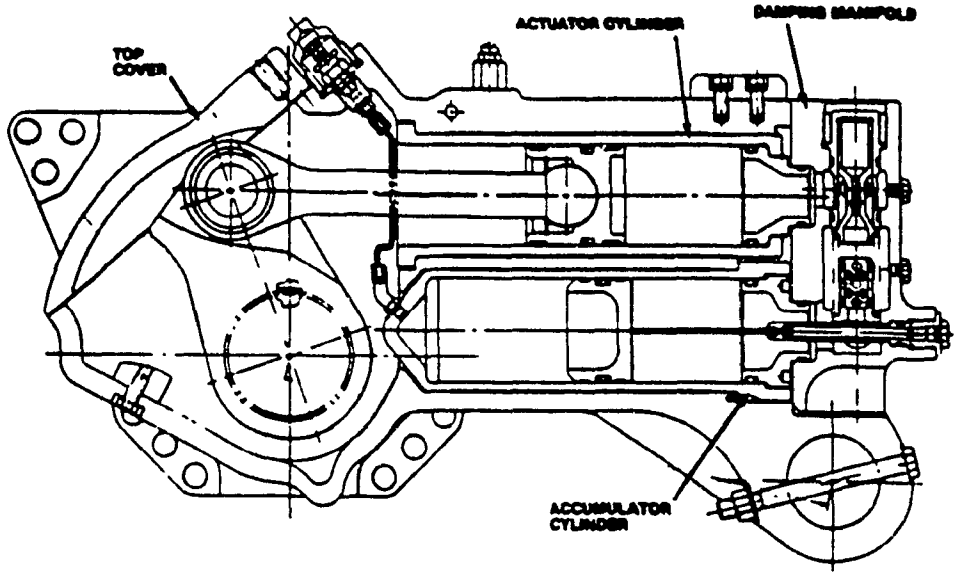

Figure 2.4 Schematic of Teledyne Continental Motors hydropneumatic suspension system [23].

and compact high pressure gas spring generates high restoring forces and provides a low static natural frequency. Low suspension weight helps reduce the unsprung mass of the vehicle, and the compact size allows the designer increased freedom for suspension packaging and design. Due to the nonlinear progressively stiffening spring rate provided by the gas, it is possible to design the vehicle suspension with a fairly constant natural frequency over a wide range of vehicle loading conditions.

Hydropneumatic suspension also offers the potential to achieve standing height control and self-leveling. A simple control system, comprising of control valve, ride height sensor and gas reservoir, can be used in conjunction with hydropneumatic suspension to provide constant and controllable ride height. Hydropneumatic suspension can thus be used in vehicles operating in the partially laden state, where the cargo load is unevenly distributed.

Force-displacement and force-velocity characteristics of suspension systems, in general, are adversely affected by an increase in operating temperature. In the absence of an effective heat dissipation mechanism, the suspension performance deteriorates as the operating temperature rises. The heat dissipation properties of conventional shock absorbers, often designed with a double wall, are quite poor when compared to those of the hydropneumatic suspension with single wall construction. The hydropneumatic suspension is, therefore, less prone to heat fade effects. Further, the lack of a separator between the air and oil mediums in double wall shock absorbers, yields poor shock and vibration attenuation due to entrained air. Since the hydropneumatic suspension employs a piston or flexible diaphragm to separate the hydraulic fluid and compressed gas, the possibilities of air-oil mixture are essentially

eliminated.

The major limitation of the hydropneumatic suspension system is that a perfect seal is required for the entire unit. Both the main and floating pistons must be adequately sealed to prevent leakage of oil and gas. These seals lead to high friction forces acting on the pistons, and the reliability of the suspension depends heavily upon the durability of these seals. Poor seals can deteriorate the suspension performance considerably, and may lead to premature suspension failure.

2.3 DEVELOPMENT OF AN ANALYTICAL MODEL

An analytical model of the hydropneumatic suspension is developed to determine its force-displacement and force-velocity characteristics, as well as shock and vibration isolation characteristics. A schematic representation of the hydropneumatic suspension is illustrated in Figure 2.5(a), and the model representation of a base excited single degree-of-freedom system employing hydropneumatic suspension is presented in Figure 2.5(b). The hydropneumatic suspension consists of two hydraulic chambers, separated by a fixed orifice damper plate, and a gas chamber. A 'floating' piston, separates the lower hydraulic chamber from the gas chamber. The main piston and strut acts on the upper hydraulic chamber, and the seals on the two pistons prevent leakage of oil and gas from their respective chambers.

An analysis of the shock and vibration isolation characteristics of hydropneumatic suspension requires systematic consideration of static equilibrium as well as dynamic forces caused by compression/extension of the gas and the flow of hydraulic fluid through the orifices.

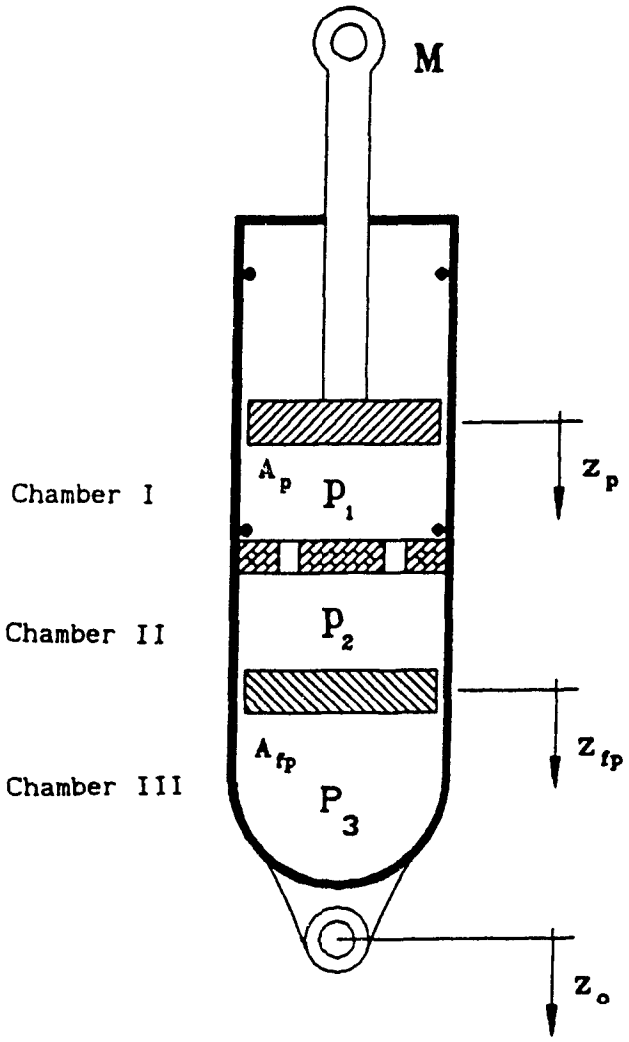

Figure 2.5(a) Spring, mass, damper representation of the single degree-of freedom hydropneumatic suspension system.

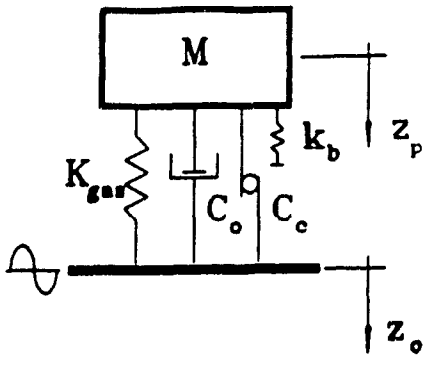

Figure 2.5(b) Schematic of base excited single degree-of-freedom hydropneumatic suspension system model.

2.3.1 Static Analysis

The static equilibrium fluid pressure within the hydropneumatic suspension is related to the static load and initial charge pressure. Under static conditions, the isolator mass is supported by the gas spring, and the internal pressures of each hydraulic chamber must be equal to the pressure within the gas chamber. Assuming that the mass of the floating piston is negligible compared to the isolator mass, the static internal pressure of hydraulic chamber I can be related to the isolator mass and piston cross-sectional area:

$$P_{1\phi} = \frac{M \cdot g}{A_p} \tag{2.1}$$

where M is isolator mass, g is acceleration due to gravity, A_p is cross-sectional area of the main piston, and $P_{1\phi}$ is pressure of the fluid in chamber I corresponding to static equilibrium conditions. Since there is no fluid flow through the damper plate under static equilibrium, the static pressure of the fluid in chamber II, $P_{2\phi}$, must be equal to that of the fluid in chamber I:

$$P_{2\phi} = P_{1\phi} \tag{2.2}$$

The absolute pressure of the gas in chamber III, corresponding to static equilibrium, may be determined by balancing the forces acting on the floating piston. Assuming negligible mass due to the floating piston, the static force balance is expressed as:

$$P_{2\phi} \cdot A_{fp} = (P_{3\phi} - P_{at}) \cdot A_{fp} \tag{2.3}$$

where $P_{3\phi}$ is absolute gas pressure corresponding to static equilibrium, P_{at} is atmospheric pressure, and A_{fp} is cross-sectional area of the floating piston. Equation (2.3) yields the following relationship between hydraulic and gas pressures:

$$P_{2\phi} = P_{3\phi} - P_{at} \tag{2.4}$$

From equations (2.1) and (2.4), the absolute gas pressure can be related to the isolator mass:

$$P_{3\phi} = \frac{M \cdot g}{A_p} + P_{at} \tag{2.5}$$

Equation (2.5) defines the absolute static internal pressure of the hydropneumatic suspension. The nitrogen gas charge is assumed to follow a polytropic compression/expansion process. The static internal pressure can thus be related to the initial preset charge pressure:

$$P_{3\phi} = P_{gi} \left(\frac{V_{gi}}{V_{3\phi}} \right)^{\gamma} \tag{2.6}$$

where P_{gi} is initial absolute charge pressure, V_{gi} is initial gas volume, $V_{3\phi}$ is gas volume corresponding to static equilibrium, and γ is the polytropic exponent. For known values of preset pressure and volume, (P_{gi} and V_{gi}), equation (2.6) may be rearranged to yield the static gas volume:

$$V_{3\phi} = V_{gi} \cdot \left(\frac{P_{gi}}{P_{3\phi}} \right)^{1/\gamma} \tag{2.7}$$

From equation (2.5) and (2.7), the static gas volume can be related to isolator mass and piston geometry:

$$V_{3\phi} = V_{gi} \cdot \left[\frac{P_{gi}}{\frac{M\,g}{A_p} + P_{at}} \right]^{1/\gamma} \tag{2.8}$$

The corresponding static deflection of the floating piston can be

determined from the change in gas volume:

$$z_{s2} = \frac{V_{g1} - V_{3\phi}}{A_{fp}} \tag{2.9}$$

where z_{s2} is the static deflection of the floating piston. Assuming incompressible hydraulic fluid, the static deflection of the primary piston can be related to the static deflection of the floating piston through the following constraint equation:

$$z_{s1} = \frac{A_{fp}}{A_p} \cdot z_{s2} \tag{2.10}$$

where z_{s1} is the static deflection of the primary piston and the isolator mass. Identical piston areas, ($A_{fp} = A_p$), yield identical static deflections of the two pistons.

The compression/expansion of the nitrogen gas follows a polytropic process leading to a nonlinear, progressively stiffening spring characteristic. Typical force-deflection characteristic of a gas spring, shown in Figure 2.6, reveals that under compression the spring force increases rapidly as the bump stop is approached.

The spring rate due to a gas spring is dependent upon the absolute pressure, volume, effective actuator area, and the polytropic exponent [24]. The spring rate, K_{gas}, is determined in the following manner:

$$K_{gas} = \frac{d}{dz} F_s = \frac{d}{dz} \left(P_g \cdot A_e \right) \tag{2.11}$$

where F_s is the spring force, A_e is the effective piston area, z is relative displacement across the gas spring, and P_g is gauge pressure. The gas pressure, P_g, is a function of relative displacement z, and, in

the case of elastic chambers, the effective piston area is also dependent upon z. The spring rate, K_{gas}, is thus expressed as:

$$K_{gas} = A_e \frac{\partial}{\partial z} P_g + P_g \frac{\partial}{\partial z} A_e \qquad (2.12)$$

The first term on the right refers to the rate of change of gas pressure with change in relative displacement, and the second term on the right refers to the rate of change of the effective piston area with change in relative displacement. For constant area floating piston employed in the proposed hydropneumatic suspension model, the second term on the right vanishes. Assuming polytropic relationship of the gas, the gauge pressure is given by:

$$P_g = \frac{C}{V_g^{\gamma}} - P_{at} \qquad (2.13)$$

where, $V_g = V_o - A_e z$, V_o is the initial gas volume, and $C = P_o V_o^{\gamma}$ is the constant. Upon substituting for P_g in equation (2.12), and applying the first-order Taylor's series approximation, a constant spring rate can be obtained as:

$$K_{gas} = \frac{\gamma \cdot P_o \cdot A_e^2}{V_o} \qquad (2.14)$$

For nitrogen gas, the value of γ has been found to be between 1.0 and 1.4, depending upon the assumed nature of compression/expansion process. For a slow compression/expansion process, where the change in temperature is insignificant, the value of the polytropic constant is taken as 1.0 (isothermal process). The polytropic constant assumes a value of 1.4 when the compression/expansion process occurs quickly enough so that no heat is lost (adiabatic process). For any value of the polytropic exponent which lies between these two limits, the process is

called 'polytropic':

$$\gamma = \begin{cases} 1.0 & ; \text{isothermal} \\ 1.0 < \gamma < 1.4 & ; \text{polytropic} \\ 1.4 & ; \text{adiabatic} \end{cases}$$

A comparison of the force-deflection characteristics associated with adiabatic and isothermal compression/expansion processes is shown in Figure 2.7. In this study, the value of the polytropic exponent γ is assumed to be constant and equal to 1.4 .

2.3.2 Dynamic Analysis - Incompressible Fluid

A schematic of the base excited hydropneumatic shock absorber, comprising of an isolator mass, hydraulic chambers, damper plate, floating piston and gas chamber, has been shown in Figure 2.5(b). An analytical model of the hydropneumatic suspension is developed by identifying the various static and dynamic forces acting upon the suspension components. The mathematical model of the hydropneumatic suspension may be developed as either a single degree-of-freedom, (SDOF), system, assuming negligible mass of the floating piston, or as a 2 DOF system when the floating piston mass is significant. For the SDOF system, the displacement of the isolator mass is taken as the only generalized coordinate, whereas in the 2 DOF model the displacement of both the isolator mass and the floating piston mass are taken as the two generalized coordinates.

Forces Acting on the Primary Piston

The equation of motion for the base excited SDOF isolator can be derived from various forces acting on the primary piston, as shown in Figure 2.8:

$$M \cdot \ddot{z}_p = M \cdot g - P_1 \cdot A_p - F_c - F_s \qquad (2.15)$$

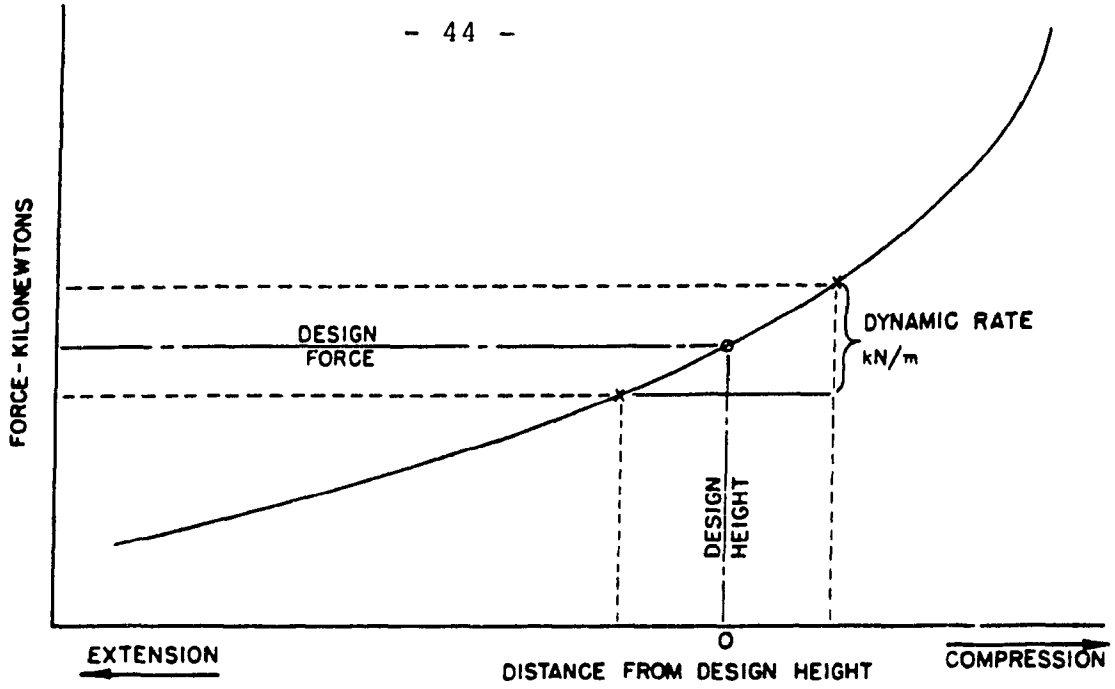

Figure 2.6 Typical force-deflection characteristic of a gas spring [7].

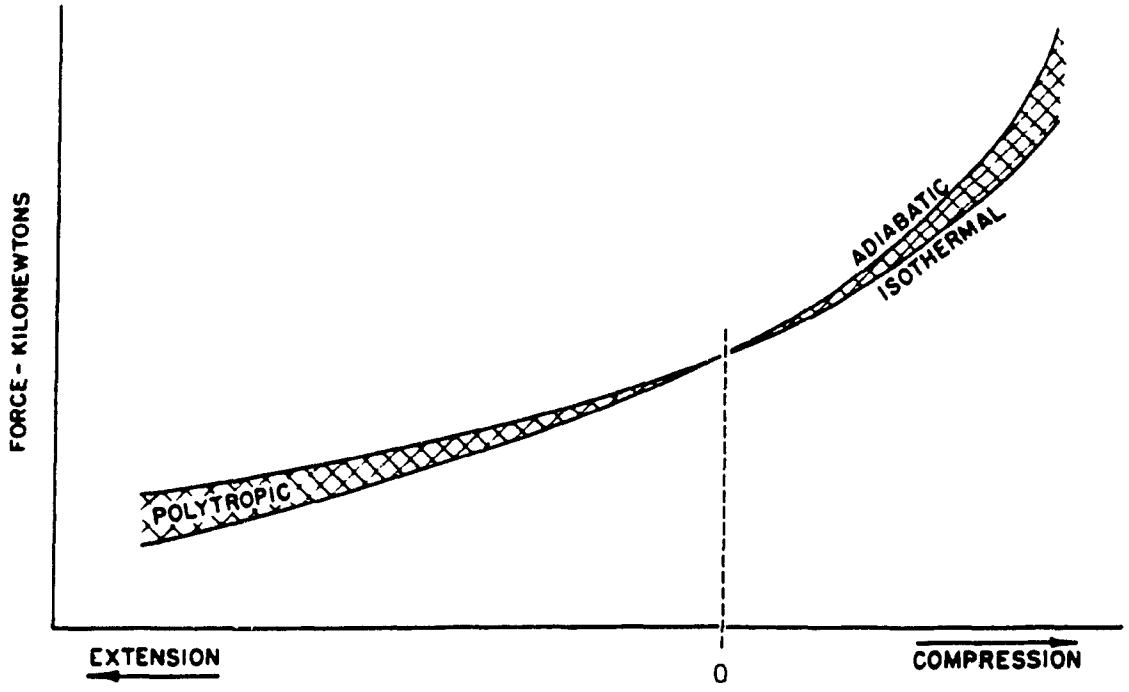

Figure 2.7 Comparison of typical force-deflection characteristics of a gas spring assuming isothermal and adiabatic processes [7].

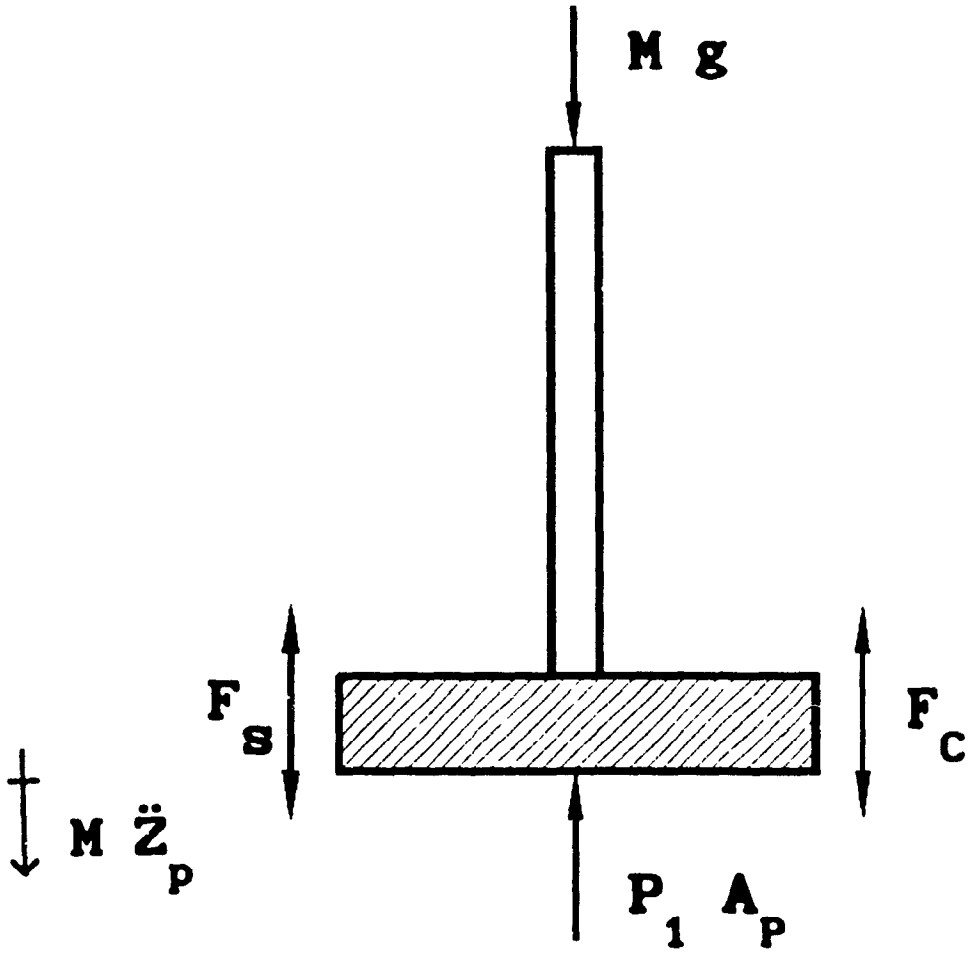

Figure 2.8 Schematic of forces acting on the primary piston.

where $\ddot{z}_p$ is acceleration of the mass, P_1 is instantaneous pressure of fluid in chamber I, F_c is Coulomb friction force due to piston seals, and F_s is bump stop force.

Force due to seal friction is assumed to behave as the ideal Coulomb friction force, as illustrated in Figure 2.9. The friction force is thus expressed as:

$$F_c = F_f \cdot \text{sgn}(\dot{z}_p - \dot{z}_o) \tag{2.16}$$

where F_f is the magnitude of the seal friction, and the sgn function ensures that the friction force is in-phase with the relative velocity, $(\dot{z}_p - \dot{z}_o)$, expressed as:

$$\text{sgn}(\dot{z}_p - \dot{z}_o) = \begin{cases} 1 & \text{for } (\dot{z}_p - \dot{z}_o) \geq 0 \\ -1 & \text{for } (\dot{z}_p - \dot{z}_o) < 0 \end{cases}$$

The ideal friction force characteristics are slightly modified to eliminate the discontinuity around zero relative velocity. A narrow viscous band is introduced around the discontinuity, as shown in Figure 2.10, such that the friction force may be expressed as:

$$F_c = \begin{cases} F_f \cdot \text{sgn}(\dot{z}_p - \dot{z}_o) & ; \ |\dot{z}_p - \dot{z}_o| \geq \delta v_p \\ \dfrac{F_f}{\delta v_p} \cdot (\dot{z}_p - \dot{z}_o) & ; \ |\dot{z}_p - \dot{z}_o| < \delta v_p \end{cases} \tag{2.17}$$

where δv_p defines the narrow viscous band in the vicinity of discontinuity.

Suspension systems, in general, are equipped with travel limiting bump stops. A bump stop force is thus generated when the piston encounters the hard rubber stops at the limits of its compression and

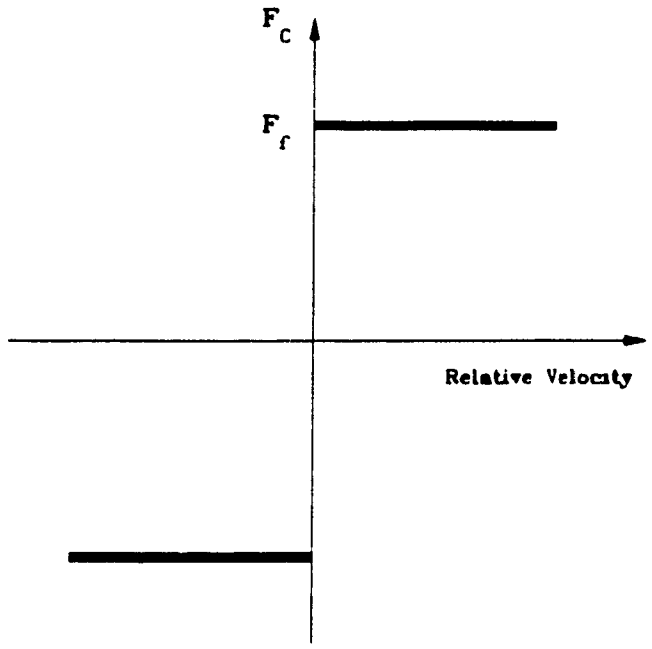

Figure 2.9 Force-velocity characteristic of ideal Coulomb friction.

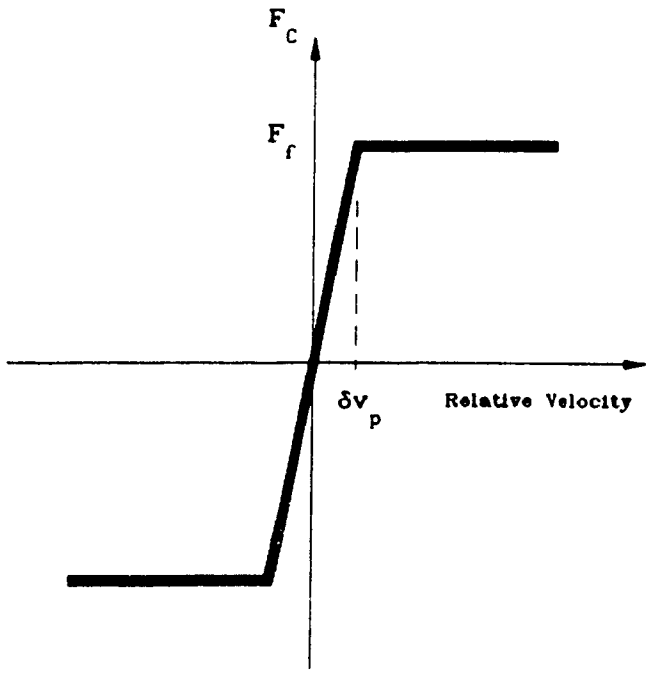

Figure 2.10 Force-velocity characteristic of Coulomb friction with a narrow viscous band at low relative velocity.

extension travel. Consequently, this force is present only when the piston travel exceeds the permissible travel. Figure 2.11 presents typical force-displacement characteristics of symmetric compression and expansion bump stops. The 'dead-band' region represents the amount of relative piston travel allowed before the bump stops are encountered. The nonlinear bump stop force can be expressed as:

$$F_s = K_s \cdot s \cdot [(z_p - z_o) - d \cdot \mathrm{sgn}(z_p - z_o)] \qquad (2.18)$$

where K_s is linear spring rate of the bump stops, and d is the permissible suspension travel during compression or expansion stroke, given by:

$$d = \begin{cases} d_1 \; ; & (z_p - z_o) \geq 0 \\ d_2 \; ; & (z_p - z_o) < 0 \end{cases}$$

and:

$$s = \begin{cases} 0 \; ; & | z_p - z_o | \leq d \\ 1 \; ; & | z_p - z_o | > d \end{cases}$$

Equation (2.15) describes the motion of the isolator mass due to base excitation. However, solution of the equation requires a knowledge of the dynamic pressure P_1 which is determined from the fluid flow equations.

Dynamic Forces Due to Hydraulic Flows

During compression and expansion modes, the hydraulic fluid flows through orifices within the damper plate. Assuming that the hydraulic fluid is incompressible, (infinitely high bulk modulus, β), and there is no leakage, the fluid flow rate into/out of chamber I is given by:

$$|Q_1| = A_p \cdot |\dot{z}_p - \dot{z}_o| \tag{2.19}$$

where $|Q_1|$ is the absolute volume flow rate through the orifices. Assuming turbulent flow through the damper plate orifices, the flow rate through the orifices can be related to pressure differential across the damper plate:

$$|Q_1| = \sum_1^n C_d \cdot A_o \cdot \left[\frac{2 | P_1 - P_2 |}{\rho} \right]^{1/2} \tag{2.20}$$

where C_d is turbulent discharge coefficient, A_o is cross-sectional area of the orifices, ρ is mass density of the oil, P_1 and P_2 are fluid gauge pressures in chambers I and II, respectively, and n is the total number of orifices in the damper plate. Assuming identical flow rates through each orifice, equation (2.20) can be simplified to:

$$Q_1 = n \cdot C_d \cdot A_o \cdot \left[\frac{2 | P_1 - P_2 |}{\rho} \right]^{1/2} \cdot \text{sgn}(dP) \tag{2.21}$$

where, $dP = P_1 - P_2$. Fluid pressure, P_1, acting on the primary piston, can thus be expressed in terms of Q_1 and P_2:

$$P_1 = \frac{\rho}{2} \cdot \left(\frac{1}{n \cdot C_d \cdot A_o} \right)^2 \cdot Q_1^2 \, \text{sgn}(dP) + P_2 \tag{2.22}$$

Substituting for Q_1 from equation (2.19), and noting that $\text{sgn}(dP) = \text{sgn}(\dot{z}_p - \dot{z}_o)$, equation (2.22) yields:

$$P_1 = \frac{\rho}{2} \cdot \left(\frac{A_p \cdot (\dot{z}_p - \dot{z}_o)}{n \cdot C_d \cdot A_o} \right)^2 \text{sgn}(\dot{z}_p - \dot{z}_o) + P_2 \tag{2.23}$$

Equation (2.23) describes the fluid pressure P_1 on the primary piston in terms of relative velocity and fluid pressure in chamber II. The fluid flow rate into/out of chamber II is related to relative velocity of the floating piston:

$$Q_2 = - A_{fp} \cdot (\dot{z}_{fp} - \dot{z}_o) \qquad (2.24)$$

where A_{fp} is cross-sectional area of the floating piston, and $\dot{z}_{fp}$ is velocity of the floating piston. Assuming no leakage and incompressible fluid, the fluid flow rate into/out of chamber I must be equal to that of chamber II:

$$A_p \cdot | \dot{z}_p - \dot{z}_o | = A_{fp} \cdot | \dot{z}_{fp} - \dot{z}_o |$$

Re-arranging the above, a constraint equation relating the velocity of the floating piston to the velocity of the main piston is obtained:

$$\dot{z}_{fp} = \frac{A_p}{A_{fp}} \cdot (\dot{z}_p - \dot{z}_o) + \dot{z}_o \qquad (2.25)$$

Similarly, the displacement of the floating piston may be expressed by the constraint equation:

$$z_{fp} = \frac{A_p}{A_{fp}} \cdot (z_p - z_o) + z_o$$

Equation of Motion of the Floating Piston

The equation of motion of the floating piston is derived upon identifying the various forces acting on the floating piston, as shown in Figure 2.12.

$$M_{fp} \cdot \ddot{z}_{fp} = M_{fp} \cdot g + P_2 \cdot A_{fp} - (P_3 - P_{at}) \cdot A_{fp} - F_{cf} \qquad (2.26)$$

where M_{fp} is mass of the floating piston, $\ddot{z}_{fp}$ is acceleration of the floating piston, P_3 is absolute pressure of the nitrogen gas charge, P_{at}

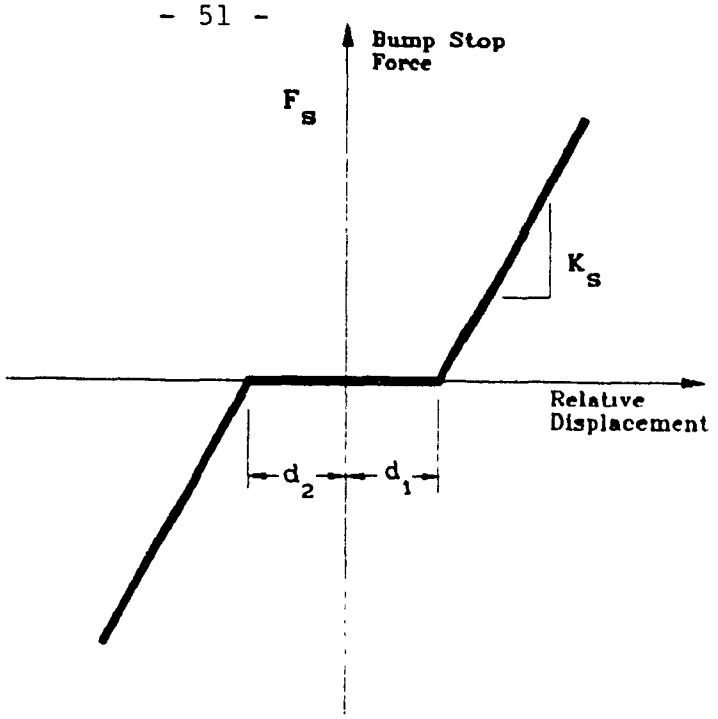

Figure 2.11 Typical force-deflection characteristic for nonlinear symmetric travel limiting, (bump), stops.

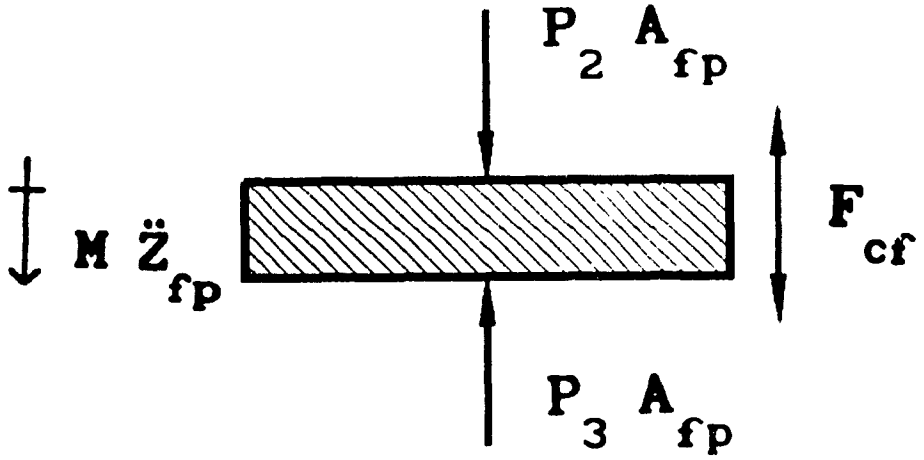

Figure 2.12 Schematic of forces acting upon the floating piston.

is atmospheric pressure, and F_{cf} is seal friction force acting on the floating piston. The acceleration of the floating piston, $\ddot{z}_{fp}$, can be derived from the constraint equation (2.25):

$$\ddot{z}_{fp} = \frac{A_p}{A_{fp}} \cdot (\ddot{z}_p - \ddot{z}_o) + \ddot{z}_o \qquad (2.27)$$

Substituting for $\ddot{z}_{fp}$ in equation (2.26) yields:

$$M_{fp} \cdot \frac{A_p}{A_{fp}} \cdot \ddot{z}_p + M_{fp} \cdot \left(1 - \frac{A_p}{A_{fp}} \right) \cdot \ddot{z}_o = M_{fp} \cdot g + P_2 \cdot A_{fp}$$

$$- (P_3 - P_{at}) \cdot A_{fp} - F_{cf} \qquad \ldots(2.28)$$

The above equation may be re-arranged to yield an expression for P_2, given by:

$$P_2 = \frac{1}{A_{fp}} \cdot \left\{ M_{fp} \cdot \frac{A_p}{A_{fp}} \cdot \ddot{z}_p + M_{fp} \cdot \left(1 - \frac{A_p}{A_{fp}} \right) \cdot \ddot{z}_o \right.$$

$$\left. + (P_3 - P_{at}) \cdot A_{fp} + F_{cf} - M_{fp} \cdot g \right\} \qquad \ldots(2.29)$$

Gas Spring

The nitrogen gas spring is assumed to follow a polytropic compression/expansion behaviour. The instantaneous pressure and volume of the gas are thus related to the static pressure and volume:

$$P_3 \cdot V_3^{\gamma} = P_{3\phi} \cdot V_{3\phi}^{\gamma} = C \qquad (2.30)$$

where P_3 and V_3 are instantaneous absolute gas pressure and instantaneous gas volume, respectively. The instantaneous gas volume, V_3, can be related to relative displacement of the floating piston:

$$V_3 = V_{3\phi} - A_{fp} \cdot (z_{fp} - z_o) \qquad (2.31)$$

The instantaneous gas pressure, P_3, can thus be expressed as:

$$P_3 = \frac{C}{[\, V_{3\phi} - A_{fp} \cdot (z_{fp} - z_o) \,]^{\gamma}} \qquad (2.32)$$

Using the constraint equation (2.25), the absolute gas pressure can be expressed in terms of the generalized coordinate z_p, the displacement of the main piston:

$$P_3 = \frac{C}{[\, V_{3\phi} - A_p \cdot (z_p - z_o) \,]^{\gamma}} \qquad (2.33)$$

Upon substituting for P_3 in equation (2.29), the fluid pressure P_2, is expressed as:

$$P_2 = M_{fp} \cdot \frac{A_p}{A_{fp}^2} \cdot \ddot{z}_p + \frac{M_{fp}}{A_{fp}} \cdot \left(1 - \frac{A_p}{A_{fp}} \right) \cdot \ddot{z}_o + \left(\frac{C}{[\, V_{g\phi} - A_p \cdot (z_p - z_o) \,]^{\gamma}} - P_{at} \right) + \frac{F_{cf}}{A_{fp}} - \frac{M_{fp} \cdot g}{A_{fp}} \qquad \ldots (2.34)$$

Upon substituting for P_2, from equation (2.34), into equation (2.23), the fluid pressure P_1 acting on the primary piston can be expressed as:

$$P_1 = \frac{\rho}{2} \cdot \left(\frac{A_p \cdot (\dot{z}_p - \dot{z}_o)}{n \cdot C_d \cdot A_o} \right)^2 \mathrm{sgn}(\dot{z}_p - \dot{z}_o) + M_{fp} \cdot \frac{A_p}{A_{fp}^2} \cdot \ddot{z}_p$$

$$+ \frac{M_{fp}}{A_{fp}} \cdot \left(1 - \frac{A_p}{A_{fp}} \right) \cdot \ddot{z}_o + \left(\frac{C}{[\, V_{3\phi} - A_p \cdot (z_p - z_o) \,]^{\gamma}} - P_{at} \right)$$

$$+ \frac{F_{cf}}{A_{fp}} - \frac{M_{fp}}{A_{fp}} \cdot g \qquad \ldots (2.35)$$

The equation of motion of the isolator mass, derived from equations (2.15) and (2.35), can thus be expressed

$$M \cdot \ddot{z}_p = M \cdot g - A_p \cdot \left\{ \operatorname{sgn}(\dot{z}_p - \dot{z}_o) \cdot \frac{\rho}{2} \cdot \left(\frac{A_p (\dot{z}_p - \dot{z}_o)}{n \cdot C_d \cdot A_o} \right)^2 \right.$$

$$+ M_{fp} \cdot \frac{A_p}{A_{fp}^2} \cdot \ddot{z}_p + \frac{M_{fp}}{A_{fp}} \cdot \left(1 - \frac{A_p}{A_{fp}} \right) \cdot \ddot{z}_o$$

$$+ \left(\frac{C}{[\, V_{3\phi} - A_p \cdot (z_p - z_o) \,]^{\gamma}} - P_{at} \right) + \frac{F_{cf}}{A_{fp}}$$

$$\left. - \frac{M_{fp}}{Afp} \cdot g \right\} - F_c - F_s \qquad \ldots (2.36)$$

Dividing by the isolator mass, M, and simplifying, the equation of motion can be expressed as:

$$\left(1 - \frac{A_p^2}{A_{fp}^2} \cdot \frac{M_{fp}}{M} \right) \cdot \ddot{z}_p = - \operatorname{sgn}(\dot{z}_p - \dot{z}_o) \cdot \frac{\rho \cdot A_p}{2 \cdot M} \cdot$$

$$\left(\frac{A_p \cdot (\dot{z}_p - \dot{z}_o)}{n \cdot C_d \cdot A_o} \right)^2 - \frac{M_{fp}}{M} \cdot \frac{A_p}{A_{fp}} \cdot \left(1 - \frac{A_p}{A_{fp}} \right) \cdot \ddot{z}_o$$

$$- \frac{A_p}{M} \cdot \left(\frac{C}{[V_{go} - A_p \cdot (z_p - z_o)]^{\gamma}} - P_{at} \right) - \frac{A_p}{A_{fp}} \cdot \frac{F_{cf}}{M} +$$

$$\left(1 + \frac{A_p}{A_{fp}} \cdot \frac{M_{fp}}{M} \right) \cdot g - \frac{F_c}{M} - \frac{F_s}{M} \qquad \ldots(2.37)$$

The equation of motion of the hydropneumatic suspension and isolator mass may be further expressed in terms of normalized parameters:

$$(1 + \mu \cdot \alpha^2) \cdot \ddot{z}_p = - \operatorname{sgn}(\dot{z}_p - \dot{z}_o) \cdot \frac{\rho \cdot A_p}{2 \cdot M} \cdot$$

$$\left(\frac{\alpha_o (\dot{z}_p - \dot{z}_o)}{n \cdot C_d} \right)^2 - \mu \cdot \alpha \cdot (1 - \alpha) \cdot \ddot{z}_o$$

$$- \frac{A_p}{M} \cdot \left(\frac{C}{[V_{g\phi} - A_p \cdot (z_p - z_o)]^{\gamma}} - P_{at} \right)$$

$$+ (1 + \alpha \cdot \mu) \cdot g - (\alpha \cdot f_{cf} + f_c) - f_s \qquad \ldots(2.38)$$

where:

$$\mu = \text{mass ratio} = \frac{M_{fp}}{M}$$

$$\alpha = \text{piston area ratio} = \frac{A_p}{A_{fp}}$$

$$\alpha_o = \text{ratio of primary piston area to orifice area} = \frac{A_p}{A_o}$$

$$f_c = \text{Coulomb friction force coefficient } (m/s^2) = \frac{F_c}{M}$$

$$f_{cf} = \text{Coulomb friction force coefficient } (m/s^2) = \frac{F_{fc}}{M}$$

$$f_s = \text{Bump stop force coefficient } (m/s^2) = \frac{F_s}{M}$$

The dynamics of a single degree-of-freedom vibration isolator employing hydropneumatic suspension are described by the second order nonlinear differential equation while assuming incompressible hydraulic fluid and negligible leakage. The isolator mass and floating piston mass are effectively combined using the constraint equation (2.25). The coefficient of $\ddot{z}_p$ in equation (2.38) represents the normalized effective mass of the isolator, μ_{eff},

$$\mu_{eff} = 1 - \mu \alpha^2$$

The first term on the right hand side of equation (2.38) represents the normalized nonlinear damping force, (f_d), due to orifice flows, while the second term represents the normalized inertial force, (f_i), of the floating piston due to base excitation. The third term on the right hand side of the equation describes the normalized gas spring force, (f_k), while the last three terms represent the normalized gravitational (f_g),

friction and bump stop forces, respectively. The differential equation of motion can thus be expressed as:

$$\mu_{eff} \cdot \ddot{z}_p + f_d + f_k + (\alpha \cdot f_{cf} + f_c) + f_s = f_g - \ell_i \quad \ldots(2.39)$$

where:

$$f_d = \text{sgn}(\dot{z}_p - \dot{z}_o) \frac{\rho A_p}{2 M} \cdot \left(\frac{\alpha_o (\dot{z}_p - \dot{z}_o)}{n \quad C_d} \right)$$

$$f_k = \frac{A_p}{M} \cdot \left(\frac{C}{[V_{3\phi} - A_p (z_p - z_o)]^{\gamma}} - P_{at} \right)$$

$$f_g = \left(1 + \alpha \cdot \mu \right) \cdot g$$

$$\ell_i = \mu \cdot \alpha \cdot \left(1 - \alpha \right) \cdot \ddot{z}_o$$

Major assumptions associated with this analytical model are as follows:

- Hydraulic fluid is incompressible (infinitely high bulk modulus)
- Turbulent and equal oil flow through each orifice of the damper plate, resulting in velocity-squared damping
- The pistons are sealed adequately so that there is no oil flow past the main or floating pistons
- The nitrogen gas follows a polytropic compression expansion process
- Temperature effects are neglected
- The seal friction is assumed to be ideal in nature
- The bump stops are assumed to be linear high rate springs

2.3.3 Dynamic Analysis - Compressible Fluid

The analytical model presented in Section 2.3.2 is developed assuming incompressible fluid flows. Studies conducted on shock and vibration isolation performance of hydraulic dampers and on the effects of entrained air on hydraulic fluid properties, have established that fluid bulk modulus can significantly influence hydraulic system performance [11, 25, 26, 27]. An analytical model of the vibration isolator is thus developed incorporating compliance due to compressible hydraulic fluid. Owing to the compressibility of the fluid, the constraint equation (2.25), relating z_p and z_{fp}, becomes invalid. Consequently, the vibration isolator is modeled as a two DOF dynamical system. Assuming that the area of the floating piston equals the area of the main piston, equations of motion for the isolator mass and floating piston mass are developed by summing the forces acting on the primary and floating pistons, respectively:

$$M \cdot \ddot{z}_p = M \cdot g - P_1 \cdot A_p - F_c - F_s$$

and,

$$M_{fp} \cdot \ddot{z}_{fp} = M_{fp} \cdot g + P_2 \cdot A_p - (P_3 - P_{at}) \cdot A_p - F_{cf} \qquad (2.40)$$

Assuming polytropic compression/expansion process for the gas spring, the instantaneous gas pressure is expressed as:

$$P_3 = \frac{C}{[V_{3\phi} - A_{fp} \cdot (z_{fp} - z_o)]^{\gamma}} \qquad (2.41)$$

Compressibility of a fluid is expressed by its bulk modulus, defined as the amount of pressure increase required to cause a decrease in the

volume occupied by a constant mass of fluid held in a rigid container. The bulk modulus, β, of a fluid is thus given by [28]:

$$\beta = - V_o \cdot \left(\frac{\delta P}{\delta V} \right)_T$$

where V_o is the initial volume occupied by the fluid, δP is infinitesimal change in pressure, δV is infinitesimal change in fluid volume, and the subscript T indicates isothermal conditions. The bulk modulus of a fluid is always positive since the quotient $(\delta P/\delta V)$ is always negative. Typically, the bulk modulus of automotive shock absorber oil may be taken as 1.374E+09 N/m^2 [25, 27].

Flow Equations

Flow rates through the damper plate orifices and due to fluid compressibility, are derived as functions of primary and floating piston velocities and effective bulk modulus. Assuming no leakage and turbulent fluid flows, the flow through the damper plate orifices can be expressed as:

$$Q_{\phi 1} = n \cdot C_d \cdot A_o \cdot \left[\frac{2 \cdot | P_1 - P_2 |}{\rho} \right]^{1/2} \cdot \mathrm{sgn}(dP) \qquad (2.42)$$

where $Q_{\phi 1}$ is flow rate through the damper plate orifices, and dP is pressure differential across the damper plate.

CHAMBER I

The rate of change of fluid volume in chamber I, Q_{v1}, can be related to the piston area and the relative velocity of the piston:

$$Q_{v1} = A_p \cdot (\dot{z}_p - \dot{z}_o) \qquad (2.43)$$

The rate of change of fluid volume, due to compressibility of fluid in chamber I, is related to the rate of change of fluid pressure P_1:

$$Q_{e1} = \frac{V_{11}}{\beta} \cdot \dot{P}_1 \qquad (2.44)$$

where Q_{e1} is the volume flow rate due to compliance of fluid in chamber I, and V_{11} is instantaneous fluid volume in chamber I, given by:

$$V_{11} = V_{1\phi} - A_p \cdot (z_p - z_o)$$

where $V_{1\phi}$ is the initial fluid volume in chamber I. Based on the law of conservation of mass, the flows in chamber I can be related using the fluid continuity, given by:

$$Q_{v1} = Q_{\phi 1} + Q_{e1} \qquad (2.45)$$

The fluid continuity equation yields the following expression for $\dot{P}_1$:

$$\dot{P}_1 = \frac{\beta}{V_{11}} \cdot \left[A_p \cdot (\dot{z}_p - \dot{z}_o) - n \cdot C_d \cdot A_o \cdot \left(\frac{2 \cdot | P_1 - P_2 |}{\rho} \right)^{1/2} \text{sgn}(dP) \right]$$

...(2.46)

CHAMBER II

The fluid flow equations for chamber II are developed in the same manner as those for chamber I. The rate of change of fluid volume in chamber II, (Q_{v2}), is related to the relative velocity of the floating piston:

$$Q_{v2} = A_{fp} \cdot (\dot{z}_{fp} - \dot{z}_o) \qquad (2.47)$$

The rate of change of fluid volume, (Q_{e2}), in chamber II, due to fluid compliance, is expressed as:

$$Q_{e2} = - \frac{V_{21}}{\beta} \cdot \dot{P}_2 \qquad (2.48)$$

where V_{21} is instantaneous fluid volume in chamber II, given by:

$$V_{21} = V_{2\phi} + A_{fp} \cdot (z_{fp} - z_o)$$

From the fluid continuity equation, the rate of change of fluid pressure in chamber II is derived as:

$$\dot{P}_2 = \frac{\beta}{V_{21}} \left[n \cdot C_d \cdot A_o \cdot \left(\frac{2 \mid P_1 - P_2 \mid}{\rho} \right)^{1/2} sgn(dP) - A_{fp} \cdot (\dot{z}_{fp} - \dot{z}_o) \right]$$

...(2.49)

Equations (2.40) form a set of second order nonlinear differential equations that describe the dynamics of a hydropneumatic suspension system, assuming compressible fluid flows. Equations (2.46) and (2.49) represent the first order differential equations that describe the fluid pressures in chambers I and II, respectively. These coupled differential equations can be solved to determine the performance characteristics of the hydropneumatic suspension systems. Parameters employed for the analysis of the hydropneumatic suspension models are presented in Table 2.1.

2.4 SUMMARY

The basic design and principles of operation of hydropneumatic suspension are presented in this chapter. Hydropneumatic suspension combines spring and damper elements into a single suspension unit, where the restoring force is generated by the compressed gas, and the damping force is generated by the hydraulic fluid through constrictions in a damper plate or valve housing. The gas and hydraulic fluids are

TABLE 2.1

PARAMETERS OF HYDROPNEUMATIC SUSPENSION

PARAMETER		VALUE
Isolator Mass, M,	(kg)	500
Floating Piston Mass, m_{fp},	(kg)	1
Damping Parameters:		
Area of Main Piston, A_p,	(m^2)	0.006
Piston Area Ratio, α,		1.0
Density of Hydraulic Fluid, ρ,	(kg/m^3)	797.68
Number of Orifices in Damper Plate, n,		4
Orifice Discharge Coefficient, C_d,		0.8
Area of Damper Plate Orifices, A_o,	(m^2)	3.17E-05
Coulomb Friction Force, F_f,	(N)	50
Viscous Band Relative Velocity, δv_p,	(m/s)	1.0E-03
Gas Spring Parameters:		
Initial Precharge Pressure, $P_{1\phi}$,	(Pa)	900,000
Initial Precharge Volume, $V_{1\phi}$,	(m^3)	1.5E-03
Polytropic Exponent, γ,		1.4
Atmospheric Pressure, P_{at},	(Pa)	101,300
Bump Stop Parameters:		
Elastic Bump Stop Stiffness, K_s,	(N/m)	3.0E+07
Compression/Expansion Relative Travel Before Encountering Bump Stops, d_1, d_2,	(m)	0.001

separated by either a flexible diaphragm or a floating piston. Potential performance benefits and limitations of various hydropneumatic suspension systems are discussed.

The first hydropneumatic suspension model is expressed by a single DOF system employing a constraint equation relating the motion of the isolator mass to that of the floating piston mass, assuming incompressible fluid. The suspension model incorporating restoring force due to gas spring, damping force due to orifice flows, seal friction and bump stop force is characterized by a second order nonlinear differential equation. The second hydropneumatic suspension model is expressed by a two DOF system assuming compressible hydraulic fluid. Consideration of fluid compressibility results in two nonlinear first order differential equations describing the rate of change of fluid pressure in chambers I and II, and two nonlinear second order differential equations describing the motions of isolator and floating piston masses.

CHAPTER 3

METHODOLOGIES FOR SUSPENSION SYSTEM RESPONSE EVALUATION

3.1 GENERAL

The performance characteristics of a vehicle suspension system are evaluated in terms of its abilities to effectively attenuate road/terrain induced shock and vibration, carry loads, and to aid in the guidance and control of the vehicle. The shock and vibration attenuation potentials of a suspension system are evaluated from the response to known dynamic excitations. These evaluations may be performed either in the laboratory or via computer simulation of the suspension dynamics as described by a mathematical model. Generally, it is more practical, versatile and economical to perform the analyses via computer simulation prior to building a prototype unit.

The primary purpose of a suspension system is to isolate the vehicle from terrain irregularities and undulations. A study of shock and vibration isolation characteristics, and thus the ride potentials, of the hydropneumatic suspension models developed in Chapter 2, requires the description of terrain excitations which the suspension will commonly encounter. Terrain excitations are typically random in nature, although some terrain irregularities may be described as deterministic excitations. The random terrain excitations are usually expressed in terms of their displacement and acceleration spectral densities, while the deterministic terrain excitations are expressed in terms of a time dependent displacement, velocity or acceleration functions.

In this chapter, analytical techniques used to simulate the shock

and vibration attenuation characteristics of the hydropneumatic suspension system models are presented.

3.2 ANALYTICAL TECHNIQUES

Shock and vibration isolation performance characteristics of the hydropneumatic suspension models can be evaluated using either time domain or frequency domain analyses techniques. In the time domain technique, the response variables are treated as functions of time and a numerical integration technique is employed to solve the differential equations of motion. The frequency domain technique involves transformation of the time dependent variables into frequency dependent variables via Fourier transform. The time domain technique may be used to analyze linear as well as nonlinear dynamical systems, whereas the frequency domain technique requires a linear or linear equivalent dynamical system.

Frequency domain analysis involves the transformation of time dependent variables into frequency dependent variables by means of Fourier transformations. The analysis technique can be best described through a linear system, expressed as:

$$[M]\{\ddot{x}\} + [C]\{\dot{x}\} + [K]\{x\} = [K_f]\{x_o\} + [C_f]\{\dot{x}_o\} \qquad (3.1)$$

where [M], [C] and [K] are mass, damping and stiffness matrices,respectively. $[K_f]$ and $[C_f]$ are forced stiffness and damping matrices, and $\{x\}$ and $\{x_o\}$ are vectors containing generalized response and excitation variables, respectively. The system of linear second order differential equations (3.1) is Fourier transformed to yield:

$$\left\{ X(j\omega) \right\} = \left[H(j\omega) \right] \left\{ X_o(j\omega) \right\} \qquad (3.2)$$

where $\{X(j\omega)\}$ and $\{X_o(j\omega)\}$ are Fourier transforms of $\{x\}$ and $\{x_o\}$

respectively. $[H(j\omega)]$ is the complex matrix representing the frequency response function of the dynamical system, given by:

$$[H(j\omega)] = \left[[K] - \omega^2[M] + j\omega[C] \right]^{-1} \left[[K_f] + j\omega[C_f] \right] \quad (3.3)$$

Since the hydropneumatic suspension system is inherently nonlinear in nature due to gas spring, orifice damping, Coulomb friction and bump stops, the frequency domain analysis techniques cannot be directly employed. The nonlinear hydropneumatic suspension model thus needs to be expressed by a linear equivalent model in order to carry out the frequency response analysis. Since the frequency domain analysis deals with the solution of algebraic equations, it offers the advantages of ease of analysis as well as reduced computational time. These techniques are thus extremely well suited for optimization and ride quality studies.

Alternatively, time domain analyses techniques employ either numerical differentiation or integration algorithms to solve the differential equations of motion. The time invariant system parameters are presented as the coefficients of time dependent variables within the set of differential equations. A set of n second order differential equations is reduced to $2n$ first order differential equations using the following substitution:

$$\dot{x}_i = x_{i+n} \quad ; \quad i = 1, 2, \ldots, n$$
$$\ddot{x}_i = \dot{x}_{i+n} \quad ; \quad i = 1, 2, \ldots, n \quad (3.4)$$

The resulting first order differential equations are then solved via a series of numerical integrations to yield time dependent response characteristics of the system. Although many algorithms have been developed to perform numerical integrations, the Runge-Kutta fourth

order algorithm [29] was employed to solve the nonlinear differential equations of motion characterizing the dynamics of the hydropneumatic suspension system. The time-domain analysis technique can effectively simulate either linear or nonlinear dynamical systems. The technique is, however, extremely demanding on computing time as compared to the frequency domain analysis technique.

3.3 DETERMINISTIC EXCITATIONS

In this thesis, deterministic base excitations are used to evaluate the shock and vibration isolation characteristics of the hydropneumatic suspension models. The shock isolation performance of the hydropneumatic suspension is evaluated for rounded step, rounded pulse and rounded bump displacement excitations, while the vibration isolation characteristics are evaluated for harmonic excitations.

The response to harmonic excitation allows the determination of vibration attenuation abilities in the frequency range of interest. Since the human body is most sensitive to whole body vibrations in the 1 - 8 Hz frequency range [30], the vibration attenuation performance is evaluated for harmonic excitations within the 0.1 - 10 Hz frequency range.

3.3.1 Rounded Step Excitation

The rounded step displacement excitation is a transient excitation encountered due to a sudden change in roadway elevation, such as a small curb, or crossing from an old to new section of paved road surface. This type of excitation allows the determination of shock isolation abilities, as well as rise time and settling time of the suspension system response.

The rounded step displacement excitation may be described as a fast

rising continuous function which achieves a steady state value after a finite period of time. The speed with which the function achieves this steady state value is controlled by the value of the *shock severity parameter*, ν. A large value of ν corresponds to a fast rise time, and a low value of ν corresponds to a slow rise time, as illustrated in Figure 3.1. As the value of ν approaches infinity, the rounded step function approaches a true square-edged step function. The displacement and corresponding velocity excitation due to the rounded step can be expressed as [31]:

$$z_o(t) = Z_{max} \cdot \left[1 - e^{-\nu\omega_o t} \cdot (1 + \nu\omega_o t) \right] \quad ; \; t \geq 0$$

$$\dot{z}_o(t) = Z_{max} \cdot (\nu\omega_o)^2 \cdot t \cdot e^{-\nu\omega_o t} \quad ; \; t \geq 0 \qquad (3.5)$$

where $e = 2.71828$ and Z_{max} is the step amplitude, ω_o is the natural frequency of the system, and ν is the shock severity parameter defined as:

$$\nu = \frac{\pi}{\omega_o \cdot \tau_1}$$

where τ_1 is the time required for the displacement to reach it's maximum value.

3.3.2 Rounded Pulse Excitation

A rounded pulse shock excitation may be used to describe the transient excitations encountered when traversing a sharp discrete obstacle in the terrain. The displacement due to rounded pulse shock

excitation rises quite rapidly, and then reduces at a somewhat slower rate. The rise and fall rates, and the pulse duration, are dependent upon the value of the shock severity parameter, ν. A large value of severity parameter corresponds to a short rise time and a short pulse duration, whereas a small value of severity parameter corresponds to a slow rise time and a long duration, as illustrated in Figure 3.2. As the value of the shock severity parameter approaches infinity, the rounded pulse function approaches a true vertical pulse profile. The displacement and corresponding velocity excitation due to a rounded pulse can be expressed as [31]:

$$z_o(t) = Z_{max} \cdot \frac{e^2}{4} \cdot (\nu\omega_o t)^2 \cdot e^{-\nu\omega_o t} \quad ; \; t \geq 0$$

and

$$\dot{z}_o(t) = Z_{max} \cdot \frac{(e\,\nu\,\omega_o)^2}{4} \cdot t\, e^{-\nu\omega_o t} \cdot (2 - t) \quad ; \; t \geq 0 \qquad (3.6)$$

where all parameters are defined as before, except for the severity parameter, ν. In the case of a rounded pulse excitation, τ_1 is duration of the pulse, and is equal to the duration of an equivalent rectangular pulse of same area with maximum displacement 17.6% greater than Z_{max}.

3.3.3 Semi-Circular Displacement Bump Excitation

The semi-circular bump is a transient displacement excitation typically used for the ride performance evaluation of tracked (usually military) vehicles. The excitation is simply defined as a 'bump' of constant radius, r_B, as shown in Figure 3.3. Assuming constant forward vehicle speed, V, the displacement excitation of the first road wheel

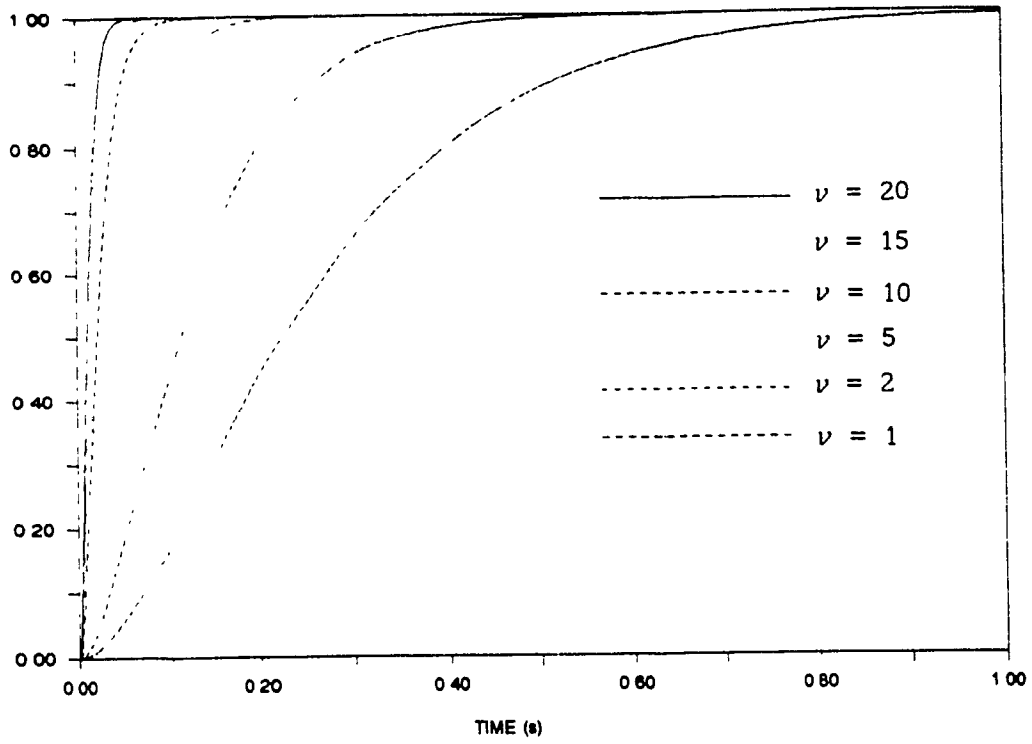

Figure 3.1 Influence of severity parameter, ν, on rounded step displacement excitation.

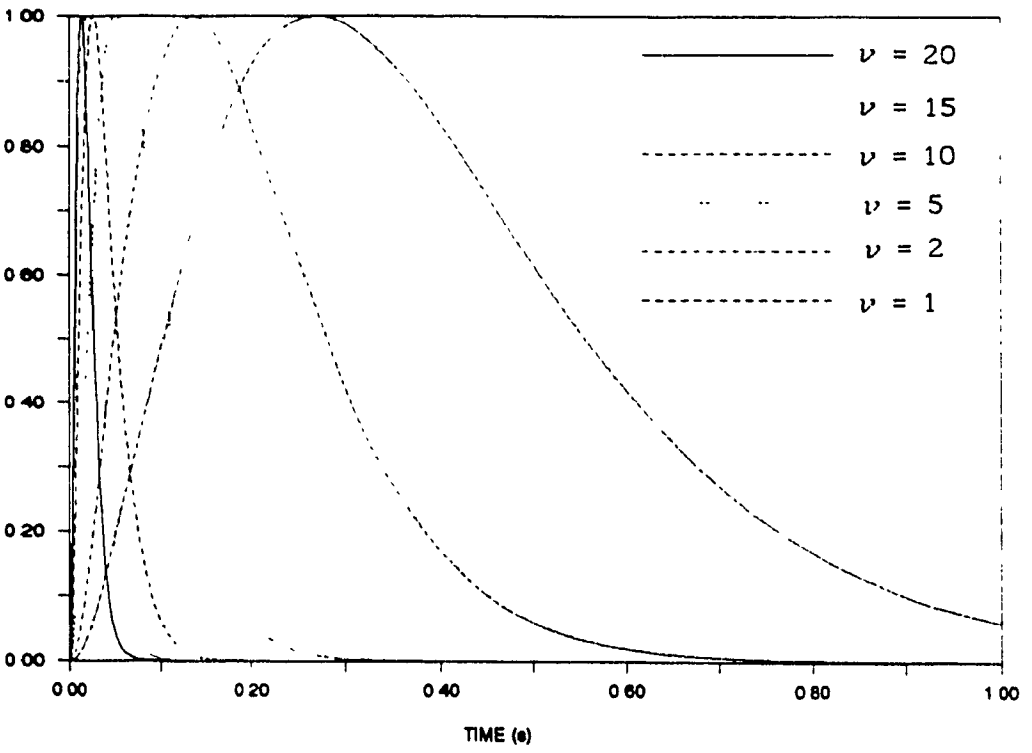

Figure 3.2 Influence of severity parameter, ν, on rounded pulse displacement excitation.

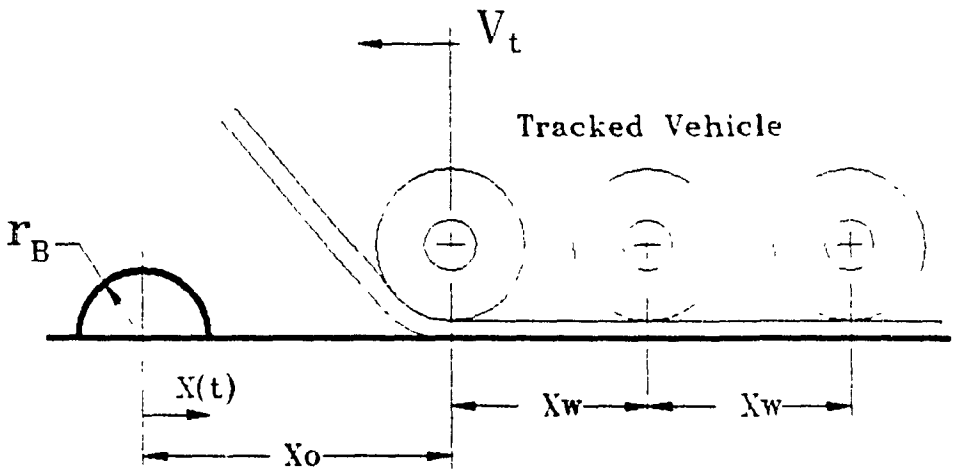

$$X(t) = Xo - V_t \bullet t$$

Figure 3.3 Schematic of semi-circular bump displacement excitation employed for tracked vehicle analysis.

due to a semi-circular bump can be expressed as:

$$z_o(t) = \begin{cases} \left[r_B^2 - (x_o - Vt)^2 \right]^{1/2} ; & x_o - r_B < x(t) < x_o + r_B \\ 0 ; & \text{otherwise} \end{cases} \quad \ldots(3.7)$$

where x(t) is the horizontal position of the wheel-bump contact point with respect to the bump center, and x_o is the initial distance from the bump. This displacement excitation will be used to evaluate the ride performance characteristics of the tracked vehicle model equipped with hydropneumatic and conventional suspension systems.

3.4 LINEARIZATION OF THE HYDROPNEUMATIC SUSPENSION SYSTEM

Since linear systems can be solved using the convenient frequency domain analysis technique, it is desirable to express the nonlinear hydropneumatic suspension model by a linear equivalent dynamic model. Development of an equivalent linear suspension model offers further advantages in view of the following:

- Solution of algebraic equations characterizing the equivalent linear system in the frequency domain is extremely economical.
- Response to stochastic excitations can be conveniently obtained.
- Ride quality analyses can be carried out in the required frequency domain.
- Optimization studies, where a large number of repetitive computations are performed, can be efficiently performed using linear equivalent suspension models.

The hydropneumatic suspension system is inherently nonlinear due to the gas spring, orifice damping, elastic motion limiting stops and

Coulomb friction. The usual engineering approach used to analyze such a nonlinear system is to consider viscous damping and linear spring equivalents to formulate the convenient linear equations of motion. Since linear systems are so much easier and economical to analyze than nonlinear systems, preliminary design and performance evaluations are conveniently achieved via the linear analytical tools. Such a methodology may be considered adequate for systems operating in the linear range, (small disturbance), where the associated effects of nonlinearities are of second order.

In general, hydropneumatic suspension systems do not operate in their linear range, thus cannot be accurately analyzed through such linear formulations. Alternatively, nonlinear analytical tools can be employed to simulate the nonlinear behaviour of the suspension system. A usual approach employed for the analysis of nonlinear systems is to replace the nonlinear dissipative and restoring elements with equivalent linear elements, such that the response characteristics of the equivalent linear system do not significantly deviate from those of the nonlinear system. A number of such linearization techniques have been developed to analyze nonlinear mechanical systems [35, 36]. Equivalent statistical linearization techniques have been extensively used to analyze nonlinear vehicle and suspension models [37, 38]. It has been established that although the linearization theory often yields correct qualitative results, it cannot characterize the often critical effects of Coulomb friction and elastic travel limiting stops. Such linear models are formulated assuming a nearly linear response of the nonlinear system, and are thus correctly applicable in a small restricted frequency band.

Alternatively, local equivalent linearization techniques have been proposed to express the nonlinear damping phenomenon by an array of average local damping constants. These local damping constants are appropriately adjusted for local excitation frequency and amplitude, such that the response characteristics can be accurately predicted over the entire frequency range [39].

In this dissertation, the nonlinear hydropneumatic suspension model is expressed by an equivalent linear model using the local equivalent linearization technique based upon energy balance. The damping mechanisms, such as orifice and Coulomb damping, are expressed by an array of local viscous damping coefficients as a function of response characteristics, excitation frequency, amplitude and type of nonlinearity. The nonlinear force-displacement characteristics of the air spring are expressed by local equivalent spring constants as a function of response characteristics, excitation frequency and amplitude. The equivalent damping constants are evaluated by equating energy dissipated per cycle by the nonlinear damper to that of a viscous damper; the equivalent spring constants are evaluated by equating the energy stored/released in one-quarter cycle by the gas spring to that stored by a linear spring. Methodology to evaluate the local equivalent constants is described in the following sub-sections.

3.4.1 Computation of Local Equivalent Damping Coefficients

The hydropneumatic suspension exhibits nonlinear damping phenomenon due to orifice flows and Coulomb damping. Assuming constant orifice and incompressible flows, the damping force F_d developed due to orifice flows is related to the square of the relative velocity across the suspension:

$$F_d = C_v \cdot \dot{z}^2 \cdot \mathrm{sgn}(\dot{z}) \tag{3.8}$$

where $\dot{z}$ is the relative velocity across the shock absorber, and C_v is the velocity-squared damping coefficient, given by:

$$C_v = A_p \cdot \frac{\rho}{2} \cdot \left(\frac{A_p}{n \cdot C_d \cdot A_o} \right)^2 \tag{3.9}$$

Assuming harmonic response, the energy dissipated by the damper over one cycle, E_d , is given by the integral:

$$E_d = \oint F_d \cdot dz \tag{3.10}$$

Substituting for F_d in the above integral, and establishing limits of integration based on one-quarter of a cycle, equation (3.10) yields:

$$E_d = 4 \int_0^z C_v \dot{z}^2 \, dz \tag{3.11}$$

For harmonic relative displacement and velocity response, and local excitation frequency ω_1, equation (3.11) is solved to yield the energy dissipated by the orifice damper in one cycle:

$$E_d = \frac{8}{3} \cdot C_v \cdot \omega_1^2 \cdot Z^3 \tag{3.12}$$

where Z is the magnitude of relative displacement across the suspension and ω_1 is the local excitation frequency in rad/s. The equivalent local damping coefficient corresponding to excitation frequency ω_1 can then be obtained by equating (3.12) to the energy dissipated per cycle by a viscous damper, $E_{eq} = \pi \, C_{eo}(\omega_1) \, \omega_1 \, Z^2$ [32]:

$$C_{eo}(\omega_1) = \frac{8}{3\pi} \cdot C_v \cdot \omega_1 \cdot Z \tag{3.13}$$

where $C_{eo}(\omega_1)$ is the local equivalent damping coefficient due to an

orifice damper corresponding to excitation frequency ω_1.

The local equivalent viscous damping coefficient due to Coulomb damping is determined in a manner similar to that of the velocity-squared damper. The force generated by ideal Coulomb damping is given by:

$$F_c = F_f \cdot \mathrm{sgn}(\dot{z}) \tag{3.14}$$

Assuming harmonic excitation, the energy dissipated in one cycle by the Coulomb damping is given by [32]:

$$E_c = 4 \cdot F_f \cdot Z \tag{3.15}$$

where E_c is the energy dissipated per cycle by Coulomb damping subject to harmonic excitation. The local equivalent damping coefficient $C_{ec}(\omega_1)$ due to a Coulomb damper is then obtained by equating (3.15) to the energy dissipated by a viscous damper:

$$C_{ec}(\omega_1) \;.= \frac{4 \cdot F_f}{\pi \cdot \omega \cdot Z} \tag{3.16}$$

The total local equivalent damping constant due to nonlinear dissipative mechanisms within the hydropneumatic suspension can then be computed from equations (3.13) and (3.16):

$$C_{eq}(\omega_1) = C_{eo}(\omega_1) + C_{ec}(\omega_1) \tag{3.17}$$

where C_{eq} is the local equivalent damping coefficient of the hydropneumatic suspension corresponding to excitation frequency ω_1, given by:

$$C_{eq}(\omega_1) = \frac{8}{3} \cdot C_v \cdot \omega_1 \cdot Z + \frac{4 \cdot F_f}{\pi \cdot \omega \cdot Z} \tag{3.18}$$

3.4.2 Computation of Local Equivalent Spring Constant

The nonlinear restoring force developed by the gas chamber within the hydropneumatic suspension is expressed as a nonlinear function of relative displacement, z:

$$F_{gas} = \left(\frac{C}{[\, V_{3\phi} - A_p \cdot z \,]^{\gamma}} - P_{at} \right) \cdot A_p - M \cdot g \qquad (3.19)$$

where γ is the polytropic exponent, (γ = 1, for an isothermal process; γ = 1.4, for an adiabatic process). The nonlinear gas spring force can be expressed by the local equivalent spring constants as functions of excitation frequency, amplitude, and response characteristics, using the similar energy balance approach. The local equivalent spring constant can be obtained by equating the energy stored/released per cycle by the nonlinear spring to that of a linear spring. The energy stored/released per cycle by a pure spring is, however, zero. The local equivalent spring constant is thus obtained by equating the energy stored/released by the gas spring in one-quarter of the cycle to that of a linear spring. The energy stored/released by the gas spring in one-quarter cycle can be evaluated from:

$$E_{gas} = \int_0^z \left[\left(\frac{C}{[V_{3\phi} - A_p \cdot z \,]^{\gamma}} - P_{at} \right) \cdot A_p - M \cdot g \right] dz \qquad (3.20)$$

where E_{gas} is the energy stored/released by the gas spring in one-quarter of the cycle. Assuming harmonic response and excitation at a frequency ω_1, equation (3.21) can be re-arranged to yield:

$$E_{gas} = \int_0^{\pi/2\omega_1} \left[\left(\frac{C}{[V_{3\phi} - A_p \cdot Z \cdot \sin(\omega_1 t)]^{\gamma}} - P_{at} \right) \cdot A_p - M \cdot g \right] \cdot$$

$$\omega_1 \cdot Z \cdot \cos(\omega t) \cdot dt$$

or

$$E_{gas} = A_p \cdot C \cdot \omega_1 \cdot Z \int_0^{\pi/2\omega_1} \frac{\cos(\omega_1 t)}{[V_{3\phi} - A_p \cdot Z \cdot \sin(\omega_1 t)]^{\gamma}} \cdot dt$$

$$- \omega_1 Z \cdot (P_{at} \cdot A_p + M \cdot g) \int_0^{\pi/2\omega_1} \cos(\omega_1 t) \cdot dt \qquad (3.21)$$

Evaluating the above integral yields the following expression for the energy stored/released in the hydropneumatic spring during one-quarter of a harmonic oscillation cycle:

$$E_{gas} = \frac{C}{(\gamma - 1)} \cdot \left[\frac{1}{[V_{3\phi} - A_p \cdot Z]^{\gamma-1}} - \frac{1}{V_{3\phi}^{\gamma-1}} \right]$$

$$- Z \cdot (P_{at} \cdot A_p + M \cdot g) \qquad \text{for } \gamma > 1 \qquad (3.22)$$

Although equation (3.22) reveals that the energy stored/released in one-quarter cycle is independent of excitation frequency, the energy is, however, dependent upon the response amplitude Z corresponding to the excitation frequency. The energy stored in one-quarter cycle by the gas spring is equated to that of a linear spring, $E_{keq} = K_{eq} \cdot Z^2/2$ to yield an expression for the local equivalent linear spring rate $K_{eq}(\omega_1)$:

$$K_{eq}(\omega_1) = \frac{2C}{Z^2(\gamma - 1)} \cdot \left[\frac{1}{[V_{3\phi} - A_p \cdot Z]^{\gamma-1}} - \frac{1}{V_{3\phi}^{\gamma-1}} \right]$$

$$- \frac{2 (P_{at} \cdot A_p + M \cdot g)}{Z} \qquad \ldots (3.23)$$

3.4.3 Algorithm for Determination of Local Equivalent Linear Coefficients

Equations (3.18) and (3.23) describe the local equivalent damping and stiffness coefficients, respectively, due to orifice flows, Coulomb friction, and gas spring corresponding to a local excitation frequency and relative displacement response amplitude. The computation of local constants thus requires prior knowledge of the response amplitude at each discrete excitation frequency. An iterative algorithm is thus employed to determine the relative displacement response and the local constants corresponding to each discrete excitation frequency [33]. The iterative algorithm is formulated in the following manner:

1. For a specified excitation frequency ω_1, and amplitude, $Z_o(\omega_1)$, the algorithm is initiated by assuming values of local equivalent constants, $C^{\circ}_{eq}(\omega_1)$ and $K^{\circ}_{eq}(\omega_1)$. The equations of motion of the assumed locally linear system are solved to determine the amplitude of the relative displacement $Z(\omega_1)$. The local equivalent damping, $C^{*}_{eq}(\omega_1)$, and stiffness, $K^{*}_{eq}(\omega_1)$, coefficients are then computed using equations (3.18) and (3.23).

2. The errors between the assumed and computed values of local damping coefficients are computed as follows:

$$\varepsilon_k = | K^{*}_{eq}(\omega_1) - K^{\circ}_{eq}(\omega_1) |$$

$$\varepsilon_d = | C^{*}_{eq}(\omega_1) - C^{\circ}_{eq}(\omega_1) |$$

where ε_k and ε_d are the errors associated with the local equivalent stiffness and damping coefficients, respectively. The assumed values are considered to be the true values of the local coefficients when the error values are observed to be within specified tolerances.

Alternatively, the local constants are updated and the iterative procedure is repeated until convergence is obtained.

3. The iterative algorithm is repeated for various discrete excitation frequencies in order to express the nonlinear mechanisms by local equivalent constants over the frequency range of interest.

A flow diagram of the iterative algorithm is illustrated in Figure 3.4.

3.5 DEVELOPMENT OF A SUSPENSION MODEL WITH LINEAR SPRING AND VELOCITY-SQUARED DAMPING

Conventional vehicle suspension systems invariably comprise of nonlinear damping mechanism, Coulomb friction and approximately linear stiffness springs. Hydropneumatic suspension offers nonlinear orifice damping characteristics similar to those of the conventional suspension while neglecting the influence of special valving characteristics. The force-deflection characteristics of a hydropneumatic suspension, however, differ considerably from those of conventional suspension springs. A suspension model with linear spring rate is thus formulated to study the relative performance characteristics of conventional and hydropneumatic suspension.

The equation of motion of the single DOF suspension model with linear spring, orifice damper and Coulomb friction, illustrated in Figure 3.5, can be derived from equation (2.37). The gas spring force is replaced by the force generated by a linear spring, F_k , given by:

$$F_k = K_{lin} \cdot (z_p - z_o) \qquad (3.24)$$

where K_{lin} is the linear spring rate. In order to conduct the relative performance analysis of conventional and hydropneumatic suspension

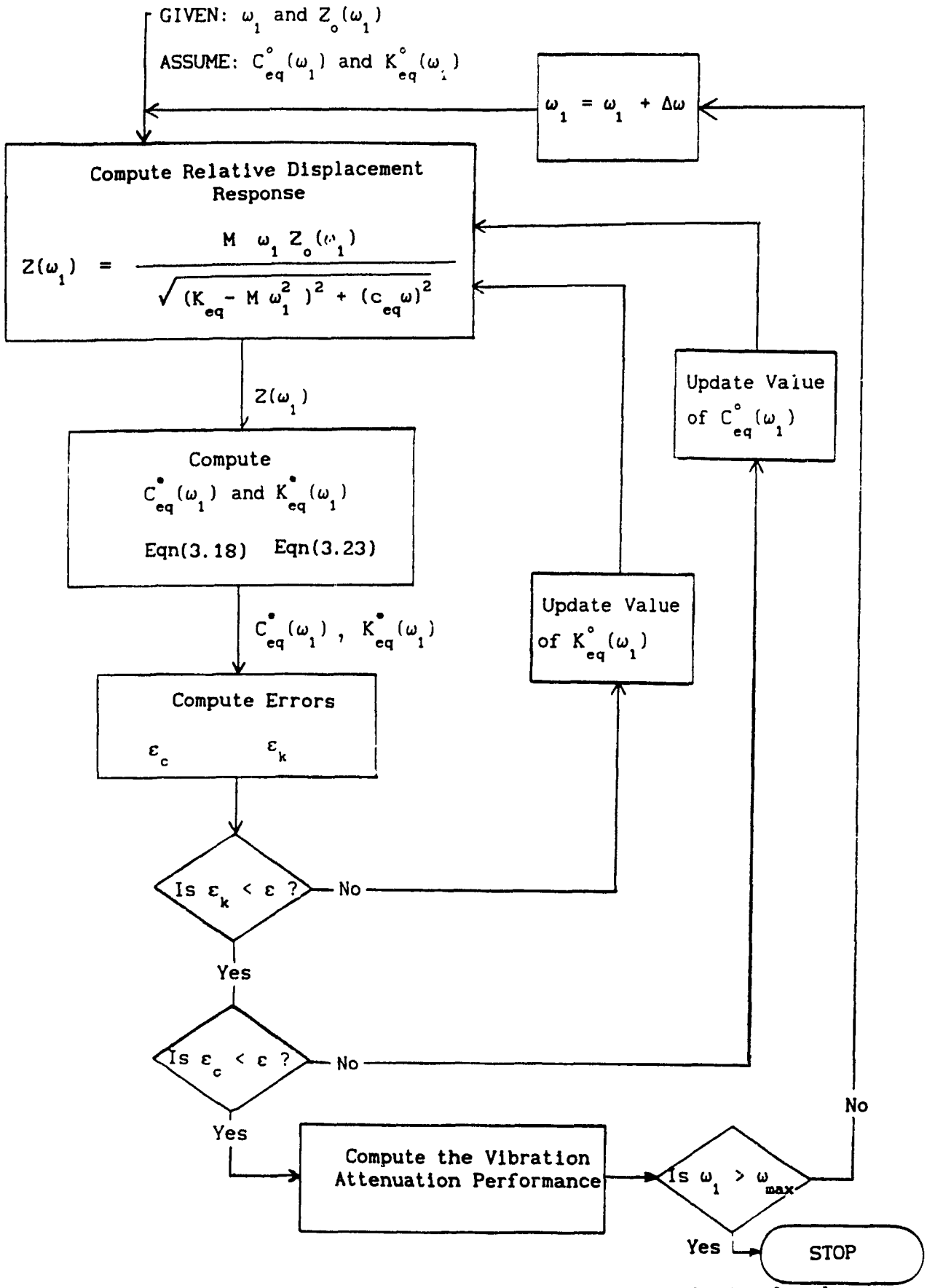

Figure 3.4 Flow diagram displaying iterative approach to local linear equivalent technique.

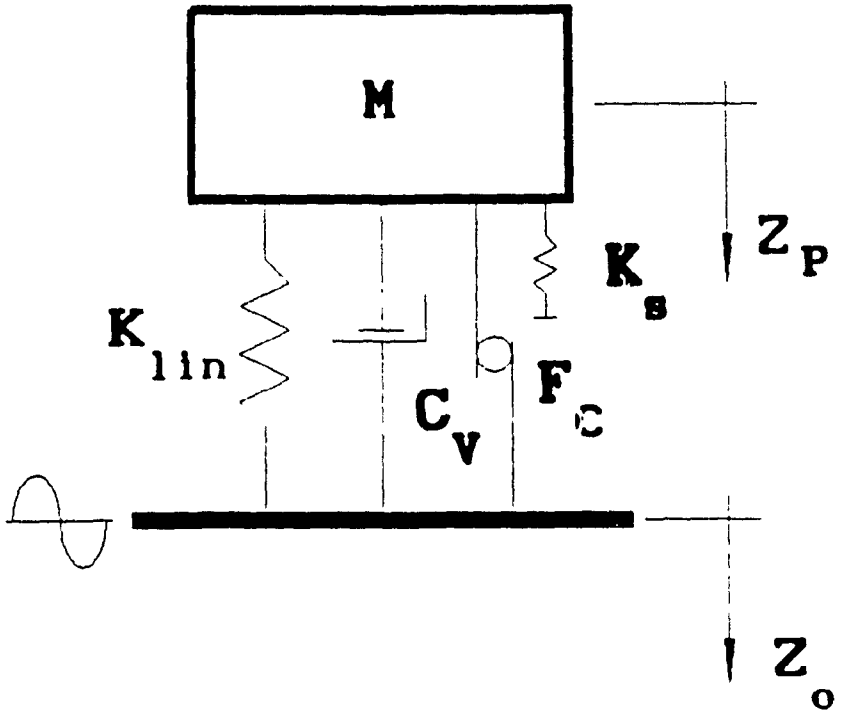

Figure 3.5 Schematic of single degree-of-freedom dynamic system with linear spring, orifice damping and Coulomb friction.

systems, the value of K_{lin} is determined from the static stiffness of the gas spring, described in equation (2.14):

$$K_{lin} = \frac{\gamma \cdot P_o \cdot A_p^2}{V_o} \tag{3.25}$$

The equation of motion for the base excited system can thus be expressed as:

$$\ddot{z}_p = - \text{sgn}(\dot{z}_p - \dot{z}_o) \cdot \frac{\rho \cdot A_p}{2 \cdot M} \cdot \left[\frac{A_p (\dot{z}_p - \dot{z}_o)}{n \cdot C_d \cdot A_o} \right]^2$$

$$+ \frac{K_{lin}}{M} \cdot (z_p - z_o) - \frac{F_c}{M} - \frac{F_s}{M} \tag{3.26}$$

Equation (3.26) represents the equation of motion of a single DOF system with a linear spring, a velocity-squared damper, Coulomb damping and elastic motion limiting bump stops. The nonlinear differential equation of motion may be solved either in the time domain using numerical integration techniques, or in the frequency domain using local equivalent linearization algorithm.

3.6 SUMMARY

Analytical techniques used for simulation of dynamical systems are briefly discussed in view of their benefits and limitations. The deterministic displacement excitations, such as rounded step, rounded pulse and semi-circular bump displacements, employed to simulate shock isolation performance of the hydropneumatic suspension are also discussed.

The nonlinear equation of motion of the hydropneumatic suspension is expressed by an array of locally equivalent equations of motion,

using the equivalent linearization technique based on energy balance. A suspension model, employing linear stiffness and nonlinear orifice damping, identical to that of the hydropneumatic suspension, is developed, such that relative performance analyses can be performed.

CHAPTER 4

DEVELOPMENT OF A TRACKED VEHICLE MODEL WITH HYDROPNEUMATIC SUSPENSION

4.1 GENERAL

Off-road vehicles, whether wheeled or tracked, experience severe ride vibrations due to extremely rough terrains. The high amplitude ride vibrations of these vehicles are of whole body nature and dominate in the lo.. frequency range to which the human driver is most fatigue and health sensitive. The driver and/or crews of such vehicles are subject to high levels of transmitted acceleration leading to driver discomfort, fatigue, poor working efficiency and limited operating speeds. In view of the increased concern for driver's health, safety and comfort, much interest has been focused in recent years on the development of innovative suspension designs which improve vehicle ride comfort and handling performance. The suspension requirements of off-road vehicles, such as earth movers, construction vehicles, battle tanks, personnel carriers, etc, are quite stringent and differ from those of conventional on-road vehicles due to high vehicle inertia, slow operating speeds and exposure to extremely rough terrains.

Tracked vehicles are often equipped with independent leading or trailing arm torsion bar suspension. A road wheel is mounted on each road arm which is splined to a transverse hull mounted torsion bar spring. Figure 4.1 illustrates the schematic of a typical trailing arm suspension employed on tracked military vehicles. A hydraulic damper is mounted between the road arm and the vehicle hull. Elastic limit stops are mounted on the vehicle hull to prevent excessive trailing arm motion.

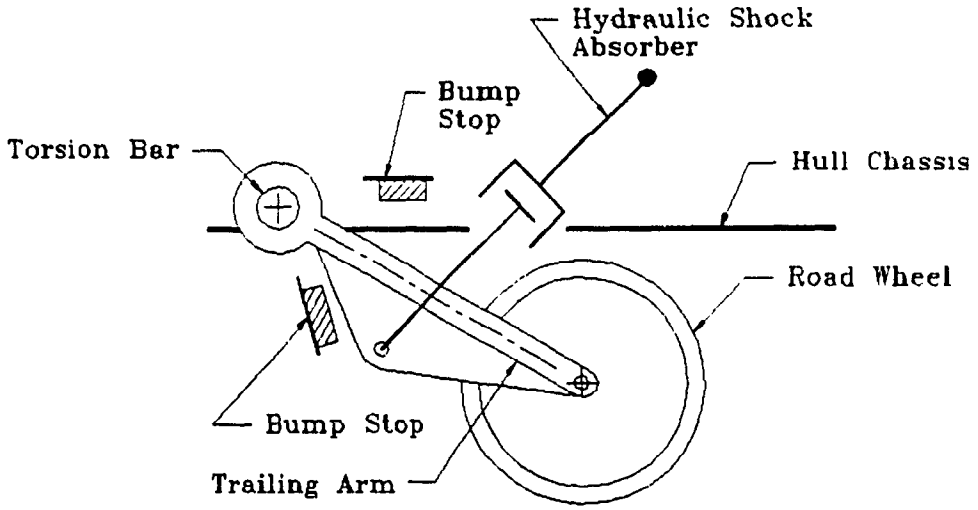

Figure 4.1 Schematic of typical trailing arm suspension configuration employed on tracked vehicles.

Although the conventional torsion bar suspensions offer the advantages of simplicity and low cost, the inherent limitations of these suspensions are well known. The primary limitations of a conventional torsion bar suspension include excessive weight and requirements for considerable mounting space. The trailing arm-torsion bar suspension tends to increase the ratio of unsprung to sprung mass, resulting in the deterioration of the ride and handling performance of the vehicle. The ride and handling performance of tracked vehicles are further deteriorated due to the lack of load-leveling capabilities of the fixed spring rate torsion bar suspension.

Hydropneumatic suspension designs have been developed by various manufacturers to improve the ride and handling performance of tracked vehicles [22, 23]. Hydropneumatic suspension offers the advantages of light weight and compact design, with a nonlinear rising rate spring characteristic. In addition, load-leveling can be conveniently achieved with this type of suspension. A multi-wheeled vehicle, equipped with hydropneumatic suspension, is analytically modeled to further investigate the shock and vibration isolation performance, and thus ride quality improvement potentials, of the hydropneumatic suspension system. A schematic of a tracked military vehicle, comprising of five road wheels per track, is illustrated in Figure 4.2. The hydraulic shock absorbers are mounted in an inclined attitude linking the trailing arm suspension with the hull chassis. The typical force-velocity characteristic of the shock absorbers employed in these vehicles is presented in Figure 4.3 [34]. The force-velocity characteristic of the nonlinear shock absorbers reveal two piece-wise linear regions representing damping coefficients corresponding to bleed control (low

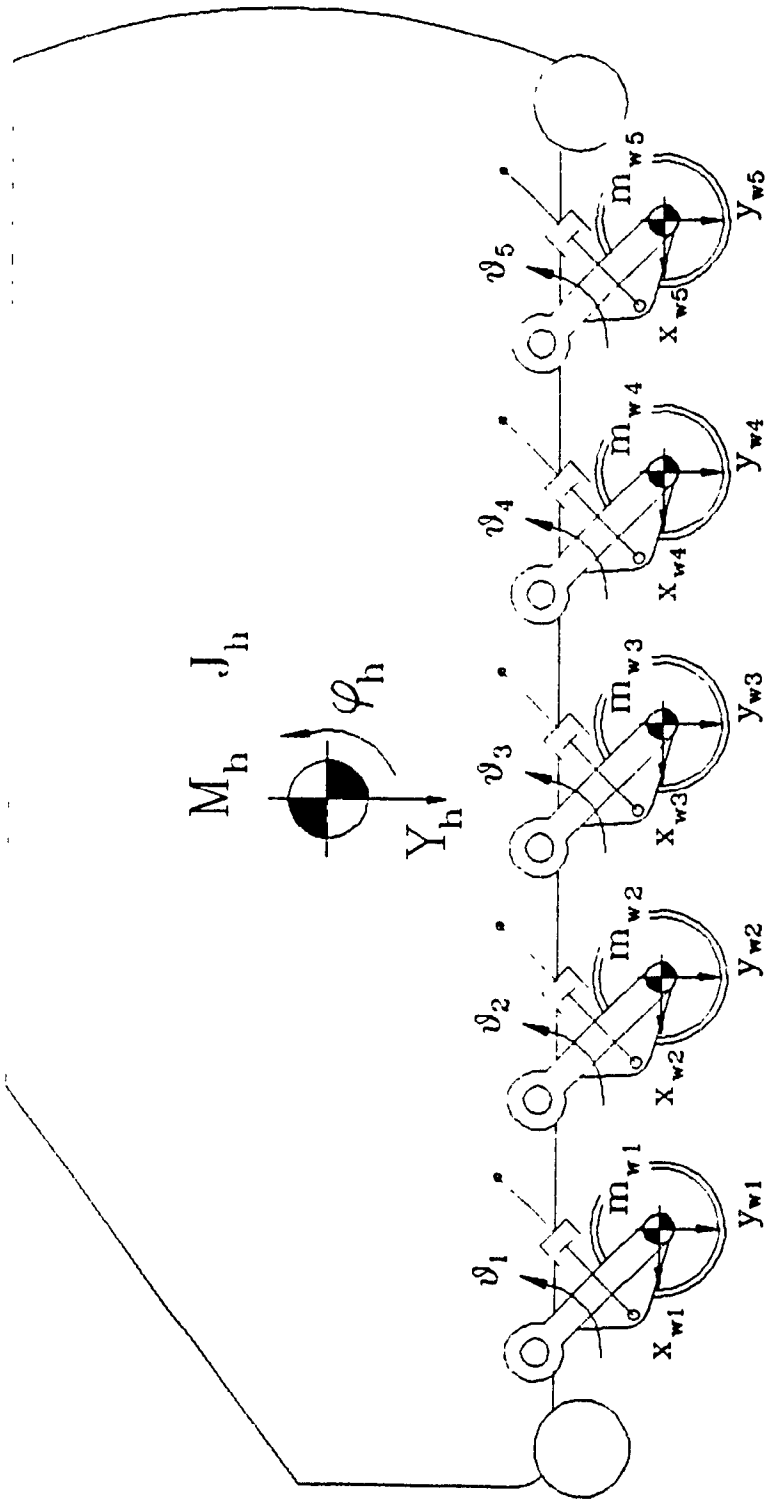

Figure 4.2 Schematic of a tracked military vehicle comprising five road wheels per track and trailing arm suspension configuration.

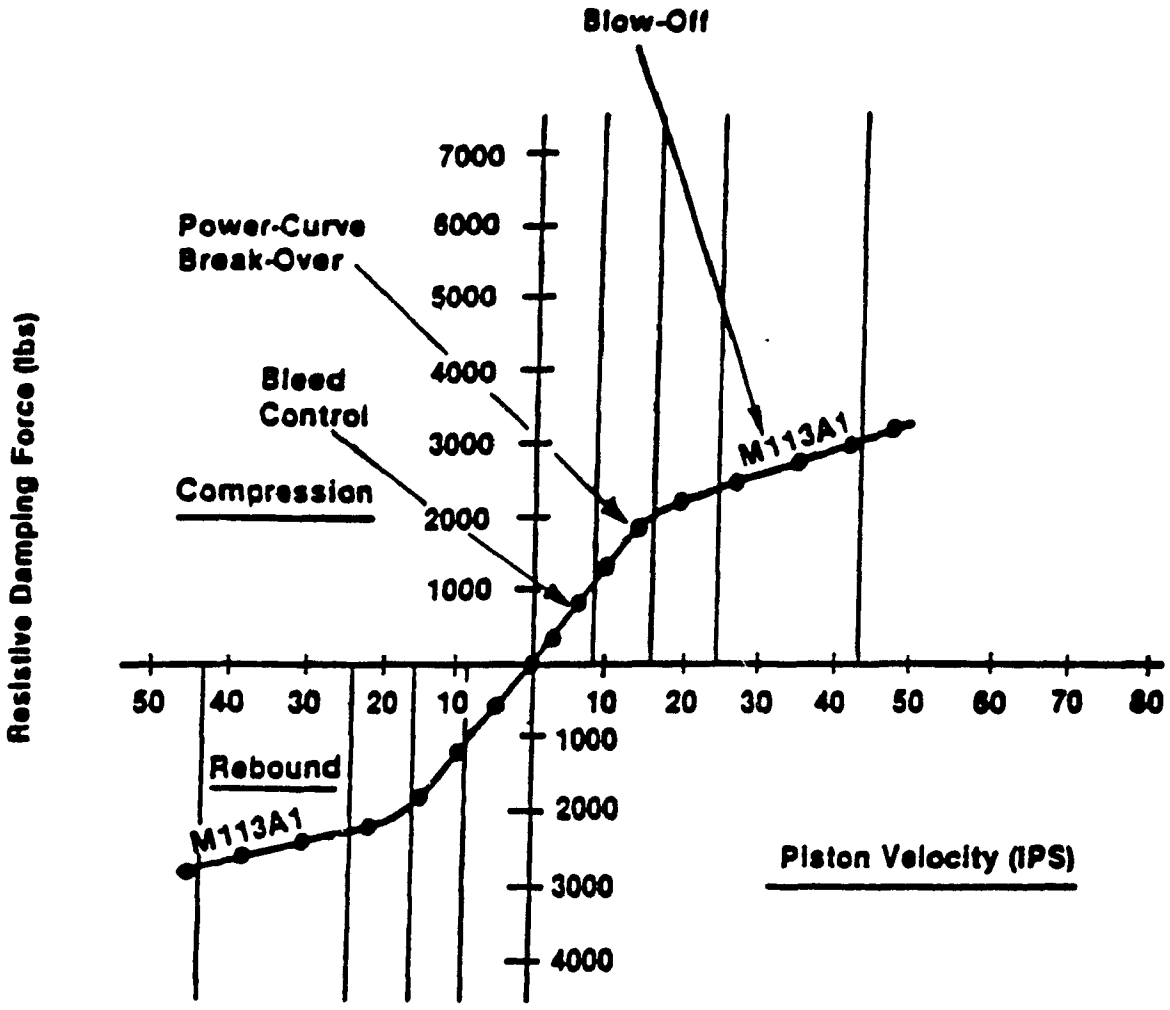

Figure 4.3 Force-velocity characteristic of hydraulic dampers employed on tracked military vehicle model [34].

velocity), and blow-off control (high velocity). The transition from bleed control (high damping) to blow-off control (low damping) occurs at a "break velocity".

4.2 DEVELOPMENT OF THE TRACKED VEHICLE MODEL

Development of a ride dynamic model involves the identification of suspension elements such as springs and shock absorbers connecting the wheels to the vehicle superstructure; unsprung and sprung masses and inertias, and elastic properties of tires, bump stops, etc. In case of a tracked vehicle, the track effects such as track pull and track pad elasticity are taken into account to study the ride dynamic behaviour of the tracked vehicle. The track loads along with the various suspension forces are then incorporated to develop a ride dynamic model to evaluate the ride vibration levels at the hull center of gravity. Dynamic analysis of this tracked vehicle has been previously performed by Afonso [34]. Modeling techniques, assumptions and parameter values, similar to those employed by Afonso, are included in the current analysis.

A pitch-plane ride dynamic model of the five road wheel tracked vehicle is developed to investigate the bounce, pitch and longitudinal ride quality of the vehicle. The roll and lateral dynamics of the vehicle are assumed to be negligible in relation to the bounce, pitch and longitudinal dynamics of the vehicle. The analytical ride dynamic models of the tracked vehicle, equipped with conventional torsion bar and hydropneumatic suspension, are formulated to carry out relative performance analyses.

A seven degrees-of-freedom ride dynamic model of the multi-wheeled tracked vehicle is developed, incorporating the kinematics and dynamics

of the linkage suspension consisting of trailing arm, torsion bar, hydraulic shock absorber and elastic limit stops. The generalized co-ordinates of the in-plane seven degrees-of-freedom model include vertical and pitch motion of the hull center of gravity (c.g.), and vertical motion of each road wheel, as shown in Figure 4.4.

The bounce motions of the road wheels are selected as generalized co-ordinates in view of convenience and ease of comparison with published results. The rotation and longitudinal motion of the trailing arms and road wheels are described by constraint equations relating hull bounce, hull pitch, road wheel bounce and suspension/vehicle geometry. The equations of motion for the in-plane ride dynamic model are derived using Lagrange's energy method. The highlights of the model and the associated assumptions are as follows [34] :

- Kinematics and dynamics associated with the trailing arm and shock absorber linkages are taken into consideration, assuming small motions.
- The damping force due to the conventional shock absorber is assumed to be proportional to the relative velocity across the shock absorber. The equivalent viscous damping coefficient is determined from the experimentally derived force-velocity characteristics of the shock absorber. (Figure 4.3)
- The damping force due to hydropneumatic suspension is derived using equation (2.39), assuming constant orifice and symmetric characteristics.
- The spring force due to hydropneumatic suspension is derived using equation (2.39), assuming a polytropic process ($\gamma = 1.4$).
- Elastic properties of the road wheel tire and the track pads are represented by linear springs in series, using a point contact model.
- The track is assumed to be a continuous belt, which remains in contact with the road wheels and terrain at all times.

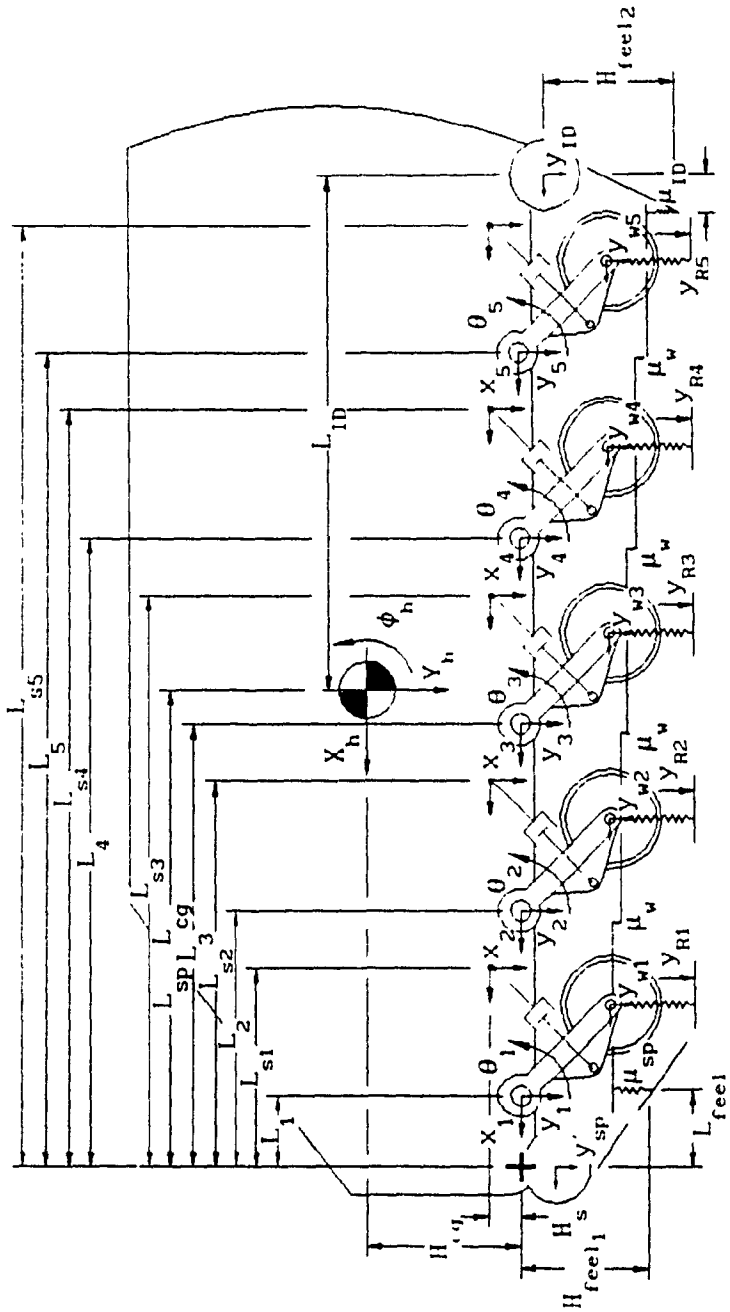

Figure 4.4 Plane model representation of a multi-wheeled tracked military vehicle employing trailing arm suspension configuration.

- The magnitude of motion along the generalized coordinates is assumed to be small.
- The elastic bump stops are represented by equivalent torsional springs in parallel with the torsion bar springs.
- The dynamic track tensions are modeled as restoring forces generated by relative springs between the forward feeler and the first road wheel, between adjacent road wheels and between the last road wheel and the trailing feeler. (Figure 4.5).

The differential equations describing the hull c.g. bounce (y_h), hull c.g. pitch (ϕ_h), and the individual wheel bounce (y_{wi}), are expressed as follows, while a detailed derivation is presented in Appendix A. Tracked vehicle geometry, suspension and road wheel tire and track parameters are presented in Tables 4.1, 4.2 and 4.3, respectively [34]. It should be noted that these equations represent a generic tracked vehicle model which conveniently displays all possible suspension forces. When the ride dynamics of the conventional torsion bar spring and hydraulic damper suspension are evaluated, the hydropneumatic suspension force, F_{Hi}, is set to zero. When the ride dynamics of the hydropneumatic suspension are evaluated, the hydraulic damper coefficients, C_{eqi}, and the torsion bar spring rates, K_{ti}, are set to zero.

Hull Bounce Motion:

$$\left(M_h - \tan^2(\theta_o - \zeta) \sum_{i=1}^{5} m_{wi} \right) \cdot \ddot{y}_h - \tan(\theta_o - \zeta) \cdot \sum_{i=1}^{5} m_{wi} \cdot d_i$$

$$\cdot \left(\tan(\theta_o - \zeta) \cdot \cos \alpha_i + \sin \alpha_i \right) \cdot \ddot{\phi}_h + \tan^2(\theta_o - \zeta) \cdot$$

$$\sum_{i=1}^{5} m_{wi} \cdot \ddot{y}_{wi} + \frac{1}{R \cdot \cos(\theta_o - \zeta)} \sum_{i=1}^{5} K_{ti} \cdot (\theta_i - \phi_h) + \mu_s \cdot$$

$$\left(y_h + L_{sp} \cdot \phi_h - y_{w1} \right) + \mu_{ID} \cdot \left(y_h - L_{ID} \cdot \phi_h - y_{w5} \right) + \frac{r_s \cdot \sin(\lambda + \theta_o)}{R \cdot \cos(\theta_o - \zeta)} \cdot \left[\sum_{i=1}^{5} C_{eqi} \cdot (V_{Ai} - V_{Bi}) + F_{H_i} \right] = 0 \quad \ldots(4.1)$$

Hull Pitch Motion:

$$\left(J_h + \sum_{i=1}^{5} m_{wi} \cdot d_i \cdot \left[\sin \alpha_i + \tan(\theta_o - \zeta) \cdot \cos \alpha_i \right]^2 \right) \cdot \ddot{\phi}_h + \tan(\theta_o - \zeta) \sum_{i=1}^{5} m_{wi} \cdot d_i \cdot \left[\sin \alpha_i + \tan(\theta_o - \zeta) \cdot \cos \alpha_i \right] \cdot \left(\ddot{y}_h - \ddot{y}_{wi} \right) + \sum_{i=1}^{5} \left(\frac{d_i \cdot \cos \alpha_i}{R \cdot \cos(\theta_o - \zeta)} - 1 \right) \cdot K_{ti} \cdot (\theta_i - \phi_h) + \mu_s \cdot L_{sp} \cdot \left(y_h + L_{sp} \cdot \phi_h - y_{w1} \right) - \mu_{ID} \cdot L_{ID} \cdot \left(y_h - L_{ID} \cdot \phi_h - y_{w5} \right) - \sum_{i=1}^{5} \left\{ d_{si} \cdot \sin(\beta_i - \lambda) + \frac{r_s \cdot d_i \cdot \cos \alpha_i}{R \cdot \cos(\theta_o - \zeta)} \cdot \sin(\theta_o + \lambda) + d_i \cdot \sin(\alpha_i - \lambda) \right\} \cdot \left[C_{eqi} \cdot (V_{Ai} - V_{Bi}) + F_{H_i} \right] = 0 \quad \ldots(4.2)$$

Road Wheel Bounce:

$$m_{wi} \cdot \left(1 - \tan^2(\theta_o - \zeta) \right) \cdot \ddot{y}_{wi} + \tan^2(\theta_o - \zeta) \cdot m_{wi} \cdot \ddot{y}_h + \tan(\theta_o - \zeta) \cdot m_{wi} \cdot d_i \cdot \left[\sin \alpha_i + \tan(\theta_o - \zeta) \cdot \cos \alpha_i \right] \cdot \ddot{\phi}_h - \frac{1}{R \cdot \cos(\theta_o - \zeta)} \cdot K_{ti} \cdot (\theta_i - \phi_h) + K_{peff} \cdot (y_{wi} - y_{Ri})$$

$$+ \mu_w \cdot \left(2\, y_{wi} - y_{wi-1} - y_{wi+1} \right) - \frac{r_s \cdot \sin(\lambda + \theta_o)}{R \cdot \cos(\theta_o - \zeta)}$$

$$\cdot \left[C_{eqi} \cdot (V_{Ai} - V_{Bi}) + F_{H_i} \right] = 0 \qquad \ldots(4.3)$$

where:

C_{eqi} = viscous damping coefficient of shock absorber 'i'

d_i = distance between hull c.g. and trailing arm pivot 'i' $= \sqrt{H_{cg}^2 + (L_{cg} - L_i)^2}$

d_{si} = distance between hull c.g. and shock absorber 'i' hull mount location $B_i = \sqrt{(H_{cg} - H_s)^2 + (L_{cg} - L_{si})^2}$

F_H = combined spring and damper force generated by hydropneumatic suspension unit 'i'

J_h = hull mass moment of inertia about hull center of gravity (in pitch-plane)

K_{peff} = effective linear stiffness of elastic track pads and road wheels

K_{ti} = linear torsional stiffness of torsion bar 'i'

L_{sp} = horizontal distance between hull c.g. and sprocket

L_{ID} = horizontal distance between hull c.g. and idler gear

M_h = sprung mass of vehicle hull

m_{wi} = mass of road wheel 'i'

R = length of trailing arm

r_s = distance between the trailing arm pivot point and the shock absorber mounting point, A_i

V_{Ai} = velocity of shock absorber end point A_i, on trailing arm, along shock absorber axis

V_{Bi} = velocity of shock absorber end point B_i, on hull, along shock absorber axis

y_{RI} = vertical displacement excitation applied at road wheel 'i'

α_i = angle between the hull chassis and a straight line from the hull c.g. to trailing arm pivot 'i'

β_i = angle between the hull chassis and a straight line from the hull c.g. to shock absorber mount B_i

λ = initial angle of inclination of shock absorber to the hull chassis

θ_i = angular deflection of trailing arm 'i'

θ_o = initial angle of inclination between the straight line from the trailing arm pivot to the shock absorber mount A_i, and the hull chassis

ζ = angle between the trailing arm centerline and the straight line from the trailing arm pivot to the shock mount A_i

μ_s = equivalent stiffness of the leading portion of track

μ_{ID} = equivalent stiffness of the trailing portion of track

μ_w = equivalent stiffness of track portion between road wheels

Assuming small displacements along the generalized co-ordinates, the pitch rotation and longitudinal motion of the trailing arms and road wheels may be given by the following constraint equations:

$$\theta_i = \frac{y_h + d_i \cdot \phi_h \cdot \cos \alpha_i - y_{wi}}{R \cdot \cos(\theta_o - \zeta)} \qquad (4.4)$$

and:

$$x_{wi} = - d_i \cdot \phi_h \cdot \sin \alpha_i - [y_h + d_i \cdot \phi_h \cdot \cos \alpha_i - y_{wi}] \cdot \tan(\theta_o - \zeta) \qquad \ldots(4.5)$$

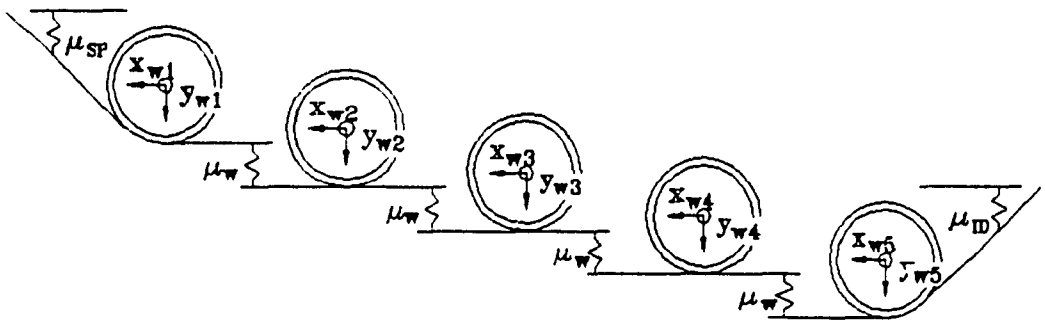

Figure 4.5 Dynamic forces generated between adjacent road wheels due to elastic track characteristics.

TABLE 4.1

TRACKED VEHICLE PARAMETERS

PARAMETER		VALUE
Mass and Inertia:		
Hull Mass, M_h,	(kg)	8,869
Road Wheel Mass, m_{w1},	(kg)	227
m_{w2},	(kg)	227
m_{w3},	(kg)	227
m_{w4},	(kg)	227
m_{w5},	(kg)	227
Pitch Moment of Inertia About Hull c.g., J_h,	($kg \cdot m^2$)	18,437
Horizontal Distance From Origin to:		
Hull c.g., L_{cg},	(m)	1.939
Torsion Bar 1, L_1,	(m)	0.362
L_2,	(m)	1.028
L_3,	(m)	1.695
L_4,	(m)	2.362
L_5,	(m)	3.029
Location of Shock Absorber:		
Shock Absorber 1, L_{s1},	(m)	0.891
L_{s2},	(m)	1.557
L_{s3},	(m)	2.224
L_{s4},	(m)	2.891
L_{s5},	(m)	3.558
Horizontal Distance from Hull c.g. to:		
Sprocket, L_{sp},	(m)	1.939
Idler Gear, L_{ID},	(m)	2.037
Vertical Distance from Origin to:		
Hull c.g., H_{cg},	(m)	0.606
Shock Absorber Ends, H_s,	(m)	0.10

TABLE 4.1 (CONTINUED)

TRACKED VEHICLE PARAMETERS

PARAMETER		VALUE
Length of Trailing Arm, R,	(m)	0.3175
Distance from Trailing Arm Pivot and Shock Absorber Mount 'A', r_s,	(m)	0.264
Trailing Arm Inclination to Horizontal, θ_o,	(rad)	1.125
Shock Absorber Inclination to Horizontal, λ,	(rad)	0.698
Angle Between Trailing Arm Axis and Line thru Trailing Arm Pivot and Shock Absorber Mount 'A', ζ	(rad)	0.724

TABLE 4.2

TRACKED VEHICLE SUSPENSION PARAMETERS

PARAMETER	VALUE
Conventional Suspension:	
Spring Rate of Torsion Bar, K_t: (N·m/rad)	
Within Normal Range of Travel,	19,768
When Contacting Bump Stops,	300,000
Permissible Rotation Before Contacting Bump Stops, θ_b, (rad)	0.401
Damping Coefficient, C_{eq}: (N·s/m)	
Bleed Control, Compression,	45,000
Expansion,	45,000
Blow-Off Control, Compression,	10,200
Expansion,	8,300
Break Velocity, v_p, (m/s)	0.4064
Hyropneumatic Suspension:	
Damping Parameters:	
Area of Main Piston, A_p, (m^2)	0.012
Piston Area Ratio, α,	1.0
Density of Hydraulic Fluid, ρ, (kg/m^3)	797.68
Number of Orifices in Damper Plate, n,	4
Orifice Discharge Coefficient, C_d,	0.8
Area of Damper Plate Orifices, A_o, (m^2)	3.17E-05
Coulomb Friction Force, F_f, (N)	444.8
Viscous Band Relative Velocity, δv_p, (m/s)	0.001
Gas Spring Parameters:	
Initial Precharge Pressure, $P_{i\phi}$, (Pa)	850,000
Initial Precharge Volume, $V_{i\phi}$, (m^3)	1.401E-03
Polytropic Exponent, γ,	1.4

TABLE 4.3

ROAD WHEEL TIRE AND TRACK PARAMETERS

PARAMETER		VALUE
Road Wheel Tire Stiffness, K_w,	(N/m)	1,225,800
Track Pad Stiffness, K_p,	(N/m)	3.0E+06
Equivalent Stiffness of the Track:		
Leading Portion of Track, μ_s,	(N/m)	210,150
Portion Between Road Wheels, μ_w,	(N/m)	131,344
Trailing Portion of Track, μ_{ID}	(N/m)	103,245

where θ_i is the angular rotation of trailing arm 'i', and x_{wi} is the longitudinal displacement of road wheel 'i'.

The analysis of the hydraulic shock absorber and hydropneumatic suspension forces requires computation of the displacements and velocities of the hull and trailing arm suspension mount locations, D_{Bi}, D_{Ai}, V_{Bi} and V_{Ai} respectively. The equations of motion of the shock absorber mounting ends, A and B, along the axis of the shock absorber are derived from the kinematic model presented in Figure 4.6:

$$D_{Ai} = \left(\frac{r_s}{R}\right)\left(\frac{\sin(\theta_o + \lambda)}{\cos(\theta_o - \zeta)}\right)\left(y_{wi} - y_h - d_i\cos\alpha_i \cdot \phi\right)$$

$$+ \phi \cdot d_i\sin(\lambda - \alpha_i) + y_h \cdot \sin\lambda \qquad (4.6)$$

and:

$$D_{Bi} = \phi \cdot d_{si}\sin(\lambda - \beta_i) + y_h \cdot \sin\lambda \qquad (4.7)$$

The velocities V_{Ai} and V_{Bi} are derived through time differentiation of equations (4.6) and (4.7).

The elastic properties of the track pads and road wheels are treated as linear springs connected in series. Combining the elastic properties of the track pads and road wheels yields an effective linear stiffness, K_{peff}, given by:

$$K_{peff} = \frac{K_p \cdot K_w}{K_p + K_w} \qquad (4.8)$$

where K_p and K_w are the constant spring rates of the track pads and road wheels, respectively.

The elastic motion limiting, or 'bump' stops, are incorporated in

the analysis by considering them as equivalent torsional springs. The torsion bars are, therefore, assumed to have two linear ranges of stiffness; a 'soft' range attributed to the torque-deflection characteristics of the torsion bars when motion of the trailing arm is in the normal range of travel, and an extremely stiff range when the trailing arm encounters the bump stop. Referring to Figure 4.7, the equivalent torsional stiffness due to the elastic bump stops is given by:

$$K_{teq} = r_b^2 \cdot K_b \qquad (4.9)$$

where r_b is the distance from the trailing arm pivot to the bump stop, and K_b is the linear stiffness of the bump stop material.

Equations (4.1), (4.2), and (4.3) form a set of coupled second order, nonlinear differential equations describing the dynamics of the tracked vehicle model in the pitch-plane. The coupled differential equations of motion can be solved using direct numerical integration techniques to determine the ride performance characteristics of conventional and hydropneumatic suspension systems.

4.3 SUMMARY

In this chapter, a vehicle application study is proposed to investigate the potential ride performance benefits of hydropneumatic suspension. A tracked military vehicle, employing a trailing arm suspension configuration, incorporating torsion bars and hydraulic dampers, is chosen for the analysis. A pitch-plane nonlinear ride dynamic model of the tracked vehicle is developed, yielding a seven DOF system. The seven generalized co-ordinates include vertical and pitch motions of the hull center of gravity (c.g.), and bounce displacement of

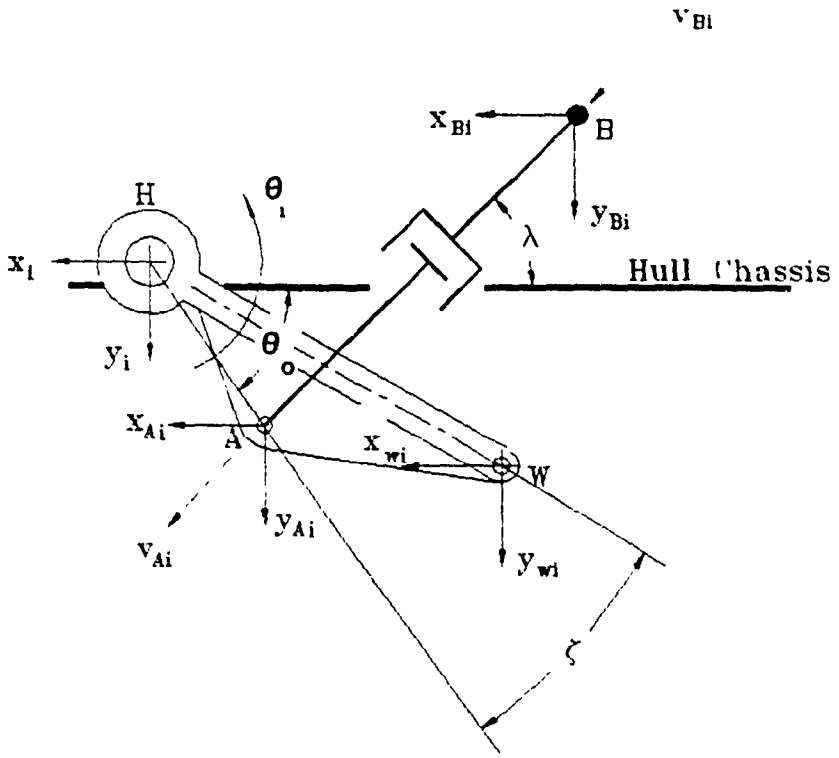

Figure 4.6 Schematic of shock absorber end geometry.

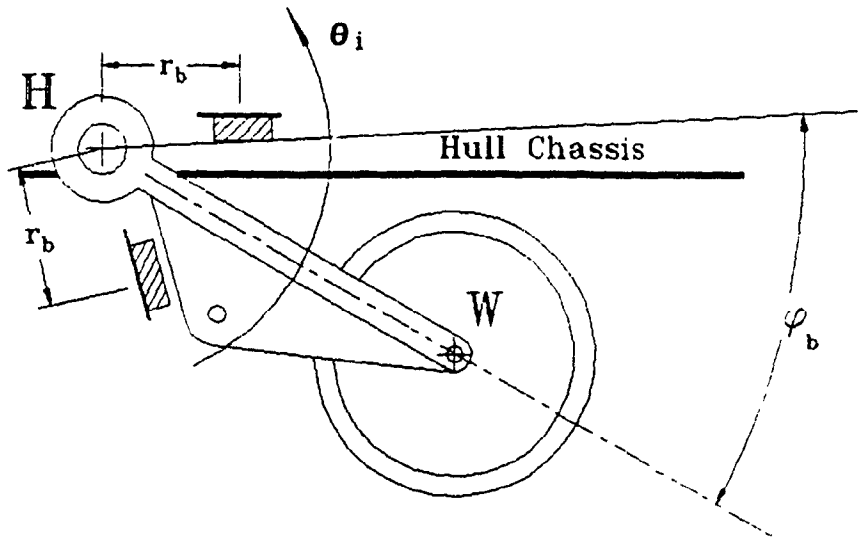

Figure 4.7 Schematic of trailing arm bump stop geometry.

each road wheel. Highlights of the tracked vehicle model include kinematics of the trailing arm linkage suspension, dynamics due to the track and track pads, and nonlinear restoring and damping forces generated by hydropneumatic suspension.

In the tracked vehicle model, it is assumed that the track is a continuous belt, and remains in contact with the terrain and road wheels at all times. The torsion bar spring rate is assumed to be linear and constant over the entire dynamic range. The force-velocity characteristics of the shock absorbers are assumed to be piece-wise linear and bump stop forces are modeled through equivalent torsional stiffnesses acting about the trailing arm pivot. The hydropneumatic suspension follows the same assumptions made in Chapter 2.

CHAPTER 5

SHOCK AND VIBRATION ISOLATION PERFORMANCE OF A HYDROPNEUMATIC SUSPENSION

5.1 GENERAL

The shock and vibration isolation performance potentials of hydropneumatic suspension are investigated via computer simulation. The nonlinear differential equations of motion, developed in Chapter 2, are solved via direct numerical integration for transient excitations to evaluate the shock isolation performance. The vibration isolation performance of the hydropneumatic suspension system is evaluated in terms of its vibration transmissibility, the ratio of steady state response amplitude to the excitation amplitude experienced at the base. A frequency sweep method, with direct numerical integration algorithm, is employed to determine the vibration transmissibility over the frequency range of interest.

5.2 SHOCK ISOLATION PERFORMANCE OF HYDROPNEUMATIC SUSPENSION

The shock isolation performance of the hydropneumatic suspension is evaluated for shock excitations arising from step and pulse displacement excitations. The shock isolation performance is evaluated in terms of the following parameters:

$$\text{Shock Displacement Ratio (SDR)} = \frac{z(t)}{Z_o}$$

$$\text{Shock Velocity Ratio (SVR)} = \frac{\dot{z}(t)}{\omega_o Z_o}$$

$$\text{Shock Acceleration Ratio (SAR)} = \frac{\ddot{z}(t)}{\omega_o^2 Z_o}$$

where Z_o is the peak displacement of the shock excitation.

Figures 5.1 and 5.2 compare the shock displacement ratio (SDR) and the shock acceleration ratio (SAR) response of the hydropneumatic suspension, respectively, to those of a conventional suspension system employing orifice damper and linear spring when subject to a rounded step displacement. The shock severity parameter was selected as $\nu = 15$. The hydropneumatic suspension provides lower peak displacement response and faster settling time than does the conventional suspension system, as shown in Figure 5.1. The SAR response of the hydropneumatic suspension, however, is quite similar to that of the conventional system, as shown in Figure 5.2.

The SDR and SAR response characteristics of the hydropneumatic and conventional suspensions, subject to a displacement pulse excitation, are presented in Figures 5.3 and 5.4, respectively. The shock severity parameter was selected as $\nu = 15$. The response characteristics reveal that the SDR and SAR response of the hydropneumatic suspension are virtually identical to the SDR and SAR responses of the conventional suspension system employing linear spring and symmetric hydraulic damping.

The influence of hydraulic fluid compliance on the shock isolation characteristics of the hydropneumatic suspension is investigated for rounded step and rounded pulse displacement excitations. The investigation compares the shock isolation characteristics of two hydropneumatic suspension system models: one assuming incompressible hydraulic fluid, ($\beta = \infty$ Pa), and the other considering a finite value of hydraulic fluid bulk modulus, (β = 1.374E+09 Pa). Figures 5.5 through 5.8 present the SDR and SAR response characteristics of the

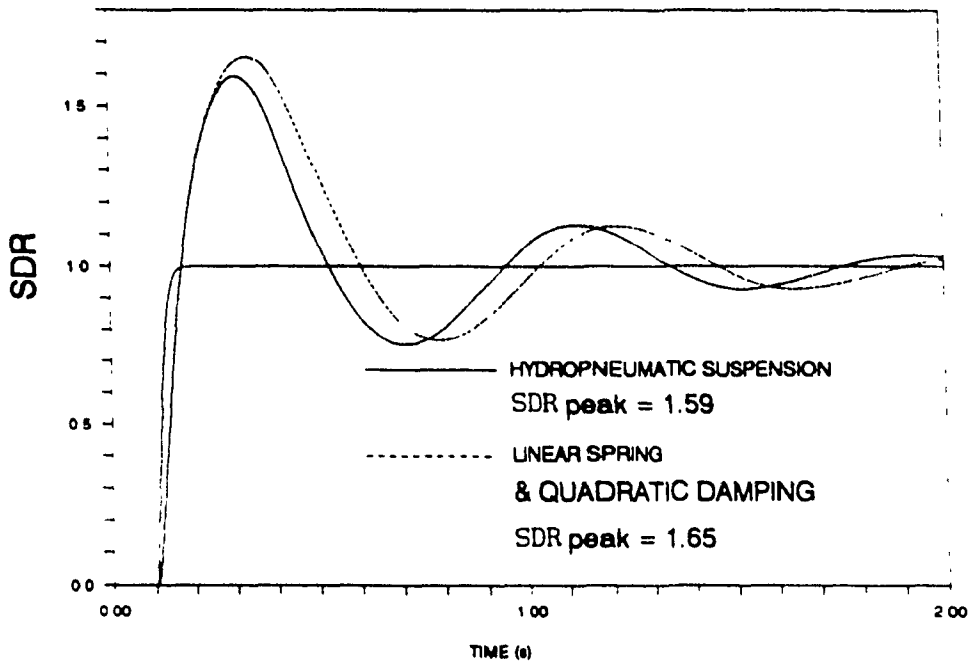

Figure 5.1 Comparison of SDR responses for hydropneumatic and conventional suspension, employing linear spring and orifice damper, when subject to rounded step excitation.

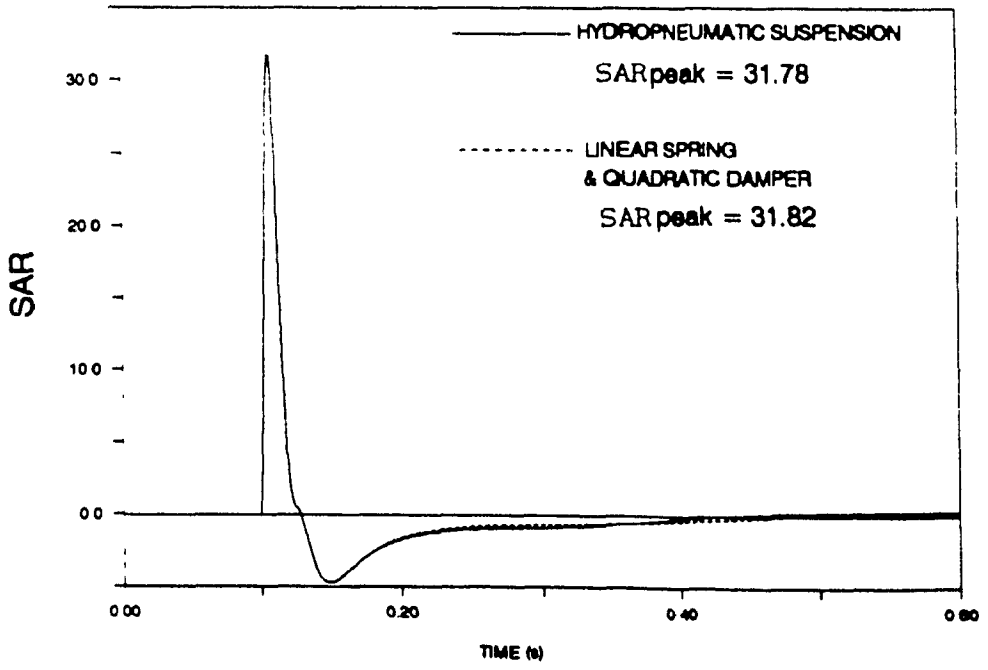

Figure 5.2 Comparison of SAR responses for hydropneumatic and conventional suspension, employing linear spring and orifice damper, when subject to rounded step excitation.

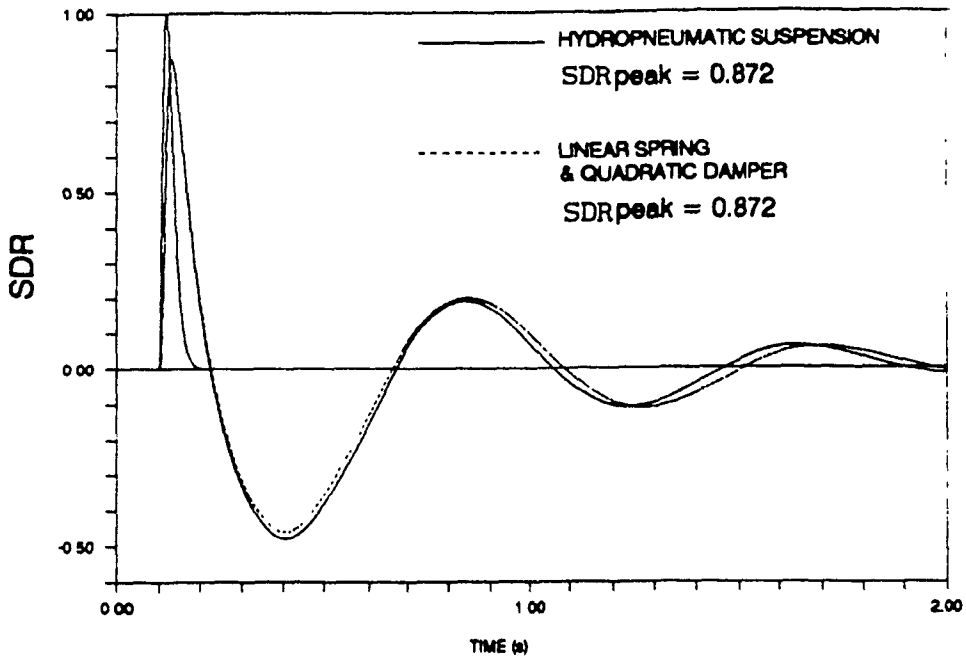

Figure 5.3 Comparison of SDR responses for hydropneumatic and conventional suspension, employing linear spring and orifice damper, when subject to rounded pulse excitation.

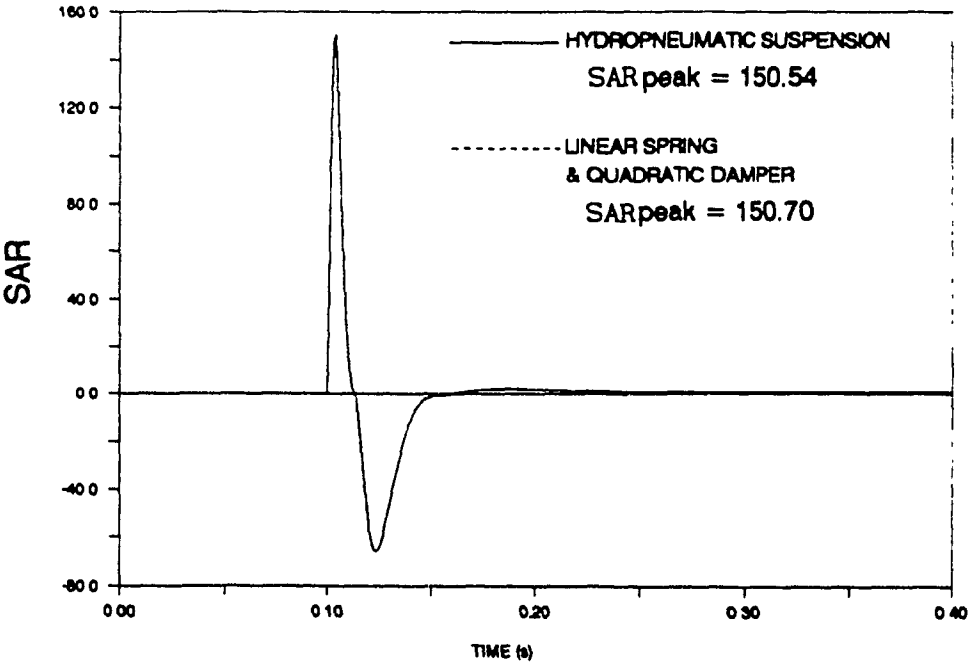

Figure 5.4 Comparison of SAR responses for hydropneumatic and conventional suspension, employing linear spring and orifice damper, when subject to rounded pulse excitation.

hydropneumatic suspension employing compressible and incompressible hydraulic fluids. Figures 5.5 and 5.6, respectively, show the SDR and SAR response characteristics of the hydropneumatic suspension models subject to a rounded step displacement excitation. Both the compressible and incompressible fluid models provide almost identical SDR and SAR characteristics. A reduction in the effective bulk modulus of the fluid yields slightly higher peak values of SDR and SAR; however, the settling time of the response remains virtually unchanged with respect to the response of the incompressible model.

Figures 5.7 and 5.8, respectively, present a comparison of the SDR and SAR response characteristics of the hydropneumatic suspension models assuming compressible and incompressible hydraulic fluid, when subjected to a rounded pulse displacement excitation. The response characteristics were obtained for a shock severity parameter of $\nu = 15$. Although the SDR response of the hydropneumatic suspension with compressible fluid is quite similar to that with incompressible fluid, the fluid compressibility tends to slightly increase the displacement response of the mass.

The SAR response characteristics of the hydropneumatic suspension models with compressible and incompressible fluids, subject to the rounded pulse displacement excitation, are presented in Figure 5.8. The compressible fluid model displays lower peak SAR response than does the hydropneumatic suspension model with incompressible fluid assumption. The increased compliance of the compressible fluid model displays slightly better SAR response when subject to this type of excitation.

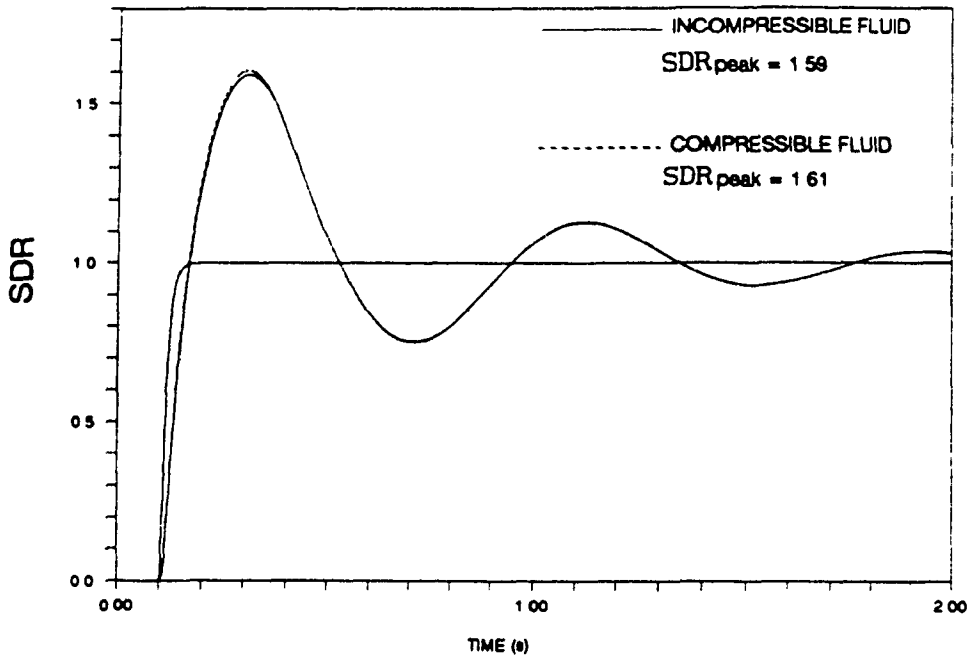

Figure 5.5 Comparison of SDR responses for hydropneumatic suspension, assuming compressible and incompressible fluid conditions, when subject to rounded step excitation.

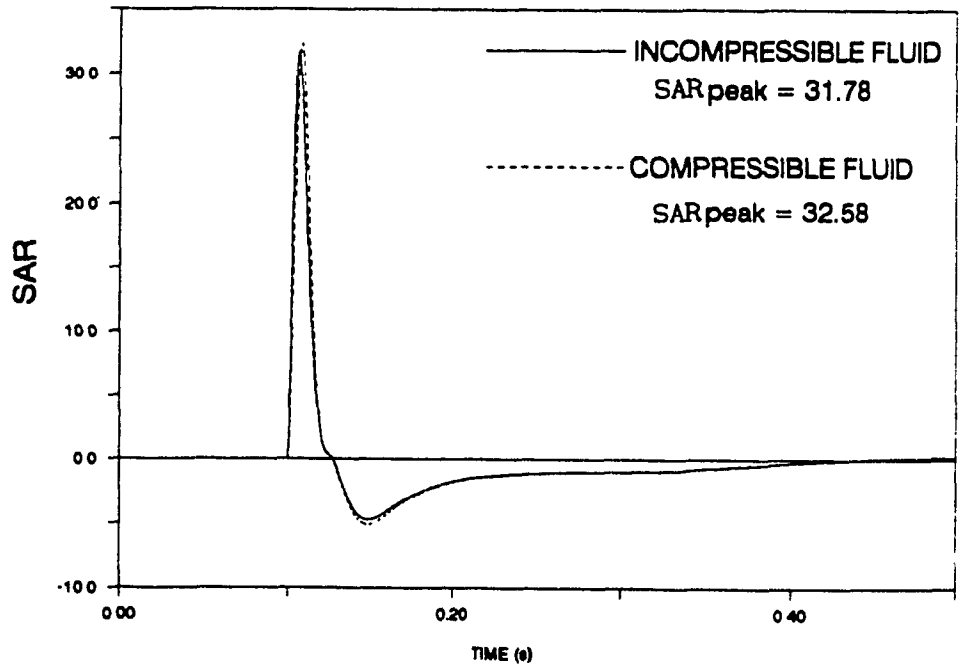

Figure 5.6 Comparison of SAR responses for hydropneumatic suspension, assuming compressible and incompressible fluid conditions, when subject to rounded step excitation.

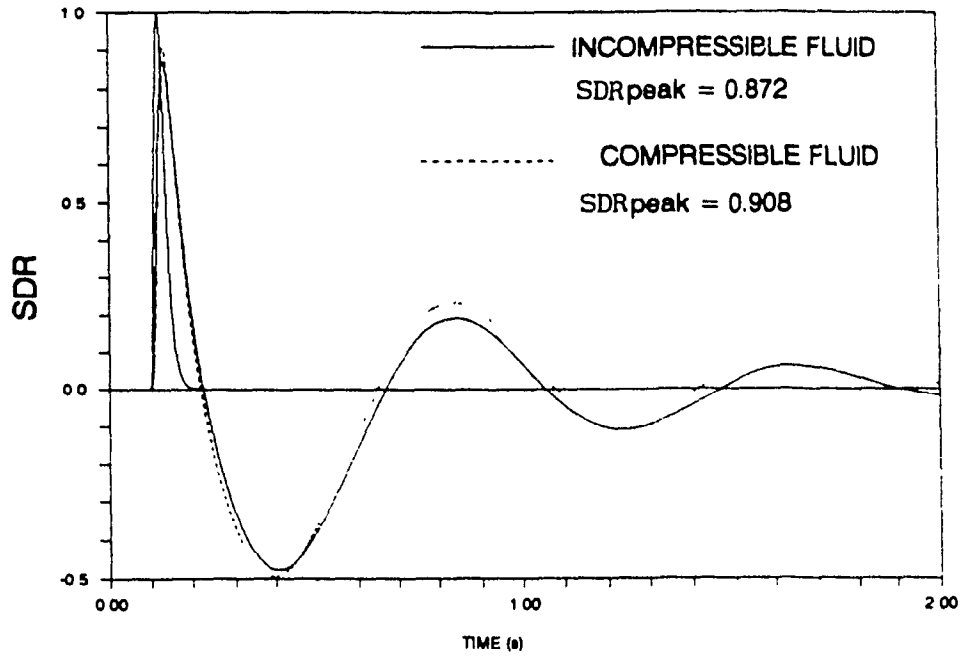

Figure 5.7 Comparison of SDR responses for hydropneumatic suspension, assuming compressible and incompressible fluid conditions, when subject to rounded pulse excitation.

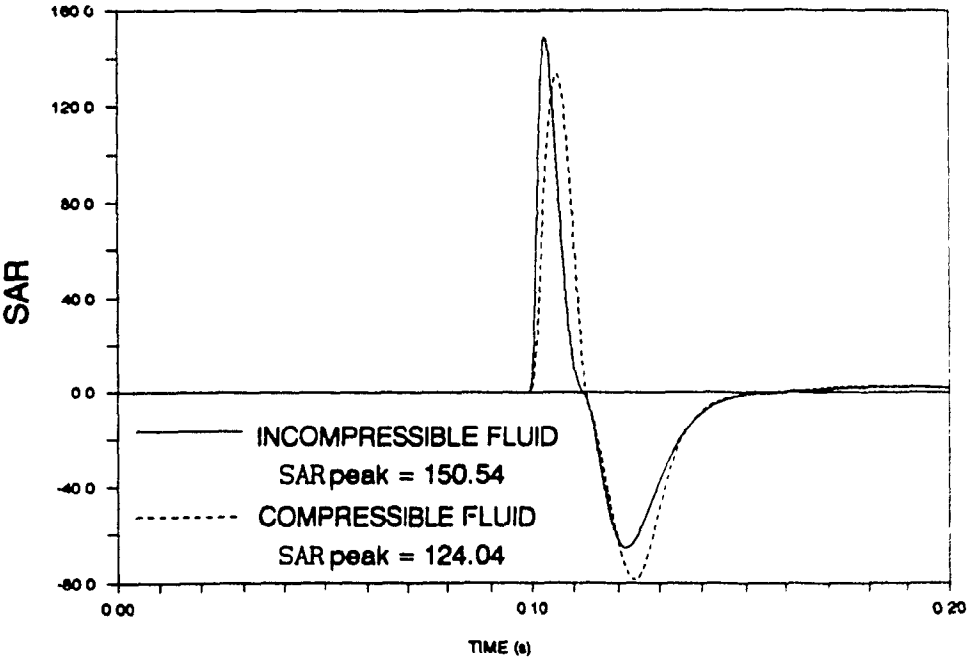

Figure 5.8 Comparison of SAR responses for hydropneumatic suspension, assuming compressible and incompressible fluid conditions, when subject to rounded pulse excitation.

5.3 VIBRATION TRANSMISSION PERFORMANCE OF THE HYDROPNEUMATIC SUSPENSION

The vibration transmissibility, or frequency response characteristic, of a suspension system provides significant insight to the steady state performance over a frequency range of interest. The vibration transmissibility characteristics of the hydropneumatic suspension are evaluated for harmonic excitations with a peak amplitude of 0.05 m. The hydropneumatic suspension exhibits nonlinear and asymmetric force-deflection characteristics due to the nitrogen gas spring, as discussed earlier in Chapter 2. Consequently, the steady state displacement response amplitude in compression differs from that in expansion, as illustrated in Figure 5.9. The steady state response amplitude in the compression mode is lower than that in the expansion mode due to the rising rate spring characteristic. In order to illustrate the inherently nonlinear and asymmetric behaviour of hydropneumatic suspension, the compression mode and expansion mode response characteristics are presented in terms of compression and expansion transmissibility ratios:

$$\text{Compression Transmissibility} = \frac{\text{Steady State Peak Amplitude During Compression}}{\text{Excitation Amplitude}}$$

$$\text{Expansion Transmissibility} = \frac{\text{Steady State Peak Amplitude During Expansion}}{\text{Excitation Amplitude}} \qquad (5.1)$$

The compression mode and expansion mode vibration transmissibility characteristics of the hydropneumatic suspension are expressed in terms of Displacement Transmissibility Ratio, (DTR), and Acceleration Transmissibility Ratio, (ACTR). The single degree-of-freedom (SDOF) hydropneumatic suspension model is subjected to harmonic base

displacement excitations to determine the DTR and ACTR characteristics.

The DTR and ACTR characteristics of the SDOF hydropneumatic suspension system are compared to those of a SDOF system employing orifice damper and a linear spring. The orifice damper is selected to possess orifice and piston geometry identical to that of the hydropneumatic suspension. The linear spring rate is selected as the static spring rate of the nitrogen gas spring.

The compression and expansion mode DTR characteristics of the hydropneumatic suspension are compared to the DTR characteristic of the SDOF system with linear spring, as shown in Figure 5.10. Since both systems employ quadratic damping due to fluid flow through orifices, the damping characteristics of the two systems are expected to be quite similar. However, the SDOF system employing hydropneumatic suspension exhibits a different DTR characteristics in compression and expansion modes. During the compression mode, the DTR response characteristics exhibit a resonant peak at approximately 0.9 hz, whereas the expansion mode response characteristics display a resonant peak at about 1.0 hz. The difference in resonant frequency of the two modes is due to the asymmetric rising rate characteristic of the gas spring. Although the undamped natural frequency in the compression mode increases due to asymmetric gas spring, the corresponding increase in fluid pressure, stiffness, and thus damping, leads to a lower damped natural frequency than in the expansion mode.

The compression and expansion mode DTR responses differ not only in resonant frequency, but also in amplitude ratio. The peak DTR response in the expansion mode is higher than that in the compression mode due to reduced damping and nature of the gas spring. The gas spring is only

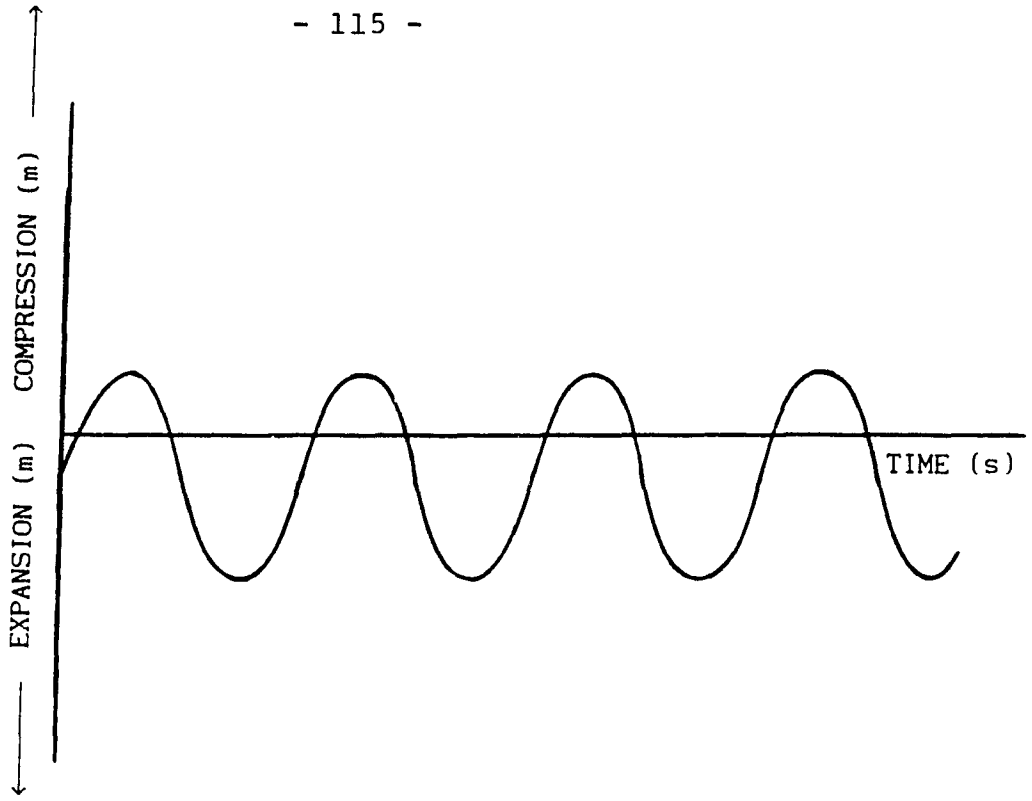

Figure 5.9 Typical steady state DTR response of hydropneumatic suspension when subject to a harmonic excitation.

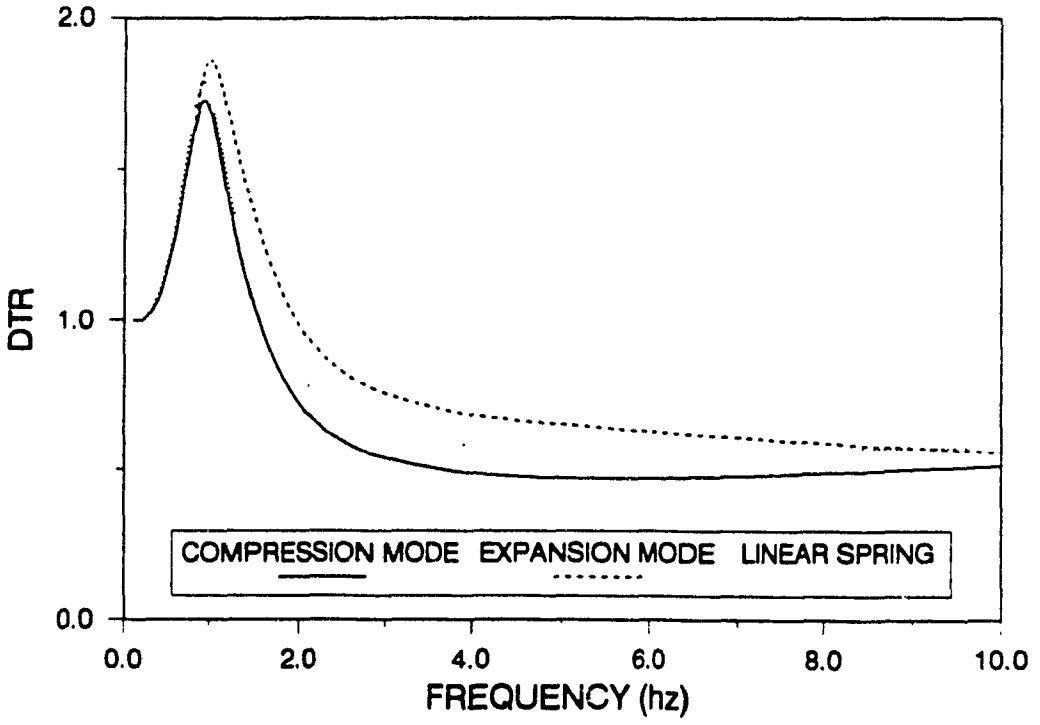

Figure 5.10 Comparison of compression and expansion mode DTR responses of hydropneumatic suspension, with DTR response of conventional suspension employing linear spring and orifice damper.

capable of storing energy in the compression mode, which must then be released in the expansion mode. However, during the expansion mode, only the damper and the increase in isolator mass potential energy are available to counteract this stored energy. Figure 5.10 further reveals that the DTR response characteristic of the conventional suspension with linear spring and orifice damper lies between the two responses of the hydropneumatic suspension over a wide range of excitation frequencies. The DTR response of the conventional system, however, approaches that of the hydropneumatic system at higher frequencies.

The acceleration transmissibility response characteristics (ACTR) of the hydropneumatic and conventional suspension systems are presented in Figure 5.11. The magnitude of the compression and expansion mode ACTR characteristics of the hydropneumatic suspension are different than the DTR characteristics due to the nonlinearities associated with orifice damping and gas spring. As shown in Figure 5.11, the ACTR resonant response in compression mode is higher than that in the expansion mode, due to the progressively stiffening spring characteristic. However, the compression and expansion mode transmissibility characteristics of the hydropneumatic suspension system converge at excitation frequencies just above the resonance. The ACTR characteristic of the conventional system, employing an orifice damper and linear spring, lies below the transmissibility responses of the hydropneumatic system around resonance. Although the ACTR response of the conventional suspension system is lower around the resonant frequency, the ACTR response of the hydropneumatic suspension is identical to that of the conventional suspension in the isolation range.

The influence of fluid compressibility on the frequency response

characteristic of hydropneumatic suspension is investigated by considering the effective bulk modulus of the hydraulic fluid. The DTR and ACTR characteristics of the hydropneumatic suspension are investigated for compressible fluid (β = 1.374E+09Pa) and incompressible fluid (β = ∞ Pa), as shown in Figures 5.12 and 5.13. The DTR characteristics, in the compression and expansion modes remain unaffected by the fluid compressibility in the resonant frequency region, as shown in Figure 5.12. However, at excitation frequencies well above the resonant frequency, the fluid compressibility affects the DTR response quite significantly. In the compression mode, the high frequency DTR response of the compressible fluid model increases, whereas the high frequency expansion mode DTR response decreases. This divergence of the DTR responses may be attributed to the dynamics associated with hydraulic fluid compliance and the floating piston mass. The combination of hydraulic fluid stiffness, gas spring stiffness and low floating piston mass create a second, high frequency resonant peak which occurs well above the limits of these graphs.

The corresponding ACTR response characteristics in compression and expansion modes of the hydropneumatic suspension models, with compressible fluid and incompressible fluid assumptions, are shown in Figure 5.13. The compression and expansion mode ACTR response characteristics of the compressible fluid model are almost identical to those of the incompressible fluid model. Slight divergence of the incompressible and compressible fluid models becomes evident at very high frequencies, again due to the added dynamics of the floating piston and compressible hydraulic fluid.

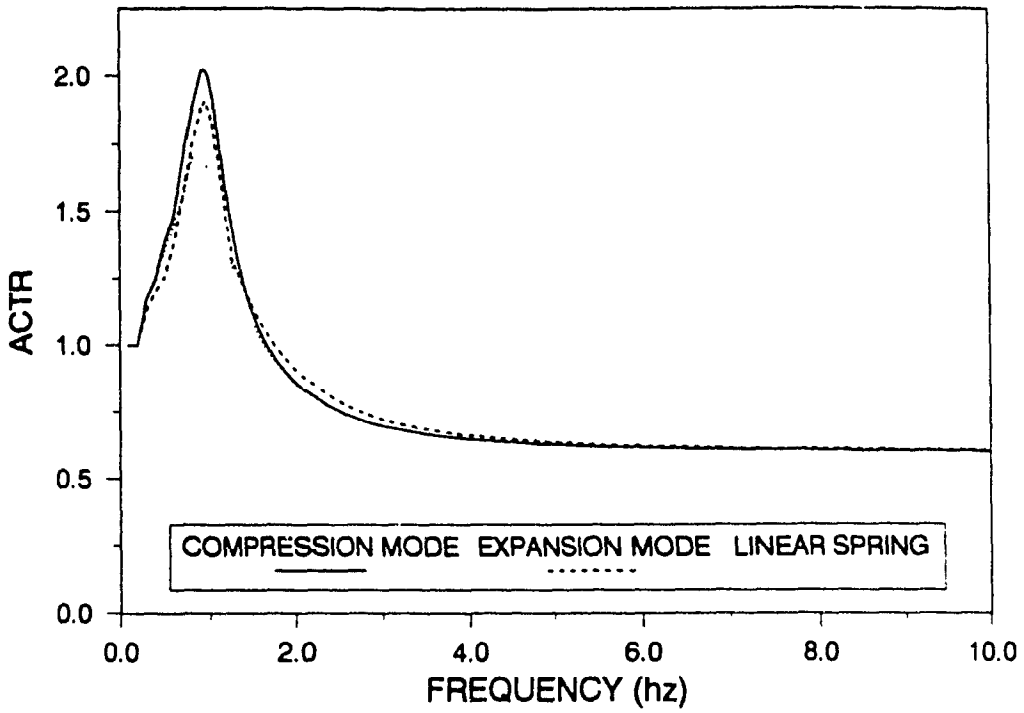

Figure 5.11 Comparison of compression and expansion mode ACTR reponses of hydropneumatic suspension, with ACTR response of conventional suspension employing linear spring and orifice damper.

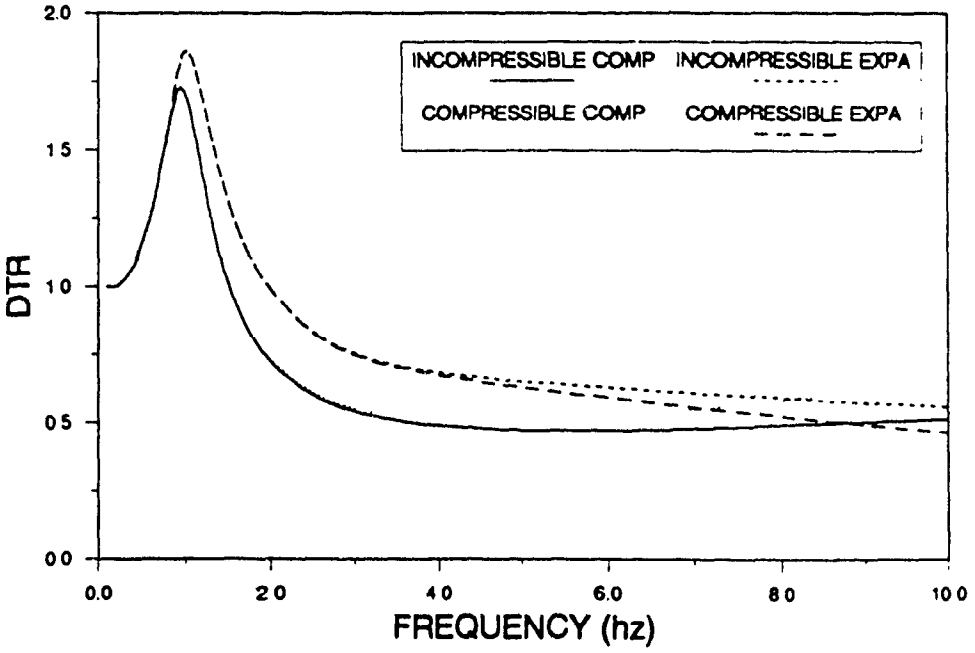

Figure 5.12 Comparison of compression and expansion mode DTR responses for hydropneumatic suspension assuming compressible and incompressible fluid conditions.

5.3.1 Frequency Response Characteristics of the Linearized Hydropneumatic Suspension Model

Analysis of linear dynamic systems is generally more convenient and economical to perform than that of a nonlinear system. Consequently, it is desirable to express the nonlinear suspension model by a linear equivalent, specifically for studies involving stochastic response evaluation and multi-variable optimization. The local equivalent linearization algorithm, presented in section 3.4.3, is employed to describe the nonlinearities arising from orifice flows, Coulomb friction and the gas spring, in terms of local equivalent damping and stiffness coefficients. The displacement (DTR), and acceleration (ACTR), transmissibility characteristics of the linearized suspension model are evaluated for harmonic base excitations, and compared to the compression and expansion transmissibility characteristics of the nonlinear suspension model established via direct integration of the nonlinear differential equations. Figures 5.14 and 5.15 present a comparison of the stiffness and damping forces, respectively, generated by the nonlinear system to those generated by the linear equivalent system. The force-deflection characteristics of the linearized spring are compared to those of the nonlinear gas spring, as shown in Figure 5.14. The force-deflection characteristics of the linearized spring correlate quite well with those of the nonlinear spring for low values of relative displacement. The error between the linear and nonlinear force, however, increases gradually when the magnitude of relative displacement increases. The error between the forces can be attributed to the fact that the linear equivalent spring is derived using only energy balance and not force balance. The force-velocity characteristics of the linear and nonlinear damper, presented in Figure 5.15, show good correlation

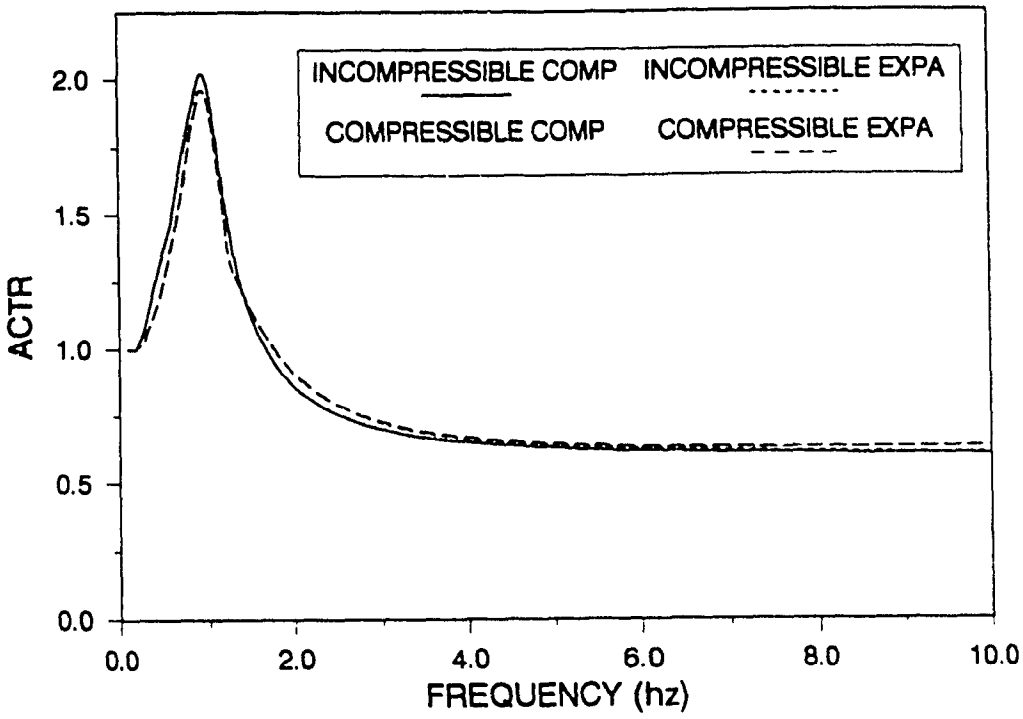

Figure 5.13 Comparison of compression and expansion mode ACTR responses for hydropneumatic suspension assuming compressible and incompressible fluid conditions.

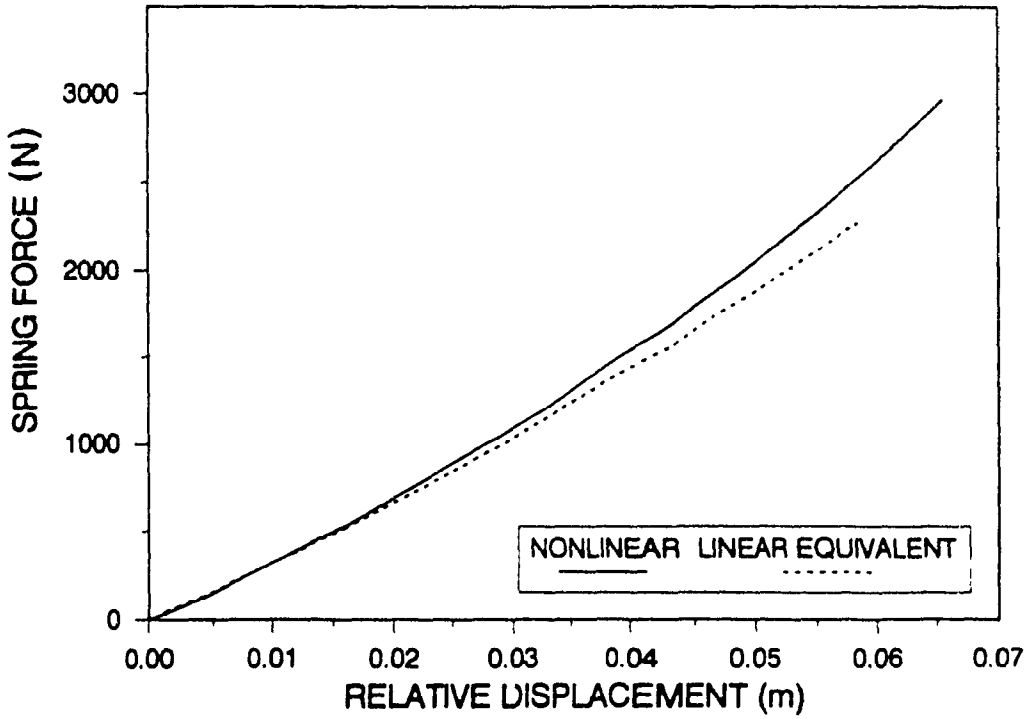

Figure 5.14 Comparison of spring force-deflection characteristics of hydropneumatic suspension and local linear equivalent system.

for low values of relative velocity response. The error between the linear and nonlinear forces, however, increases at higher velocities in a similar manner. This error, again, is attributed to the energy balance technique employed in deriving equivalent viscous damping coefficients. The peak error in the spring force, however, on the order of 10%, and peak error in the damping force is under 10%.

The DTR and ACTR response characteristics of the nonlinear hydropneumatic suspension are compared to those of the equivalent linearized suspension system, as shown in Figures 5.16 and 5.17, respectively. Figure 5.16 reveals that in the region of resonance, the DTR response of the linearized suspension follows quite closely the response characteristics of the nonlinear hydropneumatic suspension in the expansion mode. At higher excitation frequencies, the DTR response of the local equivalent linear system, however, is approximately the average of the nonlinear compression and expansion mode response characteristic. The ACTR response of the linearized system, shown in Figure 5.17, reveals a good correlation with the ACTR response of the nonlinear system only at higher excitation frequencies. The ACTR response characteristics of the local equivalent linear system do not correlate well with the response characteristics of the nonlinear hydropneumatic suspension when excitation frequencies lie in the region of resonance. Since the displacement response ratio of a linear system is identical to its acceleration response ratio, Figures 5.16 and 5.17 clearly reveal that the local equivalent linearization technique can effectively predict the displacement response and yields a large error in the acceleration response.

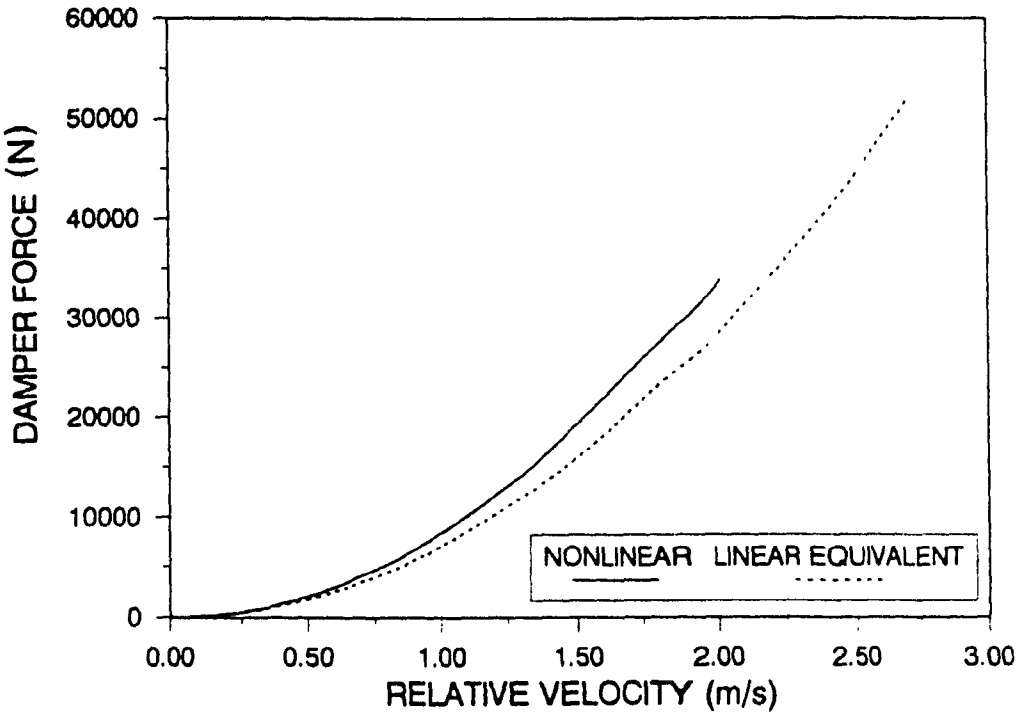

Figure 5.15 Comparison of damper force-velocity characteristics of hydropneumatic suspension and local linear equivalent system.

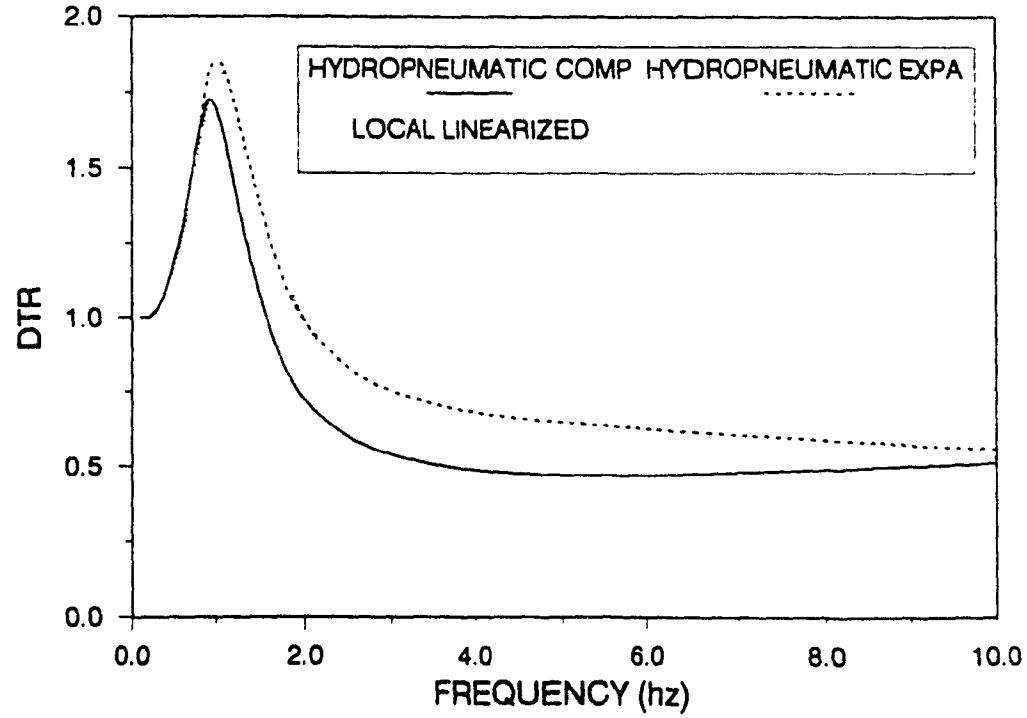

Figure 5.16 Comparison of compression and expansion mode DTR characteristics of hydropneumatic suspension and DTR characteristic of local linear equivalent system.

5.4 PARAMETRIC SENSITIVITY ANALYSES

The shock and vibration isolation characteristics of the hydropneumatic suspension are strongly influenced by various suspension parameters, such as: fluid bulk modulus, β; piston area ratio, α; polytropic gas exponent, γ; initial gas volume, V_{g1}; initial gas pressure, P_{g1}; damper plate design, etc. Parametric sensitivity analyses are conducted to establish the influence of the suspension parameters on the shock and vibration transmissibility characteristics. The results of the study are summarized in the following sub-sections.

5.4.1 Bulk Modulus

Figure 5.18 presents the influence of the fluid compressibility on the displacement transmissibility ratio DTR, in compression and expansion modes. The low frequency resonant peak occurs around 1 Hz and remains unaffected by variations in the bulk modulus, indicating that the gas spring dominates performance in the low frequency range. The DTR response, however, becomes increasingly divergent at higher excitation frequencies when the value of the bulk modulus is decreased. In the compression mode, the high frequency DTR response increases considerably with decrease in the effective bulk modulus. This significant increase in DTR response is attributed to the shifting of the second resonant peak to a lower frequency due to lower bulk modulus. On the other hand, an increase in hydraulic fluid compliance results in a decrease in the high frequency DTR response in the expansion mode.

It is evident that the vibration transmissibility characteristics of the hydropneumatic suspension are increasingly asymmetric with reduction in effective bulk modulus, since the compliant hydraulic fluid behaves as a fluid spring with asymmetric characteristics. The fluid

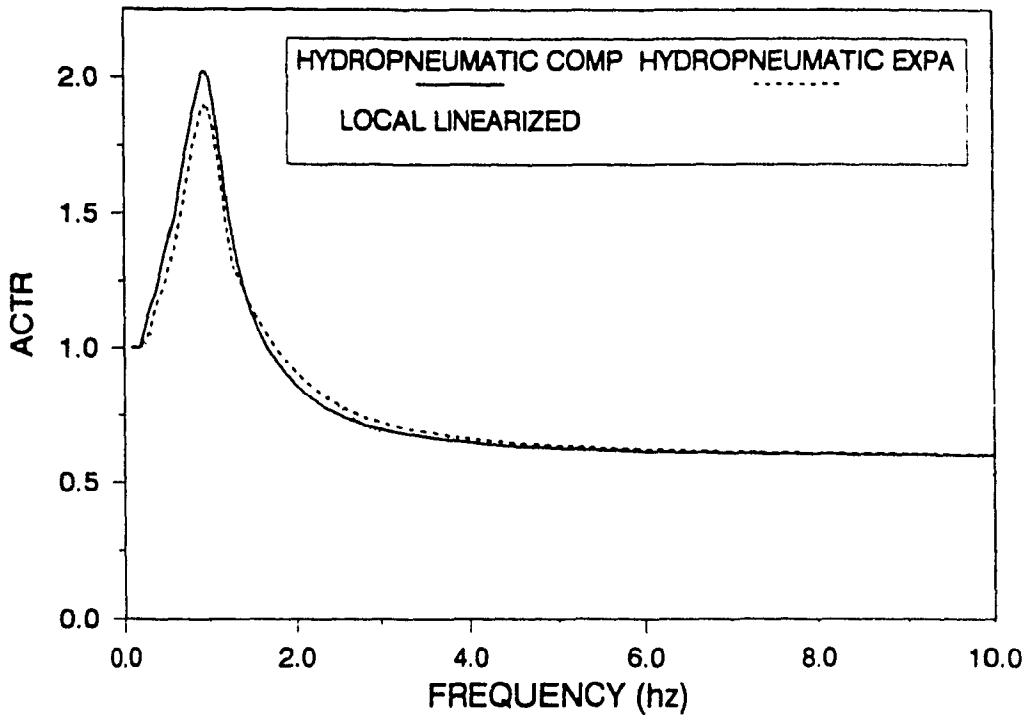

Figure 5.17 Comparison of compression and expansion mode ACTR characteristics of hydropneumatic suspension and ACTR characteristic of local linear equivalent system.

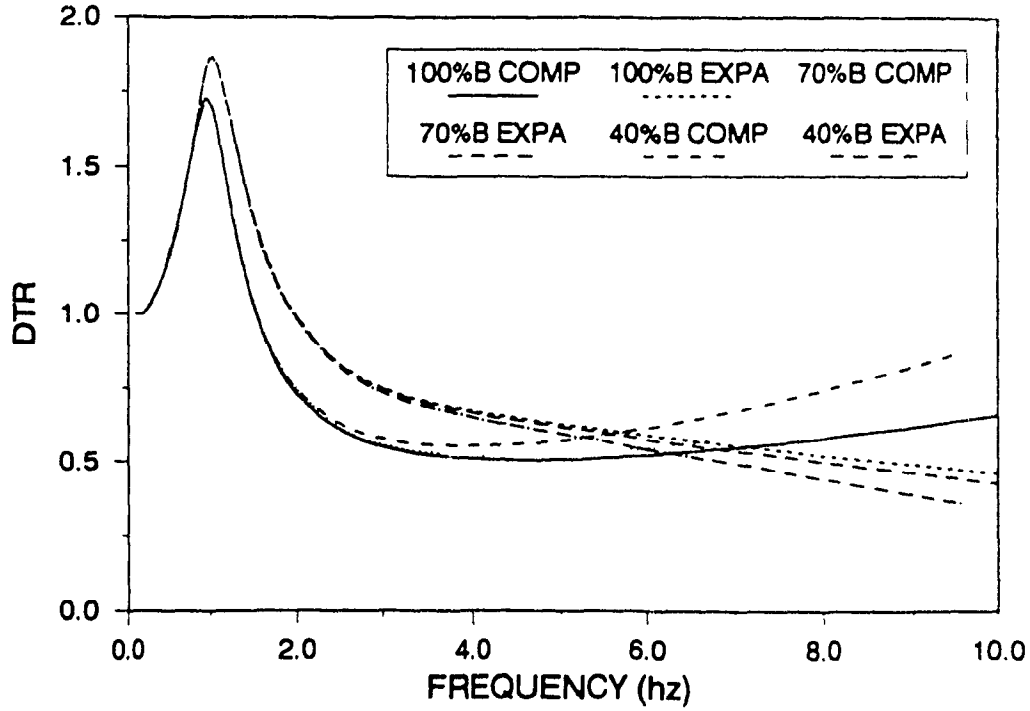

Figure 5.18 Influence of reduced fluid bulk modulus on compression and expansion mode DTR characteristics of hydropneumatic suspension.

spring affects the compression mode transmissibility considerably at higher excitation frequencies; the influence on the expansion mode transmissibility, however, is not as significant. Such an asymmetric behaviour can also be attributed to the design of the hydropneumatic suspension, where the hydraulic fluid only experiences compression during the compression stroke. This is unlike a conventional damper where the oil chambers above and below the main piston are subject to compression as well as expansion during a compression stroke.

Figure 5.19 presents the influence of hydraulic fluid compliance on the ACTR response in the compression and expansion modes for various values of the fluid bulk modulus. The figure clearly illustrates that the ACTR characteristics are significantly less sensitive to variations in the fluid bulk modulus. The influence of the hydraulic fluid compliance on the shock isolation performance of the hydropneumatic suspension is also investigated for rounded step and rounded pulse displacement excitations. The influence of hydraulic fluid compliance on the shock response is presented in terms of the shock spectrum, a plot of peak displacement (SDR), and acceleration (SAR), ratio versus the ratio of bulk modulus, β, to the nominal bulk modulus, β_o (1.374E+09 Pa). Figure 5.20 presents the SDR and SAR response spectra for a 0.10 m rounded step displacement excitation. The magnitude of SDR remains almost unchanged until the value of the bulk modulus is reduced below 10% of the nominal value, while the peak value of the SAR is considerably influenced by variations in the effective bulk modulus. The results clearly indicate that the shock isolation performance of the suspension is not affected by small variations in the value of the fluid bulk modulus; however, a significant reduction in the fluid bulk modulus

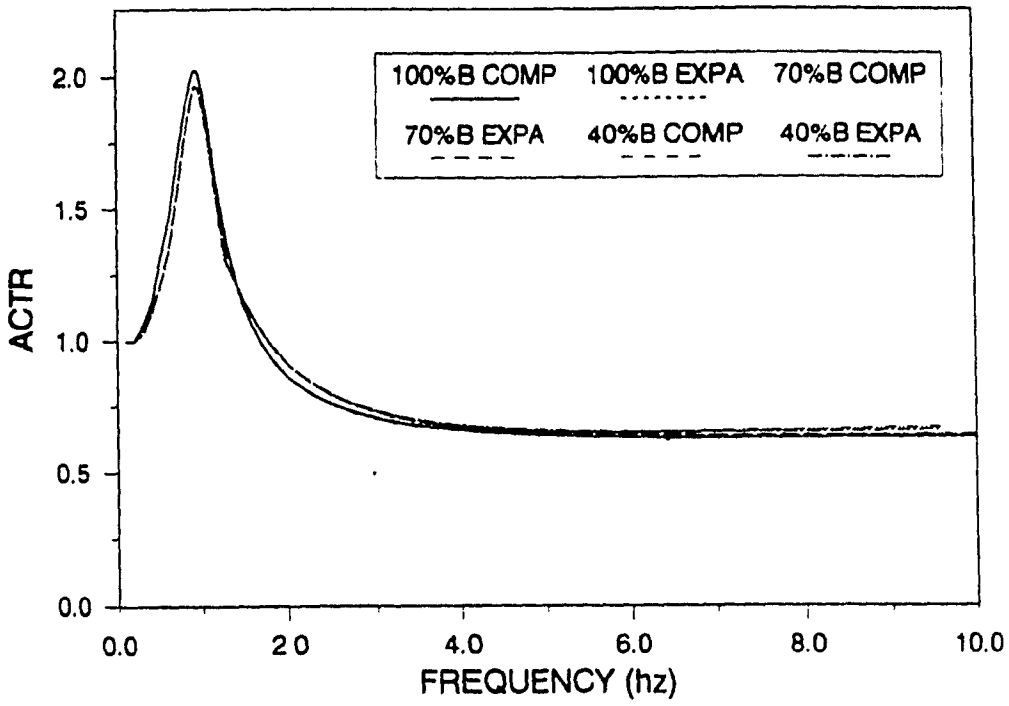

Figure 5.19 Influence of reduced fluid bulk modulus on compression and expansion mode ACTR characteristics of hydropneumatic suspension.

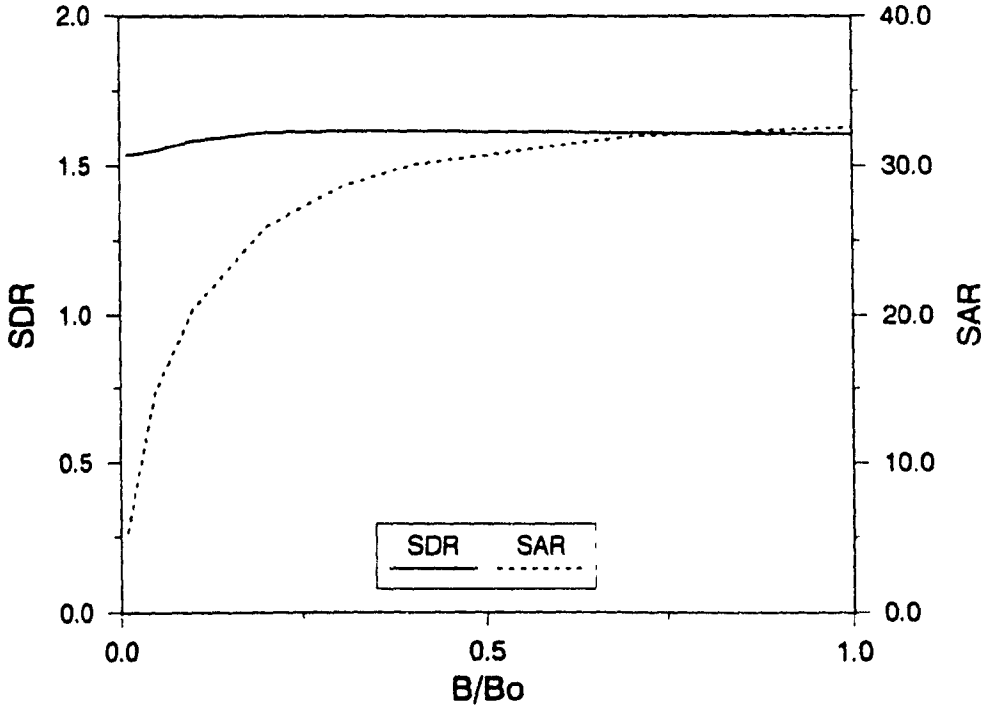

Figure 5.20 Influence of reduced fluid bulk modulus on SDR and SAR responses of hydropneumatic suspension, when subject to rounded step excitation.

can cause a considerable impact on the shock isolation performance.

Figure 5.21 presents the SDR and SAR response spectra of the hydropneumatic suspension subjected to a 0.10 m rounded pulse displacement excitation. The peak SDR response decreases only slightly with moderate reduction in effective bulk modulus, while the peak SAR response decreases considerably under the same conditions. Significant reductions in SDR occur as the value of β is reduced below 10% of the nominal value of the bulk modulus. The shock response spectra again reveals that the acceleration response is far more sensitive to variations in the bulk modulus. Although Figures 5.20 and 5.21 reveal that SDR and SAR response characteristics are affected only by significant decrease in the bulk modulus, it should be noted that only a small amount of entrained air can lead to considerable reduction in the effective bulk modulus.

5.4.2 Piston Area Ratio

Computer simulations are performed to investigate the influence of the floating piston area on the shock and vibration isolation performance of the hydropneumatic suspension model. The floating piston area is varied via the piston area ratio, ($\alpha = A_p/A_{fp}$), while the total gas volume of the spring is held constant.

Figure 5.22 presents the influence of varying piston area ratio, α, on the vibration isolation performance of the hydropneumatic suspension, while the total gas volume is held constant. The DTR characteristics reveal that variations in area ratio have only a slight influence on the response in the expansion mode at excitation frequencies above the resonant frequency, while the influence on the compression mode response is negligible. The ACTR characteristics of the hydropneumatic

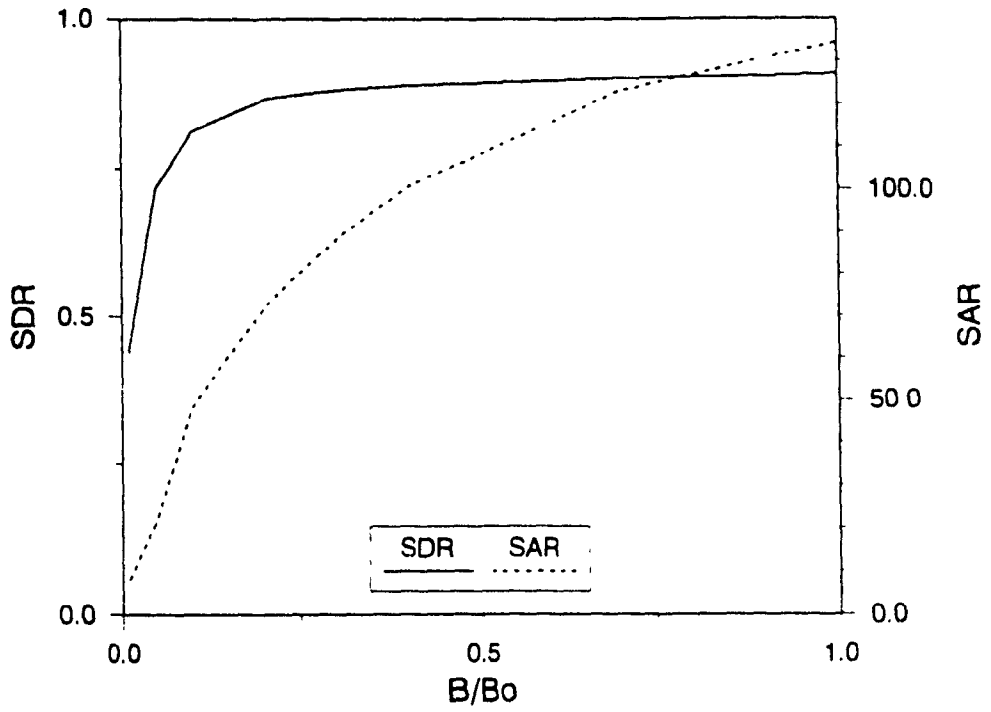

Figure 5.21 Influence of reduced fluid bulk modulus on SDR and SAR responses of hydropneumatic suspension, when subject to rounded pulse excitation.

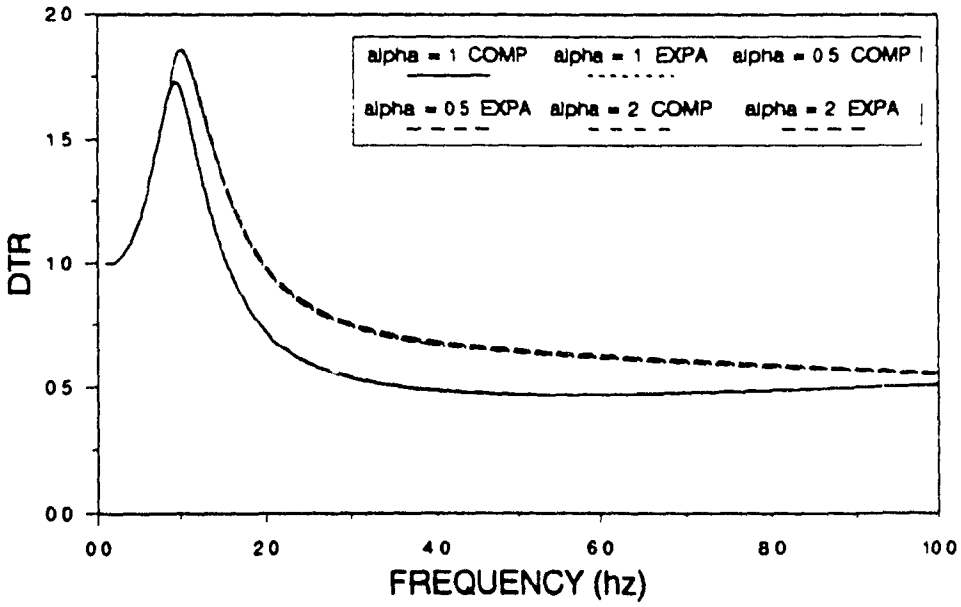

Figure 5.22 Influence of piston area ratio, α, on the compression and expansion mode DTR responses of hydropneumatic suspension.

suspension, presented in Figure 5.23, also reveal that variations in the piston area ratio is insignificant.

The shock displacement and acceleration response spectra of the hydropneumatic suspension are evaluated for a rounded step displacement excitation subject to different values of α. The results reveal that variations in the piston area ratio have virtually no effect on the peak values of SDR and SAR response.

5.4.3 Polytropic Gas Exponent

Variations in polytropic gas exponent γ, strongly influence the force-displacement characteristics of the gas spring, and thus the shock and vibration isolation characteristics of the suspension system. The instantaneous gas pressure also varies directly with variations in the polytropic gas exponent and thus affects the spring and damping forces generated by the suspension. Variations in the polytropic gas exponent are typically encountered due to temperature changes. Figures 5.24 and 5.25, respectively, present the influence of variations in polytropic gas exponent on the DTR and ACTR characteristics of the hydropneumatic suspension. Computer simulations are carried out for the following values of γ :

$$\gamma = 1.0 \quad \text{(Isothermal)}$$

$$\gamma = 1.4 \quad \text{(Adiabatic)}$$

$$\gamma = 2.0$$

The resonant frequency and the peak DTR response both increase with increasing value of γ, as shown in Figure 5.24. An increase in the value of γ yields a relatively stiffer spring and, thus, the resonant frequency of the system increases. The DTR response during compression decreases slightly in the isolation frequency range with increase in the

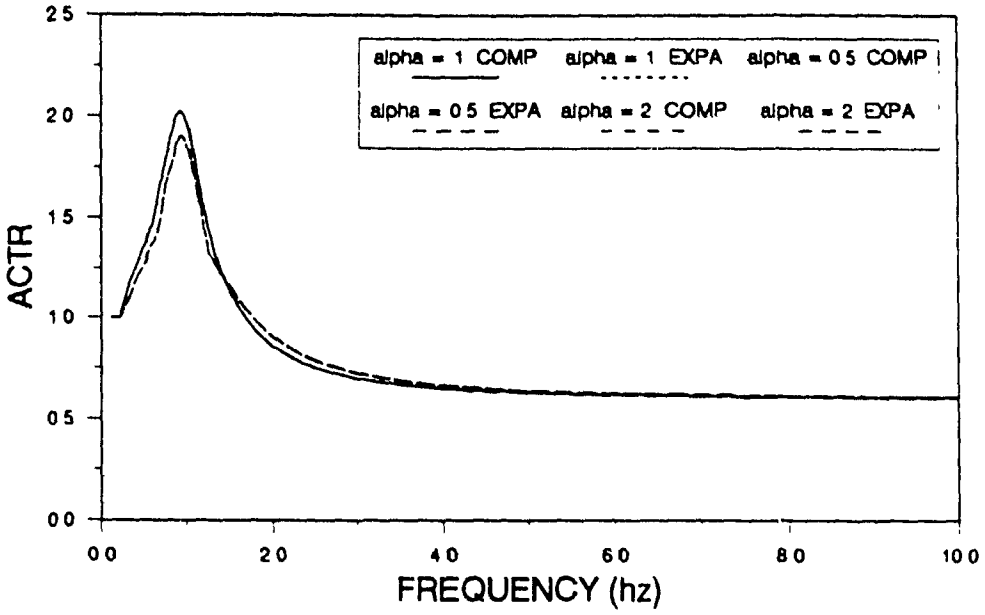

Figure 5.23 Influence of piston area ratio, α, on the compression and expansion mode ACTR responses of hydropneumatic suspension.

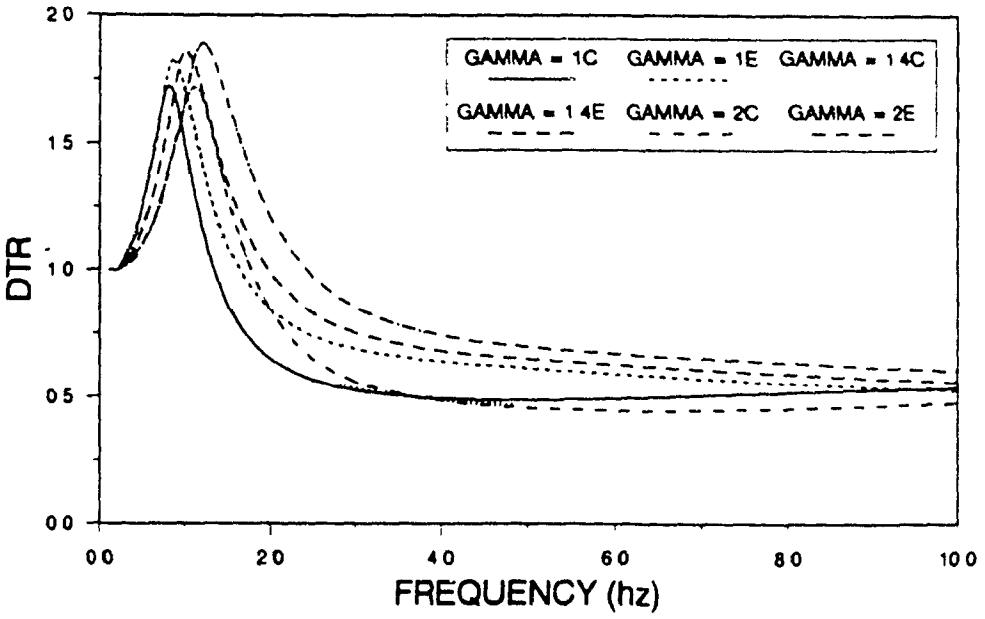

Figure 5.24 Influence of polytropic exponent, γ, on the compression and expansion mode DTR responses of hydropneumatic suspension.

value of γ. The corresponding DTR response during the expansion mode, however, increases with an increase in the value of γ over the entire frequency range. This behavior in the compression and expansion modes is due to the increased capacity of the gas spring to store energy as the polytropic exponent is increased.

The peak ACTR response, during compression and expansion modes, also increases as the value of γ increases, as shown in Figure 5.25. The ACTR response at higher excitation frequencies, however, remains unaffected by variations in the value of γ.

5.4.4 Initial Gas Volume

The initial gas volume determines the static and dynamic spring rate of the gas spring, and thus directly influences the shock and vibration isolation performance of the hydropneumatic suspension. The nominal initial gas volume, preset at the factory prior to static loading, is referred to as $V_{g1\phi}$. Parametric analysis is performed by selecting initial gas volumes of 50% and 200% of the nominal initial gas volume. Figures 5.26 and 5.27 present the DTR and ACTR response characteristics, respectively, in compression and expansion modes for three values of initial gas volume. An increase in the initial gas volume, $V_{g1\phi}$, yields a lower gas spring rate and thus a lower resonant frequency, as shown in Figures 5.26 and 5.27. The peak DTR response in the compression mode decreases when the value of $V_{g1\phi}$ is decreased. The DTR response in the expansion mode, however, increases with lower gas volume, as shown in Figure 5.26. At excitation frequencies beyond resonance, the variations in gas volume affect the DTR response in a considerable manner, as shown in Figure 5.26. A reduction in the gas volume causes high internal pressure and thus high damping. The

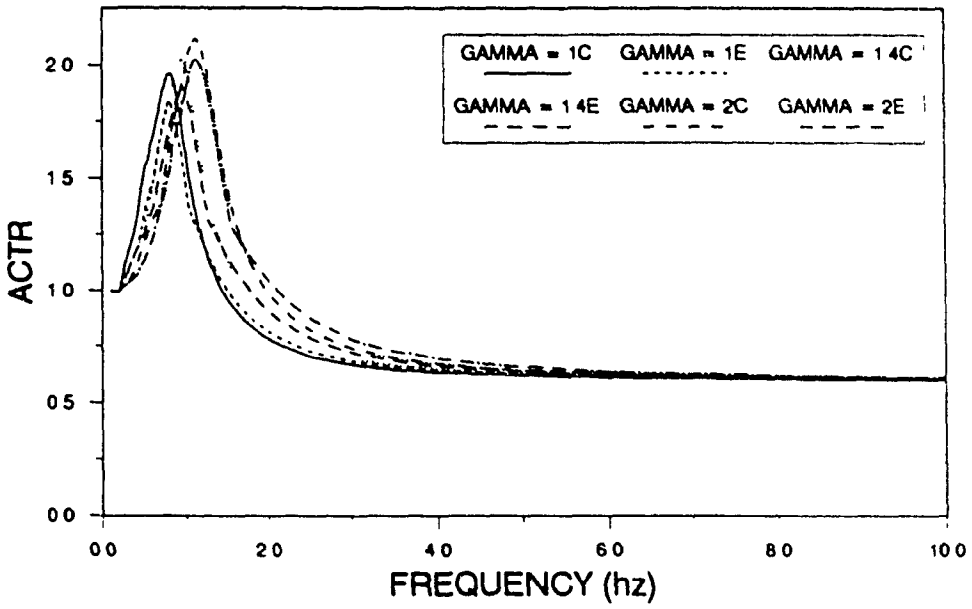

Figure 5.25 Influence of polytropic exponent, γ, on the compression and expansion mode ACTR responses of hydropneumatic suspension.

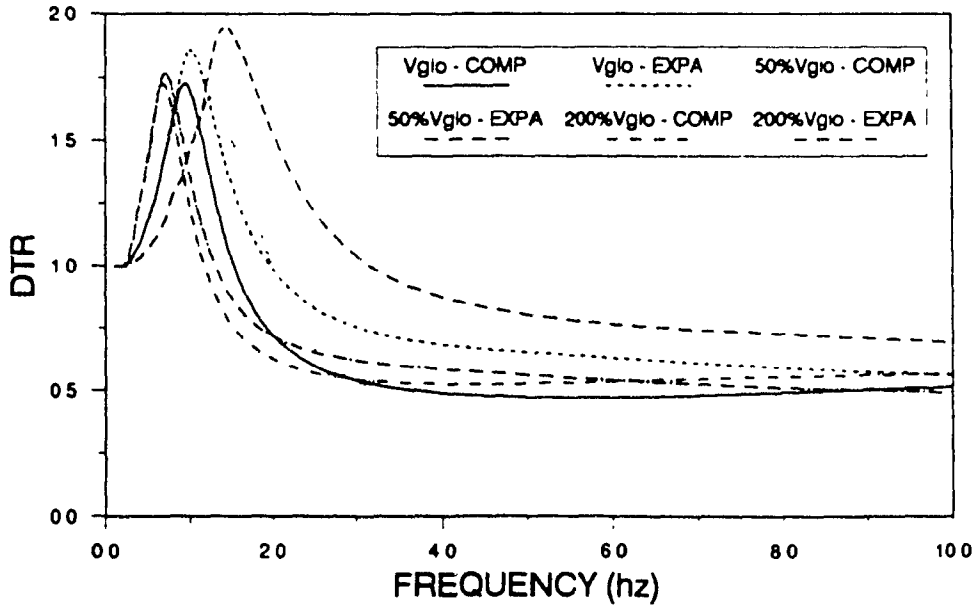

Figure 5.26 Influence of initial gas volume on the compression and expansion mode DTR responses of hydropneumatic suspension.

expansion mode transmissibility at higher frequencies, specifically, increases considerably when the gas volume is reduced.

The resonant frequency and the resonant ACTR response in the compression as well as the expansion mode increase considerably when the gas volume is decreased, as shown in Figure 5.27. At excitation frequencies well beyond the resonant frequency, the variations in initial gas volume have only negligible influence on the ACTR response. The compression and expansion mode response characteristics reveal a sharp increase in the magnitude at low excitation frequencies, when the gas volume is increased to 200%$V_{g1\phi}$. This sharp increase is caused by the lock-up due to friction force, which is relatively larger than the restoring force generated by the soft gas spring.

The shock displacement and acceleration response spectra of the hydropneumatic suspension are evaluated for a rounded step displacement excitation subject to different values of $V_{g1\phi}$. The results reveal that variations in initial gas charge volume have almost no effect on the peak SDR and SAR responses. The changes in initial gas volume, however, influence transient response characteristics such as rise time and settling time.

5.4.5 Initial Gas Charge Pressure

The initial gas charge pressure also strongly influences the force-deflection and force-velocity characteristics of the hydropneumatic suspension system. The shock and vibration isolation performance of the hydropneumatic system is investigated for various values of initial gas charge pressure, $P_{g1\phi}$, preset at the factory prior to static loading. Although the gas spring rate is directly related to the charge pressure, an increase in the charge pressure

yields a high static gas volume which, in turn, yields a softer spring. Consequently, the natural frequency of the suspension decreases when the precharge pressure, and resulting equilibrium volume, are increased.

The compression and expansion mode DTR response characteristics are presented in Figure 5.28 for three values of initial gas charge pressure: nominal pressure, $P_{g1\phi}$; 50% of nominal pressure, and 200% of nominal pressure. As the value of $P_{g1\phi}$ is increased, the peak expansion mode DTR response and corresponding resonant frequency decrease, whereas the peak compression mode DTR response increases very slightly. An increase in the initial gas pressure may tend to increase the static stiffness; however, this increase in static stiffness is compensated by the corresponding increase in gas volume. At excitation frequencies above the resonant frequency, the compression and expansion mode DTR response appear to converge gradually, regardless of the charge pressure.

Figure 5.29 presents the ACTR response characteristics in the compression and expansion modes for three values of initial gas pressure, $P_{g1\phi}$. The resonant frequency and peak ACTR response increase as the charge pressure decreases. This may be attributed to the resulting lower static gas volume and, thus, increased gas spring constant. The compression and expansion mode ACTR response, for 200% $P_{g1\phi}$, show an initial sharp rise at low frequency, due to lock-up associated with relatively high value of of static Coulomb friction force. The ACTR response characteristic in the compression and expansion modes, at higher excitation frequencies, quickly converge to a common value, regardless of the charge pressure.

The shock displacement and acceleration response spectra of the

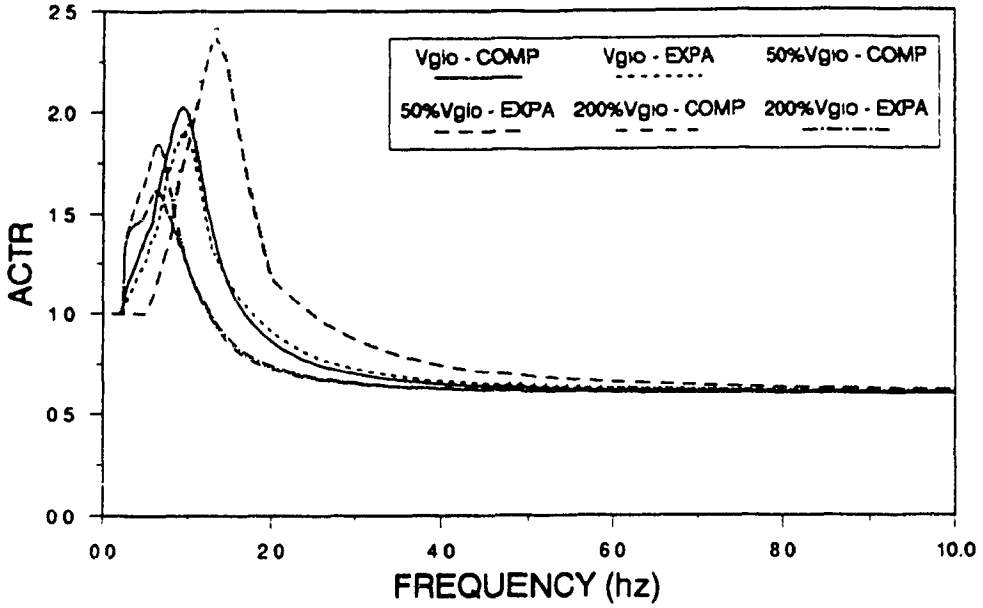

Figure 5.27 Influence of initial gas volume on the compression and expansion mode ACTR responses of hydropneumatic suspension.

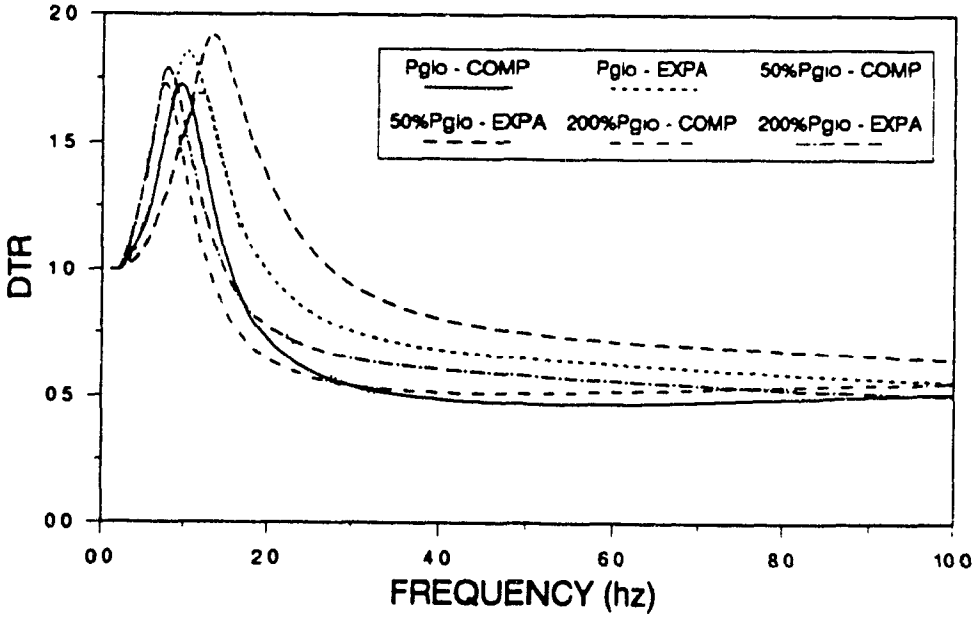

Figure 5.28 Influence of initial gas charge pressure of the compression and expansion mode DTR responses of hydropneumatic suspension.

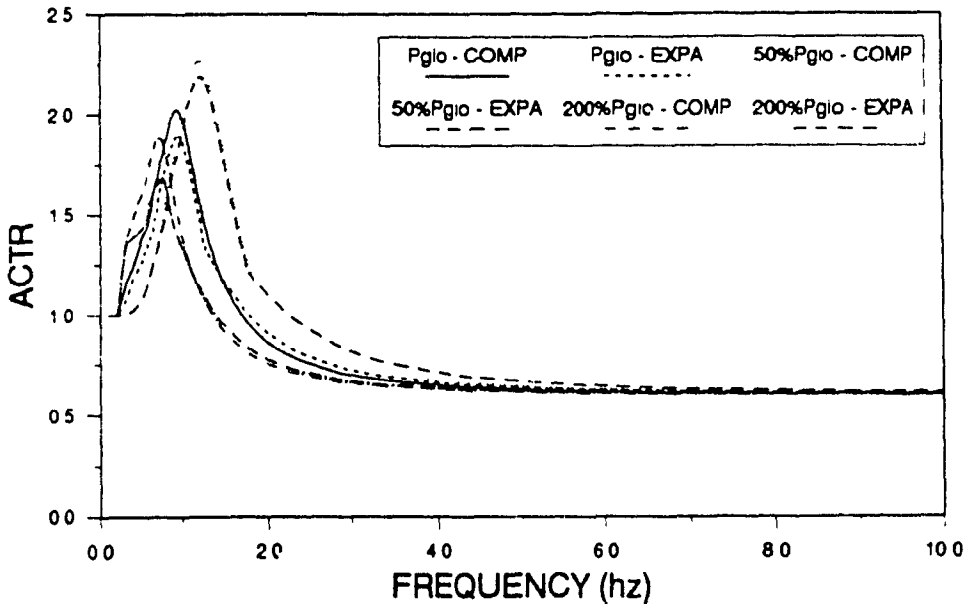

Figure 5.29 Influence of initial gas charge pressure on the compression and expansion mode ACTR responses of hydropneumatic suspension.

hydropneumatic suspension are evaluated for a rounded step and rounded pulse displacement excitations subject to different values of $P_{g1\phi}$. The results reveal that variations in the initial gas charge pressure have no significant effect on the SDR and SAR response characteristics, although the rise and settling times are influenced.

5.4.6 Highlights of the Parametric Sensitivity Analyses

The parametric sensitivity analyses of the nonlinear hydropneumatic suspension system, presented in this study, consider two types of parameters: system design parameters, such as piston area ratio, initial gas pressure, and initial gas volume, and operating parameters, including polytropic gas exponent and fluid bulk modulus. The variations in polytropic gas constant and bulk modulus are often caused by the operating conditions, and cannot be controlled during the design and manufacturing stages. These parameters can vary considerably over the life and application environment of the suspension system.

The analyses are performed to study the influence of variations in design and operating parameters on the shock and vibration isolation characteristics, such as SDR, SAR, DTR and ACTR. The analyses revealed that the most significant system design parameters are $P_{g1\phi}$ and $V_{g1\phi}$, and the significant operating parameter is γ. The results of the single parameter sensitivity study indicate that improved vibration isolation performance can be achieved through low values of $P_{g1\phi}$ and γ , and a high value of $V_{g1\phi}$. The study, however, cannot conclude on the influence of simultaneous variations in two or more parameters. The parametric analyses also revealed that the peak values of SDR and SAR response to rounded pulse and step excitations are not significantly influenced by variations in the selected parameters. The response characteristics,

such as rise and settling times and oscillation frequency, however, are influenced by changes in these parameters.

5.5 SUMMARY

In this chapter, the shock and vibration isolation performance of the hydropneumatic suspension models, developed in Chapters 2 and 3, are investigated. The hydropneumatic suspension models investigated include nonlinear model with incompressible hydraulic fluid, nonlinear model with compressible hydraulic fluid, and local linear equivalent model. The shock isolation performance is investigated in the time domain for rounded step and rounded pulse displacement excitations. Vibration isolation performance of the nonlinear suspension models are evaluated using numerical integration in conjunction with frequency sweep, and local equivalent linearization techniques.

Parametric sensitivity analyses are performed to investigate the effects of piston area ratio, initial gas charge pressure, initial gas volume, polytropic exponent, and fluid bulk modulus. The parametric sensitivity analyses reveal that variations in individual parameters $P_{g1\phi}$, $V_{g1\phi}$, and γ have the most significant effects on the vibration isolation performance of the hydropneumatic suspension system. SDR and SAR response characteristics revealed that variations in α, $P_{g1\phi}$, $V_{g1\phi}$ and γ do not have a significant influence on the shock isolation performance. The SDR and SAR response characteristics, however, are strongly affected by reduction in the effective bulk modulus of the fluid.

CHAPTER 6

TRACKED VEHICLE RIDE PERFORMANCE ANALYSIS

6.1 GENERAL

The unique characteristics of the hydropneumatic suspension system demonstrate potential for improving the ride comfort and handling control of ground vehicles. These characteristics include a low natural frequency, nonlinear progressively stiffening spring rate, light weight and compact design, and the ability to provide ride height control. The low natural frequency of the hydropneumatic suspension system presents the greatest potential for improved ride quality. This is particularly important since the human body is most fatigue sensitive to vibrations occurring in the low frequency range, between 2 - 8 Hz.

The nonlinear rising rate, or stiffening, spring characteristic of the hydropneumatic suspension provides potential benefits for both ride comfort and handling control. The progressively increasing restoring force, due to rising rate spring characteristic, prevents excessive suspension travel and, thus, impacts with the vehicle chassis. Consequently, the hydropneumatic suspension is able to generate progressive control forces and amortize shocks as it negotiates severe terrain irregularities. Further, the rising rate spring characteristics of the hydropneumatic suspension offer the potential to achieve nearly constant natural frequency under various loading conditions, by varying the gas spring parameters during the design stage.

The ride comfort potentials of the hydropneumatic suspension are investigated via computer simulation of the tracked military vehicle

model presented in Chapter 4. The shock and vibration isolation performance of the tracked vehicle, equipped with both the conventional and hydropneumatic suspension, are investigated. The conventional suspension comprises a linear torsion bar spring at each trailing arm, and an inclined hydraulic shock absorber located only at the first and last trailing arms. In the hydropneumatic suspension configuration, hydropneumatic suspension units are mounted, in an inclined manner identical to the hydraulic shock absorbers, at the first and last trailing arms, while the trailing arms 2, 3 and 4 are equipped with linear torsion bar springs. The parameters of the hydropneumatic gas spring are selected such that the static stiffness of the hydropneumatic suspension is the same as the linear spring rate of the torsion bar spring. The hydropneumatic suspension, however, provides nonlinear orifice damping, while the conventional suspension provides dual-phase damping characteristics due to bleed and blow-off control as shown in Figure 4.3.

6.2 FREQUENCY RESPONSE CHARACTERISTICS OF THE TRACKED VEHICLE MODEL

The ride performance characteristics of the tracked vehicle model, equipped with hydropneumatic and conventional suspension systems, are investigated via frequency response analysis. The frequency response characteristics are presented in terms of vertical displacement, vertical acceleration and pitch transmissibility response at the hull c.g., and vertical displacement transmissibility response of road wheels 1, 3 and 5, expressed as:

$$\text{Vertical displacement transmissibility of hull c.g.} = \frac{|\, y_h \,|}{|\, y_o \,|}$$

$$\text{Vertical acceleration transmissibility of hull c.g.} = \frac{|\ddot{y}_h|}{|\ddot{y}_o|}$$

$$\text{Pitch displacement transmissibility about hull c.g.} = \frac{|\phi_h|}{|y_o|}$$

$$\text{Pitch acceleration transmissibility about hull c.g.} = \frac{|\ddot{\phi}_h|}{|y_o|}$$

$$\text{Vertical displacement transmissibility of road wheel 'i'} = \frac{|y_{wi}|}{|y_o|}$$

The vibration transmissibility characteristics of the tracked vehicle model are obtained via direct numerical integration in the time domain employing a frequency sweep technique for identical harmonic excitations at each road wheel.

6.3 RIDE PERFORMANCE POTENTIALS OF HYDROPNEUMATIC SUSPENSION

Figures 6.1 through 6.7 present a comparison of the frequency response characteristics of the tracked vehicle models equipped with hydropneumatic and conventional suspension systems. The vertical displacement response at the hull c.g. of the tracked vehicles equipped with hydropneumatic and conventional suspensions are presented in Figure 6.1. The comparison of the frequency response characteristics reveals that the hydropneumatic suspension yields considerably lower transmissibility in the 1-2 Hz excitation frequency range. The peak response in this frequency range corresponds to the bounce and pitch resonances of the vehicle hull [34]. The frequency response of the vehicle equipped with hydropneumatic suspension is also lower than that

with the conventional suspension system at excitation frequencies above 7.5 Hz.

Figure 6.2 compares the vertical acceleration response characteristics of the tracked vehicles equipped with both hydropneumatic and conventional suspensions. The hydropneumatic suspension provides a considerably lower resonant response, and slightly larger response in the frequency range of 2.5-10 Hz, when compared to that of the conventional suspension.

Figures 6.3 and 6.4 illustrate the pitch displacement and acceleration response characteristics of the tracked vehicles, equipped with hydropneumatic and conventional suspensions. The hydropneumatic suspension suppresses the resonant peaks considerably; the peak pitch displacement response of the hydropneumatic suspension is approximately 0.2 rad/m, while that of the conventional suspension is 1.9 rad/m. The hydropneumatic suspension continues to yield lower pitch displacement transmissibility at higher excitation frequencies. The pitch acceleration response of the hydropneumatic suspension at higher excitation frequencies, corresponding to road wheel resonance, however, is larger than that of the conventional suspension, as shown in Figure 6.4.

The bounce displacement transmissibilities of the first, third and fifth road wheels are presented in Figures 6.5, 6.6 and 6.7, respectively. The displacement transmissibility of these three road wheels, corresponding to the hull resonant frequencies, is considerably small when the vehicle equipped with hydropneumatic suspension. The bounce response of the first and last road wheels of the vehicle equipped with hydropneumatic suspension is also significantly lower at

higher frequencies, (road wheel resonance), when compared to that with conventional suspension. The road wheel bounce resonant frequencies occur between 9 and 14 Hz, and the hydropneumatic suspension at the first and last road wheels virtually eliminates these resonant peaks, as shown in Figures 6.5 and 6.7 respectively. In the absence of a damped suspension, the bounce transmissibility of the third road wheel exhibits high transmissibility response corresponding to hull and road wheel resonant frequencies, when the vehicle is equipped with conventional suspension. However, the resonant peak corresponding to the hull resonance is almost attenuated when hydropneumatic suspension is employed. The hydropneumatic suspension, however, yields high transmissibility corresponding to road wheel resonances, similar to the conventional suspension, as shown in Figure 6.6.

Figures 6.1 through 6.7 clearly illustrate that the hydropneumatic suspension provides considerably superior vibration isolation, specifically in the low excitation frequencies to which the human body is most fatigue sensitive, as compared to the conventional suspension configuration.

6.4 TRANSIENT RESPONSE OF THE TRACKED VEHICLE MODEL

Transient response characteristics of the tracked vehicle model with hydropneumatic and conventional suspensions are investigated for discrete obstacles described in Chapter 3. The transient response behaviour is evaluated when the vehicle traverses a semi-circular bump at a constant forward speed. The response characteristics of the hydropneumatic and conventional suspension systems are presented in terms of the following ratios:

$$\text{Hull c.g. bounce displacement response} = \frac{(y_h)_{peak}}{r_B}$$

$$\text{Hull c.g. bounce acceleration response} = \frac{(\ddot{y}_h)_{peak}}{r_B}$$

$$\text{Pitch deflection response ratio} = \frac{(\phi_h)_{peak}}{r_B}$$

$$\text{Pitch acceleration response ratio} = \frac{(\ddot{\phi}_h)_{peak}}{r_B}$$

$$\text{Bounce displacement response of road wheel 'i'} = \frac{(y_{wi})_{peak}}{r_B}$$

The transient response of the vehicle is evaluated for two different vehicle speeds, (4.17 m/s and 6.94 m/s), and two bump radii (0.2032 m and 0.3048 m). The results, presented in Figures 6.8 through 6.49, are discussed in view of the above response ratios.

The transient vertical displacement response characteristics at the hull c.g., due to a 0.2032 m semi-circular bump excitation at 4.17 m/s, are presented in Figure 6.8. The hull experiences large vertical displacements as the vehicle negotiates the bump, and the hull oscillates at its resonant frequency regardless of suspension configuration. The vertical displacement response gradually decays as the vehicle traverses past the obstacle. Although the transient response characteristics of the hydropneumatic suspension are quite similar to those of the conventional suspension, the peak amplitudes of oscillations of the hydropneumatic suspension are slightly lower than that of the conventional suspension. Figure 6.9 illustrates the transient vertical displacement response at the hull c.g. when the vehicle traverses a 0.3048 m bump at a constant forward speed of 4.17

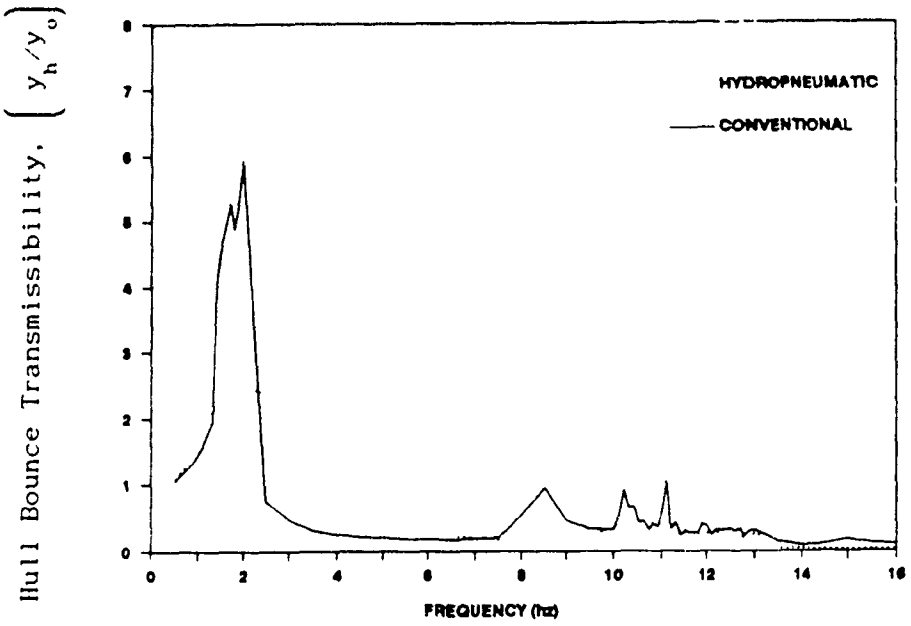

Figure 6.1 Comparison of hull c.g. bounce transmissibilities of the tracked vehicle equipped with hydropneumatic and conventional suspension configurations.

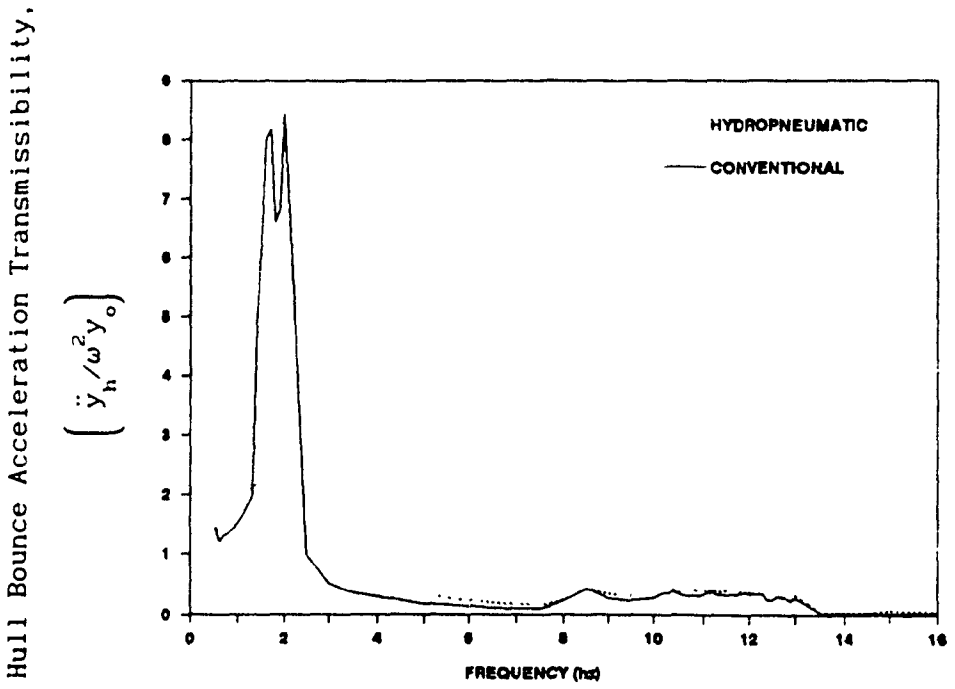

Figure 6.2 Comparison of hull c.g. bounce acceleration transmissibilities of the tracked vehicle equipped with hydropneumatic and conventional suspension configurations.

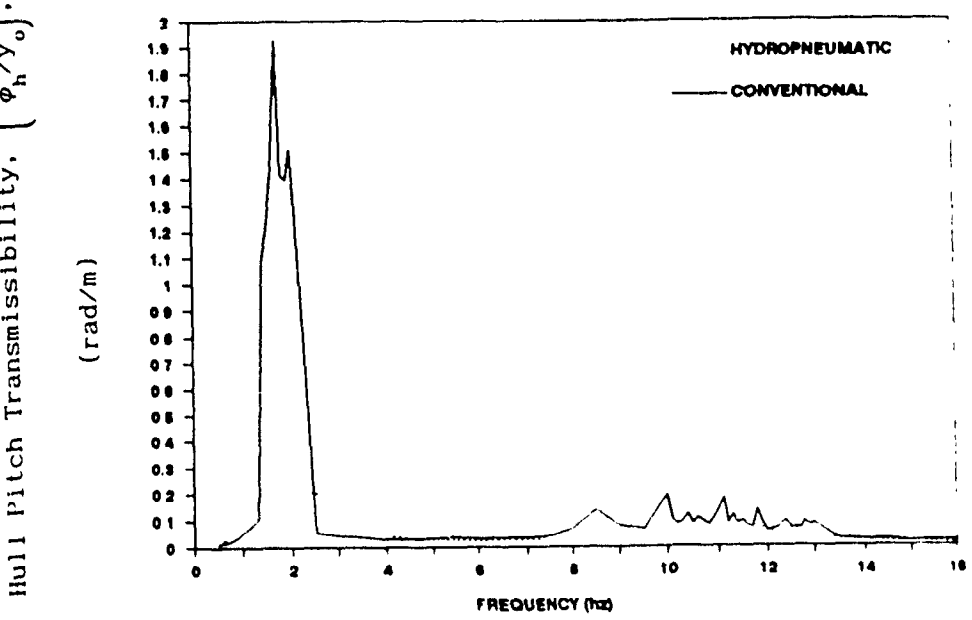

Figure 6.3 Comparison of hull c.g. pitch transmissibilities of the tracked vehicle equipped with hydropneumatic and conventional suspension configurations.

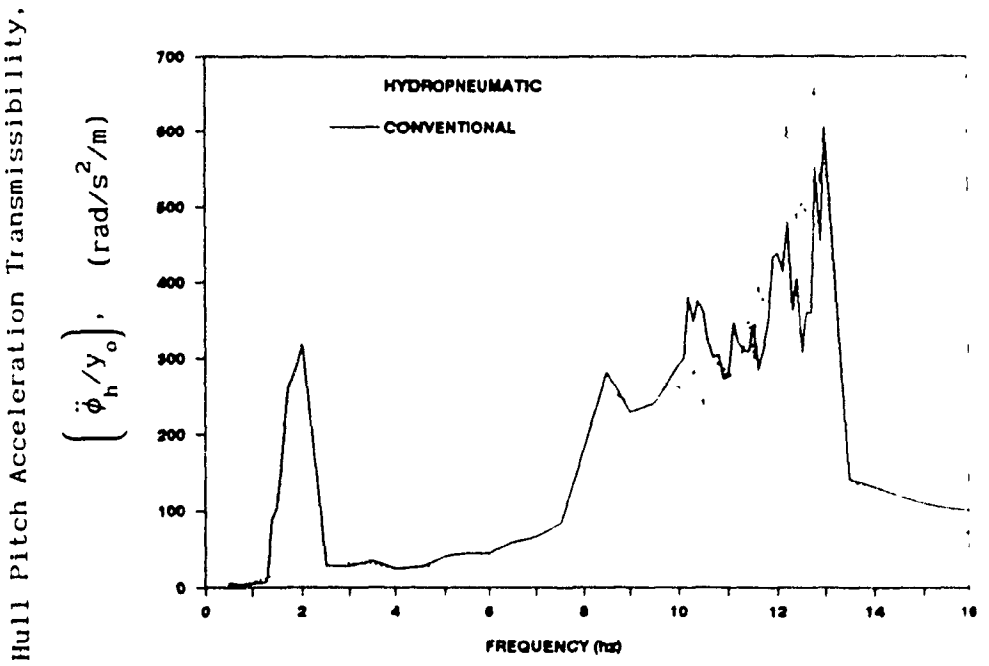

Figure 6.4 Comparison of hull c.g. pitch acceleration transmissibilities of the tracked vehicle equipped with hydropneumatic and conventional suspension configurations.

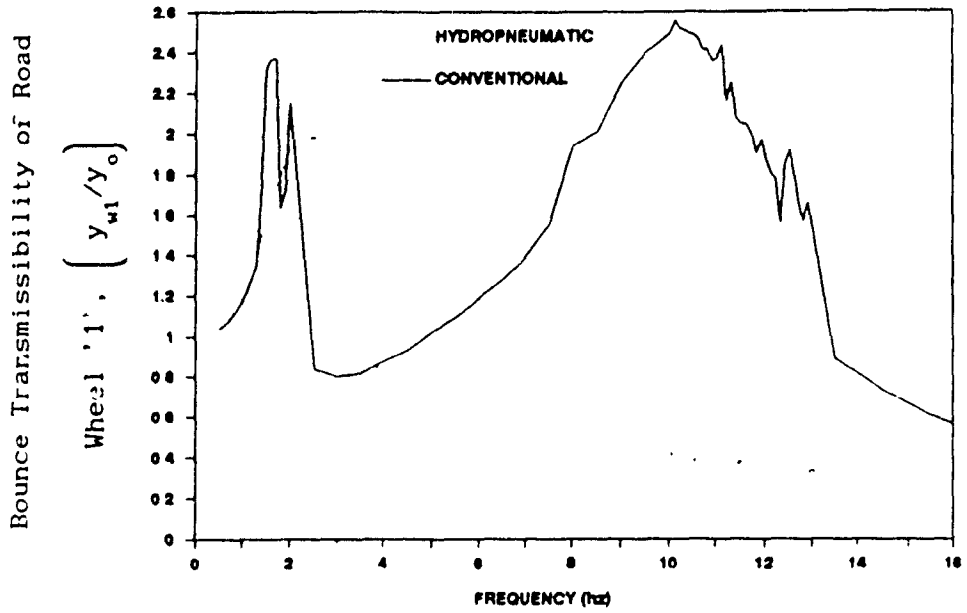

Figure 6.5 Comparison of road wheel #1 bounce transmissibilities of the tracked vehicle equipped with hydropneumatic and conventional suspension configurations.

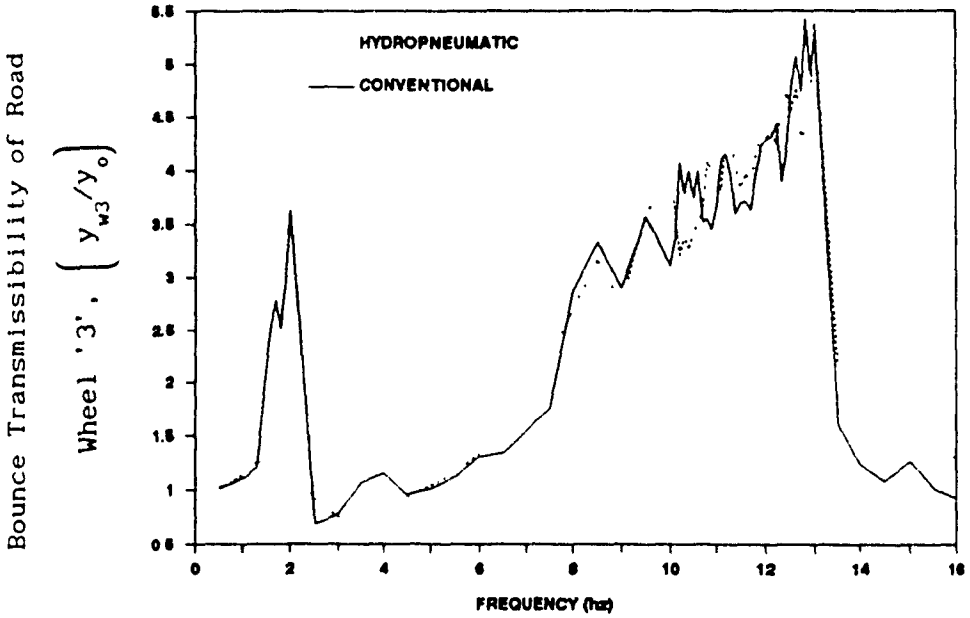

Figure 6.6 Comparison of road wheel #3 bounce transmissibilities of the tracked vehicle equipped with hydropneumatic and conventional suspension configurations.

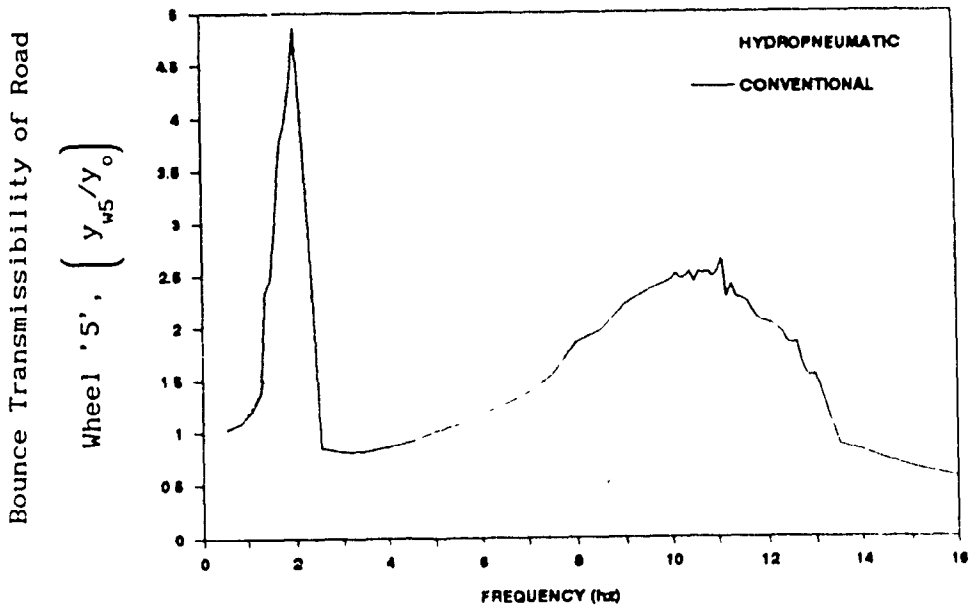

Figure 6.7 Comparison of road wheel #5 bounce transmissibilities of the tracked vehicle equipped with hydropneumatic and conventional suspension configurations.

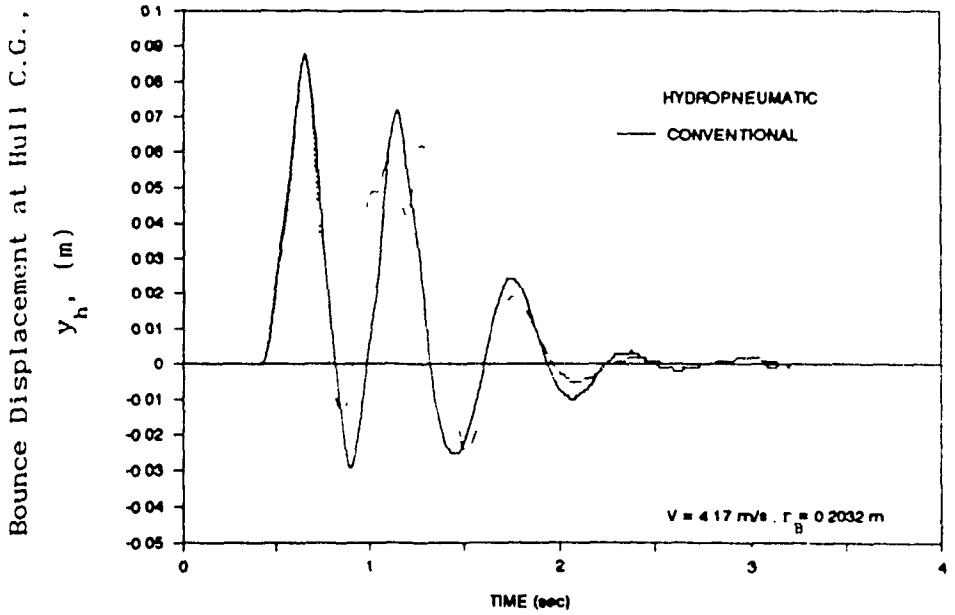

Figure 6.8 Comparison of hull c.g. bounce responses of tracked vehicle equipped with hydropneumatic and conventional suspension configurations when traversing 0.2032 m bump at 4.17 m/s

m/s. The two suspensions yield identical response, initially, as shown in the figure. The transient response of the vehicle equipped with hydropneumatic suspension, however, decays quite rapidly when compared to that of the vehicle equipped with the conventional suspension. Rapid decay of the bounce response, of the vehicle equipped with hydropneumatic suspension, is due to the superior bounce control of the first and last road wheels. Figure 6.10 presents a comparison of peak hull bounce displacement response ratios of hydropneumatic and conventional suspension for 0.2032 m and 0.3048 m bump excitations. The hydropneumatic suspension yields a slightly higher peak response than the conventional suspension, when traversing the smaller 0.2032 m bump; however, the peak response of hydropneumatic suspension is considerably smaller when the vehicle traverses the large 0.3048 m bump.

The bounce acceleration response at the hull c.g. of the tracked vehicles traversing the 0.2032 m and 0.3048 m bumps, are presented in Figures 6.11 and 6.12, respectively. Both the conventional and hydropneumatic suspension systems yield similar hull c.g. acceleration response when traversing a 0.2032 m bump, as shown in Figure 6.11. The acceleration response of the vehicle equipped with hydropneumatic suspension, however, is considerably lower than that of the vehicle equipped with conventional suspension when traversing the 0.3048 m bump, as shown in Figure 6.12. The hydropneumatic suspension initially yields acceleration response similar to that of conventional suspension; however, the acceleration response settles at a faster rate. Figure 6.13 compares the peak acceleration response at the hull c.g. of the vehicles equipped with conventional and hydropneumatic suspension traversing the two different bumps at 4.17 m/s. The figure clearly illustrates that the

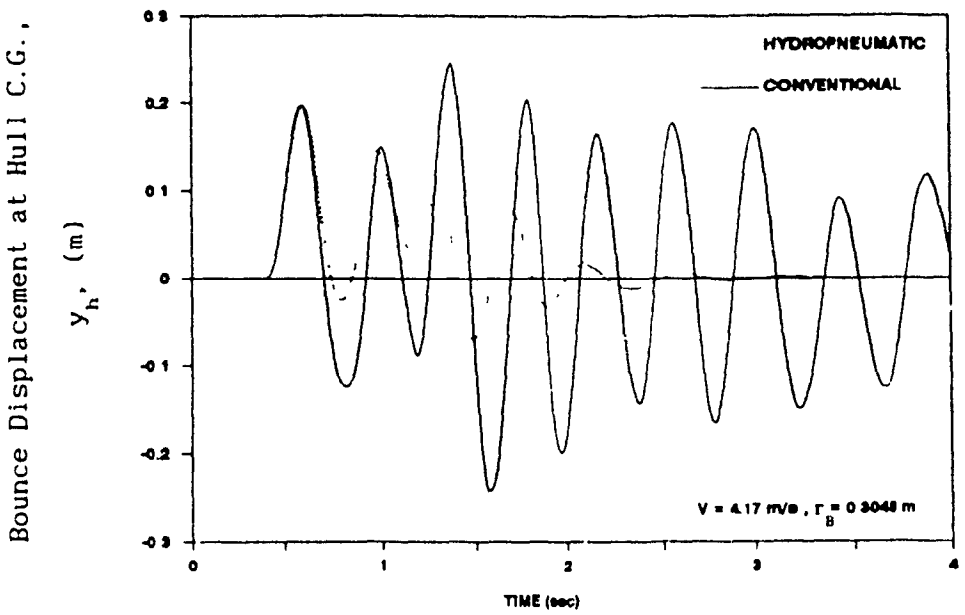

Figure 6.9 Comparison of hull c.g. bounce responses of tracked vehicle equipped with hydropneumatic and conventional suspension configurations when traversing the 0.3048 m bump at 4.17 m/s.

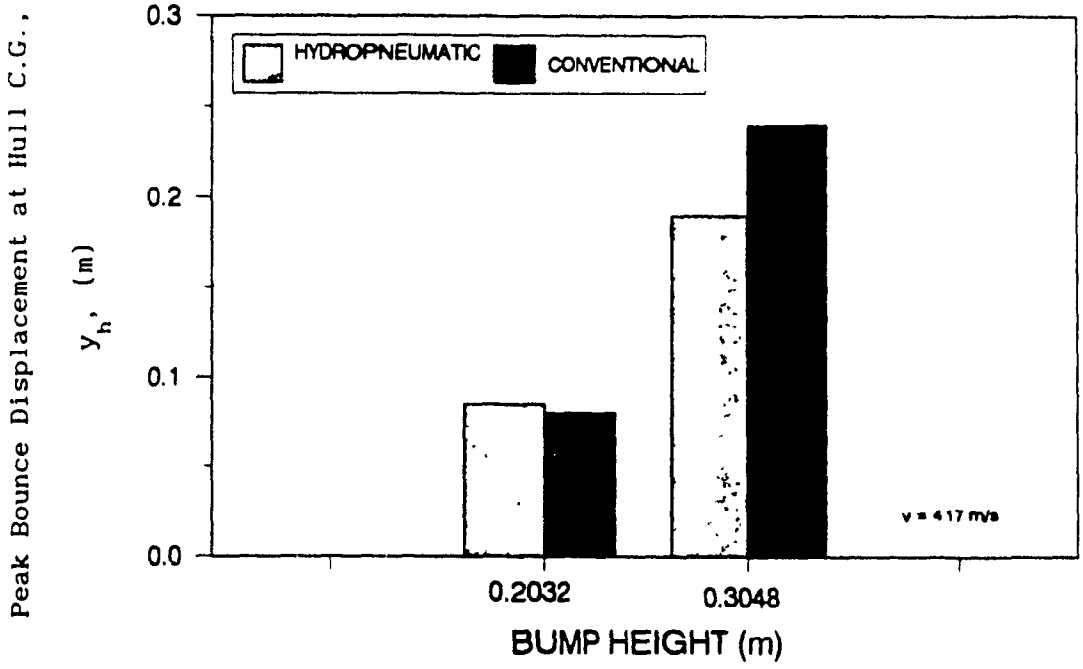

Figure 6.10 Comparison of peak hull c.g. bounce response of tracked vehicle equipped with hydropneumatic and conventional suspension configurations when traversing bumps at 4.17 m/s.

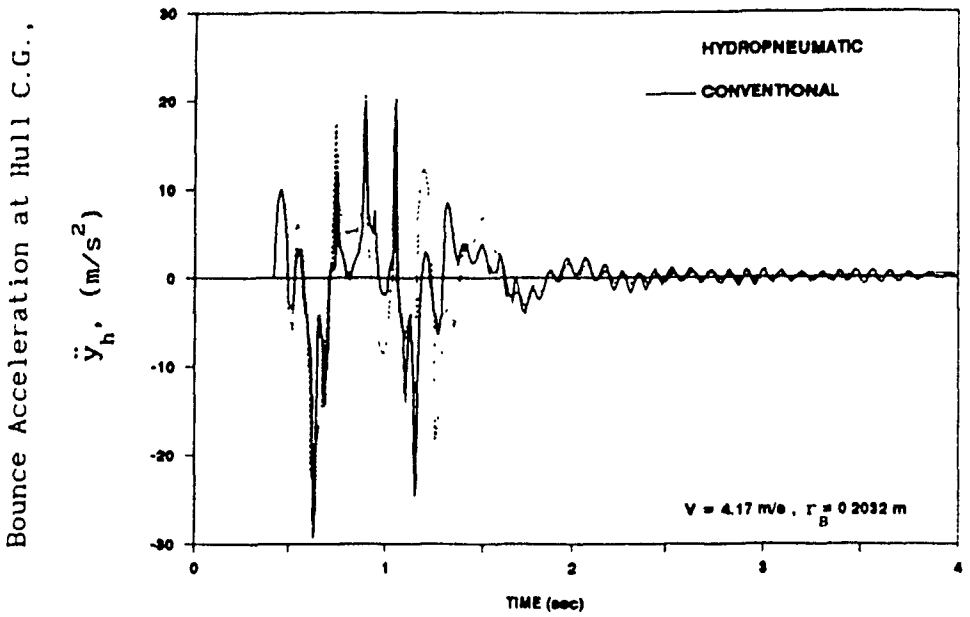

Figure 6.11 Comparison of hull c.g. bounce acceleration responses of the tracked vehicle equipped with hydropneumatic and conventional suspension configurations when traversing the 0.2032 m bump at 4.17 m/s.

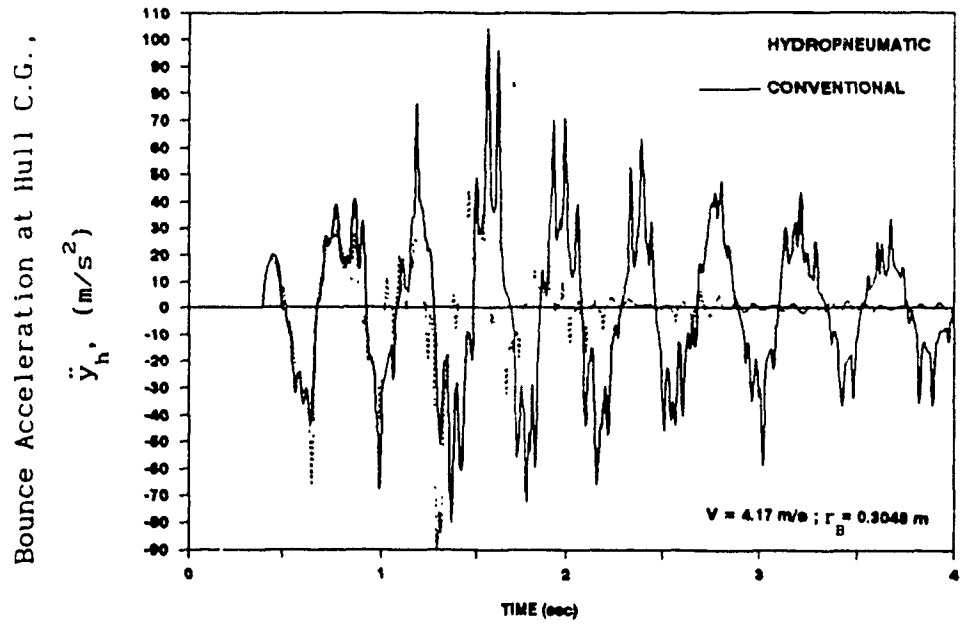

Figure 6.12 Comparison of hull c.g. bounce acceleration responses of tracked vehicle equipped with hydropneumatic and conventional suspension configurations when traversing the 0.3048 m bump at 4.17 m/s.

hydropneumatic suspension yields lower peak acceleration at the hull c.g. for both sizes of bump excitation.

Figures 6.14 and 6.15, respectively, present the pitch deflection response about the hull c.g. of the tracked vehicles, equipped with conventional and hydropneumatic suspension, traversing the 0.2032 m and 0.3048 m bumps at 4.17 m/s. The two vehicles yield similar pitch response when traversing the 0.2032 m bump as shown in Figure 6.14. The pitch response of the conventional suspension vehicle, however, tends to settle faster than the hydropneumatic suspension vehicle. The pitch response of the vehicle equipped with hydropneumatic suspension, however, is considerably lower than that of the vehicle equipped with conventional suspension, as shown in Figure 6.15. The pitch response of the vehicle with hydropneumatic suspension settles down at approximately 2.5 s, while the pitch response of the conventional suspension continues to oscillate beyond 4 s. A comparison of the peak values of pitch displacement response ratios of the two suspensions, presented in Figure 6.16, reveals that the hydropneumatic suspension continues to out perform the conventional suspension for high amplitude bump excitations. The superior ride performance of the hydropneumatic suspension is attributed to the progressively stiffening gas spring characteristic. The nature of the gas spring permits shock energy to be quickly stored resulting in smaller suspension relative displacements and velocities.

Figures 6.17 and 6.18 present the comparison at 4.17 m/s constant forward vehicle speed of hull pitch acceleration response of the tracked vehicles, equipped with hydropneumatic and conventional suspensions, for 0.2032 m and 0.3048 m bump excitation, respectively. Both the tracked vehicles exhibit similar pitch acceleration response when negotiating

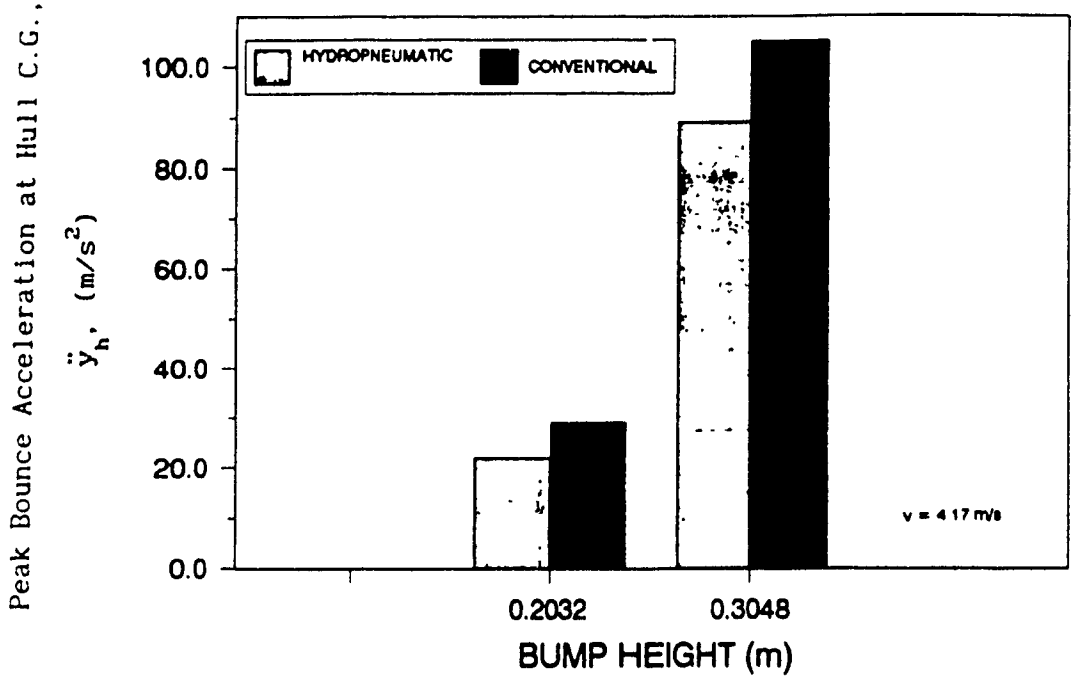

Figure 6.13 Comparison of peak hull c.g. bounce acceleration responses of the tracked vehicle equipped with hydropneumatic and conventional suspension configurations when traversing bumps at 4.17 m/s.

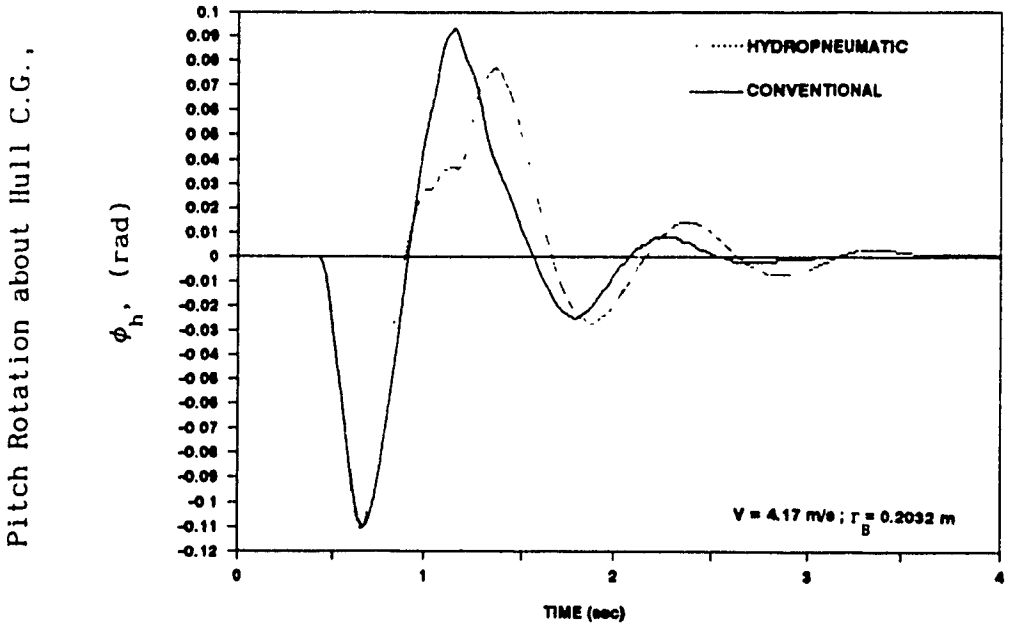

Figure 6.14 Comparison of hull c.g. pitch responses of the tracked vehicle equipped with hydropneumatic and conventional suspension configurations when traversing the 0.2032 m bump at 4.17 m/s.

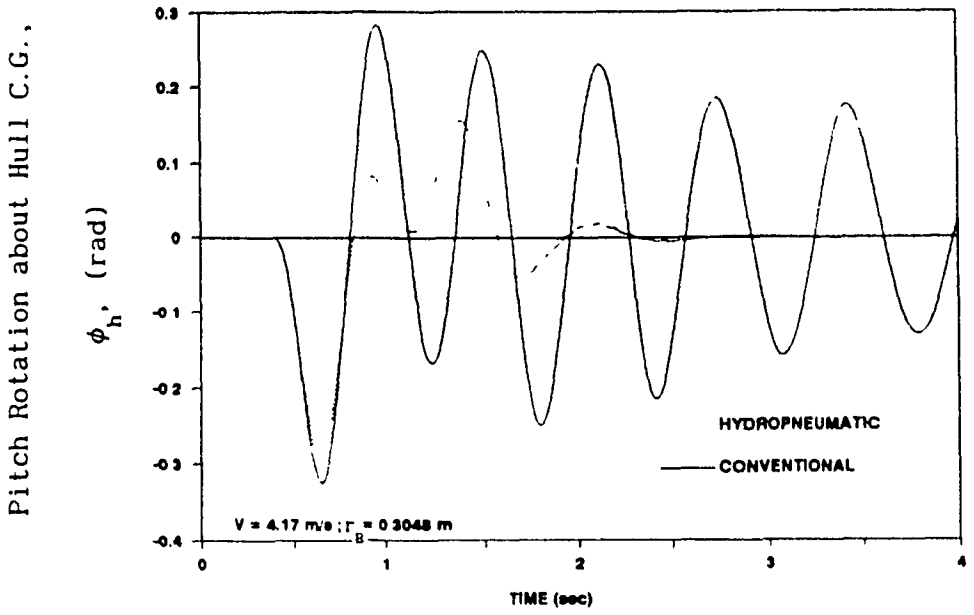

Figure 6.15 Comparison of hull c.g. pitch responses of the tracked vehicle equipped with hydropneumatic and conventional suspension configurations when traversing the 0.3048 m bump at 4.17 m/s.

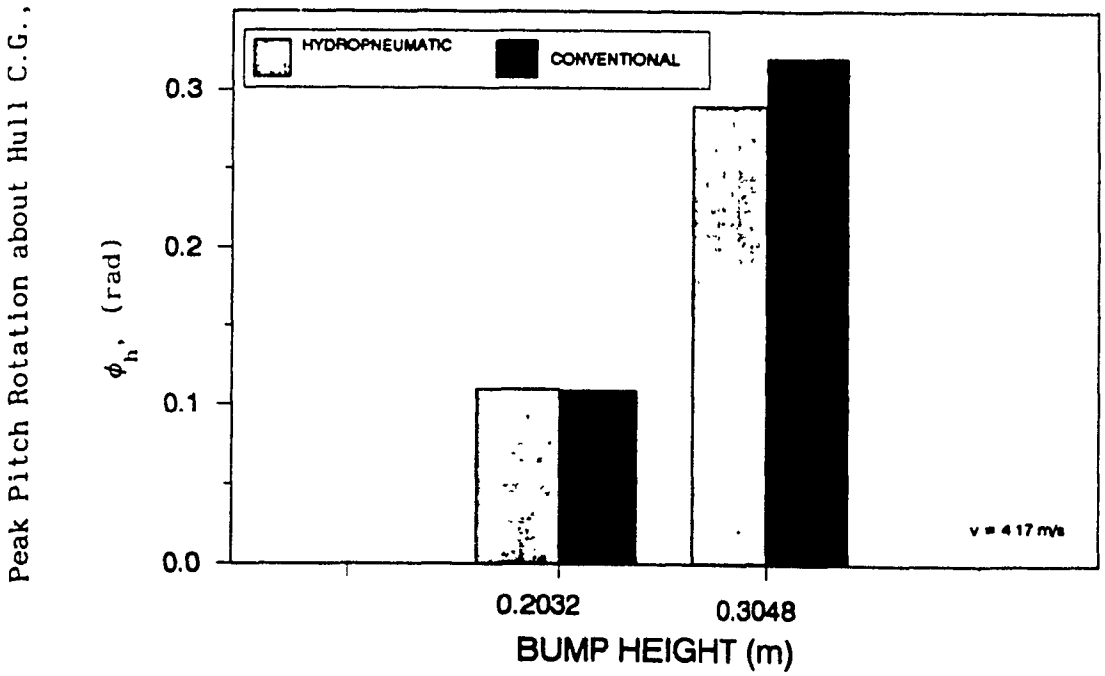

Figure 6.16 Comparison of peak hull c.g. pitch responses of the tracked vehicle model equipped with hydropneumatic and conventional suspension configurations when traversing bumps at 4.17 m/s.

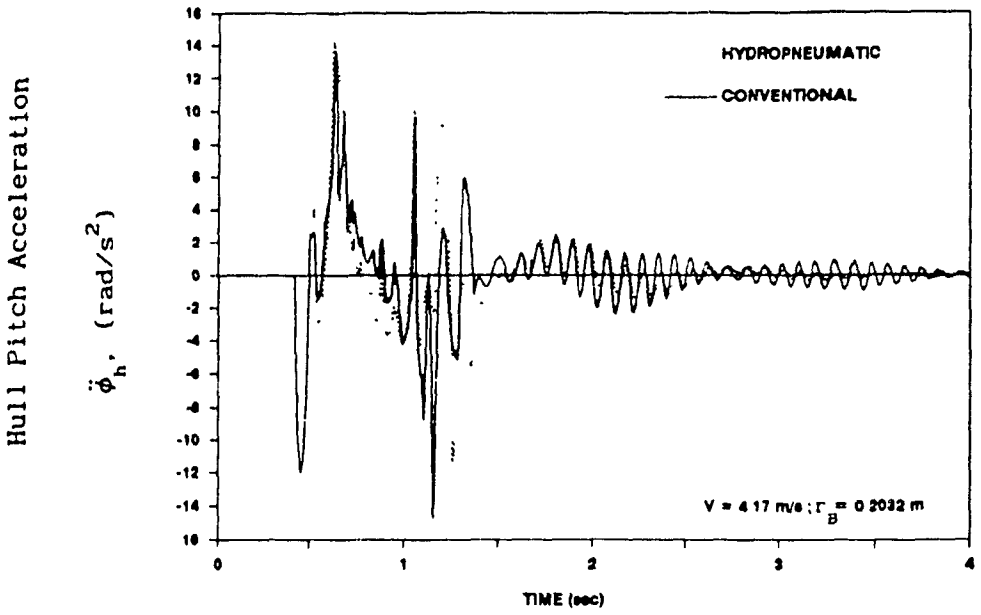

Figure 6.17 Comparison of hull c.g. pitch acceleration responses of the tracked vehicle equipped with hydropneumatic and conventional suspension configurations when traversing the 0.2032 m bump at 4.17 m/s.

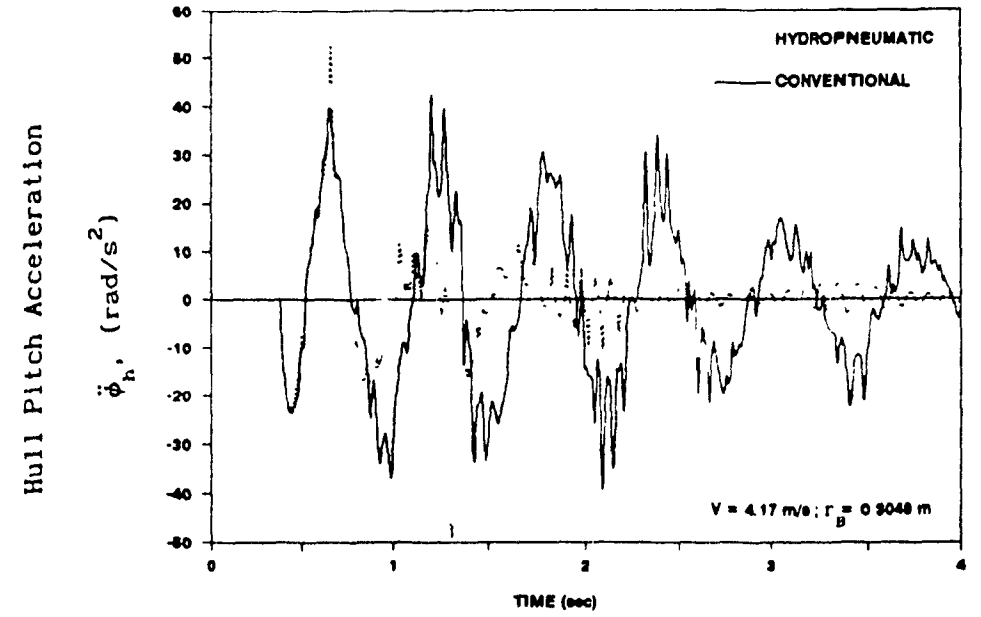

Figure 6.18 Comparison of hull c.g. pitch acceleration responses of the tracked vehicle equipped with hydropneumatic and conventional suspension configurations when traversing the 0.3048 m bump at 4.17 m/s.

the 0.2032 m semi-circular bump, as shown in Figure 6.17. The tracked vehicle with hydropneumatic suspension, however, exhibits significantly higher pitch acceleration peaks compared to those of the vehicle with conventional suspension, as shown in Figure 6.18, when traversing the 0.3048 m bump at 4.17 m/s. The pitch acceleration response of the vehicle with hydropneumatic suspension settles at a much higher rate than that of the vehicle with conventional suspension. Further, Figure 6.19 compares the peak pitch acceleration response of the vehicles traversing the two bumps. Although the peak pitch acceleration response of the hydropneumatic suspension is almost identical to that of the conventional suspension for the small bump, the conventional suspension provides significantly lower peak pitch acceleration when traversing the 0.3048 m bump.

The vertical displacement response of the first and last road wheels of the tracked vehicles, equipped with hydropneumatic and conventional suspensions, negotiating a 0.2032 m semi-circular bump at a speed of 4.17 m/s, are presented in Figures 6.20 and 6.21, respectively. The first road wheel exhibits peak displacement near 0.6 s, and peak response of hydropneumatic suspension is considerably lower than that of the conventional suspension, as shown in Figure 6.20. The displacement response of the last road wheel is quite similar to that of the first road wheel, except that the peak response occurs near 1.2 s. The displacement response of the first and last road wheels increases considerably, regardless of suspension type, when the bump height is increased to 0.3048 m, as shown in Figures 6.22 and 6.23. The displacement response of the first road wheel, of the vehicle equipped with hydropneumatic suspension, is initially similar to that of the

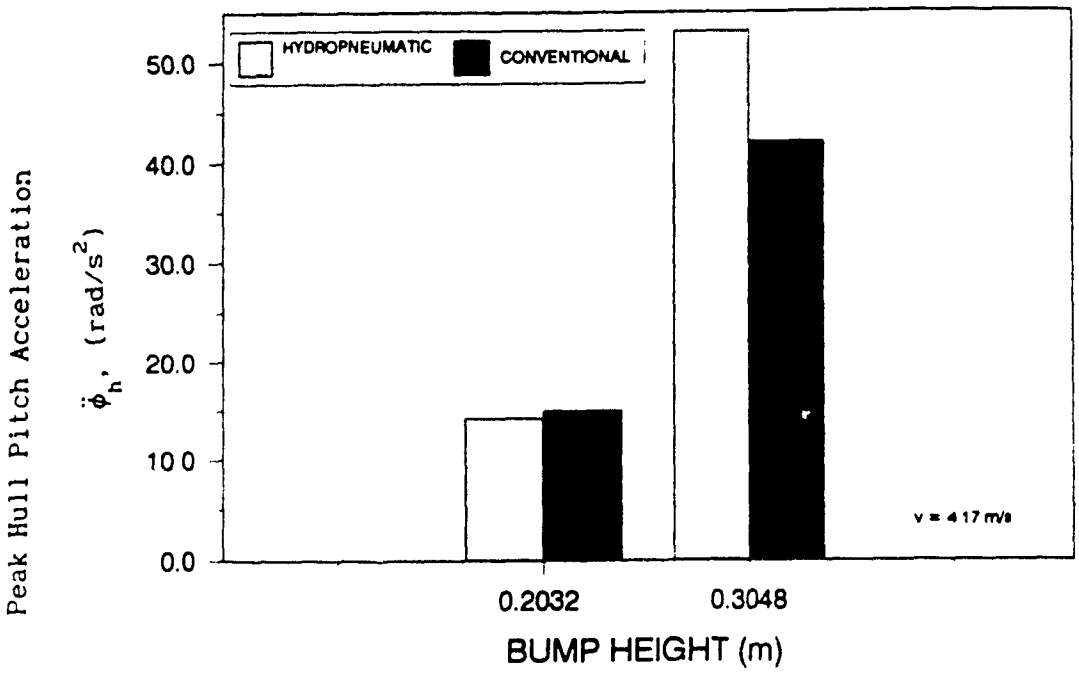

Figure 6.19 Comparison of peak hull c.g. pitch acceleration responses of the tracked vehicle equipped with hydropneumatic and conventional suspension configurations when traversing bumps at 4.17 m/s.

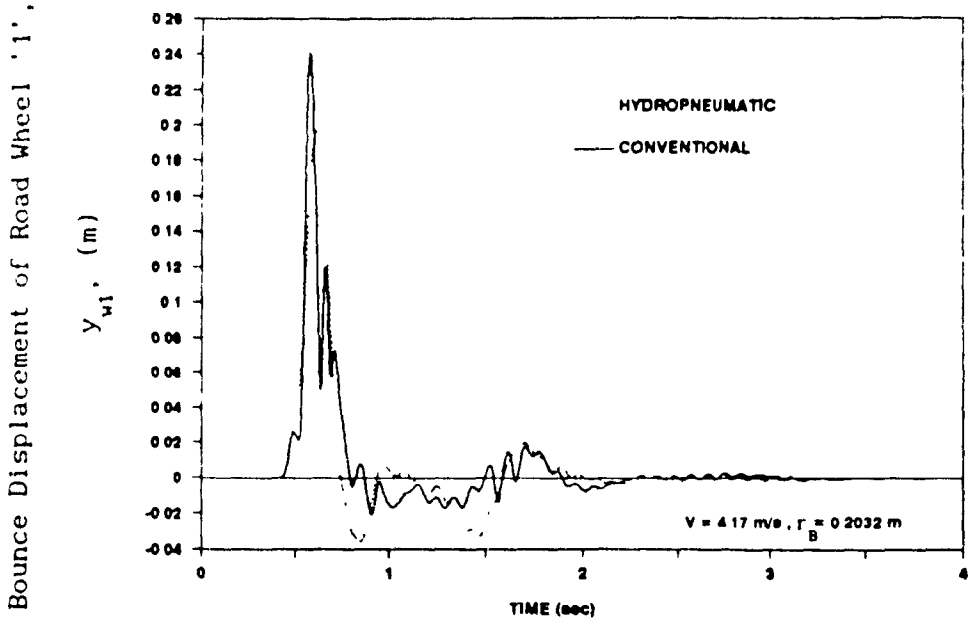

Figure 6.20 Comparison of road wheel #1 bounce responses of the tracked vehicle equipped with hydropneumatic and conventional suspension configurations when traversing the 0.2032 m bump at 4.17 m/s.

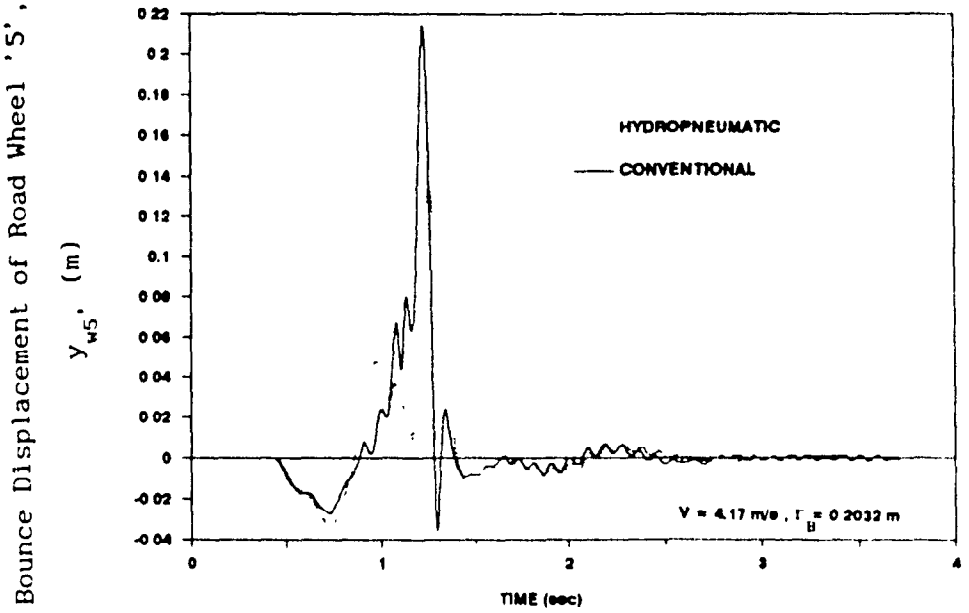

Figure 6.21 Comparison of road wheel #5 bounce responses of the tracked vehicle equipped with hydropneumatic and conventional suspension configurations when traversing the 0.2032 m bump at 4.17 m/s.

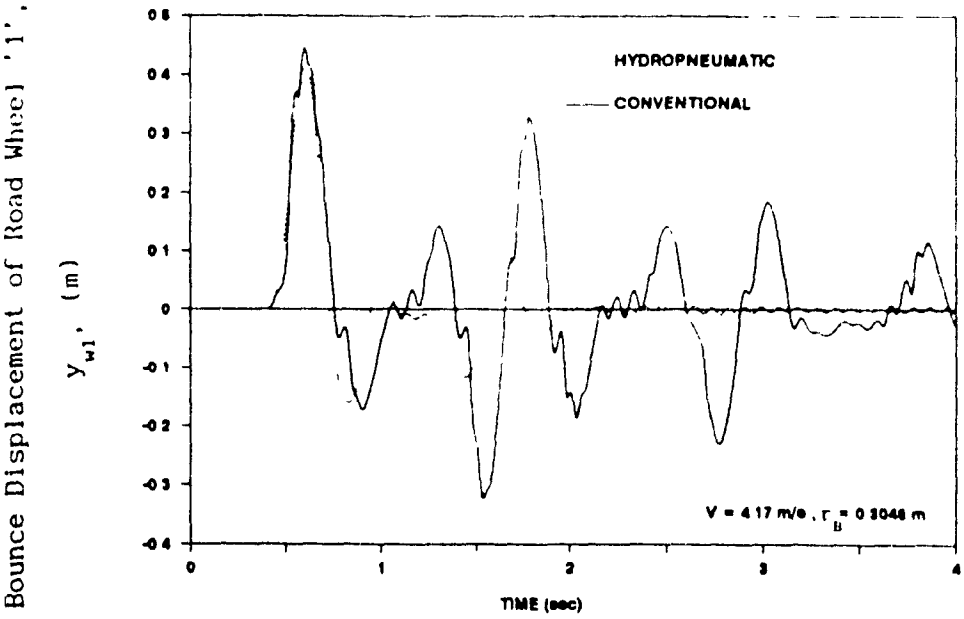

Figure 6.22 Comparison of road wheel #1 bounce responses of the tracked vehicle equipped with hydropneumatic and conventional suspension configurations when traversing the 0.3048 m bump at 4.17 m/s.

vehicle equipped with conventional suspension, as shown in Figure 6.22. The road wheel displacement response of the hydropneumatic suspension, however, decays very rapidly, (settles around 2 s), while the road wheel displacement response of the conventional suspension exhibits high amplitude oscillations beyond 4 s. The displacement response characteristics of the last road wheel are quite similar to that of the first road wheel, as shown in Figure 6.23. The peak displacement response of first and last road wheels of the vehicle equipped with a hydropneumatic suspension is considerably lower than that of the vehicle equipped with conventional suspension, regardless of bump height, as shown in Figures 6.24 and 6.25, respectively.

Figures 6.26 and 6.27 illustrate the displacement response of the undamped road wheel '3' of the vehicles traversing 0.2032 m and 0.3048 m bumps at a speed of 4.17 m/s, respectively. The displacement response of the road wheel '3' of the vehicle equipped with hydropneumatic suspension exhibits higher peak response when compared to that of the vehicle equipped with conventional suspension, as shown in Figure 6.28. The hydropneumatic suspension, however, causes the road wheel response to settle very rapidly when negotiating the 0.2032 m bump, as shown in Figure 6.26. The road wheel response of the vehicle with hydropneumatic suspension, however, continues to oscillate similar to the conventional suspension when traversing the 0.3048 m bump.

6.4.1 Influence of Vehicle Speed on the Transient Response

Figures 6.29 and 6.30 present the vertical response of the hull c.g. of the vehicles, equipped with hydropneumatic and conventional suspensions, for 0.2032 m and 0.3048 m bump excitations, when the vehicle speed is increased to 6.94 m/s. When subject to the 0.2032 m

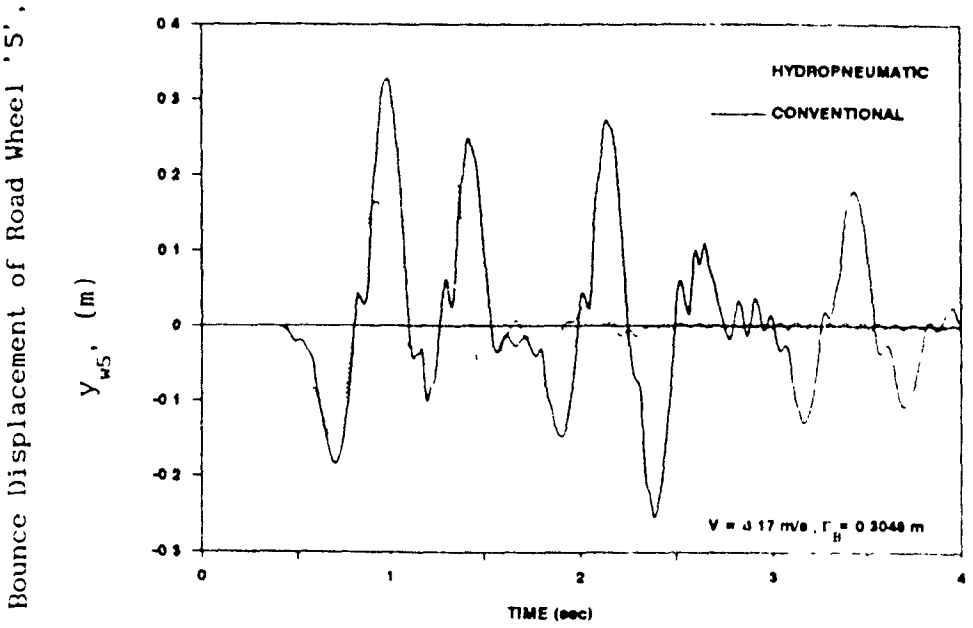

Figure 6.23 Comparison of road wheel #5 bounce responses of the tracked vehicle equipped with hydropneumatic and conventional suspension configurations when traversing the 0.3048 m bump at 4 17 m/s.

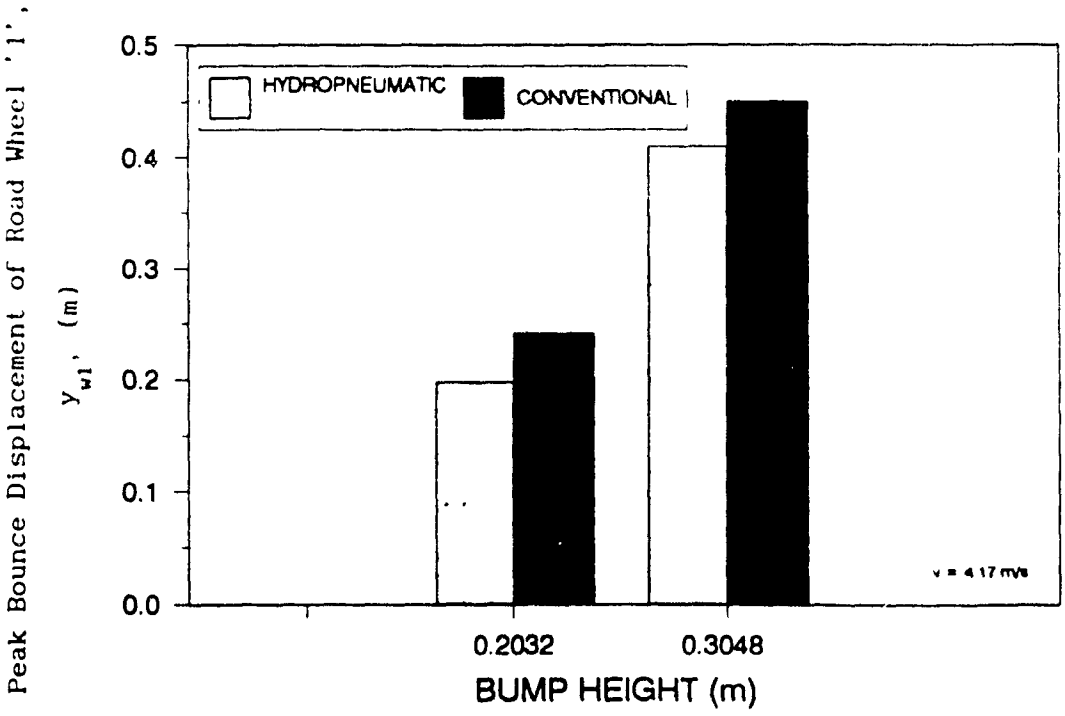

Figure 6.24 Comparison of peak road wheel #1 bounce responses of the tracked vehicle equipped with hydropneumatic and conventional suspension configurations when traversing bumps at 4.17 m/s.

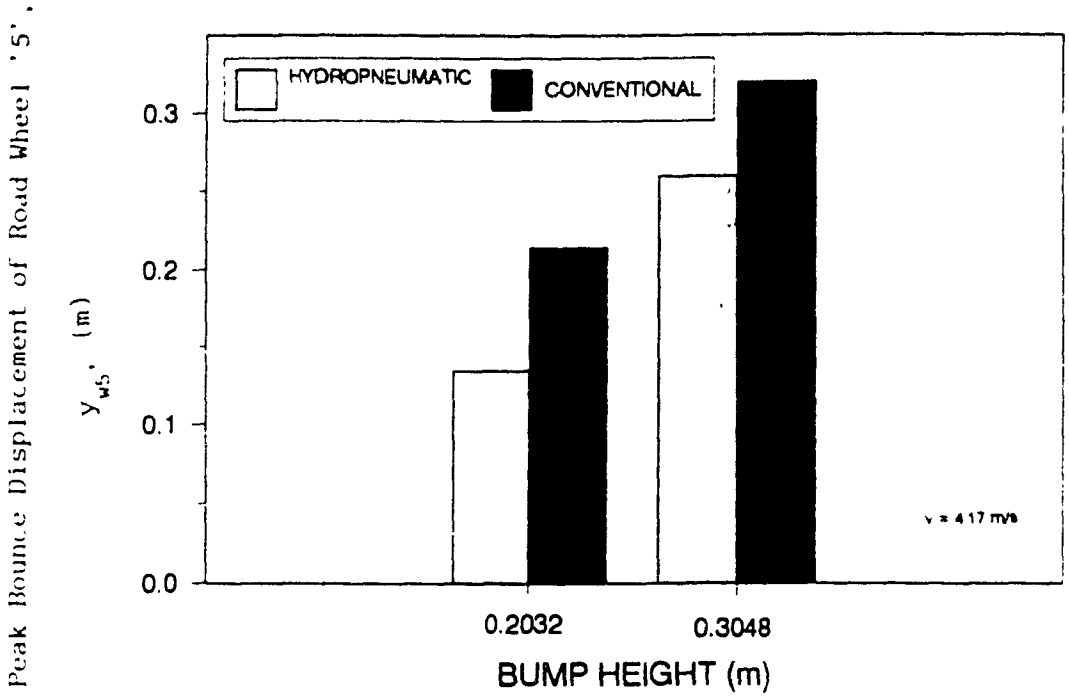

Figure 6.25 Comparison of peak road wheel #5 bounce responses of the tracked vehicle equipped with hydropneumatic and conventional suspension configurations when traversing bumps at 4.17 m/s.

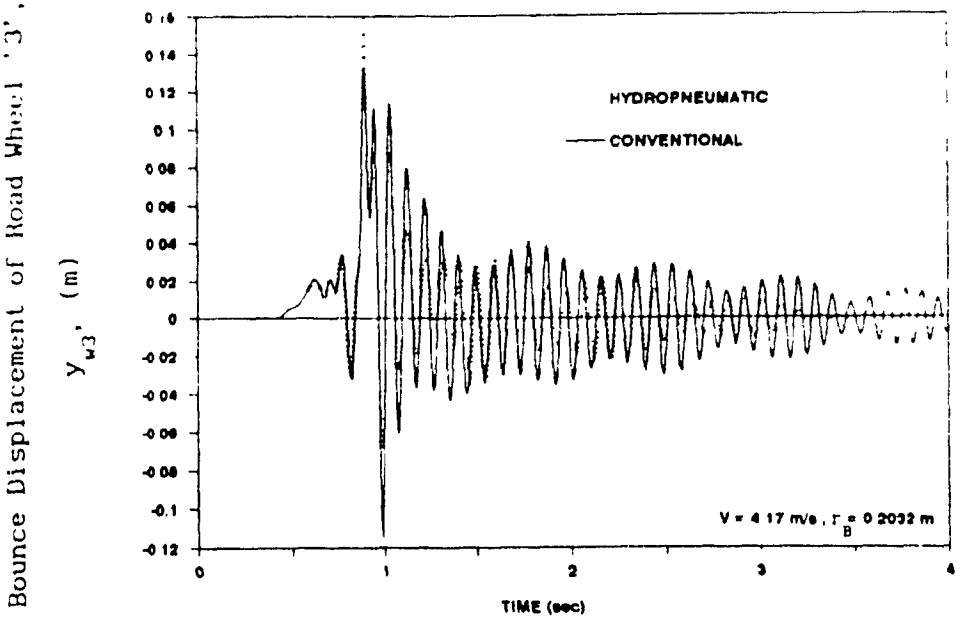

Figure 6.26 Comparison of road wheel #3 bounce responses of the tracked vehicle equipped with hydropneumatic and conventional suspension configurations when traversing the 0.2032 m bump at 4.17 m/s.

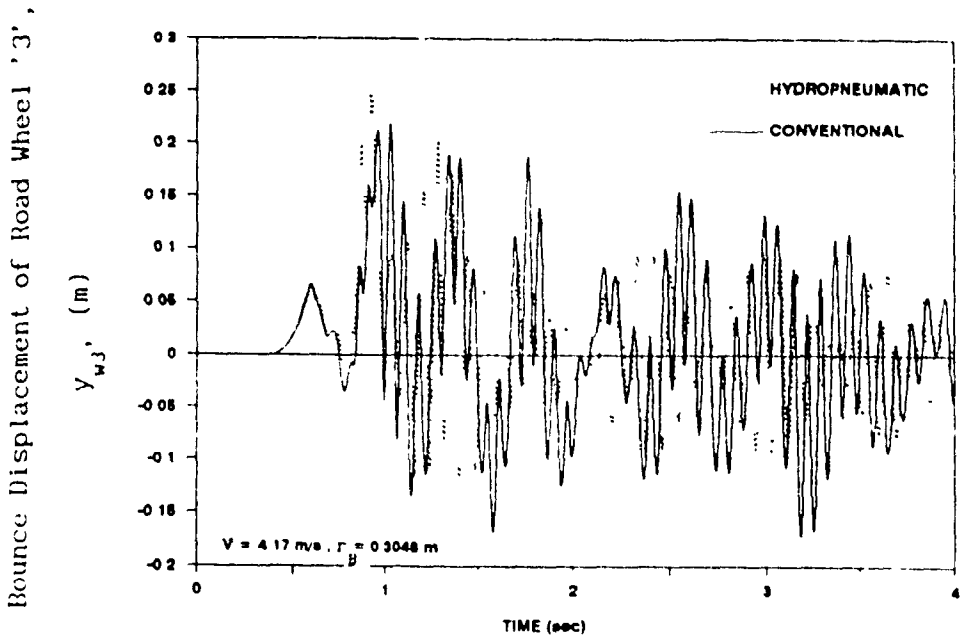

Figure 6.27 Comparison of road wheel #3 bounce responses of the tracked vehicle equipped with hydropneumatic and conventional suspension configurations when traversing the 0.3048 m bump at 4.17 m/s.

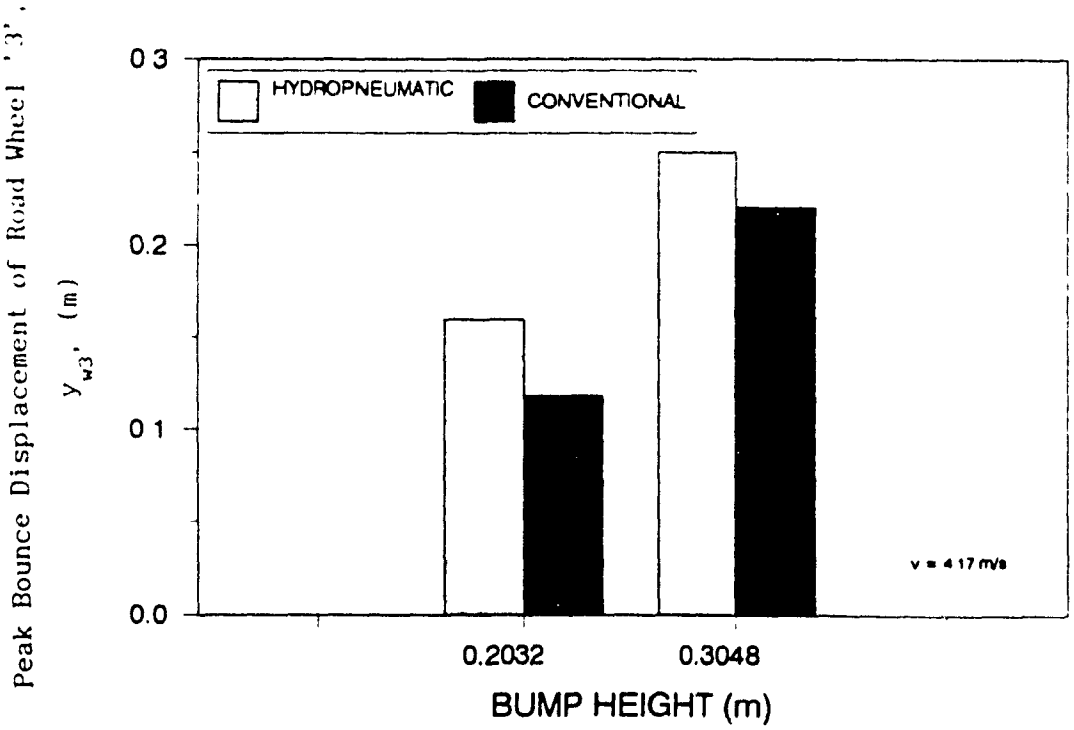

Figure 6.28 Comparison of peak road wheel #3 bounce responses of the tracked vehicle equipped with hydropneumatic and conventional suspension configurations when traversing bumps at 4.17 m/s.

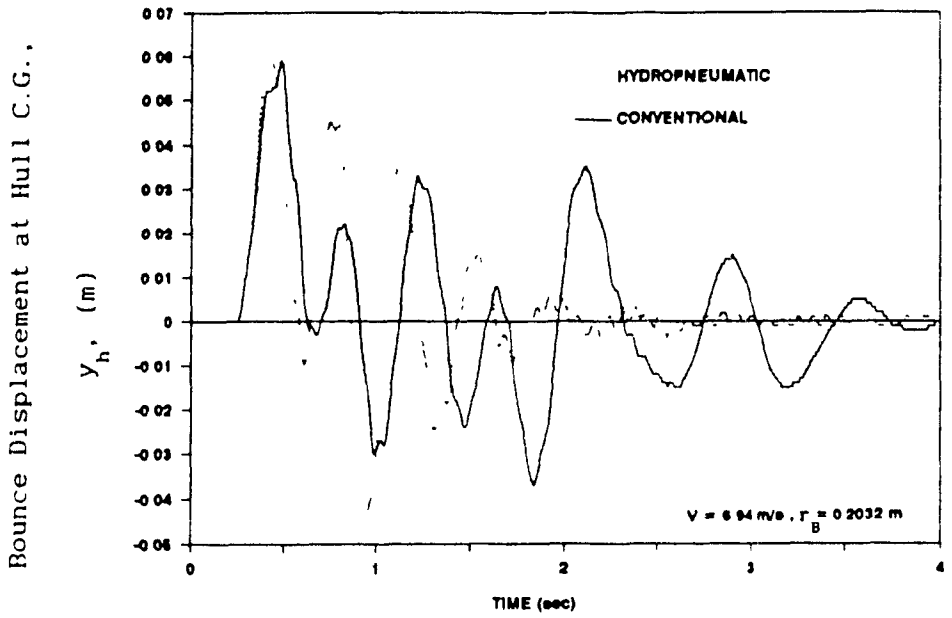

Figure 6.29 Comparison of hull c.g. bounce responses of the tracked vehicle equipped with hydropneumatic and conventional suspension configurations when traversing the 0.2032 m bump at 6.94 m/s.

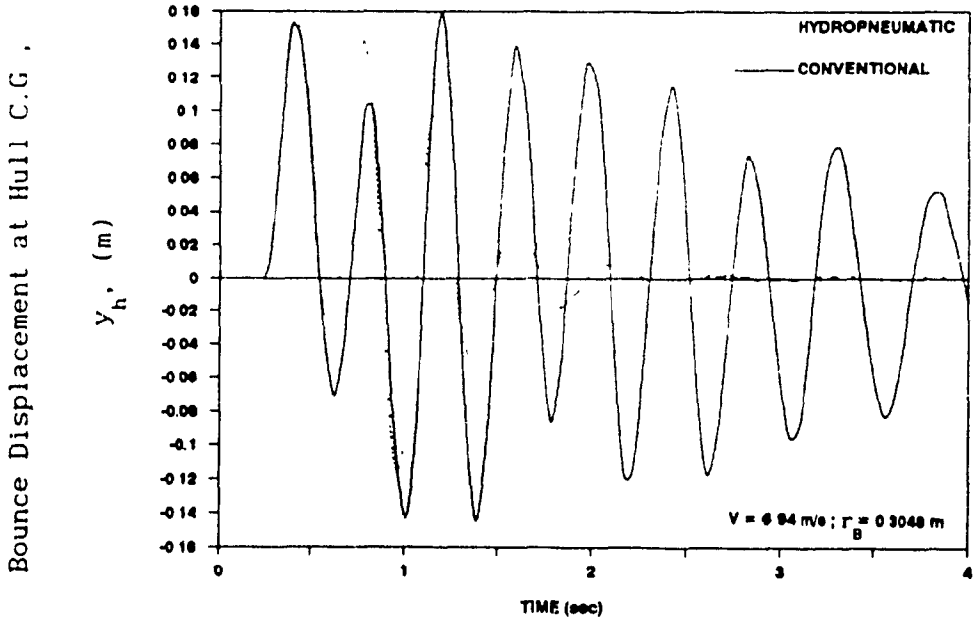

Figure 6.30 Comparison of hull c.g. bounce responses of the tracked vehicle equipped with hydropneumatic and conventional suspension configurations when traversing the 0.3048 m bump at 6.94 m/s.

bump, the hydropneumatic suspension yields larger peak displacement response which decays quite rapidly due to its high damping, as shown in Figure 6.29. The vertical displacement response of the hydropneumatic suspension decays at even faster rate when subject to the 0.3048 m bump, as shown in Figure 6.30. The peak values of the vertical displacement response of the two suspensions, however, are quite similar, as shown in Figure 6.31.

The hull bounce acceleration response characteristics of the tracked vehicles, equipped with hydropneumatic and conventional suspensions, traversing the 0.2032 m and 0.3048 m bump at 6.94 m/s, are shown in Figures 6.32 and 6.33, respectively. As shown in Figure 6.32, the vehicle equipped with hydropneumatic suspension experiences higher peak values of hull bounce acceleration and slower response settling time, than the tracked vehicle equipped with conventional suspension. However, when traversing the 0.3048 m bump at 6.94 m/s, the tracked vehicle equipped with hydropneumatic suspension experiences lower peak values of bounce acceleration response, at the hull c.g., than the tracked vehicle equipped with conventional suspension, as shown in Figure 6.33. In addition, the bounce acceleration response at the hull c.g. of the vehicle equipped with hydropneumatic suspension settles significantly faster (around 2 s), than the response of the vehicle equipped with conventional suspension. The coupled nature of the 7 DOF tracked vehicle model is evident in the vibration responses of Figures 6.32 and 6.33; the shock responses show superimposed vibrations from the low frequency hull bounce and pitch modes, as well as the higher frequency road wheel bounce modes. Figure 6.34 compares the peak values of bounce acceleration, at the hull c.g., experienced by the tracked

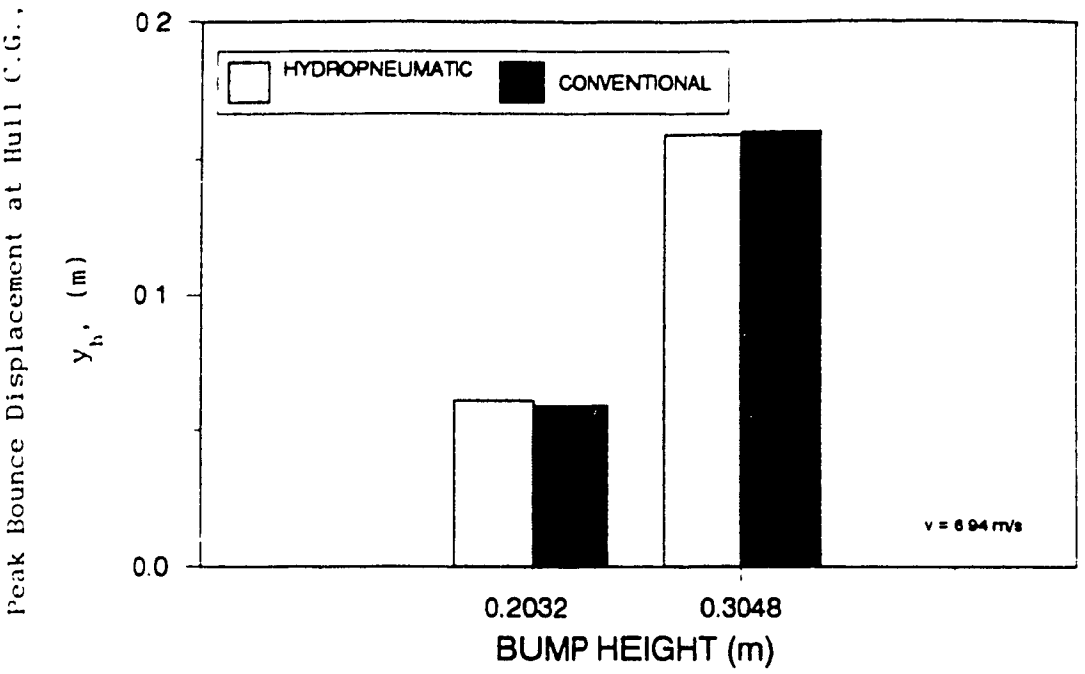

Figure 6.31 Comparison of peak hull c.g. bounce responses of the tracked vehicle equipped with hydropneumatic and conventional suspension configurations when traversing bumps at 6.94 m/s.

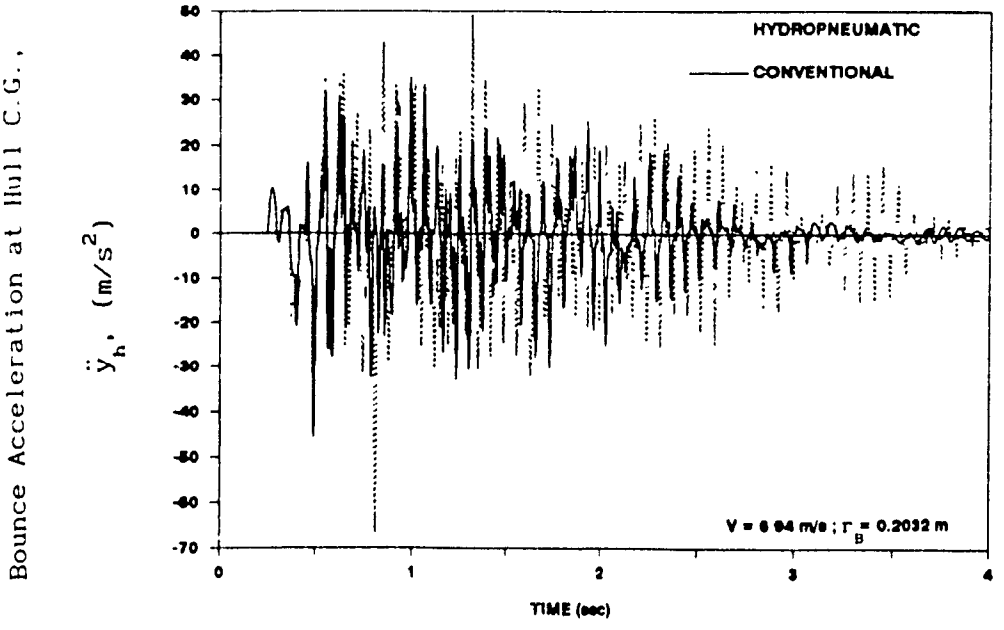

Figure 6.32 Comparison of hull c.g. bounce acceleration responses of the tracked vehicle equipped with hydropneumatic and conventional suspension configurations when traversing the 0.2032 m bump at 6.94 m/s.

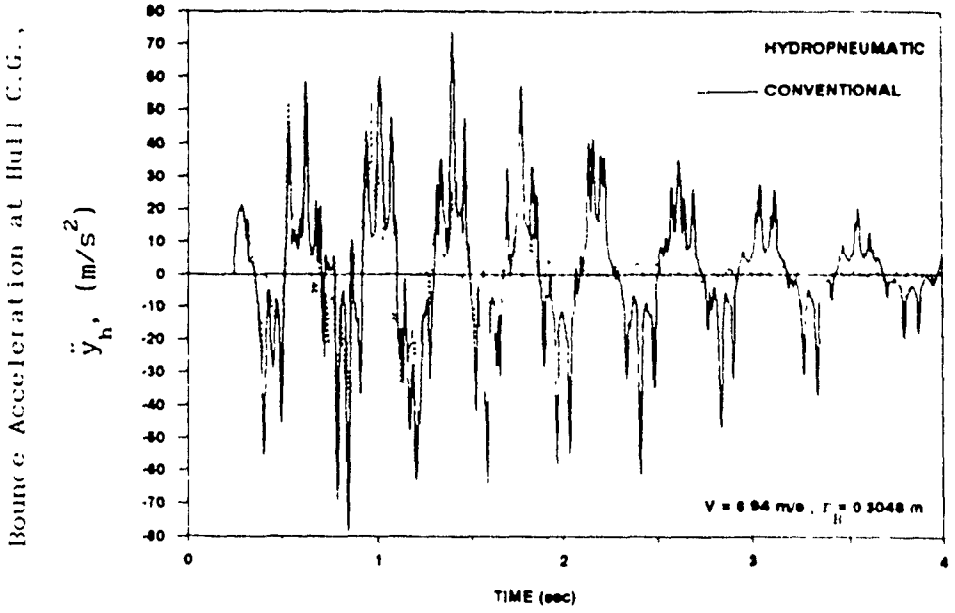

Figure 6.33 Comparison of hull c.g. bounce acceleration responses of the tracked vehicle equipped with hydropneumatic and conventional suspension configurations when traversing the 0.3048 m bump at 6.94 m/s.

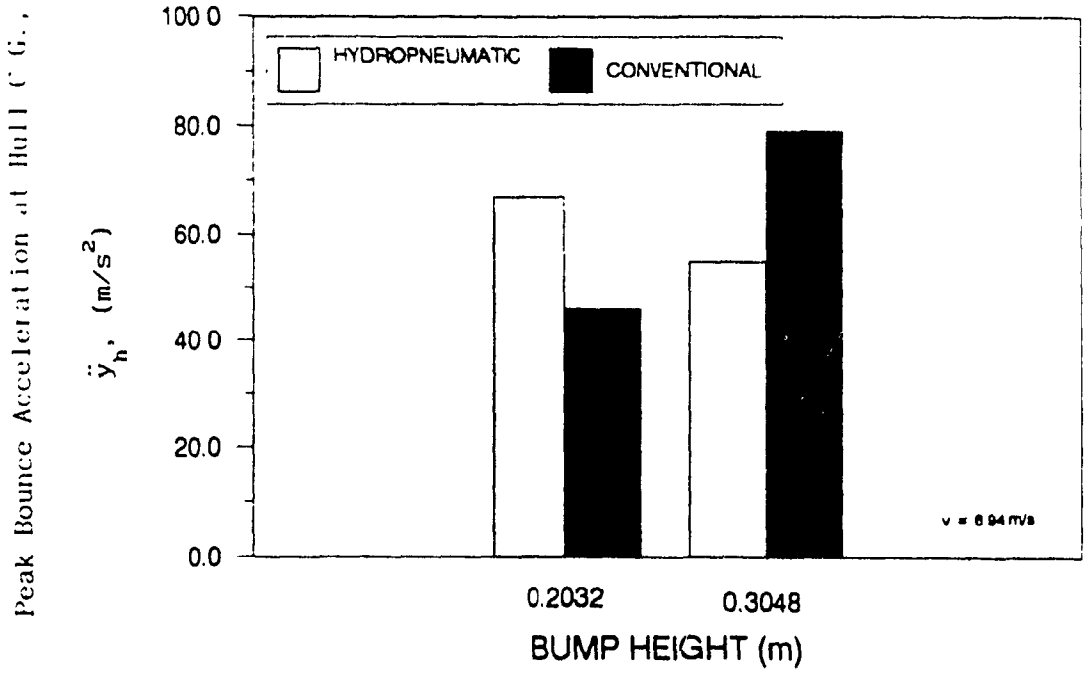

Figure 6.34 Comparison of peak hull c.g. bounce acceleration responses of the tracked vehicle equipped with hydropneumatic and conventional suspension configurations when traversing bumps at 6.94 m/s.

vehicles equipped with hydropneumatic and conventional suspensions, when traversing the two sizes of bump obstacle at 6.94 m/s. As shown in this figure, the vehicle with hydropneumatic suspension experiences greater peak hull bounce acceleration when traversing the 0.2032 m excitation, but yields significantly lower peak bounce acceleration when traversing the 0.3048 m excitation.

Figures 6.35 and 6.36, respectively, present the pitch deflection response about the hull c.g. of the tracked vehicles, equipped with conventional and hydropneumatic suspensions, traversing the 0.2032 m and 0.3048 m bumps at 6.94 m/s. The two vehicles experience almost identical pitch deflection response for the first half cycle after encountering the bump. However, the pitch deflection response of the tracked vehicle, equipped with hydropneumatic suspension, settles at a significantly faster rate (between 1.5 s and 2 s), than the vehicle equipped with conventional suspension. Figure 6.37 compares the peak pitch deflection responses about the hull c.g. of the tracked vehicles when traversing the two sizes of bump obstacle at 6.94 m/s; the tracked vehicle equipped with hydropneumatic suspension, experiences considerably lower peak pitch deflection response for both sizes of bump excitation.

The pitch acceleration response characteristics of the tracked vehicles, equipped with hydropneumatic and conventional suspensions, traversing the 0.2032 m and 0.3048 m bumps at 6.94 m/s, are shown in Figures 6.38 and 6.39, respectively. As shown in Figure 6.38, the pitch acceleration response of the tracked vehicles traversing the 0.2032 m bump at 6.94 m/s are almost identical, except that the hydropneumatic suspension experiences slightly higher peak acceleration response. The coupled nature of the tracked vehicle models is evidenced again by the

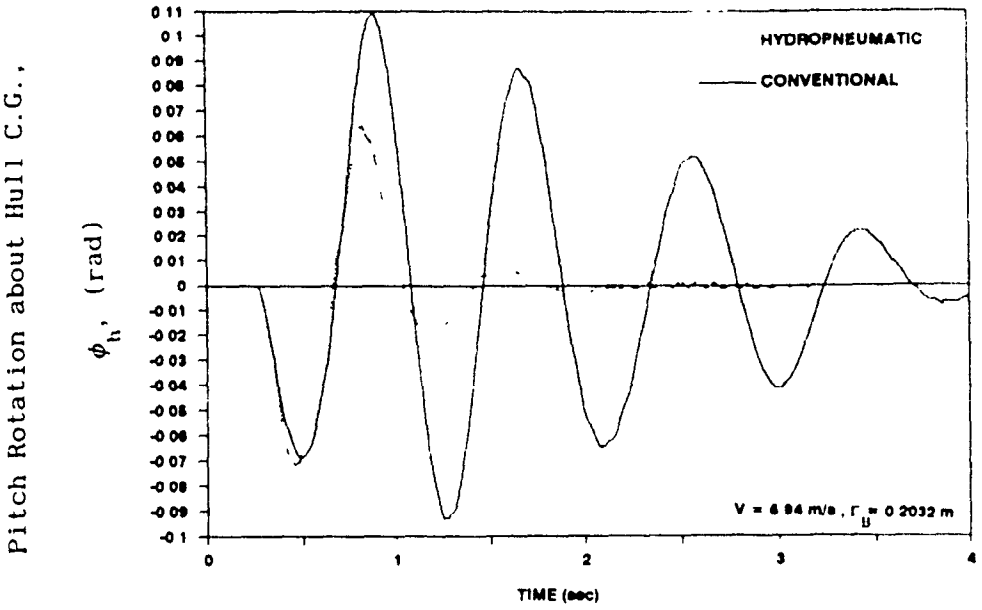

Figure 6.35 Comparison of hull c.g. pitch responses of the tracked vehicle equipped with hydropneumatic and conventional suspension configurations when traversing the 0.2032 m bump at 6.94 m/s.

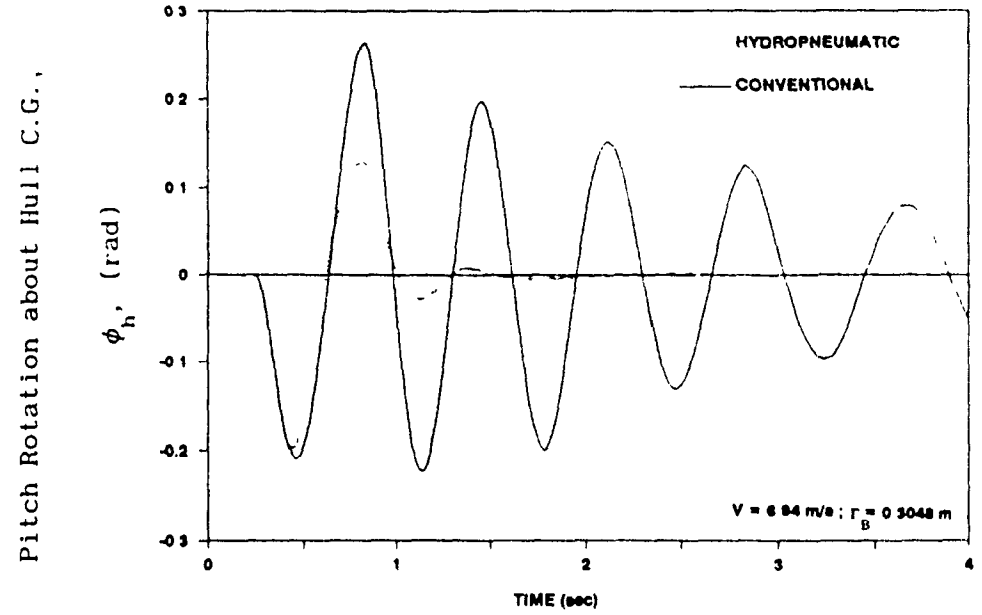

Figure 6.36 Comparison of hull c.g. pitch responses of the tracked vehicle equipped with hydropneumatic and conventional suspension configurations when traversing the 0.3048 m bump at 6.94 m/s.

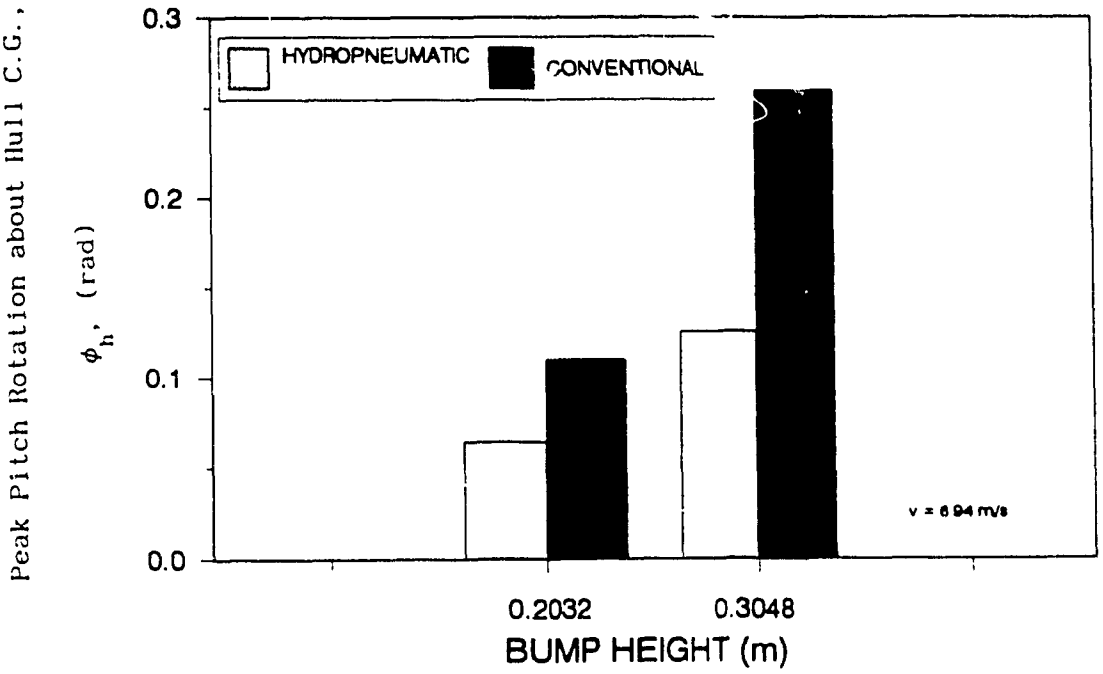

Figure 6.37 Comparison of peak hull c.g. pitch responses of the tracked vehicle equipped with hydropneumatic and conventional suspension configurations when traversing bumps at 6.94 m/s.

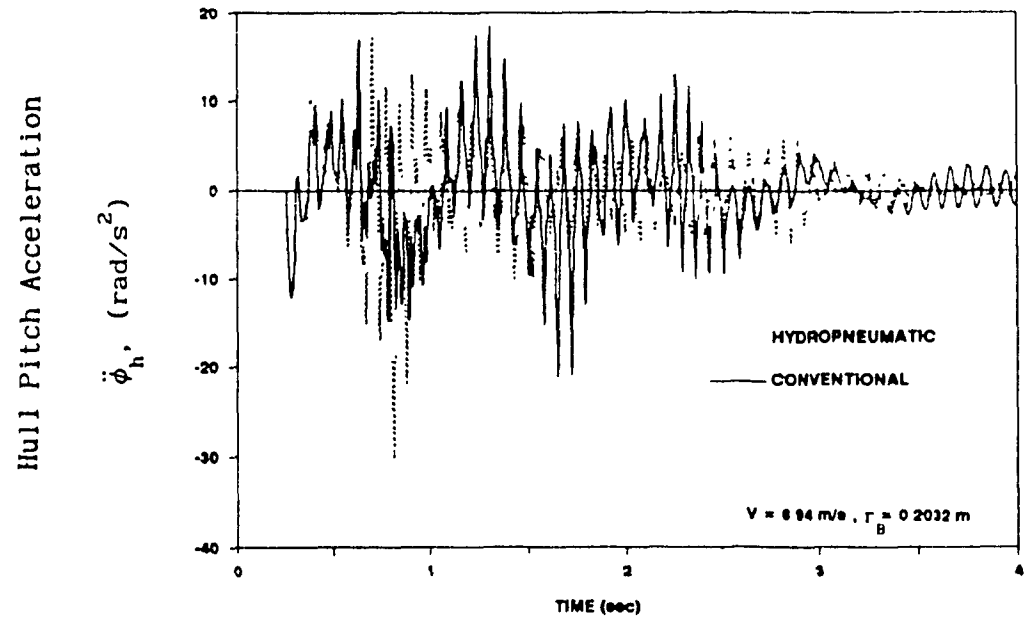

Figure 6.38 Comparison of hull c.g. pitch acceleration responses of the tracked vehicle equipped with hydropneumatic and conventional suspension configurations when traversing the 0.2032 m bump at 6.94 m/s.

superimposed high and low frequency vibration responses, as shown in Figure 6.38. The pitch acceleration response of the tracked vehicle equipped with hydropneumatic suspension, traversing the 0.3048 m bump at 6.94 m/s, experiences lower peak acceleration response and settles at a considerably faster rate than the vehicle equipped with conventional suspension, as shown in Figure 6.39. Figure 6.40 compares the peak pitch acceleration response, about the hull c.g., of the tracked vehicle traversing the two bumps at 6.94 m/s. As shown in this figure, the tracked vehicle equipped with conventional suspension experiences lower peak pitch acceleration response when traversing the 0.2032 m bump, whereas the tracked vehicle equipped with hydropneumatic suspension experiences significantly lower peak hull pitch acceleration when traversing the 0.3048 m bump.

The vertical displacement response of the first and last road wheels of the tracked vehicles equipped with hydropneumatic and conventional suspensions, negotiating the 0.2032 m bump at 6.94 m/s, are presented in Figures 6.41 and 6.42, respectively. The first road wheel exhibits a significantly reduced peak response and faster settling time for the vehicle equipped with hydropneumatic suspension, as shown in Figure 6.41. The response of the last road wheel is similar to that of the first road wheel; peak response and settling time are considerably lower for the hydropneumatic suspension. The displacement response of the first and last road wheels increases considerably, regardless of suspension type, when the bump size is increased to 0.3048 m, as shown in Figures 6.43 and 6.44. The initial peak displacement responses of the first road wheel of the hydropneumatic and conventional suspensions are almost identical, as shown in Figure 6.43; however, the response of the

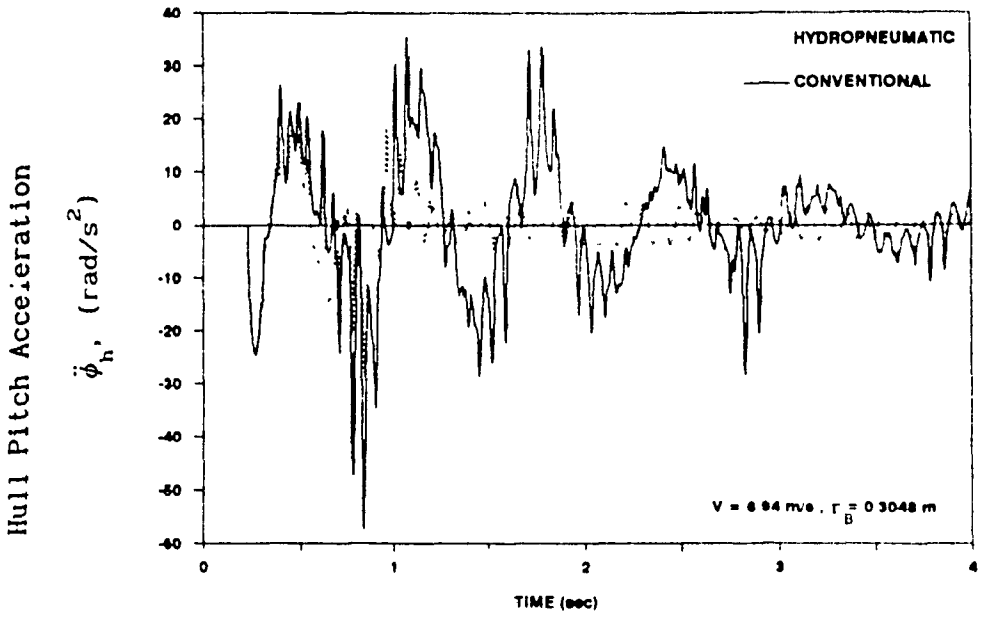

Figure 6.39 Comparison of hull c.g. pitch acceleration responses of the tracked vehicle equipped with hydropneumatic and conventional suspension configurations when traversing the 0.3048 m bump at 6.94 m/s.

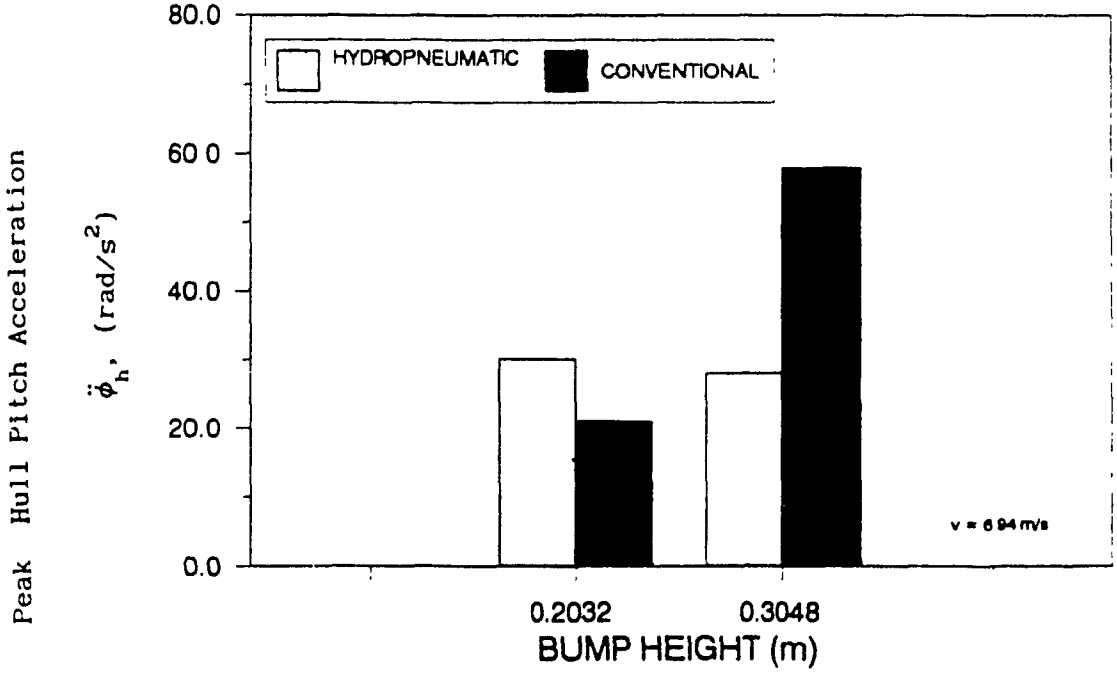

Figure 6.40 Comparison of peak hull c.g. pitch acceleration responses of the tracked vehicle equipped with hydropneumatic and conventional suspension configurations when traversing bumps at 6.94 m/s.

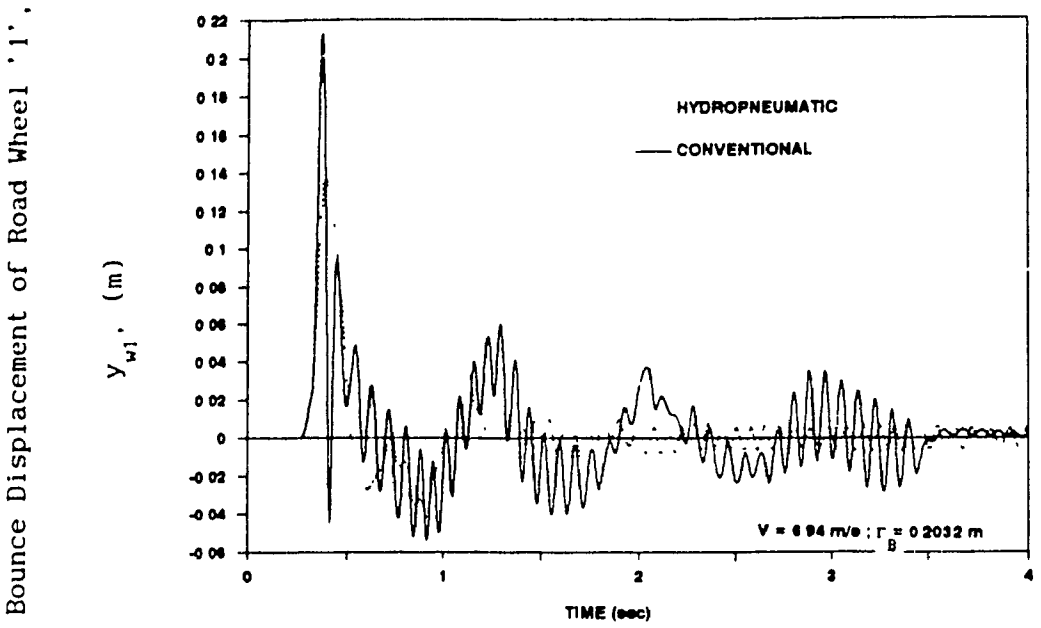

Figure 6.41 Comparison of road wheel #1 bounce responses of the tracked vehicle equipped with hydropneumatic and conventional suspension configurations when traversing the 0.2032 m bump at 6.94 m/s.

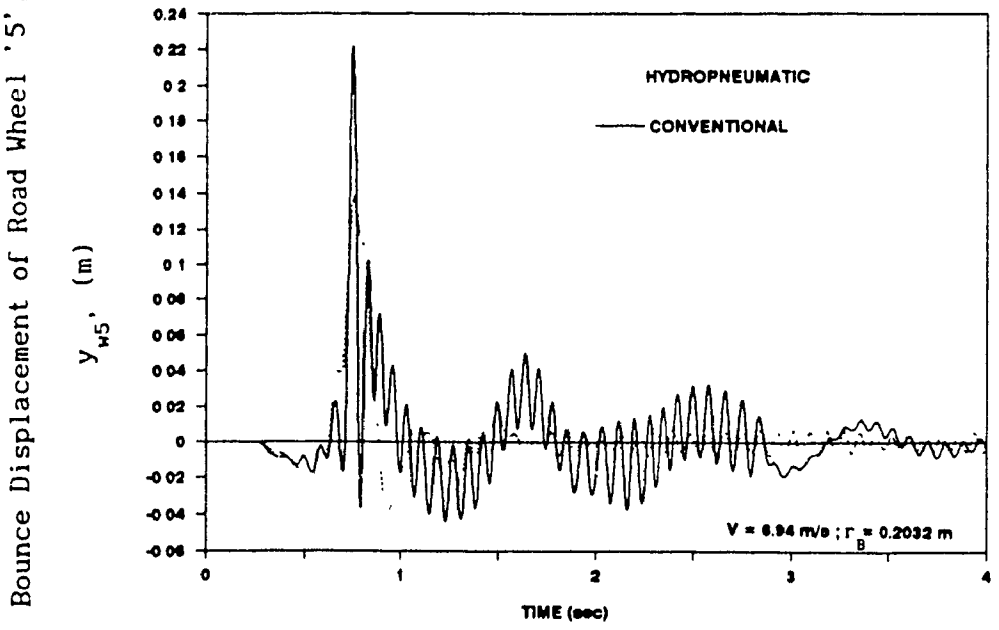

Figure 6.42 Comparison of road wheel #5 bounce responses of the tracked vehicle equipped with hydropneumatic and conventional suspension configurations when traversing the 0.2032 m bump at 6.94 m/s.

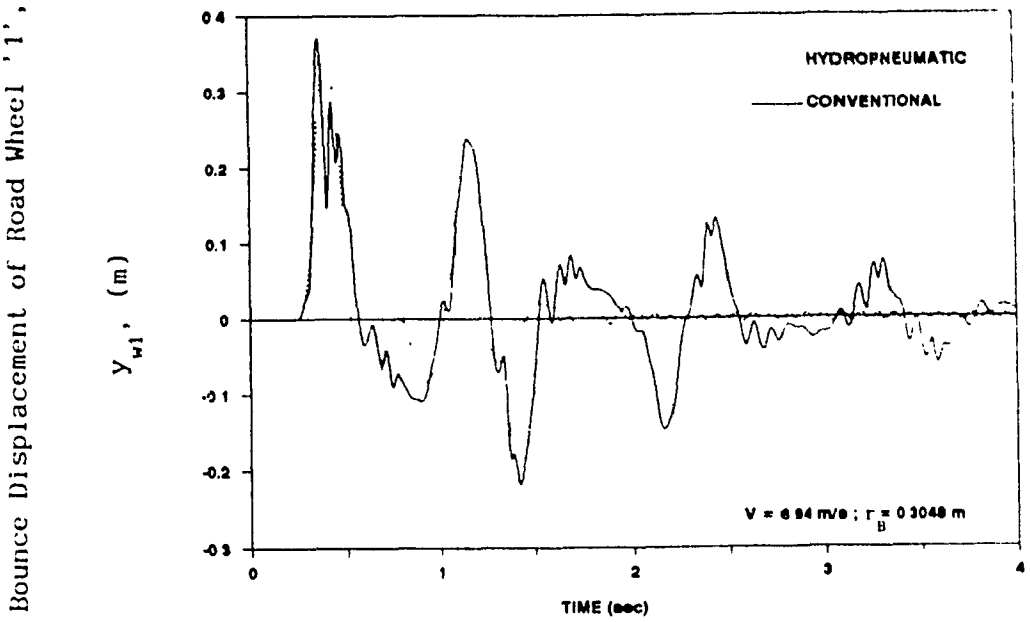

Figure 6.43 Comparison of road wheel #1 bounce responses of the tracked vehicle equipped with hydropneumatic and conventional suspension configurations when traversing the 0.3048 m bump at 6.94 m/s.

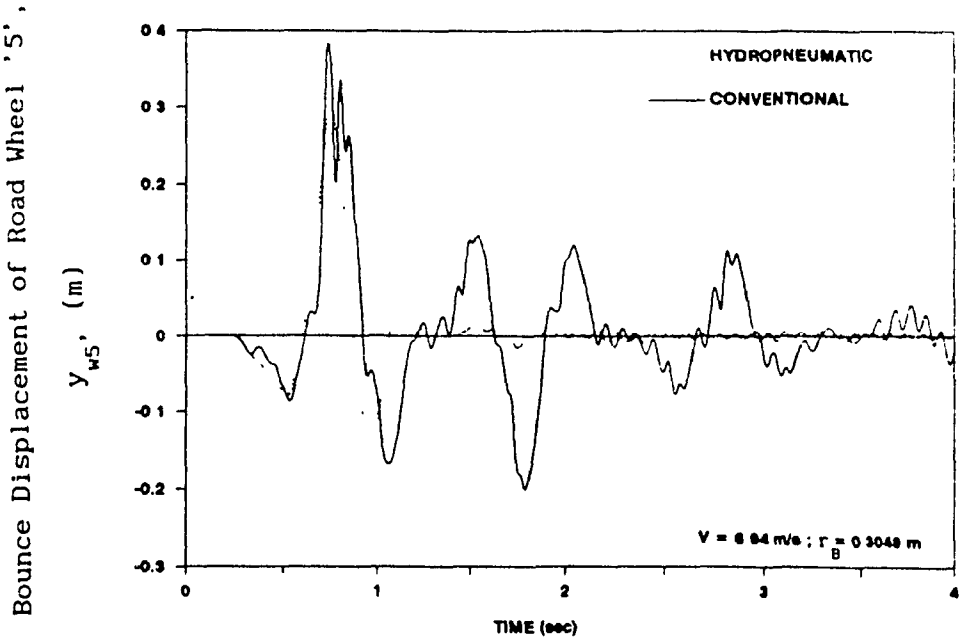

Figure 6.44 Comparison of road wheel #5 bounce responses of the tracked vehicle equipped with hydropneumatic and conventional suspension configurations when traversing the 0.3048 m bump at 6.94 m/s.

hydropneumatic suspension settles faster (around 1.5 s), as compared to the conventional suspension. The last road wheel experiences similar bounce response, as shown in Figure 6.44. The response of the hydropneumatic suspension is slightly lower and settles at a faster rate than the response of the conventional suspension; the response of the hydropneumatic suspension settles around 1.7 s, whereas the response of the conventional suspension only begins to settle around 3.5 s. The peak displacement response of the first and last road wheel of the vehicle, equipped with hydropneumatic suspension, is lower than that of the vehicle equipped with conventional suspension, regardless of bump height, as shown in Figures 6.45 and 6.46, respectively.

Figures 6.47 and 6.48 illustrate the displacement response of undamped road wheel '3' of the vehicles traversing the 0.2032 m and 0.3048 m bumps at 6.94 m/s, respectively. The peak displacement response of road wheel '3' is virtually identical for both hydropneumatic and conventional suspension, regardless of bump height, as shown in Figure 6.49. Although peak response is almost identical, the bounce response of road wheel '3' of the vehicle equipped with hydropneumatic suspension, oscillates at a higher magnitude, as shown in Figure 6.47. In addition, superimposed low frequency vibrations, due to the hull bounce and pitch modes, are evident in both Figures 6.47 and 6.48. As shown in Figure 6.48, the entire bounce response of road wheel '3' is very similar for both hydropneumatic and conventional suspensions.

6.6 SUMMARY

In this chapter, the ride performance potentials of hydropneumatic suspension are investigated using the pitch-plane model of a vehicle.

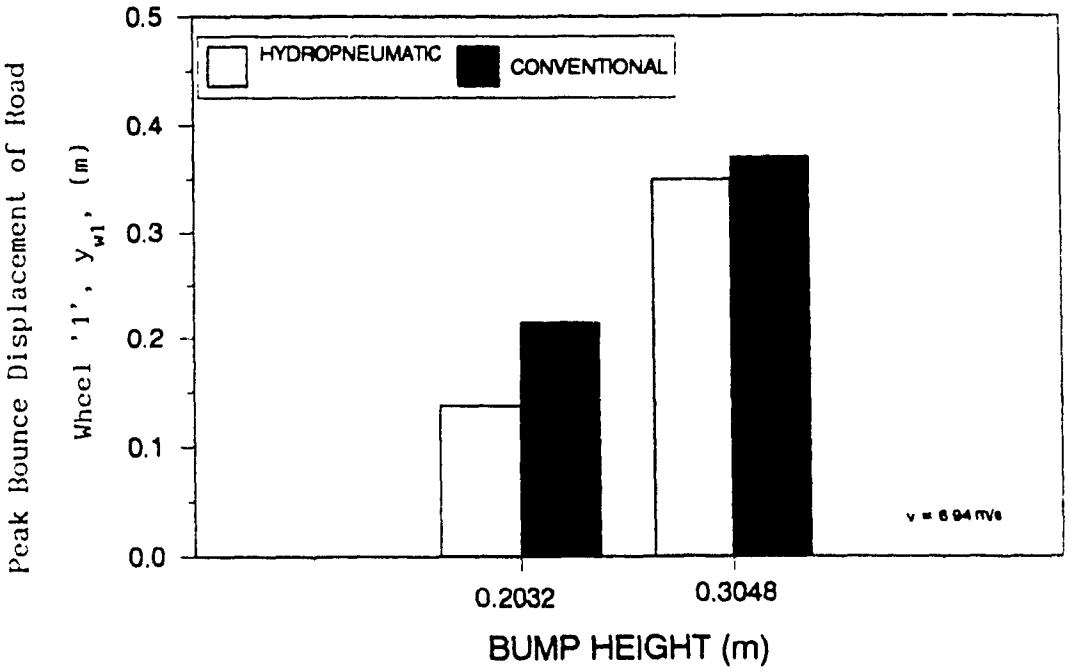

Figure 6.45 Comparison of peak road wheel #1 bounce responses of the tracked vehicle equipped with hydropneumatic and conventional suspension configurations when traversing bumps at 6.94 m/s.

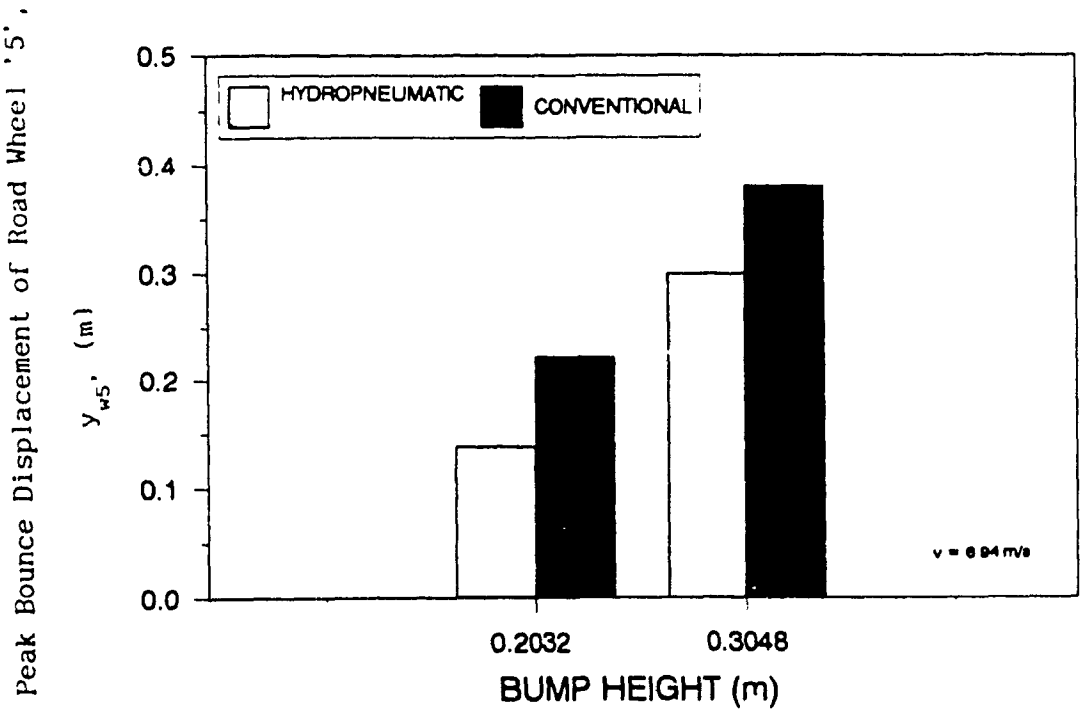

Figure 6.46 Comparison of peak road wheel #5 bounce responses of the tracked vehicle equipped with hydropneumatic and conventional suspension configurations when traversing bumps at 6.94 m/s.

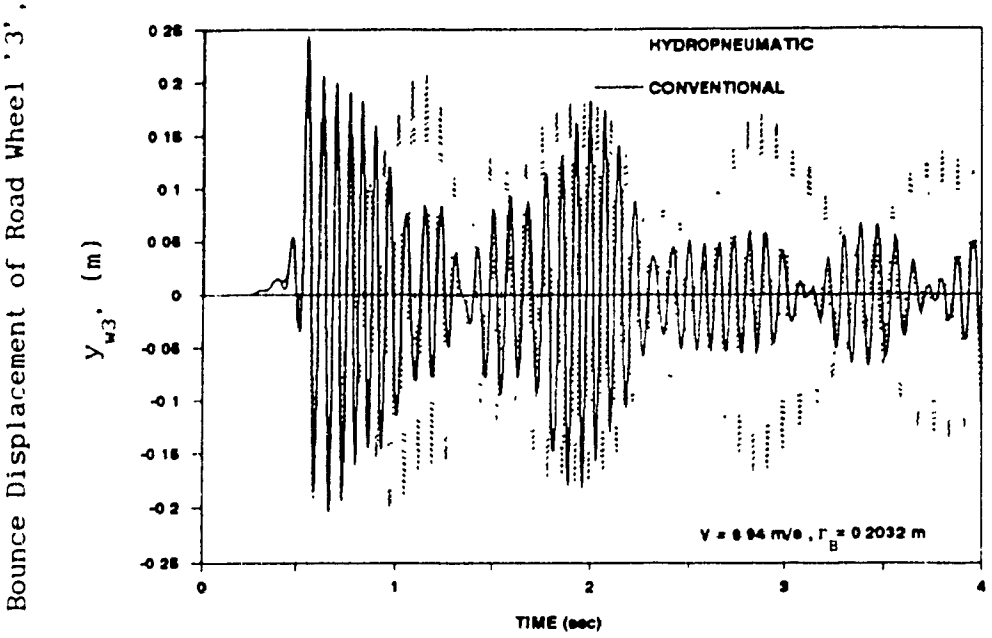

Figure 6.47 Comparison of road wheel #3 bounce responses of the tracked vehicle equipped with hydropneumatic and conventional suspension configurations when traversing the 0.2032 m bump at 6.94 m/s.

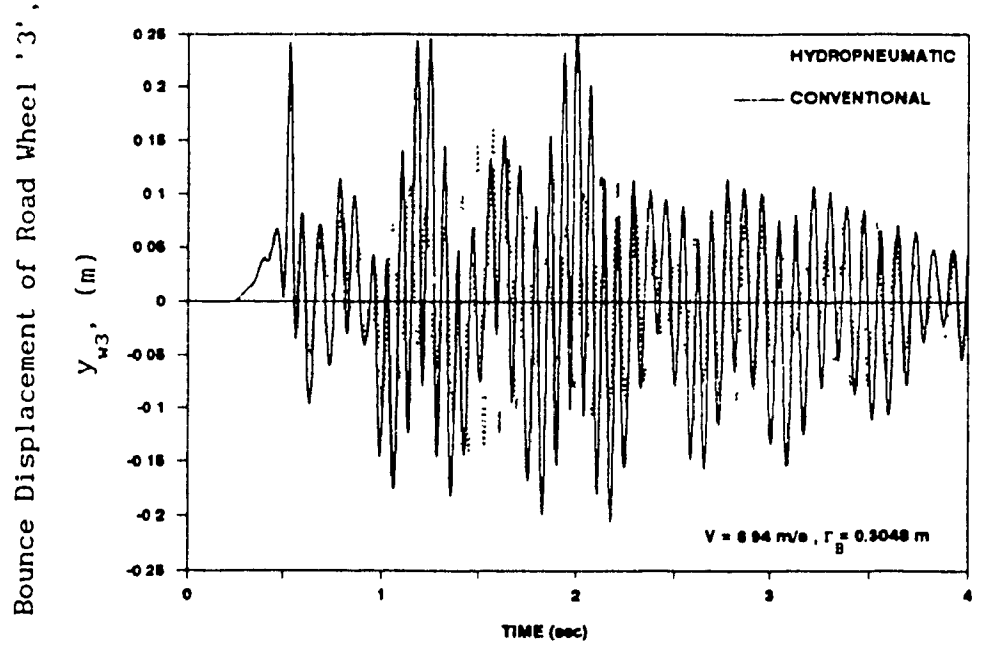

Figure 6.48 Comparison of road wheel #3 bounce responses of the tracked vehicle equipped with hydropneumatic and conventional suspension configurations when traversing the 0.3048 m bump at 6.94 m/s.

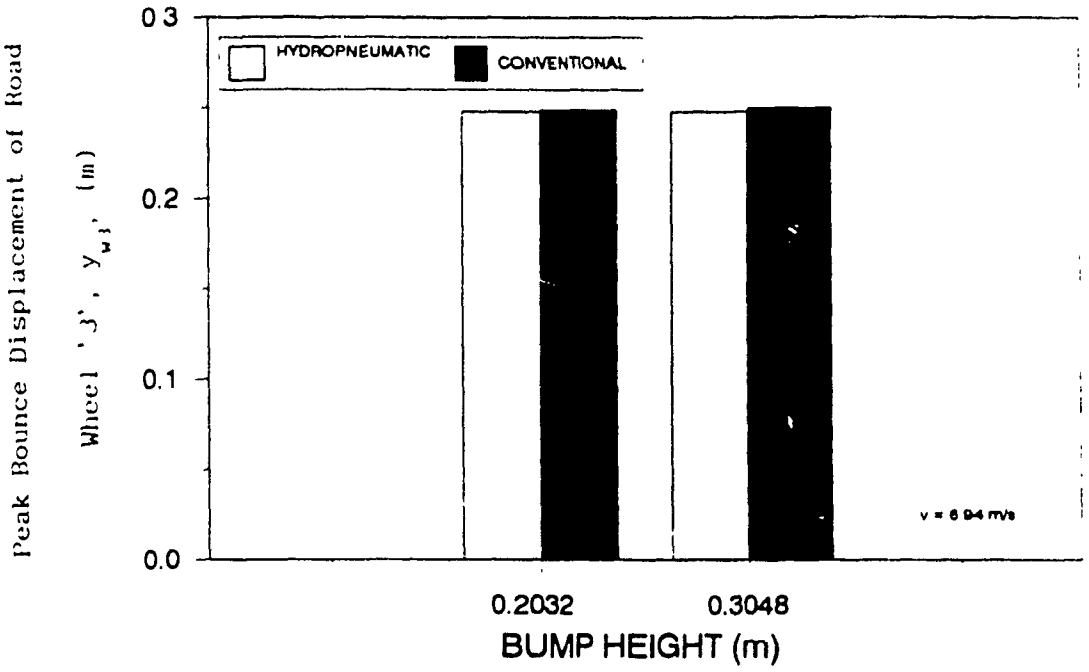

Figure 6.49 Comparison of peak road wheel #3 bounce responses of the tracked vehicle equipped with hydropneumatic and conventional suspension configurations when traversing bumps at 6.94 m/s.

The pitch-plane nonlinear model of a tracked vehicle, developed in Chapter 4, employing trailing arm linkage suspension configuration, is selected for this study. The ride quality improvement potentials are investigated for harmonic displacement excitation, whereas the shock isolation potentials for semi-circular discrete obstacles. The shock isolation performance of the suspension system is investigated for two different semi-circular bump obstacles and vehicle approach speeds. The investigations on ride performance potentials revealed that the hydropneumatic suspension can significantly attenuate transmitted vibrations over the frequency range of interest. The magnitude of transmitted vibrations around the low frequency hull bounce and hull pitch resonances can be reduced considerably with the use of the hydropneumatic suspension. The high frequency vibration responses, corresponding to road wheel resonances, can also be reduced significantly by the hydropneumatic suspension.

Investigations on the shock isolation potentials of hydropneumatic suspension revealed that the hydropneumatic suspension generally provides a more controlled response and faster settling times. The hydropneumatic suspension generally provides lower peak shock response than that provided by the conventional suspension system. The hydropneumatic suspension yields improved shock isolation performance, specifically when the vehicle is subjected to higher amplitude bump excitation at higher approach speeds.

CHAPTER 7

CONCLUSIONS AND RECOMMENDATIONS FOR FUTURE WORK

7.1 GENERAL

In this thesis, the shock and vibration isolation characteristics of the hydropneumatic suspension system are analyzed via mathematical modeling and computer simulation. Two analytical models of the hydropneumatic suspension system are developed: a single degree-of-freedom dynamic model assuming incompressible hydraulic fluid; and a two DOF dynamic model assuming compressible hydraulic fluid. The models are developed to incorporate the nonlinearities of orifice damping, gas spring, Coulomb friction, and travel limiting elastic bump stops.

Transient response characteristics of the hydropneumatic suspension are evaluated for rounded step and rounded pulse displacement excitations using a numerical integration algorithm. Vibration isolation performance is evaluated in terms of transmissibility characteristics using a numerical integration and frequency sweep technique. The shock and vibration response characteristics of the hydropneumatic suspension system are compared to those of a conventional suspension, employing linear spring and orifice damping characteristics, to investigate the relative performance benefits of the hydropneumatic suspension. A linearization technique is employed to establish local linear equivalent spring and damping characteristics over the frequency range of interest for the hydropneumatic suspension system.

The ride performance potentials of the hydropneumatic suspension system are investigated using a tracked vehicle model. A pitch-plane,

nonlinear, seven DOF ride dynamic model of a tracked military vehicle, employing trailing arm suspension linkage configuration, is developed for the analysis. Transient response of the tracked vehicle is evaluated for semi-circular displacement excitations. Vibration isolation, in terms of transmissibility characteristics, is evaluated for harmonic excitation using a numerical integration and frequency sweep technique.

7.2 HIGHLIGHTS OF PRESENT INVESTIGATION

The highlights of the present investigation are summarized in the following sub-sections:

7.2.1 Hydropneumatic Suspension: Modeling and Analysis

Study of hydropneumatic suspension includes complex dynamics associated with floating piston, gas spring, fluid flows and fluid compressibility. The hydropneumatic suspension system is modeled using two methodologies. The first modeling approach assumes the hydraulic fluid to be incompressible. The dynamics of the floating piston are represented and incorporated by deriving a constraint equation relating the motions of floating and primary pistons. The hydropneumatic suspension is thus modeled as a single degree-of-freedom (SDOF) system incorporating nonlinearities due to gas spring, seal friction, orifice flows and motion limiting stops.

The second model of the suspension system is developed by considering the fluid compressibility. The dynamics of the floating piston are then characterized by an additional DOF. The suspension model is thus represented by two coupled and nonlinear second order differential equations, and two first order differential equations relating the fluid pressure, compressibility, and flow in chambers I and

II. The fluid compressibility yields a second resonant frequency, which is considerably higher than the first resonance in the low frequency range. The second resonant frequency occurs well beyond the frequency range of interest in this study, and is only evident in the compression mode. Analysis of the hydropneumatic suspension model revealed that the fluid compliance dominates the system compliance at higher excitation frequencies during the compression mode, and when fluid bulk modulus is low. The gas spring, however, remains the predominant system compliance during the expansion mode. The shock and vibration attenuation performance of the suspension system are not significantly affected by the hydraulic fluid compressibility. The two suspension models, therefore, yield identical dynamic behaviour and performance characteristics. However, a reduction in the fluid bulk modulus, caused by only a small amount of entrained air, affects the suspension performance in a significant manner.

7.2.2 Linearization of Suspension Model

The hydropneumatic suspension exhibits nonlinearities due to gas spring, orifice damping, seal friction and bump stops. Since the linear system models are simpler and more convenient to analyze than the nonlinear models, the nonlinear suspension model is linearized using the local linearization scheme based upon energy balance. The nonlinear damping forces due to orifice damping and seal friction are represented by an array of local equivalent damping coefficients, where each coefficient is valid only in the vicinity of the selected excitation frequency and magnitude. The nonlinear restoring forces due to gas spring are characterized by an array of local equivalent stiffness coefficients for isothermal, adiabatic and polytropic conditions. An

iterative algorithm is employed to determine the local equivalent linear coefficients and thus the frequency response of the linearized hydropneumatic suspension model. A comparison of the linearized system response to that of the nonlinear system revealed that the linearization technique yields reasonable correlation with the nonlinear suspension model except in the region of resonance. For small relative displacements and relative velocities, the linearization technique accurately predicts the spring and damping forces generated by the hydropneumatic suspension.

7.2.3 Transient Response of the Hydropneumatic Suspension

Transient response of the hydropneumatic suspension is evaluated in terms of shock displacement and shock acceleration characteristics for rounded step and rounded pulse displacement excitations. In order to establish relative shock isolation performance potentials, the performance characteristics of the hydropneumatic suspension are compared to those of a conventional suspension. The conventional suspension is configured with a linear spring of stiffness equal to the static stiffness of the gas spring, and velocity-squared, (orifice), damping characteristic. The results showed that the hydropneumatic suspension yields improved shock isolation performance when compared to the conventional suspension system.

7.2.4 Vibration Isolation of the Hydropneumatic Suspension

Vibration isolation is investigated in terms of displacement and acceleration transmissibilities of the sprung mass. The vibration isolation characteristics of the hydropneumatic suspension are compared to those of an equivalent conventional suspension, configured for transient response analyses, in order to demonstrate its relative

performance potentials.

The frequency response characteristics of the hydropneumatic suspension exhibit different magnitudes of transmitted vibration during compression and expansion modes, due to asymmetric force-deflection characteristics of the gas spring. The conventional suspension, however, yields identical frequency response in the compression and expansion modes. The vibration isolation performance of the hydropneumatic suspension are thus presented in terms of compression and expansion mode vibration transmissibilities.

7.2.5 Parametric Sensitivity Analyses

A comprehensive parametric study is performed to establish the influence of variations in design and operating parameters on the performance characteristics of hydropneumatic suspension. The sensitivity of suspension performance to variations in hydraulic fluid bulk modulus, polytropic exponent, ratio of primary piston area to floating piston area, gas charge pressure and initial gas volume, is specifically investigated. The following conclusions are drawn from the parametric study:

(a) The hydropneumatic suspension performance is most significantly affected by variations in polytropic exponent, gas charge pressure and initial gas volume.

(b) A low value of polytropic exponent provides best vibration isolation in terms of lowest transmitted acceleration and displacement.

(c) An increase in initial gas volume and initial gas pressure yields improved vibration isolation.

(d) Reduction in effective fluid bulk modulus yields increasingly

asymmetric vibration transmissibility response.

(e) Moreover, the vibration transmissibility response characteristics exhibit a second high frequency resonance, evident only in the compression mode. This second resonance is due to the added dynamics of the floating piston mass and fluid compressibility.

(f) Significant reduction in fluid bulk modulus results in reduction of transmitted shock displacement and acceleration.

7.2.6 Vehicle Ride Potential Analysis

The ride performance potentials of hydropneumatic suspension are investigated using a tracked vehicle ride dynamic model. The tracked vehicle is represented by a seven DOF dynamical system in the pitch plane, while assuming negligible dynamics in the roll plane. Two tracked vehicle models are developed using two different suspension configurations: (i) trailing arm torsion bar suspension at each road wheel, and conventional shock absorber at first and last road wheels, and (ii) trailing arm torsion bar suspension at road wheels 2, 3, 4, and hydropneumatic suspension at first and last road wheels.

The relative ride performance potentials of hydropneumatic suspension are established by comparing its shock and vibration attenuation characteristics to those of the tracked vehicle with conventional suspension. The vibration attenuation performance is evaluated for harmonic excitations occurring simultaneously at all road wheels, and shock attenuation performance characteristics are evaluated for semi-circular obstacles and different vehicle speeds. A comparison of shock and vibration attenuation characteristics of the two suspension

systems revealed the following:

(a) The vibration transmission performance of the hydropneumatic suspension is considerably superior to that of the conventional suspension. The hydropneumatic suspension thus offers considerable potentials for ride improvement of these vehicles.

(b) The hydropneumatic suspension, specifically, provides superior vibration attenuation of low frequency excitations around sprung mass resonances corresponding to hull pitch and bounce modes. Since the low frequency vibrations are the primary contributing factor to driver/crew discomfort and fatigue, the hydropneumatic suspension offers excellent potential to minimize the impact of low frequency whole body ride vibration on the driver/crew.

(c) The hydropneumatic suspension also yields improved attenuation of high frequency vibration around the resonant frequency of the road wheels.

(d) The hydropneumatic suspension effectively reduces the magnitude of transmitted shock displacement and acceleration, specifically due to large obstacles and high vehicle approach speeds.

(e) The improved ride performance potentials of the hydropneumatic suspension system are attributed to the progressively stiffening spring characteristic and simple orifice damping scheme.

7.3 RECOMMENDATIONS FOR FUTURE INVESTIGATIONS

The present investigation yields dynamic models which provide a basic insight to the shock and vibration isolation performance of the hydropneumatic suspension system. The modeling and analyses techniques employed in this study lend themselves well to the analysis of hydropneumatic as well as other suspension systems employing a nonlinear spring characteristic. The knowledge gained from this investigation is a starting point and establishes the direction for future work.

It is recommended that future investigations include extensive laboratory testing of the hydropneumatic suspension system in order to validate the mathematical models presented herein. Validation of the present models will increase confidence in both the modeling techniques employed in this study, and the ability for the models to accurately predict the performance of the nonlinear suspension system. Laboratory testing will also highlight any shortcomings of the current models and the need for refinements.

It is also recommended that the sophistication of the current mathematical models be increased so as to include thermal effects, compliance of cylinder walls and suspension internals, the affects of tuned damper valving, and a control scheme for ride height control. The consideration of thermal effects is very important since the gas polytropic exponent, hydraulic fluid viscosity, friction, and material expansion properties are all affected by changes in operating temperature.

The current analyses have concentrated on the response to deterministic excitations. Future work should explore the response of the hydropneumatic suspension to stochastic excitation. This natural

extension in the investigation would provide another aspect for comparison of the shock and vibration isolation potentials of the hydropneumatic suspension. In addition, comparison of the hydropneumatic suspension with various types of suspension systems, such as other gas spring or semi-active suspension configurations, will increase understanding of the relative ride quality benefits provided by the hydropneumatic suspension system. It would also be beneficial to perform additional vehicle application studies to evaluate the ride potentials of hydropneumatic suspension for different classes of vehicles, including both on and off-road applications.

Finally, optimization techniques can be employed to 'tune' the hydropneumatic suspension characteristics to provide optimal shock or vibration isolation performance for a specific terrain or vehicle application. The parametric analyses provide the background for further study in this area by highlighting the parameters which have a significant effect on the performance of the hydropneumatic suspension system.

REFERENCES

1. Fukushima, N., Hidaka, K and Iwata, K, "Optimum Characteristics of Automotive Shock Absorbers Under Various Driving Conditions and Road Surfaces", *International Journal of Vehicle Design*, Volume 4, Number 5, 1983. pp. 463-472.

2. Anderson, R.J. and Fan, Y., "Dynamic Testing and Modelling of a Bus Shock Absorber", *SAE Technical Paper series 902282*, 1990.

3. Hall, B.B. and Gill, K.F., "Performance of a Telescopic Dual-Tube Automotive Damper and the Implications for Vehicle Ride Prediction", *Proceedings of the Institution of Mechanical Engineers*, Volume 200, Number D2, 1986. pp. 115-123.

4. "Guide to the Evaluation of Human Exposure to Whole-Body Vibration" *ISO 2631-1978(E)* and *Amendment 1, ISO 2631-1978/A1-1982(E), (International Standards Organization)*

5. Su, H., Rakheja, S. and Sankar, T.S., "Analysis of a Passive Sequential Damper for Vehicle Suspension", *Vehicle System Dynamics*, Volume 19, 1990. pp.289-312.

6. Bank, T.A., "Some ABC's of Air Spring Suspensions for Commercial Road Vehicles", *SAE Technical Paper Series No. 800482*, International Congress and Exposition, Detroit, Michigan, 1980.

7. Burkley, T.E. and Meyers, P.F., "Design and Validation of Variable Rate Pneumatic Springs", *SAE Technical Paper Series No. 800483*, International Congress and Exposition, Detroit, Michigan, 1980.

8. Hundal, M.S.,"Damped Pneumatic Spring as Shock Isolator: Generalized Analysis and Design Procedure", *Shock and Vibration Bulletin*, Volume 53, Part 4, 1983. pp. 73-83.

9. Hundal, M.S. and Fitzmorris, D.J., "Response of a Symmetric Self-Damped Pneumatic Shock Isolator to an Acceleration Pulse", *Shock and Vibration Bulletin*, Part 4, 1984. pp. 139-154.

10. Wahi, M.K., "Oleopneumatic Shock Strut Dynamic Analysis and Its Real-Time Simulation", *Journal of Aircraft*, Volume 13, Number 4, 1976. pp. 303-308.

11. Wahi, M.K., "Oil Compressibility and Polytropic Air Compression Analysis for Oleopneumatic Shock Struts", *Journal of Aircraft*, Volume 13, Number 7, 1976. pp. 527-530.

12. Moulton, A.E. and Best, A., "From Hydrolastic to Hydragas Suspension", *Proceedings of the Institution of Mechanical Engineers*, Volume 193, 1979. pp. 15-37.

13. Félez, J. and Vera, C., "Bond Graph Assisted Models for Hydropneumatic Suspensions in Crane Vehicles", *Vehicle System Dynamics*, Volume 16, 1987. pp. 313-332.

14. Craighead, I.A. and Brown, P.R., "Vibration and Dynamics of Off-Road Vehicles", *Institution of Mechanical Engineers*, C135/84, 1984. pp.65-76.

15. Maclaurin, B., "Progress in British Tracked Vehicle Suspension Systems", *SAE Technical Paper Series No. 830442*, International Congress and Exposition, Detroit, Michigan, 1983.

16. "Comparison of the Ride and Shock Responses of the M60 STB and M60 HSS/ATB Hybrid Tanks", *W.E.S. Miscellaneous Paper No. GL-79-2*, Geotechnical Laboratory, U.S. Army Engineer Waterways Experiment Station, Vicksburg, Mississippi, 1979.

17. Karnopp, D. and Margolis, D., "Adaptive Suspension Concepts for Road Vehicles", *Vehicle System Dynamics*, Volume 13, 1984. pp. 145-160.

18. Horton, D.N.L. and Crolla, D.A., "Theoretical Analysis of a Semi-Active Suspension Fitted to an Off-Road Vehicle", *Vehicle System Dynamics*, Volume 15, 1986. pp. 351-372.

19. Crolla, D.A., Pitcher, R.H. and Lines, J.A., "Active Suspension Control for an Off-Road Vehicle", *Proceedings of the Institution of Mechanical Engineers*, Volume 201, Number D1, 1987. pp. 1-10.

20. Dominy, J. and Bulman, D.N., "An Active Suspension for a Formula One Grand Prix Racing Car", *Journal of Dynamic Systems, Measurement, and Control*, Volume 107, 1985. pp. 73-78.

21. "Aircraft Landing Gear Systems", edited by J.A. Tanner, *SAE PT-37*, 1990. pp. 179-196.

22. "DUNLORIDE Hyro-Pneumatic Suspension System - Type 40-60 Tonne", Product Brochure, *Dunlop Aviation Division - Military Equipment*, Coventry, England.

23. "Hydropneumatic Suspension System for Tracked/Wheeled Military Vehicles", Model 2880 In-Arm Hydropneumatic Suspension Unit Product Brochure, *Teledyne Continental Motors, General Products Division*, Muskegon, Michigan.

24. "Manual for Incorporating Pneumatic Springs in Vehicle Suspension Designs", *SAE HS 1576*, Report of the Spring Committee, June 1988.

25. Mayne, R.W., "The Effects of Fluid and Mechanical Compliance on the Performance of Hydraulic Shock Absorbers", *Transactions of the ASME, Journal of Engineering for Industry*, February 1974. pp. 101-106.

26. Dalibert, A., "Progress in Shock Absorber Oil Technology", *SAE Technical Paper No. 77085*, 1970.

27. Hanly, F.J., "Fluids for High-Pressure Industrial Hydraulic Systems", *SAE Technical Paper No. 670697*, 1969.

28. Merritt, H.E., *Hydraulic Control Systems*, John Wiley & Sons, Inc., New York, 1967.

29. Hornbeck, R.W., "*Numerical Methods*", Prentice-Hall Inc., New Jersey, 1975.

30. Bastow, D., "*Car Suspension and Handling*", Second Edition, Pentech Press, London, 1987.

31. Rakheja, S. and Sankar, S., "Response of a Sequential Damper to Shock Inputs", *The Shock and Vibration Bulletin*, Bulletin 57, Part 3, January 1987.

32. Thomson, W.T., "*Theory of Vibration with Applications*", Second Edition, Prentice-Hall Inc., New Jersey, 1981.

33. Su, H., "Random Response of Pressure Limited Hydraulic Damper", Technical Report, Concordia University, Montreal, February 1988.

34. Afonso, M.F.R., "Ride Dynamic Rsponse of Tracked Vehicles", Master of Engineering Thesis, Department of Mechanical Engineering, Concordia University, Montreal, 1989.

35. Cochin, I., *Analysis and Design of Dynamic Systems*, Dun-Donnely Publisher, New York, 1977.

36. Roberts, J.B., "Response of Non-Linear Mechanical Systems to Random Excitation. Part 2: Equivalent Linearization and Other Methods", *Shock and Vibration Digest*, Volume 13, Number 5, May 1981. pp. 15-29.

37. Caughey, T.K., "Equivalent Linearization Techniques", *Journal of the Acoustical Society of America*, Volume 35, Number 11, 1963. pp. 1706-1711.

38. Bandstra, J.P., "Comparison of Equivalent Viscous Damping and Nonlinear Discrete and Continuous Vibrating Systems", *ASME Paper No. 81-DET-89*, Presented at the 8th ASME Design Engineering Conference, Hartford, Conn., September 1981.

39. Rakheja, S., Van Vliet, M. and S. Sankar, "A Discrete Harmonic Linearization Technique for Simulation of Nonlinear Mechanical Systems", *Journal of Sound and Vibration*, Volume 100, Number 4, 1985. pp. 511-526.

APPENDIX A

DEVELOPMENT OF TRACKED VEHICLE EQUATIONS OF MOTION

The equations of motion for the seven degrees-of-freedom, (DOF), ride dynamic model of a tracked military vehicle are derived using Lagrange's Method. Lagrange's Method is chosen for its simplicity since the tracked vehicle represents a multi-degree-of-freedom (MDOF) dynamical system which can be efficiently analyzed with the use of generalized co-ordinates. Generalized co-ordinates, q_i , are defined as the "n" independent co-ordinates which are necessary to describe the equations of motion of a dynamic "n" DOF system [32]. Seven generalized co-ordinates are required to completely describe the dynamic motion of the pitch-plane model of the tracked vehicle. The resulting generalized co-ordinates chosen for the dynamic analysis are: vertical motion of the hull c.g., y_h ; pitch displacement of the hull c.g., ϕ_h, and vertical displacement each road wheel, y_{wi} , $i = 1, 2, \ldots, 5$.

The equations of motion are derived from the kinetic, potential and dissipative energy functions of the dynamic system [32]:

$$\frac{d}{dt}\left(\frac{\delta T}{\delta \dot{q}_i}\right) - \frac{\delta T}{\delta q_i} - \frac{\delta D}{\delta \dot{q}_i} + \frac{\delta U}{\delta q_i} = 0 \qquad (A.1)$$

where **T** is the kinetic energy, **D** is the dissipative energy, and **U** is the potential energy.

Static Analysis

Static analysis of the tracked vehicle poses a statically indeterminate problem. For the tracked vehicle, equipped with conventional suspension, it is therefore assumed that each road wheel

supports an equal amount of the vehicle weight. For the tracked vehicle equipped with hydropneumatic suspension, it is necessary to determine the initial gas spring characteristics which match those of the conventional torsion bar spring suspension. The hydropneumatic suspension systems replace both the torsion bar and hydraulic damper sets at the first and last road wheels. The hydropneumatic suspension mounting points coincide directly with those of the conventional damper. Due to the suspension linkage design, a force multiplication exists on each trailing arm linkage suspension set. This suspension linkage 'gain' may be easily determined by referring to Figure A.1.

Under static conditions, a couple is produced on the trailing arm due to the static weight being supported. This static couple is given by:

$$\text{Static Couple} = W \cdot R \cdot \cos(\theta_o - \zeta) \qquad (A.2)$$

where W is the static weight supported at the wheel station, R is the length of the trailing arm, and $(\theta_o - \zeta)$ is the angle between the trailing arm axis and the horizontal. This couple must be balanced by a reaction torque supplied by the hydropneumatic suspension. The reaction torque produced by the hydropneumatic suspension is given by:

$$\text{Reaction Torque} = F_{Hs} \cdot r_s \cos(\tfrac{\pi}{2} - \lambda - \theta_o) \qquad (A.3)$$

where F_{Hs} is the static force developed by the hydropneumatic suspension, and r_s is the perpendicular distance from the trailing arm pivot to the hydropneumatic suspension mounting point. The suspension geometry, however, results in an approximately perpendicular orientation of the hydropneumatic suspension with respect to the trailing arm. Assuming small angle, $\cos(\pi/2 - \lambda - \theta_o) \cong 1$, and the reaction torque can

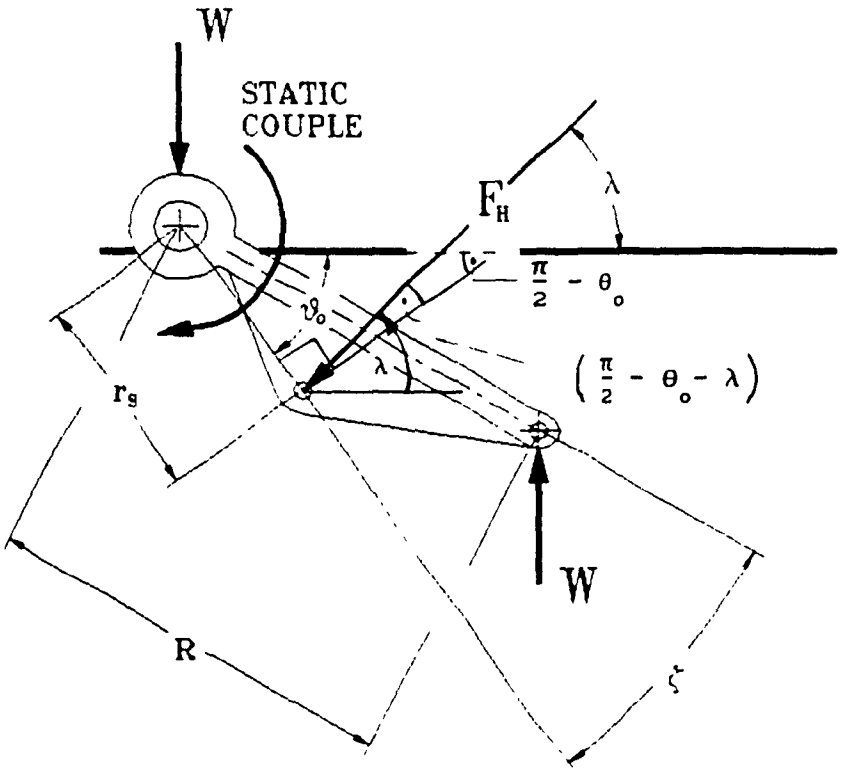

Figure A.1: Forces acting on trailing arm linkage under static conditions.

be expressed as:

$$\text{Reaction Torque} \cong F_{Hs} \cdot r_s \tag{A.4}$$

Equating the static couple and the reaction torque, it is possible to determine the amount of static force required from the hydropneumatic suspension in order to maintain equilibrium:

$$F_{Hs} = W \cdot \frac{R}{r_s} \cos \theta_o \tag{A.5}$$

The term:

$$\frac{R}{r_s} \cdot \cos \theta_o$$

is the linkage gain due to the trailing arm suspension design. Multiplication of the static weight by the linkage gain yields the static force required from the hydropneumatic suspension.

The initial stiffness of the hydropneumatic suspension is determined by equating the torque developed by the torsion bar spring and that of the hydropneumatic suspension. The torque, T_{bar}, developed by the linear torsion bar is:

$$T_{bar} = K_t \cdot \theta \tag{A.6}$$

where K_t is the torsion bar stiffness, and θ is the angle of rotation. The torque, T_H, developed by the hydropneumatic suspension about the trailing arm pivot is given by:

$$T_H = K_{Hs} \cdot X \cdot r_s \tag{A.7}$$

where K_{Hs} is the static stiffness of the hydropneumatic suspension, X is the amount of static linear displacement, and r_s is defined as before.

Assuming small angular displacement, the displacement, X, may be approximated by:

$$X = r_s \cdot \theta$$

Substituting for X in equation (A.7) with the above expression yields the following approximation for the torque developed by the

hydropneumatic suspension:

$$T_H = K_{Hs} \cdot \theta \cdot r_s^2 \qquad (A.8)$$

Equating the two expressions for torque, the equivalent initial stiffness of the hydropneumatic suspension obtained as:

$$K_{Hs} = \frac{1}{r_s^2} \cdot K_t \qquad (A.9)$$

Equations (A.5) and (A.9) provide the necessary information for sizing the hydropneumatic suspension to provide initial spring characteristics similar to those of the conventional torsion bar springs.

Dynamic Analysis

Referring to Figure A.2, the equation for the kinetic energy of the system, T, is given by:

$$T = \frac{1}{2} \cdot M_h \cdot \dot{y}_h^2 + \frac{1}{2} \cdot J_h \cdot \dot{\phi}_h^2 + \frac{1}{2} \sum_{i=1}^{5} m_{wi} \cdot \dot{y}_{wi}^2 + \frac{1}{2} \sum_{i=1}^{5} m_{wi} \cdot \dot{x}_{wi}^2 \qquad \ldots(A.10)$$

where M_h is the mass of the hull, J_h is the pitch-plane mass moment of inertia of the hull about the hull c.g., m_{wi} is the mass of the i^{th} road wheel, $\dot{y}_h$ is the bounce velocity of the hull c.g. , $\dot{\phi}_h$ is the hull pitch velocity about the hull c.g., and $\dot{x}_{wi}$ and $\dot{y}_{wi}$ are the horizontal and vertical components, respectively, of the velocity of the i^{th} road wheel.

The longitudinal velocity of road wheels, $\dot{x}_{wi}$, can be related to the generalized coordinates using the constraint equations. Referring to Figure A.3, and assuming small angles, the horizontal motion of the road wheels can be expressed in terms of trailing arm rotation:

$$x_{wi} = x_i - R\,\theta_i \sin(\theta_o - \zeta) \qquad (A.11)$$

where x_i is the horizontal displacement of the i^{th} trailing arm pivot,

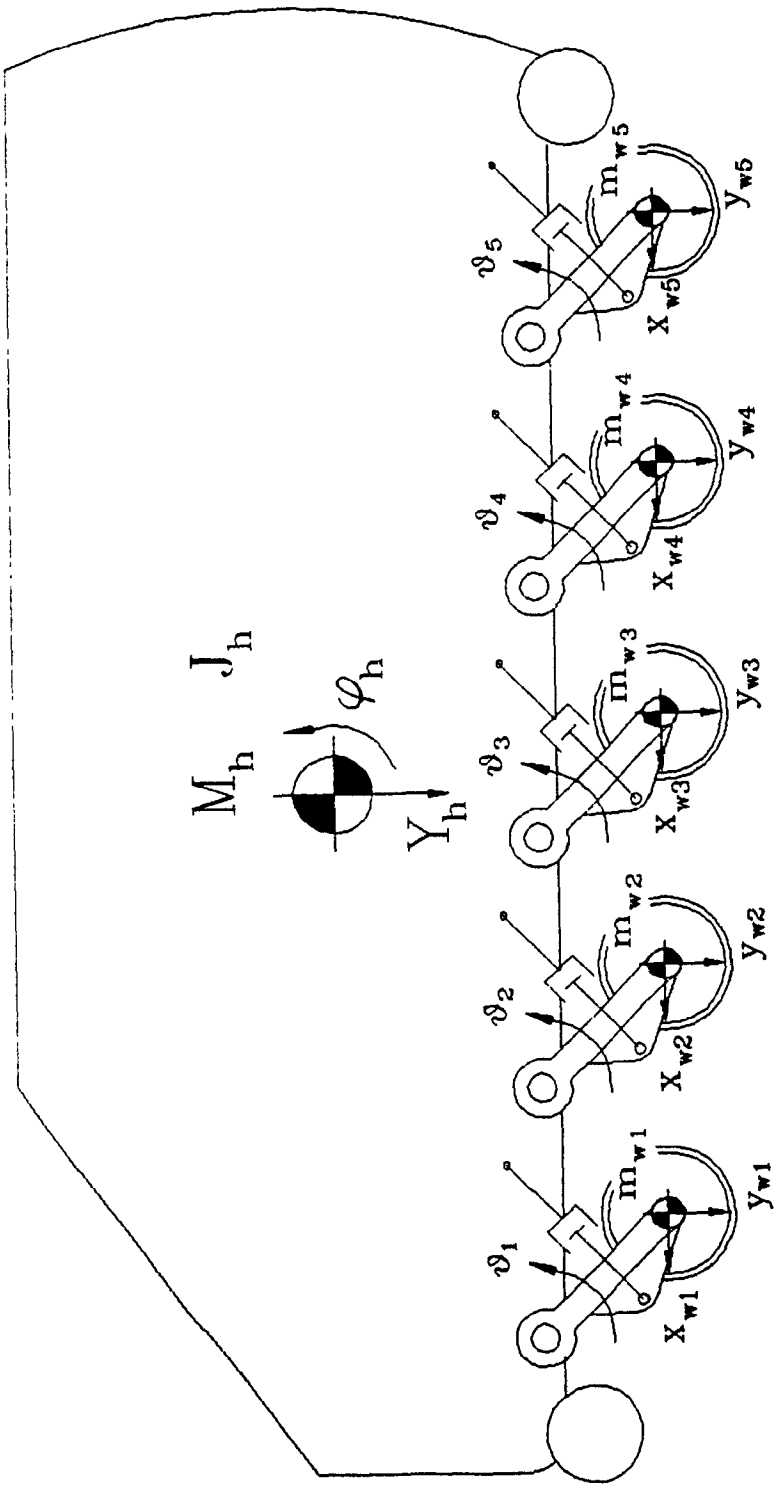

Figure A.2: Lumped-mass representation of the seven-degrees-of-freedom tracked vehicle.

θ_i is the angular rotation of the i^{th} trailing arm, θ_o is the initial angle between the hull floor and a line passing from the trailing arm pivot to the trailing arm shock mount (point A), and ζ is the offset angle between the trailing arm center line and the line passing from the trailing arm pivot to the trailing arm shock mount. The horizontal displacement of the trailing arm pivot, x_i, can be related to the pitch displacement of the hull:

$$x_i = - d_i \cdot \phi_h \cdot \sin \alpha_i \qquad (A.12)$$

where d_i is the distance between the i^{th} trailing arm pivot and the hull c.g., and α_i is the angle formed between the horizontal and the line between hull c.g. and trailing arm pivot.

The vertical displacement of the road wheels can also be related to the trailing arm rotation and hull pitch using the following constraint equation:

$$y_{wi} = y_h + d_i \cdot \phi_h \cdot \cos \alpha_i - R \cdot \theta_i \cdot \cos(\theta_o - \zeta) \qquad (A.13)$$

Equation (A.13) thus yields an expression for the trailing arm rotational coordinates in terms of the generalized coordinates:

$$\theta_i = \frac{y_h + d_i \cdot \phi_h \cdot \cos \alpha_i - y_{wi}}{R \cdot \cos(\theta_o - \zeta)} \qquad (A.14)$$

Equations (A.11), (A.12) and (A.14) then yield an expression for x_{wi} in terms of the generalized coordinates:

$$x_{wi} = - d_i \cdot \phi_h \cdot \sin \alpha_i - [y_h + d_i \cdot \phi_h \cdot \cos \alpha_i - y_{wi}] \cdot \tan(\theta_o - \zeta) \qquad ...(A.15)$$

Differentiating once with respect to time yields the expression for the horizontal velocity of the road wheels:

$$\dot{x}_{wi} = - d_i \cdot \dot{\phi}_h \cdot \sin \alpha_i - [\dot{y}_h + d_i \cdot \dot{\phi}_h \cdot \cos \alpha_i - \dot{y}_{wi}] \cdot \tan(\theta_o - \zeta) \qquad ...(A.16)$$

The equation for the potential energy, U, is derived from the energy storage elements, consisting of the torsion bars, bump stops, and the track. The effect of the track is two fold, acting both as a linear spring between the individual road wheels and the ground, and as a continuous belt applying a tension to the road wheel sets. The track tension is modeled as relative springs acting between the adjacent road wheels as well as between the front sprocket and wheel 1, and between wheel 5 and the rear idler gear. The potential energy is thus expressed as:

$$U = \frac{1}{2}\sum_{i=1}^{5} K_{ti} \cdot (\theta_i - \phi_h)^2 + \frac{1}{2}\sum_{i=1}^{5} K_{peff} \cdot (y_{wi} - y_{Ri})^2 + \frac{1}{2}\mu_s (y_{w1} - y_s)^2 + \frac{1}{2}\sum_{i=1}^{4} \mu_{wi} (y_{wi+1} - y_{wi})^2 + \frac{1}{2}\mu_I (y_{ID} - y_5)^2 \quad \ldots(A.17)$$

where K_{ti} is the linear stiffness of the i^{th} torsion bar, K_{peff} is the effective linear stiffness of the elastic track pad and elastic road wheels, y_{Ri} is the vertical displacement excitation at the i^{th} road wheel, y_s is the vertical displacement of the sprocket, y_{ID} is the vertical displacement of the idler gear, μ_s, μ_I, and μ_w are the relative spring rates between the sprocket and road wheel 1, road wheel 5 and the idler gear, and between adjacent road wheels, respectively.

Assuming small angles, the vertical displacements of the sprocket, y_s, and the idler gear, y_{ID}, are expressed as:

$$y_s = y_h + L_{sp} \cdot \phi_h$$
$$y_{ID} = y_h - L_{id} \cdot \phi_h \quad (A.18)$$

where L_s and L_{id} are the horizontal distances between the hull c.g. and the sprocket and idler gear, respectively.

The linear stiffness of the elastic track pads (K_p), and road wheels (K_w), are assumed to be series-connected. The equivalent stiffness is, thus, computed as:

$$K_{peff} = \frac{K_p \cdot K_w}{K_p + K_w} \qquad (A.19)$$

The elastic bump stops which limit the travel of the trailing arms, as shown in Figure A.4, are incorporated in the analysis as equivalent torsional stiffnesses acting at the trailing arm pivot. The torsion bars are thus modeled with two linear ranges of stiffness as shown in Figure A.5: one soft range due to torsion bar alone, and an extremely stiff range when the trailing arm encounters the bump stop. The equivalent torque about the trailing arm pivots due to the bump stops, K_{teq}, is given by:

$$K_{teq} = r_b^2 \cdot K_b \qquad (A.20)$$

where r_b is the distance from the road arm pivot to the bump stop, and K_b is the linear stiffness of the elastic bump stop.

The dissipative energy, D, of the tracked vehicle system is determined from the hydraulic shock absorbers, and is given by:

$$D = \frac{1}{2} \sum_{i=1}^{5} C_{eqi} \cdot (V_{ai} - V_{bi})^2$$

where C_{eqi} is viscous damping coefficient due to shock absorber at road wheel i, V_{ai} is the velocity of the i^{th} trailing arm shock mount along the shock absorber axis and V_{bi} is the velocity of the i^{th} hull shock mount along the shock absorber axis, computed as:

$$V_{ai} = \dot{x}_{sri} \cdot \cos\lambda + \dot{y}_{sri} \cdot \sin\lambda$$
$$V_{bi} = \dot{x}_{shi} \cdot \cos\lambda + \dot{y}_{shi} \cdot \sin\lambda \qquad (A.21)$$

where λ is the inclination of the shock absorber with respect to the

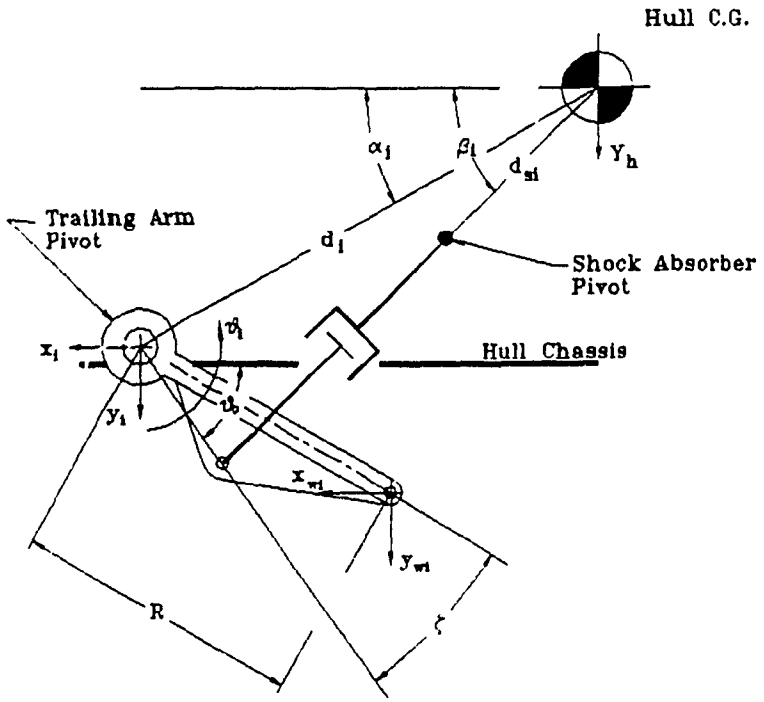

Figure A.3: Geometry of trailing arm linkage 'i'.

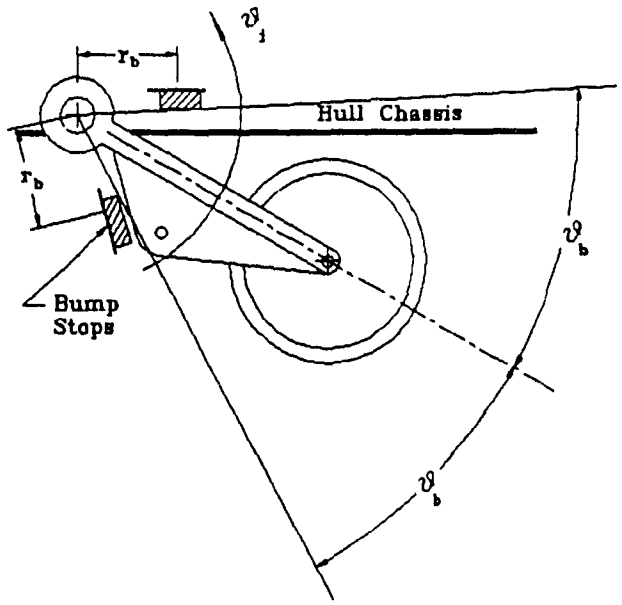

Figure A.4: Geometry of elastic bump stops acting on trailing arm linkages.

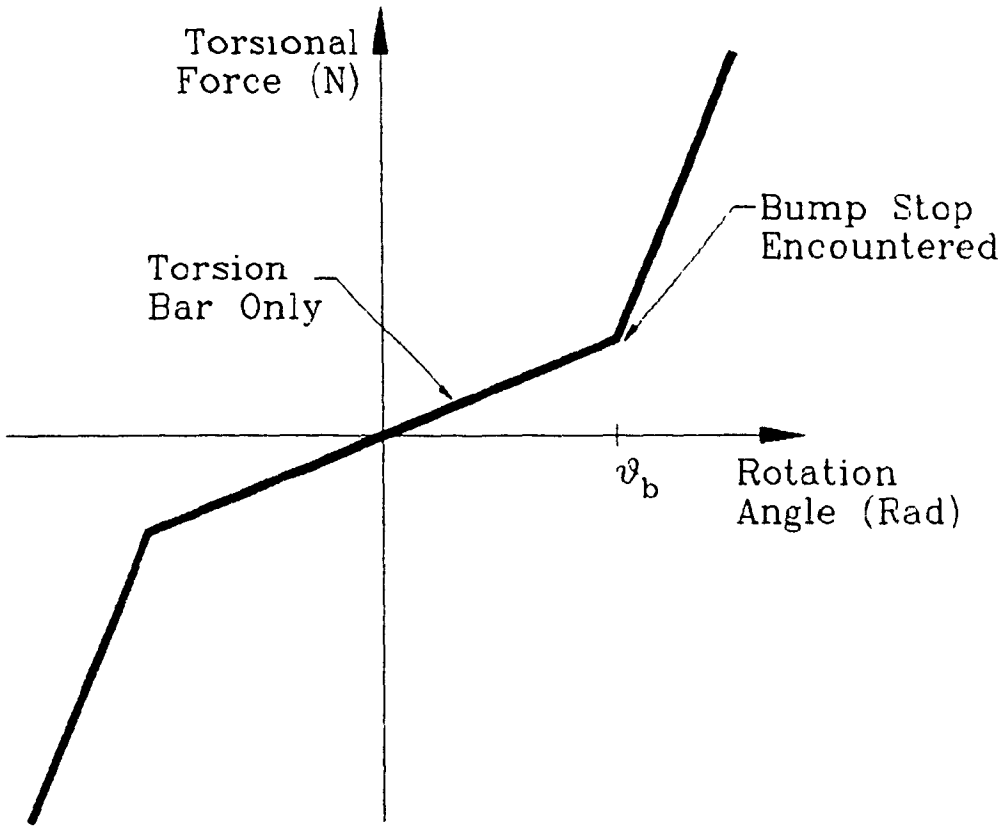

Figure A.5: Piece-wise linear torsion bar characteristic resulting from the addition of elastic bump stops.

hull floor; $\dot{x}_{sri}$ and $\dot{y}_{sri}$ are the horizontal and vertical components, respectively, of the i^{th} trailing arm shock mount velocity, and $\dot{x}_{shi}$ and $\dot{y}_{shi}$ are the horizontal and vertical components, respectively, of the i^{th} hull shock mount velocities. These velocity components can be expressed in terms of the generalized co-ordinates in the following manner:

$$\dot{x}_{sri} = -\frac{r_s}{R} \cdot \frac{\sin\theta_o}{\cos(\theta_o - \zeta)} \cdot \dot{y}_h - [d_i \cdot \sin\alpha_i + \frac{r_s}{R} \cdot \frac{\sin\theta_o}{\cos(\theta_o - \zeta)} \cdot d_i \cdot \cos\alpha_i] \cdot \dot{\phi}_h + \frac{r_s}{R} \cdot \frac{\sin\theta_o}{\cos(\theta_o - \zeta)} \cdot \dot{y}_{wi}$$

$$\dot{y}_{sri} = \left[1 - \frac{r_s}{R} \frac{\cos\theta_o}{\cos(\theta_o - \zeta)}\right] \dot{y}_h + \left[1 - \frac{r_s}{R} \cdot \frac{\cos\theta_o}{\cos(\theta_o - \zeta)}\right] d_i \cos\alpha_i \cdot \dot{\phi}_h + \frac{r_s}{R} \cdot \frac{\cos\theta_o}{\cos(\theta_o - \zeta)} \cdot \dot{y}_{wi}$$

$$\dot{x}_{shi} = -d_{si}\ \dot{\phi}_h \sin\beta_i$$

$$\dot{y}_{shi} = \dot{y}_h + d_{si}\ \dot{\phi}_h \cos\beta_i \qquad \text{(A.22)}$$

where d_{si} is the distance between the hull c.g. and the i^{th} hull shock mount; β_i is the angle with respect to the horizontal made by the line passing from the i^{th} hull shock mount to the hull c.g..

The equations of motion of the seven DOF model, derived using Lagrange's equation, can be expressed as:

Hull Bounce:

$$\left(M_h - \tan^2(\theta_o - \zeta) \sum_{i=1}^{5} m_{wi}\right) \cdot \ddot{y}_h - \tan(\theta_o - \zeta) \cdot$$

$$\sum_{i=1}^{5} m_{wi} \cdot d_i \left[\tan(\theta_o - \zeta) \cos \alpha_i + \sin \alpha_i \right] \cdot \ddot{\phi}_h +$$

$$\tan^2(\theta_o - \zeta) \sum_{i=1}^{5} m_{wi} \cdot \ddot{y}_{wi} + \frac{1}{R \cdot \cos(\theta_o - \zeta)} \cdot \sum_{i=1}^{5} K_{ti} \cdot (\theta_i - \phi_h)$$

$$+ \mu_s \cdot \left(y_h + L_{sp} \cdot \phi_h - \dot{y}_{wi} \right) + \mu_{ID} \cdot \left(y_h - L_{ID} \cdot \phi_h - y_{ws} \right)$$

$$+ \frac{r_s}{R \cdot \cos(\theta_o - \zeta)} \cdot \sin(\lambda + \theta_o) \cdot \sum_{i=1}^{5} C_{eqi} \cdot (V_{ai} - V_{bi}) = 0$$

...(A.23)

Hull Pitch:

$$\left(J_h + \sum_{i=1}^{5} m_{wi} \cdot d_i \left[\sin \alpha_i + \tan(\theta_o - \zeta) \cdot \cos \alpha_i \right]^2 \right) \cdot \ddot{\phi}_h$$

$$+ \tan(\theta_o - \zeta) \sum_{i=1}^{5} m_{wi} \cdot d_i \cdot \left[\sin \alpha_i + \tan(\theta_o - \zeta) \cdot \cos \alpha_i \right]$$

$$\cdot \left(\ddot{y}_h - \ddot{y}_{wi} \right) + \sum_{i=1}^{5} \left(\frac{d_i \cdot \cos \alpha_i}{R \cdot \cos(\theta_o - \zeta)} - 1 \right) \cdot K_{ti} \cdot (\theta_i - \phi_h)$$

$$+ \mu_s \cdot L_{sp} \cdot \left(y_h + L_{sp} \cdot \phi_h - y_{wi} \right) - \mu_{ID} \cdot L_{ID} \cdot \left(y_h - L_{ID} \right.$$

$$\left. \cdot \phi_h - y_{ws} \right) - \sum_{i=1}^{5} \left\{ \left[d_{si} \cdot \sin \beta_i - d_i \cdot \sin \alpha_i - \right. \right.$$

$$\frac{r_s \cdot \sin \theta_o}{R \cdot \cos(\theta_o - \zeta)} \cdot d_i \cdot \cos \alpha_i \left. \right] \cdot \cos \lambda + \left[\left(1 - \right. \right.$$

$$\left. \left. \frac{r_s \cdot \cos \theta_o}{R \cdot \cos(\theta_o - \zeta)} \right) \cdot d_i \cdot \cos \alpha_i - d_{si} \cdot \cos \beta_i \right] \cdot \sin \lambda \Big\} \cdot$$

$$C_{eqi} \cdot (V_{ai} - V_{bi}) = 0 \qquad \ldots(A.24)$$

Wheel Bounce:

$$m_{wi}\left(1 - \tan^2(\theta_o - \zeta)\right) \cdot \ddot{y}_{wi} + \tan^2(\theta_o - \zeta) \cdot m_{wi} \cdot \ddot{y}_h + \tan(\theta_o - \zeta) \cdot m_{wi} \cdot d_i \left[\sin\alpha_i + \tan(\theta_o - \zeta) \cdot \cos\alpha_i\right] \cdot \ddot{\phi}_h - \frac{1}{R \cdot \cos(\theta_o - \zeta)} \cdot K_{ti} \cdot (\theta_i - \phi_h) + K_{peff} \cdot (y_{wi} - y_{Ri}) + \mu_w \left(2y_{wi} - y_{wi-1} - y_{wi+1}\right) - \frac{r_s}{R \cdot \cos(\theta_o - \zeta)} \cdot \sin(\lambda + \theta_o) \cdot C_{eqi} \cdot (V_{ai} - V_{bi}) = 0 \quad \ldots(A.25)$$

Equations (A.23) to (A.25) represent the dynamic equations of motion for the tracked vehicle equipped with conventional torsion bar/hydraulic damper linkage suspension. When the tracked vehicle is equipped with hydropneumatic suspension systems, the above equations must be modified to include its effects. Assuming identical locations of the hydropneumatic suspension, the vertical and horizontal velocities across the suspension system can be derived from equations (A.21) and (A.22). The relative displacement across the hydropneumatic suspension can be expressed in a similar manner:

$$\begin{aligned} D_{ai} &= x_{sri} \cdot \cos\lambda + y_{sri} \cdot \sin\lambda \\ D_{bi} &= x_{shi} \cdot \cos\lambda + y_{shi} \cdot \sin\lambda \end{aligned} \qquad (A.26)$$

where D_{ai} and D_{bi} are the displacements along the shock absorber axis of the trailing arm and hull mount suspension locations, respectively; x_{sri} and y_{sri} are the horizontal and vertical components, respectively, of the trailing arm shock absorber mounts, and x_{shi} and y_{shi} are the horizontal and vertical components, respectively, of the hull shock

absorber mounts.

The hydropneumatic suspension forces, due to gas spring, orifice damping, Coulomb friction, and bump stops, described in Chapter 2, are integrated in the equations of motion to yield the ride dynamics of the tracked vehicle with hydropneumatic suspension. Denoting the total hydropneumatic suspension force as F_H, the equations of motion are expressed as:

Hull Bounce:

$$\left(M_h - \tan^2(\theta_o - \zeta) \sum_{i=1}^{5} m_{wi} \right) \cdot \ddot{y}_h - \tan(\theta_o - \zeta) \cdot$$

$$\sum_{i=1}^{5} m_{wi} \cdot d_i \cdot \left(\tan(\theta_o - \zeta) \cdot \cos \alpha_i + \sin \alpha_i \right) \cdot \ddot{\phi}_h +$$

$$\tan^2(\theta_o - \zeta) \sum_{i=1}^{5} m_{wi} \cdot \ddot{y}_{wi} + \frac{1}{R \cdot \cos(\theta_o - \zeta)} \sum_{i=1}^{5} K_{ti} \cdot$$

$$(\theta_i - \phi_h) + \mu_s \cdot \left(y_h + L_{sp} \cdot \phi_h - y_{wi} \right) + \mu_{ID} \cdot \left(y_h - \right.$$

$$\left. L_{ID} \cdot \phi_h - y_{ws} \right) + \frac{r_s}{R \cdot \cos(\theta_o - \zeta)} \cdot \sin(\lambda + \theta_o) \left[\sum_{i=1}^{5} C_{eqi} \cdot \right.$$

$$\left. (V_{ai} - V_{bi}) + F_{Hi} \right] = 0 \qquad \ldots(A.27)$$

Hull Pitch:

$$\left(J_h + \sum_{i=1}^{5} m_{wi} \cdot d_i \left[\sin \alpha_i + \tan(\theta_o - \zeta) \cdot \cos \alpha_i \right]^2 \right) \cdot \ddot{\phi}_h$$

$$+ \tan(\theta_o - \zeta) \sum_{i=1}^{5} m_{wi} \cdot d_i \cdot \left[\sin \alpha_i + \tan(\theta_o - \zeta) \cdot \cos \alpha_i \right] \cdot$$

$$\left(\ddot{y}_h - \ddot{y}_{w1} \right) + \sum_{i=1}^{5} \left(\frac{d_i \cdot \cos \alpha_i}{R \cdot \cos(\theta_o - \zeta)} - 1 \right) \cdot K_{ti} \cdot (\theta_i - \phi_h)$$

$$+ \mu_s \cdot L_{sp} \cdot \left(y_h + L_{sp} \cdot \phi_h - y_{w1} \right) - \mu_{ID} \cdot L_{ID} \cdot \left(y_h - L_{ID} \cdot \phi_h - y_{w5} \right)$$

$$- \sum_{i=1}^{5} \left\{ d_{si} \cdot \sin(\beta_i - \lambda) + \frac{r_s \cdot d_i \cdot \cos \alpha_i}{R \cdot \cos(\theta_o - \zeta)} \sin(\theta_o - \zeta) + d_i \cdot \sin(\alpha_i - \lambda) \right\}$$

$$\cdot \left[C_{eqi} \cdot (V_{ai} - V_{bi}) + F_{Hi} \right] = 0 \qquad \ldots(A.28)$$

Wheel Bounce:

$$m_{wi} \cdot \left(1 - \tan^2(\theta_o - \zeta) \right) \cdot \ddot{y}_{wi} + \tan^2(\theta_o - \zeta) \cdot m_{wi} \cdot \ddot{y}_h$$

$$+ \tan(\theta_o - \zeta) \cdot m_{wi} \cdot d_i \cdot \left[\sin \alpha_i + \tan(\theta_o - \zeta) \cdot \cos \alpha_i \right]$$

$$\cdot \ddot{\phi} - \frac{1}{R \cdot \cos(\theta_o - \zeta)} \cdot K_{ti} \cdot (\theta_i - \phi_h) + K_{peff} \cdot (y_{wi} - y_{Ri})$$

$$+ \mu_w \cdot \left(2y_{wi} - y_{wi-1} - y_{wi+1} \right) - \frac{r_s \cdot \sin(\lambda + \theta_o)}{R \cdot \cos(\theta_o - \zeta)}$$

$$\cdot \left[C_{eqi} \cdot (V_{ai} - V_{bi}) + F_{Hi} \right] = 0 \qquad \ldots(A.29)$$

The above equations form a set of general equations of motion valid for the pitch-plane analysis of the tracked vehicle with conventional as well as hydropneumatic suspension. Depending upon the desired analysis, suspension elements at the individual wheel sets may be selected in any combination: torsion bar and hydraulic damper; torsion bar alone; hydropneumatic alone, etc.